DOCTOR OF HEALTH (DHEALTH)

Estimating musculoskeletal loading and muscular adaptations to hypogravity using an optimal control approach

Cowburn, James

Award date:
2022

Awarding institution:
University of Bath

Estimating musculoskeletal loading and muscular adaptations to hypogravity using an optimal control approach

submitted by

James Cowburn

for the degree of Doctor of Philosophy

University of Bath

Department for Health

March 2022

Declarations

Declaration of any previous submission of the work.

The material presented here for examination for the award of a higher degree by research has not been incorporated into a submission for another degree.

Candidate's signature ....

Declaration of Authorship

I am the author of this thesis, and the work described therein was carried out by myself personally.

Candidate's signature ....

Abstract

In this thesis a computational framework was developed to profile the musculoskeletal loading during exercise in hypogravity and to model muscular adaptations to disuse. The aims were i) to create a *Biomechanical Handbook* of normative internal musculoskeletal loading profiles when exercising in hypogravity, and ii) to assess how muscular adaptations to unloading can be replicated with a Hill-type muscle model. A direct collocation framework was used to estimate muscle and joint reaction forces, validated against the Knee Grand Challenge dataset. The framework was then used to estimate lower-limb joint reaction forces during single-leg hopping at five hypogravity levels, and predict exercise volume to avoid detrimental adaptations. Joint reaction forces were estimated within 0.62 - 0.85 BW relative to the Knee Grand Challenge data, with a peak error of 1.24 $\pm$ 0.17 BW. The framework was also able to detect the increase in peak joint reaction force as walking speed increased. The hypogravity case-study revealed an increased quadriceps muscle forces and a shift in rectus femoris force as gravity approached 1 g. When quadriceps muscle forces were input into a muscle adaption model, predicted exercise volumes needed to combat muscle adaptations decreased substantially with gravity. The framework allows for the comparison between different movements and gravity levels needed to create a Biomechanical Handbook. An experimental protocol, which expands on the handbook vision, is presented to provide a blueprint for the analysis of a catalogue of gait and jumping exercises in hypogravity to provide reference values to the handbook. Finally, a Monte Carlo sampling technique was used to perturb Hill-type muscle model parameters during an isokinetic knee extension task. The results highlighted the Hill-type muscle model can replicate muscular adaptations to unloading as long as optimal fibre length is adjusted appropriately.. This information is key for future research to adjust musculoskeletal models to achieve appropriate simulation results, which will improve application of simulation methods to space science contexts.

Acknowledgements

First and foremost, my most sincere thanks must go to my supervisors. Dario, your passion, optimism, and friendship have been a constant source of inspiration and reassurance to keep learning and improving my work. You have always made time for meetings, to provide feedback, and to discuss all things modelling. I always felt you were in my corner, and that is something I cannot thank you enough for. Steffi, you helped introduce me to biomechanics during first year labs, and now you have helped guide me through a PhD. Your ability to both challenge and encourage me with one question always helped me see the bigger picture, and this is a stronger PhD because of it. Aki, I want to thank you for putting your faith in me when you first invited me to discuss this project during the MSci. You set me on this path and for that I am grateful.

To Dr Gil Serrancolí for hosting me at Universitat Politècnica de Catalunya and guiding me through the crazy world of optimal control. Without your troubleshooting, feedback, and creative solutions I would not be where am. To Dr Tobias Weber, Dr David Green, and Dr Jonathan Scott from the European Space Agency (ESA) for their knowledge of all things space science during my PhD. Without the funding from the ESA I would not have been able to undertake such novel and exciting research. To Prof Alberto Minetti and Dr Gaspare Pavei for supporting me in securing funding to visit the University of Milan. I would also like to thank Dr Elena Seminati and Dr Polly McGuigan. Without the IAA project I would not have been able to fund the final stages of this PhD.

To the ABS family, past and present, thank you for providing welcome distractions and friendship throughout my PhD. In particular to the PhD office for creating an easy-going and, on occasion, chaotic working environment, and for always being willing to engage in (not so) topical discussions. To my friends across the Department for Health for the endless supply of memories and laughs over the years.

Finally, to my family. To my mum and dad, Carolyn and Terry. To my brothers, Ian and Terry, their partners, Alex and Claire, and the newest member, Edward. Thank you for your unconditional love and support in pursuit of every goal I have ever had. I would not be the person I am today without you.

Thesis Dissemination

Conference Proceedings

Cowburn, J., Serrancolí, G., Pavei, G., Minett, A., Salo, A., Colyer, S., & Cazzola, D. (2021). *Estmating muscle forces and adaptations during plyometric hopping in emulated hypogravity.* Proceedings of the 26th Congress of the European Socoiety of Biomechanics, Milan, Italy.

(This conference proceeding formed the basis for worked carried out in chapter 3)

Cowburn, J., Serrancolí, G., Pavei, G., Minett, A., Salo, A., Colyer, S., & Cazzola, D. (2021). *Estmating muscle forces and adaptations during plyometric hopping in emulated hypogravity.* Proceedings of the 6th German Human Physiology Workshop, Cologne, Germany.

(This conference proceeding formed the basis for worked carried out in chapter 3)

Cowburn, J., Baldwin, M., Serrancolí, G., Salo, A., Colyer, S., & Cazzola, D. (2022). *Optimal Fibre length and Maximum Isometric Force are the most influential parameters when modelling muscular adaptations to unloading using Hill-Type muscle models.* Proceedings of the 9th World Congress of Biomechanics, Taipei, Taiwan.

(This conference proceeding formed the basis for worked carried out in chapter 5)

Funding Acquired

University of Bath IRO International Research Funding Schemes - Strand 3 Future Research Leaders (2019)	£1,800

Public Engagement

Take off for partial gravity rehabilitation project (Physics World)	2019
Take off for European Space Agency-funded project (University of Bath)	2019

Contents

List of Figures

List of Tables

Chapter 1

Introduction

1.1 Motivation

Almost five decades since Apollo 17 last carried humans to the Moon, space exploration is again a main focus of international space organisations. The European Space Agency (ESA) announced their long-term aim of returning to the lunar surface as early as 2025 (Eurpoean Space Agency, 2022), with the National Aeronautics and Space Administration (NASA) aiming to transport humans to Mars before 2040 (Wilson, 2021). Commercial spaceflight, or space tourism, is also becoming a reality with two companies, Virigin Galactic and Blue Origin, launching the first civilian-only flights into space in July 2021 (Blue Origin, 2021; Virgin Galactic, 2021). However, the musculoskeletal (MSK) systems, amongst other physiological systems, undergo adaptations during spaceflight that impact human health. These adaptations can occur in as little as seven days (Ferrando *et al.*, 1995), and, in some instances, may not return to their pre-flight condition (Kramer, Kümmel, *et al.*, 2018a). The MSK system is integral to performing work to allow locomotion and to maintain posture. Consequently, space-induced adaptations impact an individual's functional capacity during and following spaceflight (Berg *et al.*, 1997; English *et al.*, 2020). During the Apollo program, the last and still only manned program to the Lunar surface, NASA spent ∼\$25 billion in 1960s currency (Gisler & Sornette, 2009); over \$180 billion adjusting for inflation. As space activities continue grow in number and duration, and as they extend further from Earth orbit, the financial outlay will equally continue to grow.

The severe environmental and physiological challenges of spaceflight have long been acknowledged. Before Neil Armstrong stepped foot on the moon (1969), before Yuri Gagarin made the first human voyage into Space (1961), and even before the creation of NASA, (1958), mitigation against the deleterious physiological affects of spaceflight were being considered (National Advisory Committee for Aeronautics, 1958). Since then a substantial research effort has taken place to better understand adaptations of physiological systems, including the MSK system, so as to minimise the impact to astronaut health and well-being upon return-to-Earth. Exercise has become an integral part of an astronaut's routine to maintain MSK health (Loehr *et al.*, 2015; Petersen *et al.*, 2016). The health of MSK tissue, such as muscle and bone, reflects the mechanical load to which it has been exposed to. The equipment aboard the International Space Station (Figure 1-1) has been optimised for the unique time, mission, space, and resource constraints associated with space travel whilst trying to target the multi-system adaptations associated with the reduced gravitational environment. These devices have evolved over time but are still limited in the movement patterns they allow and the resistance they can provide. This is reflected in the adaptations observed in astronauts post-spaceflight, which are relatively quick to emerge (Winnard *et al.*, 2019) and show considerable inter-individual variation (Scott *et al.*, 2021). Although the evolution of exercise devices and innovation of different countermeasures appears to have reduced the magnitude of adaptations (English *et al.*, 2015), the fact astronauts still experience MSK deterioration highlights the need for further research to protect their health in- and post-spaceflight.

(a)

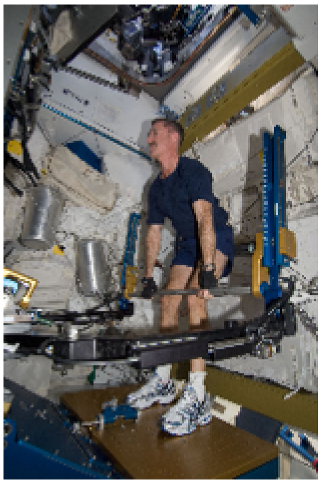

(b)

(c)

Figure 1-1 Astronauts on the International Space Station currently have access to multiple exercise devices. Aerobic conditioning via a treadmill and cycle ergometer (a & c) and an advance resistance exercise device (b) for strength training.

1.2 Rationale of Musculoskeletal Modelling

Hypogravity encapsulates environments, both ground-based (e.g. body weight support systems) and extra-terrestrial (e.g. the Moon), where gravitational forces are below terrestrial levels (i.e. $\leq$1 g). In this context, the mechanoresponsive MSK tissues, such as muscle and bone, adapt to the reduced habitual mechanical stimuli that are applied to them due to the reduced gravitational forces. Astronauts are prescribed comprehensive exercise programs pre-, in-, and post-spaceflight to mitigate against MSK adaptations (Loehr *et al.*, 2015; Petersen *et al.*, 2016). However, astronauts still experience multi-system MSK adaptations that highlights there is a gap in our understanding of mechanical loading in hypogravity that if addressed can improve the outlook for astronaut health in space. Previous work aiming to describe MSK loading in hypogravity has been driven by external parameters, including ground reaction forces and impulses, internal and external work performed to oscillate the centre of mass, and net joint moments (Apte *et al.*, 2018; Richter *et al.*, 2017). Notwithstanding the valuable information that can be garnered from these variables, they do not provide a complete picture but rather a net affect on the whole or part of the MSK system. The human body is a redundant system with the number of muscles exceeding the degrees of freedom of the skeletal system, meaning it is not possible to divide these parameters across the individual MSK structures using traditional biomechanical analyses. Musculoskeletal modelling is the application of physics-based mathematical methods to describe the MSK system, and is often combined with traditional biomechanical workflows to allow for the estimation of internal parameters that are otherwise not possible *in vivo*. In particular, the inclusion of muscle-tendon unit (MTU) elements, including geometrical information (i.e. lines of action and moment arms about a joint) and force-generating dynamics (Zajac, 1989), allows for optimisation-based algorithms to estimate the muscle forces required to generate the analysed movement. With the estimated muscle forces, joint reaction forces can then be calculated that describe the overall joint loading between two segments. These internal parameters provide a more detailed picture of the loading profile on the MSK tissue. This approach has shown promise in clinical contexts through identifying MSK loading parameters that are implicated in the progression of degenerative diseases (e.g. osteoarthritis), rehabilitation, assistive device deign, and surgical planning (Killen *et al.*, 2020). For example, Von Rossom and colleague (2018) estimated the knee joint loading for a catalogue of activities of daily living and rehabilitation exercises, allowing for a patient's rehabilitation stage to be aligned with the prescribed exercise. In a similar way, estimating internal MSK loading during exercise in hypogravity can improve exercise prescription in two main ways:

1. In-flight exercise programs can be categorised according to their loading profile to better target and prevent MSK adaptations.

2. Exercise programs can be personalised during post-spaceflight rehabilitation to the type and magnitude of MSK adaptations experienced by the astronaut.

1.3 Research Aims

The overarching purpose of this thesis was to inform hypogravity exercise prescription by applying MSK modelling and optimal control simulation methods to hypogravity exercise contexts. This would, for the first time, provide insight into internal biomechanical loading (i.e. muscle and joint forces) during movement in hypogravity. Knowledge of this is key for space agencies, and other disuse rehabilitation contexts, as expected MSK loading profiles can be better aligned with astronaut-specific exercise requirements based on their adaptations to disuse. This can inform preventative monitoring tools to intervene in-flight before adaptations become severe, or rehabilitation strategies to minimise recovery time. To this end, the aims of this thesis were:

1. To create a *Biomechanical Handbook* of normative muscle and joint loading profiles when exercise is performed in different gravity levels.

2. To assess how muscular adaptations to unloading can be replicated with a Hill-type muscle model.

To achieve this the following objectives were set:

1. To develop a computational framework, based on optimal control theory, that quantifies the lower-limb internal loading during exercises performed at different levels of gravity (aim 1).

2. To devise a comprehensive experimental protocol for the collection of biomechanical data for a variety of exercises across a spectrum of gravity levels (aim 1).

3. To systematically adjust Hill-type muscle model parameters to replicate experimental data of muscular adaptations due to unloading (aim 2).

4. To integrate a stochastic sampling technique with the optimal control framework to explore all the feasible combinations of Hill-type muscle model parameters that reflect muscular adaptations to disuse (aim 2).

1.4 Thesis Structure

Chapter Two: Review of Literature

The contents of this chapter review the pertinent literature relating to MSK adaptation to unloading, biomechanical loading during hypogravity exercise, the application of MSK modelling to quantify loading (i.e. muscles and joints) during exercise, and simulation methods used to optimise for and solve the muscle redundancy problem.

Chapter Three: The Biomechanical Handbook

The development and validation of an integrated experimental and direct collocation optimal control framework is presented in this first study, before the concept of a *Biomechanical Handbook* is provided via a hypogravity case-study. An open source repository of biomechanical data, including *in vivo* knee contact forces from a force instrument knee prosthetic, from a single male participant was used to assess the accuracy with which the framework could estimate joint reaction forces. The *Biomechanical Handbook* was presented by applying the validated framework to a case-study of a single male participant performing single-leg hopping using a body weight support system. A novel approach of using a muscle adaptation model was used to assess, for the first time, hypothetical training volumes (i.e. repetitions) to better bridge the gap between theoretical simulations and application to practice.

Chapter Four: The MoLo-Milano Study Protocol

Experimental and MSK modelling methods are combined to create an experimental protocol for analysing internal MSK loading in hypogravity (i.e. $\leq$1 g). This builds upon the *Biomechanical Handbook* concept presented in Chapter Three by collecting biomechanical data for a catalogue of exercise types, including gait and jumping movements, using a body weight support system to replicate a spectrum of hypogravity conditions from 0.16 g (Luna gravity) to 1 g (terrestrial gravity). The same data-tracking simulation framework is described to estimate the internal MSK loading (i.e. muscle forces and joint reaction force). An analysis plan is presented to define MSK loading profiles based on the movement and gravity level, and the application to in-flight and post-spaceflight exercise prescription is considered.

Chapter Five: Modelling Muscle-Tendon Unit Adaptations to Unloading

Within this chapter a Monte Carlo sampling technique was used to explore all feasible combinations of Hill-type muscle model parameters that were able to recreate an experimental isokinetic knee extension task. The capacity of the Hill-type muscle model to replicate adaptations to unloading is considered and strategies for adjusting MTU parameters based on the results are discussed.

Chapter Six: General Discussion

The contents of the studies presented within this thesis are contextualised in the wider literature. The impact of the results are discussed, and the limitations and directions of future research are considered before final concluding remarks are made.

Chapter 2

Review of Literature

This chapter evaluates the relevant literature in relation to aims outlined in the first chapter of this thesis. Particular focus is given to four main themes:

1. Musculoskeletal Adaptation to Unloading
2. Musculoskeletal Loading in Hypogravity
3. Musculoskeletal Modelling to Estimate Load
4. Optimisation to Solve the Muscle Redundancy Problem

This chapter begins with introducing adaptations musculoskeletal (MSK) tissue experiences when gravitational forces are reduced. This aims to highlight the severe physiological challenge spaceflight represents to the human body, and gives contexts to the important role exercise plays in mitigating against the deleterious adaptations. The limitations of previous biomechanical assessment of MSK loading when exercising hypogravity are then discussed in relation to previous literature from spaceflight and ground-based methods to replicate load gravity. In the final two themes, MSK modelling and computer simulations are introduced as methods for estimating internal loading (i.e. muscle and joint forces) that are not possible using traditional *in vivo* biomechanical methods. A particular focus is placed on the key aspects that influence the physiological realism of muscle force and joint reaction force estimations.

This chapter is concluded with a restatement of the thesis aims in the context of the gaps that are present in the literature.

Key Definitions

Before advancing to overview the relevant literature, it is important outline the definitions used in this thesis. Within the literature, the terms *hypogravity* and *partial gravity* are interchangeable ways of describing gravity below terrestrial levels (i.e. < 1 g). They encapsulate another term, *microgravity*, which specifically refers to $\sim$0 g, such as on the International Space Station. Within this thesis the term hypogravity is used to describe ¡ 1 g, and microgravity is used when specifically referencing 0 g. Terrestrial or Earth gravity is used to describe 1 g.

2.1 Musculoskeletal Adaptation to Unloading

The health of MSK tissue, such as muscle and bone, reflects the mechanical load to which it has been exposed to. Mechanical load acts as a stimulus that regulates homeostasis through triggering remodelling and maintenance processes (Frost, 1987, 2003; Wang, 2006). The state of MSK system adapts to the degree of overload borne by its structures. Equally, by removing habitual mechanical load, such as during spaceflight, the MSK system adapts in a way that would be considered detrimental to *normal* free living. This leaves the MSK system less able to meet the demands of societal functioning, which may impact an individuals well-being. This includes a reduced functional capacity of the muscular system and reduced bone strength that both leave the individual less able to perform activities of daily living, and more susceptible to potential injuries. This section summaries the MSK adaptations associated with disuse to contextualise the challenge faced by individuals embarking on long-duration spaceflight.

2.1.1 Muscular adaptations

Weakening of the muscular system is a common symptom of disuse. This has been demonstrated in various unloading paradigms including spaceflight (Koryak, 2019), bed rest (Winnard *et al.*, 2019), unilateral lower-limb support (ULLS) (Berg *et al.*, 1991), cast immobilisation (Hvid *et al.*, 2017), and as a consequence of aging (Bruce *et al.*, 1989). Evidence from short duration spaceflight highlights that maximum voluntary isometric contraction (MVC) moment can decline by as much as 15% in as little as 2-5 days (Convertino & Tsiolkovsky, 1990). Although there can be substantial variability between muscles and between individuals. Continued exposure to microgravity shows that MVC performance can decrease 8 - 37% after 14 to ∼180 days of spaceflight (Koryak, 2019; Lambertz *et al.*, 2001; Tesch *et al.*, 2005; Trappe *et al.*, 2009), and 3 - 55% after 14 to 120 days bed rest (Bamman *et al.*, 1998; Berg *et al.*, 2007; Berg *et al.*, 1997; Blottner *et al.*, 2006; Gallagher *et al.*, 2005; Kawakami *et al.*, 2001; Koryak, 1995, 1999, 2010, 2014, 2015; Kramer, Kümmel, *et al.*, 2018a; Moriggi *et al.*, 2010; Reeves *et al.*, 2002; Schneider *et al.*, 2016). This has been shown to manifest in reduced functional performance in one repetition maximum of lower-limb extension (English *et al.*, 2020), and reduced countermovement jump height (Kramer, Kümmel, *et al.*, 2018b). The majority of studies have utilised isometric or isokinetic movements about a single joint, either via dynamometry or flywheel equipment. While this provides an objective method to evaluate the influence on muscle moment-joint angle/velocity interactions, which are relevant in the study of movement, these measures do not necessarily scale well to the muscle level (Lieber & Fridén, 2000). Muscle biopsies allow for isolation of single fibres to overcome a number of the limitations with *in vivo* measurements through chemical stimulation via immersion in a calcium solution. Since the sarcoplasmic reticulum is rendered non-functional, this technique is assumed to represent muscular function at the level of the cross-bridges. Biopsies taken from the soleus and gastrocnemius show reduced fibre force of 21% and 15%, respectively, after 17-d spaceflight (Widrick *et al.*, 2001; Widrick *et al.*, 1999). By the time an astronaut has been exposed to ≥160-d spaceflight, the decline in fibre force can reach as much as 35%, depending on the muscle and fibre type (Fitts *et al.*, 2010). The remaining content of this section will overview the structural and architectural adaptations reported to the muscular system that underpin the decline muscular strength.

Muscle Size

Muscle atrophy is a common reported adaption to disuse. Decrease in cross-sectional area (CSA) has been demonstrated that atrophy can manifest at both the whole muscle level and the fibre level. Medical imaging, such as MRI and CT scans, highlight that muscle CSA declines by as much as 4 - 10% within just 8 to 17 days of spaceflight (LeBlanc *et al.*, 1995; Tesch *et al.*, 2005) and within 5 to 7 days of bed rest (Dirks *et al.*, 2016; Ferrando *et al.*, 1995; Tanner *et al.*, 2015). Continued exposure to unloading Although, data collated by Nirici and de Boer (2011) from various disuse paradigms, the rate of atrophy appears to slow overtime. Muscle biopsies from the vastus lateralis and triceps surae muscles highlight reduced fibre CSA between 16 - 36% after 7 - 11 day (Edgerton *et al.*, 1995), 2 - 21% after 17-d (Riley *et al.*, 2000; Trappe *et al.*, 2001; Widrick *et al.*, 2001; Widrick *et al.*, 1999), and 24 - 44% after $\geq$160-d (Fitts *et al.*, 2010). The decrease in muscle tissue is believed to be due to decreases in muscle protein synthesis, and consequently a net breakdown, due to the reduced mechanical stimuli. There is evidence that protein synthesis rate is decreased after 3-months spaceflight and halved after 21 days ULLS (De Boer *et al.*, 2007; Stein *et al.*, 1999), but limited data showing changes to protein breakdown when disuse is not accompanied with confounding variables (e.g. disease or diet). The decrease in CSA is believed to represent a loss of muscle fibres in parallel, compromising the potential for cross-bridge formation required for force generation. This is supported by a reduction in specific force/tension (muscle force normalised to CSA) following bed rest (Larsson *et al.*, 1996) and immobilisation (Hvid *et al.*, 2017), which may, in part, be explained by a reduction in actin myofilament density impacting cross-bridge formation (Riley *et al.*, 2000). Furthermore, the decrease in CSA is experienced across the entire length of the muscle (Akima, Kawakami, *et al.*, 2000; Miokovic *et al.*, 2012), contributing to a loss of muscle volume (Gopalakrishnan *et al.*, 2010; Rittweger *et al.*, 2018; Trappe *et al.*, 2009). Albeit, CSA loss across the muscle is non-uniform (Akima, Kawakami, *et al.*, 2000; Miokovic *et al.*, 2012) meaning CSA can, depending on the region measured, appear greater than volume atrophy as volume represents the average CSA changes (Narici & De Boer, 2011).

An important observation from literature is susceptibility of so called *antigravity* muscles to disuse. The volume of the soleus (19.6%), gastronemius (23.8%), quadriceps femoris (12.1%), hamstrings (15.7%), anterior leg muscles (16%), intrinsic back muscles (20.0%) and psoas (10.9%) have all been shown to decrease to varying degrees following 16 - 28 weeks of spaceflight (LeBlanc, Lin, *et al.*, 2000). Similarly, Miokovic *et al.* (2012) showed muscle volumes of the soleus (23%), gastronemius (24%), vasti (16%) atrophy to a greater extent than the hamstrings (13%) and tibialis anterior (12%). Although contentious within the literature, there is evidence that type I fibres atrophy to a greater extent than faster fibre types (Narici & De Boer, 2011). For example, following 180 days spaceflight single fibre analyses showed a heirachial decrease in fibre CSA of the order soleus type I > soleus type II > gastronemius type I > gastronemius type II (Fitts *et al.*, 2010). This likely reflects the fact the soleus is a greater contributor to progression during walking and running gaits (Cronin *et al.*, 2013; Hamner & Delp, 2013), therefore the relative decrease in habitual loading of the soleus is greater when gravitational forces are removed. Additionally, the regions within the same muscle that experienced the greatest CSA atrophy was muscle-specific, with the greatest atrophy seen between 5 - 50% of the rectus femoris' length (muscle origin being 0%), between 15 - 70% for the hamstring muscles, and 30 - 100% for the gastronemius heads (Miokovic *et al.*, 2012). Muscles that perform multiple functions may explain the different CSA atrophy within muscles. For example, the rectus femoris has been hypothesised to have two or more sub-volumes due to split nerve innervation and blood supply to the proximal and distal portions of the muscle (Yang & Morris, 1999). Muscle compartmentalisation is this manor allows multiple functions to be performed by the same muscle (Hasselman *et al.*, 1995), and may contribute to within-muscle heterogeneity.

Muscle Architecture

As demonstrated in the literature, muscle weakening and muscle atrophy adapt asynchronously in response to disuse. A systematic review of non-exercise control groups during bed rest found that muscle weakening (7-d) proceeds muscle atrophy (14-d) during short-term disuse, but, although both continue to decline, muscle atrophy does so at a faster rate with continued disuse (Winnard *et al.*, 2019). Additionally, isometric and isokinetic moment generation may still decline even in the absence of concurrent muscle atrophy following spaceflight (Bamman *et al.*, 1998; Greenisen *et al.*, 1999) and bed rest (Alkner & Tesch, 2004; Kawakami *et al.*, 2001). This highlights that additional adaptations contribute to changes in muscle strength beyond CSA. The limitation of medical imaging to measure CSA is that they provide a planer representation of the muscle, which is not necessarily representative of the fibre architecture. An in-depth description of muscle fibre arrangement is beyond this review (see Lieber & Fridén, 2000), but, in brief, fibres are typically non-parallel to the axis of force generation (i.e. are pennate) and may be distributed at various angles (θ) within the same muscles. Physiological CSA (PCSA) is an architectural parameter that expresses muscle volume (muscle mass/density [ρ]) whilst accounting for fibre length and pennation angle (eq. 2.1). It is considered to represent the total CSA of the muscle fibres and, therefore, the only parameter directly proportional to maximum force generating capacity of the muscle (Lieber & Fridén, 2000; Martin *et al.*, 2020).

$$PCSA(mm^2) = \frac{musclemass(g) \cdot cosine\theta}{\rho(g \cdot mm^3) \cdot fibrelength(mm)} \tag{2.1}$$

Pennation angle represents the angle at which the muscle fibres are orientated with respects to the aponeurosis. It represents the projection of the muscle fibres along the aponeurosis, and consequently governs the effective force that is applied to the bones for movement. It has been consistently shown that pennation angle decreases with disuse, with values reported between 3% - 27% reported after spaceflight (Koryak, 2019; Rittweger *et al.*, 2018), 1% - 14% after bed rest (De Boer *et al.*, 2008; Kawakami *et al.*, 2001; Kawakami *et al.*, 2000; Reeves *et al.*, 2002), and 4% - 10% following ULLS (Campbell *et al.*, 2013; De Boer *et al.*, 2007; Seynnes *et al.*, 2008). Pennation angle is positively correlated with fibre thickness (Kawakami *et al.*, 1993), hence increased pennation angle is used to indicate an increase parallel sarcomere orientation (Narici *et al.*, 2016). The increased pennation, although reduces the effective force a fibre projects along the aponeurosis, allows for increased fibres to be arranged within the muscle. Given muscle atrophy is a common adaption following disuse, the reduced pennation angle supports the hypothesis that the decrease in CSA is caused by reduced parallel sarcomere. It is unclear whether the reduced pennation angles partially offset the decreased PCSA (i.e. force generating capacity) by allowing more fibre force to be projected along the tendon, however, it is clear that muscle atrophy supersedes this. A functional role of pennation angle is to control fibre shortening velocity through rotating during contraction (Lieber & Fridén, 2000). The increase in pennation angle as the muscle shortens results in a disproportionate decrease on muscle length relative to fibre length. Koryak (2019) measured pennation angle of the ankle plantarflexors before and after 180 days spaceflight in two different ankle angle positions. The results indicated that although there was a tendency for the medial gastrocnemius to rotate less during shortening after spaceflight, this was not substantial and not observed in the lateral head and the soleus. The impact on shortening velocity due to pennation angle changes in likely minimal.

Muscle fibre length is an important characteristic in muscle force-generation. Muscle adapts in response to overstretch and understretch, as demonstrated by the increased and decreased serial sarcomere number seen in mice with immobilised ankles in lengthened and shortened configurations, respectively (Williams & Goldspink, 1978). Ultrasonographic images have shown that resting muscle fascicle length is shorter following disuse, indicating removal of gravitational load understretches the muscles. Data from spaceflight (Koryak, 2019; Rittweger *et al.*, 2018), bedrest (De Boer *et al.*, 2008; Reeves *et al.*, 2002), and ULLS (De Boer *et al.*, 2007; Suetta *et al.*, 2007) show lower-limb muscle fascicles can shorten between 5 - 13% following disuse. The observation that postural muscles, particularly the ankle plantarflexors, are more susceptible to unloading was shown in fascicle lengths, with the gastrocnemius (12%) and the vastus lateralis (8%) shortening while the biceps brachii do not (De Boer *et al.*, 2008). Additionally, in microgravity astronauts adopt a more flexed resting posture (Han Kim *et al.*, 2019; Simons, 1964), which likely further exacerbates the understretch stimulus. It is theorised that muscle fascicle length adapts by additional serial sarcomere to ensure the sarcomere work within the ascending limb and plateau regions of the force-length relationship (Lieber & Fridén, 2000). However, this is yet to be confirmed experimentally in adult human muscle *in vivo* with increased sarcomere length appearing to be the primary underlying adaption following short-term eccentric training (Pincheira *et al.*, 2022). Adaptation to the resting sarcomere length is supported by some disuse studies, with the distance between consecutive z-lines, indicative of sarcomere length, shown to decrease following spaceflight and bed rest (Riley *et al.*, 2000, 1998). Regardless, this highlights there is a shift in the operating region within the muscle has adapted to work efficiently in. Shorter muscle fibres will have two potential impacts on force-generation (Lieber & Fridén, 2000). First, maximum shortening velocity will be reduced as it is proportional to fibre length, meaning less force can be produced for the same absolute fibre velocity. Disuse research provides some support for this as fibre shortening velocity, as assessed via slack test procedures, can change in some fibres (Fitts *et al.*, 2010). Although this outcome is influenced by adaptations to fibre type composition within the muscle. Second, the absolute range of the force-length relationship is shifted causing peak absolute force to occur at a shorter length. While geometry of the muscle, particularly moment arm about a joint, will influence the range of motion of the muscle, this reduced absolute range of the fibre impacts muscle function. Again, disuse research can provide some support for this as reduced flexibility, as demonstrated by reduced sit-and-reach performance, is present in some astronauts post-spaceflight (English *et al.*, 2020; Laughlin *et al.*, 2015). Where muscle fascicle shortening is present it may explain the increased muscle weakening observed in some participants, as the architectural adaptations may compound muscle atrophy. While there is little data to support this hypothesis in practice, reduced muscle volume and physiological CSA with and without concurrent fascicle shortening has been observed in both human (Rittweger *et al.*, 2018) and animal studies (Caiozzo *et al.*, 1996).

Shortening Velocity

Muscle shortening velocity plays an important role in the active force generation of the muscle. Fundamental to the force-velocity relationship, maximum shorten velocity determines the absolute range of shortening velocities of a muscle. When maximum isometric force is kept constant, this allows for greater absolute force to be generated for the same shortening velocity (Lieber & Fridén, 2000; Miller *et al.*, 2012) and a greater shortening velocity to be achieved before zero force can be generated. Thus, adaptations to the muscle that influence the velocity at which a muscle can shorten will influence muscular strength. As mentioned above, it is assumed that muscle fibre length is proportional to fibre velocity and that rotation of the fibres (i.e. increased pennation angle) during contraction can influence the velocity a fibre shortens (Lieber & Fridén, 2000). It would be expected then that the shortening velocity of the fibre would exclusively decline following disuse because fascicle length tends to shorten and pennation rotation appears to be unaffected. However, this is not always the case. *In vitro* analyses of single-fibres have reported that maximum shortening velocity can decline by as much as 44% (Fitts *et al.*, 2010), but increase by a factor of two (Yamashita-Goto *et al.*, 2001) following disuse. Short-term disuse is associated with increased shortening velocity. Soleus fibres presented with increased shortening velocity after 17 days spaceflight (22 - 44% Widrick *et al.*, 2001; Widrick *et al.*, 1999) and 17 days bed rest (15 - 33% Widrick *et al.*, 1998; Widrick *et al.*, 1997). However, with the exception of soleus type II fibres, following 160 days spaceflight the shortening velocity of grastrocnemius and soleus fibres was reduces by $\sim 20\%$ (Fitts *et al.*, 2010). The authors of these papers suggest thin filament density influences this finds, reduced thin myofilament density during short-term disuse allowing for greater spacing between actin and myosin and less drag (Riley *et al.*, 2000, 1998). Further complication arises due to a preferential shift to type II fibres within the muscle. Long-term bed rest has been associated with the shift from type I to type II fibres (Trappe *et al.*, 2004), believed to restore parity to fibre power generation after the loss of fibre force (Qaisar *et al.*, 2020). Despite reduced maximum shortening velocity appears to occur across all fibre types, at least with long-term disuse, the shift from type I to type II fibres makes it difficult to understand how this might manifest at the whole muscle level. This likely explains the large variation values reported in the literature.

It is important to note that the neuromuscular system is complex and there are other adaptations not discussed in detail here that will contribute to the decrease in muscular strength. For example, Koryak (Koryak, 1995, 1998, 1999, 2010, 2014, 2015) presented a series of studies assessing maximal involuntary contraction (MIC), assessed during titanic supramaximal stimulation via surface electrodes in a stepwise manor, and voluntary contraction of a muscle group after bed rest. From these studies it was found that MVC was reduced to a greater extent than MIC after 60-d (33.5% vs 17.3%, Koryak, 2010) and 120-d (36.1 - 45.5% vs 11.5 - 36.7%, Koryak, 1995, 1999, 2014), suggesting factors extrinsic to the contraction apparatus (e.g. calcium-dynamics or neural drive) influences the force-generating capacity. This is supported by the electromyographic (EMG) activity of the plantarflexors fallng by 35-40% following long-duration spaceflight (Lambertz *et al.*, 2001).

2.1.2 Tendon adaptations

The role of tendon in human movement is to transfer the contractile force to the bone to allow motion and to stabilise joints. It works in tandem with the muscle, and is typically considered part of a muscle-tendon unit (MTU). A key mechanical property of tendon is its stiffness, and describes it's resistance to elongation when force is applied. All else being equal, a more compliant tendon will experience greater strain when pulled by the same magnitude of force. This has important implications for muscle contraction dynamics as the elongation of the tendon will directly impact the lengths at which the fibres operate (Narici & Maganaris, 2007). Stiffness of the vastus lateralis aponeuross is reported to decline by 28% - 32% after 20 days bed rest (Kubo *et al.*, 2004a; Kubo *et al.*, 2004b), while Achilles tendon is reported to decline to 58% by 90 days bed rest (Reeves *et al.*, 2005). The onset can occur rapidly with 10% and 20% decrease in Patella and Achilles tendon stiffness, respectively, occurring after 14 days ULLS (Couppé *et al.*, 2012; De Boer *et al.*, 2007), rising to 29% by day 23 (De Boer *et al.*, 2007). An observation from De Boer *et al.* (2007) was that the reduction in stiffness accelerated after day 14, which is in contrast to the muscular and skeletal adaptations. The decline in tendon stiffness is similar to the degree in decline observed in Young's modulus (De Boer *et al.*, 2007; Reeves *et al.*, 2005), tendon stiffness normalised to tendon dimensions, suggesting tendon dimensions do not adapt substantially to disuse. Indeed, no previous study has reported changes to Achilles nor Patella tendon CSA in health adults following bed rest, ULLS and cast immobilisation (De Boer *et al.*, 2007; Reeves *et al.*, 2005). Furthermore, turnover of collagen tissue in Achilles tendon does not change after 6 - 10 weeks cast immobilisation (Christensen *et al.*, 2008).

This suggests that bed rest and ULLS disuse are insufficient stimuli to trigger tendon CSA atrophy and collagen remodelling. It appears that the decrease in tendon stiffness is driven by other structural consequences, such as collagen quality (Narici & De Boer, 2011). This places the disused tendon at greater risk of injury due to the potential for increased elongation under the same tensile load, because straining a tendon beyond ~4% and ~8 - 10% can lead microscopic and macroscopic tearing, respectively (Wang, 2006).

2.1.3 Bone and Cartilage Adaptations

Bone provides various functions from being a reservoir for minerals (e.g. calcium) to protection for internal structures such as organs, to name a couple. Most importantly for human movement is that bones provide structural support and attachment sites for muscles to transmit force to motion. Early spaceflight from NASA's Apollo (1968 - 1972) and Skylab programs (1973 - 1974) showed calcaneal bone mineral content can declined by as much as ~2 % in 13 days (Rambaut & Johnston, 1979), and continued to ~8 % by 84 days (Rambaut & Johnston, 1979). This aligned with data from the U.S.S.R's manned space programs with cosmonauts presenting with up to 8.2 % loss at the calcaneus after 175 days spaceflight (Gazenko *et al.*, 1981). These early findings were followed by further study that confirmed disuse via spaceflight and bed rest is associated with substantial mineral loss within the bones. It is often cited that bone mineral content loss occurs at a rate of 1 - 1.5% per month during spaceflight (LeBlanc, Schneider, *et al.*, 2000), which, for context, suggests astronauts would experience a similar rate of loss in just one month as post-menopausal women do in a year (Mendoza-Pinto *et al.*, 2021; Pouilles *et al.*, 1993). However, within the same study, LeBlanc *et al.* (2000) found those that spent longer in space (311 and 438 days) than the group average (188 days) has substantially lower rates of bone loss (0.51 - 0.68% per month). While this might be a consequence of inter-individual variability (Rittweger *et al.*, 2005; Scott *et al.*, 2021), the rate of loss appears to decline with extended exposure to hypogravity. Furthemore, bone mineral density, a measure of bone mineral content normalised to area scanned, declines at a similar rate at the hip (1.2% - 1.5% per month) but slightly slower in the vertebrae (0.8% - 0.9% per month) following 4 - 6 months spaceflight (Lang *et al.*, 2004). Bone mineral density represents the quantity of minerals within the bone structures, and even though it is not the only parameter of bone strength (e.g. quality of architecture), it is still considered a major determinant of bone strength (Ammann & Rizzoli, 2003). The mechanisms underpinning the decline in bone is related to altered bone remodelling. Bone remodelling occurs due to relative activities of osteoclasts (i.e. bone resorption) and osteoblasts (i.e bone formation), with the net effect resulting in an increase or decrease in bone mass. Markers of bone resorption increase more rapidly than formation markers during spaceflight (Stavnichuk *et al.*, 2020a) and bed rest (Spatz *et al.*, 2012), suggesting a net resorption dominates as a consequence of disuse. Furthermore, the increased resorption appears to plateau after 25 days while formation continues to rise through long-duration spaceflight (Stavnichuk *et al.*, 2020a), which supports the hypothesis that rate of bone loss decreases over time. The role of muscle in bone loss during disuse should not be discounted as bone and muscle strength are closely related, highlighting that muscle contractions are an important factor in skeletal loading (Schönau *et al.*, 1996).

The loss of bone has been shown to be regional and bone-type specific. Data from spaceflight and bed rest show that the lumbar spine, pelvis and lower-limb bones are particularly vulnerable to bone mineral loss in comparison to the upper limbs, upper thorax/spine and skull (Kramer *et al.*, 2017; Lang *et al.*, 2004; LeBlanc, Schneider, *et al.*, 2000; Rittweger *et al.*, 2005; Stavnichuk *et al.*, 2020a). There is also heterogeneity in bone mineral loss at different regions along the length of the bone (Kramer *et al.*, 2017; Rittweger *et al.*, 2005). Given the close relationship between bone mass and muscle mass, it is logical that the locations within that body that experience greater adaptations for muscle (e.g. the lower-limbs) are observed in the corresponding bones. The transmission of load from muscles to the bone occurs at the origin and insertions of the tendon, and these sites on the bone will experience the largest decline in mechanical load. However, markers of bone remodelling are typically assessed through blood and urine samples, and are therefore not sensitive enough to determine regions of concentrated remodelling to confirm. The introduction of quantitative computed tomography (QCT) allowed to separate compartments of the bones to assess mineral density of trabeculae and cortical bone. Using this approach, Lang and colleagues (2004) demonstrated that trabecular lost mineral density (2.2% - 2.7% per month) at a faster rate than cortical bone (0.4% - 0.5%) during spaceflight. Although the duration of disuse may be important, as total bone mass loss was greater than the trabecular bone mass during shorter duration bed rest (¡60 days), but trabecular bone mass loss was greater as disuse continued (Cervinka *et al.*, 2014). Using computational finite element modelling, Keyak *et al.* (2009) modelled the proximal femur of astronauts pre- and post-spaceflight (4 - 6 months), and applied representative loads of standing and falling activities to assess strength loss due to disuse. Their findings indicated bone strength losses were comparable to reported trabecular mineral density loss (2.4% - 2.7% per month), although the variability between astronauts was considerable. Bone mineral density is a good predictor of bone strength (Ammann & Rizzoli, 2003), and the substantial decrease in both cortical and trabecular bone underpins the decrease n bone strength following spaceflight.

Hyaline cartilage is a smooth, durable, avascular tissue that provides a low friction interface between articulating surfaces. The cartilage experiences compressive strain during human movement, and altered strain profiles are regularly implicated in joint-disease pathology (Crook *et al.*, 2021), such as osteoarthritis (Wang *et al.*, 2011). Evidence from studies comparing habitual loading indicate that cartilage displayed increase proteoglycan content (Slowman & Brandt, 1986) and increased stiffness (Swann & Seedhom, 1993) in area of increased stress. This highlights that cartilage is mechanoresponsive to compressive joint loading (Zhao *et al.*, 2020). Cartilage helps to redistribute load at the joint to prevent high concentration stress being applied to the bone. Given the reduced mechanical stimuli associated with disuse, adaptations to the cartilage will influence bone health.

The adaption of cartilage following disuse is not well understood. The majority of studies have either been conducted using animal models (Ramachandran *et al.*, 2018) or with participants with pathology (e.g. ACL-reconstruction, Crook *et al.*, 2021). A 14 day bed rest study in healthy young adults did demonstrate that knee cartilage thickness decreased by 8% in both the medial and lateral compartments (Liphardt *et al.*, 2009). Reduced thickness was found post-knee surgery patients (Hinterwimmer *et al.*, 2004), spinal cord injury patients (Vanwanseele *et al.*, 2003), and in animal (Kwok *et al.*, 2021). The reduction in thickness may be underpinned by a reduction is proteoglycan content, which has been shown to decrease after 6 - 8 weeks of crutch use (Souza *et al.*, 2012). Cartilage thickness and proteoglycan content are directly related to the stiffness of the tissue (Korhonen *et al.*, 2002; Lu *et al.*, 2009), leaving a joint structures more vulnerable to high strain rates when the cartilage layer is thinner. Since cartilage is avascular, loading the tissue is important for promoting fluid shift within the cartilage to assist remodelling. The removal of stimulating load in hypogravity is likely implicated in the adaptations observed in cartilage (Vico & Hargens, 2018). The concurrent adaptations to cartilage alongside those discussed to bone mineral density increased the vulnerability of the skeletal structures to injury when load is reintroduced following disuse.

2.2 Musculoskeletal Loading in Hypogravity

The term *load* is an umbrella term describing any physical quantity that is being applied to a system. The definition of load in biomechanical studies, and in other disciplines, is determined by the research question and the outcome measure used to describe the load borne by the system. In this thesis, the term is used to describe the forces and moments that are applied to the MSK system. The MSK tissues, including bone, muscle, tendons and ligaments, are mechanoresponsive, and perform self-maintenance in response to external mechanical stimuli (Frost, 1987; Goldberg *et al.*, 1975; Wang & Li, 2010). The phenomenon of translating mechanical stimuli to biological events, called mechanotransduction (Wang & Li, 2010), is key in triggering remodelling processes to promote MSK adaptations. Quantifying MSK loading during exercise in hypogravity is important for understanding the nature of the adaptations observed following disuse. The premise being that there is an optimal range of load required to maintain tissue homeostasis and to prevent adaptations that increase susceptibility to injury and disease progression, as has been shown in other clinical settings (Saxby *et al.*, 2016). In biomechanics, mechanical loads can be categorised as external or internal (Vanrenterghem *et al.*, 2017), based on whether the metrics that describe quantities describing net effects on the body or segments (e.g. ground reaction forces) or directly to an internal MSK tissue (e.g. muscle and joint contact forces). Knowledge of the loading profile during exercise in hypogravity allows for: (1) the determination of factors and mechanisms that contribute to adaptations, and (2) the development of appropriate preventive measures to mitigate against (i.e. through countermeasures) or rehabilitate post-disuse (i.e. through grading exercises according the individuals condition). This section overviews the biomechanical research in hypogravity exercise, with a particular focus on outcome measures that describe the mechanical loading on the MSK system.

2.2.1 Spaceflight

Exercise is one of the main countermeasures for mitigating against MSK adaptations during spaceflight. Astronauts are prescribed 2.5 hours a day, 6 days a week (including equipment preparation and pack-up, and showering) across three main devices (Lambrecht *et al.*, 2017; Loehr *et al.*, 2015; Petersen *et al.*, 2016). Two devices, a modified treadmill with gravity replacement load bungee chords (Figure 2-1a) and an advanced resistive exercise device (ARED) (Figure 2-1b), are aimed at providing a mechanical stimulus to mitigate against MSK deterioration. However, biomechanical analyses on the International Space Station is limited due to lack of equipment (e.g. motion capture), expertise, space, and time constraints. Consequently, quantification of MSK skeletal loading has been almost exclusively been related to external forces at the foot, initially via force-measuring insoles (Cavanagh *et al.*, 2009) and later via an instrumented treadmill installed in 2009 (De Witt & Ploutz-Snyder, 2014). The results of these studies demonstrate that it is not possible to achieve the same peak forces in microgravity (i.e. ∼0 g) for the equivalent movement on Earth, even with gravity replacement equipment (Cavanagh *et al.*, 2010; De Witt & Ploutz-Snyder, 2014; Genc *et al.*, 2010). For context, Genc *et al.* (2010) reported foot-shoe interaction forces measured by the insoles was 50 - 77% of the forces in terrestrial gravity at equivalent running speeds. The rate of loading was also substantially diminished (43 - 84%) compared to 1 g (Genc *et al.*, 2010). Strain magnitude and strain rate are believed to be important in the stimulation of tissue maintenance (e.g., Frost, 1987).

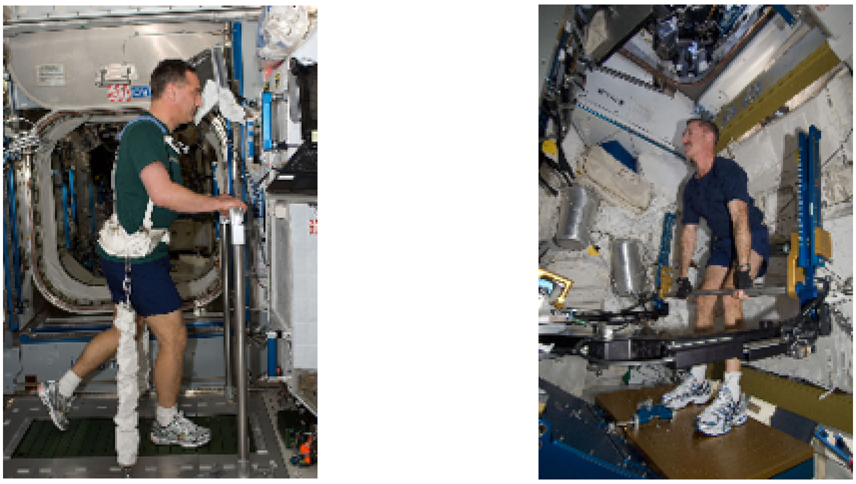

(a) **(b)**

Figure 2-1 Examples of the modified treadmill (a) and advanced resistive exercise device (ARED, b) currently available on the International Space Station for astronaut exercise prescription.

The inability to attain high loading rates on the International Space Station, as speculated by De Witt *et al.* (2014), likely stems from the vibration isolation systems absorbing some of the impact forces, as it works to dissipate vibrations from exercise transmitting to the ISS structure.

An obvious approach to increase mechanical loading in hypogravity is to increase the work required to complete a task. However, this is limited by the equipment (e.g. the maximum resistance it can apply), and astronaut comfort, as astronauts cannot tolerate gravity replacement loads that are too high (Novotny *et al.*, 2013). Rather the manipulation of the task, or utilising the equipment in different configurations may provide a more quality mechanical stimulus. For example, astronauts were able to achieve larger peak ground reaction forces, but not rate of loading, by running at faster speeds (De Witt & Ploutz-Snyder, 2014). This aligns with findings in 1 g that show running faster is associated with greater peak ground reaction forces (Nilsson & Thorstensson, 1989). Similarly, shifting the feet positions forward and backward relative to the centre of mass can increased the net joint moments about the trunk and lower-limbs to achieve magnitudes similar to those in 1 g (Fregly *et al.*, 2015). Although some studies have shown promise in being able to achieve similar magnitudes of external loads to 1 g, they cannot account for the substantially lower loading conditions when exercise is not being performed. Using the insoles, Cavanagh and colleagues (2010) reported only 30% of the astronauts' assigned exercise time was *measureable*, suggesting that even the entirety of the presumed exercise time is not necessarily providing a quantifiable mechanical stimulus. It is clear that exercise in microgravity is not providing a quality and regular external mechanical stimulus to the MSK system. Additionally, it is unclear from the external load measurements how these transfer to the internal structures. While some studies have reported it is possible to replicate terrestrial external loading (i.e. ground reaction forces and net joint moments) in certain conditions, the loading on the internal structures (i.e. muscles and forces) remains unstudied.

2.2.2 Ground-based Hypogravity Emulators

Due to the limitations of biomechanical measurement briefly outlined in the previous section, apparatus that attempts to emulate the hypogravity conditions on Earth are needed. Additionally, the main focus of this thesis is focused on understanding musculoskeletal loading upon return-to-Earth, as opposed to during long-duration spaceflight. The role of ground-based analogues of spaceflight are such that scientific data can be collected in a control laboratory environment to isolate key variables to understand the influence of gravity on the MSK system. This improves our understanding of why the body adapts to disuse in the way it does, and how we can rehabilitate the MSK system upon return-to-Earth. Various different pieces of equipment have been used in the literature (Figure 2-2), each with their own advantages and disadvantages. A summary of these systems is provided elsewhere (e.g., Lacquaniti *et al.*, 2017), but all these devices assist or manipulate posture to counter the gravitational force on the body. By doing so they reduce the external mechanical work required to move the body against gravity, thereby mimicking different levels of hypogravity. For example, the tension placed in the vertical body weight support spring-elements, the angle of attack of the plane during parabolic flight, and the angle of tilt in the tilted body weight support can all be manipulated to offset or realign gravity to replicate, or emulate, a desire hypogravity.

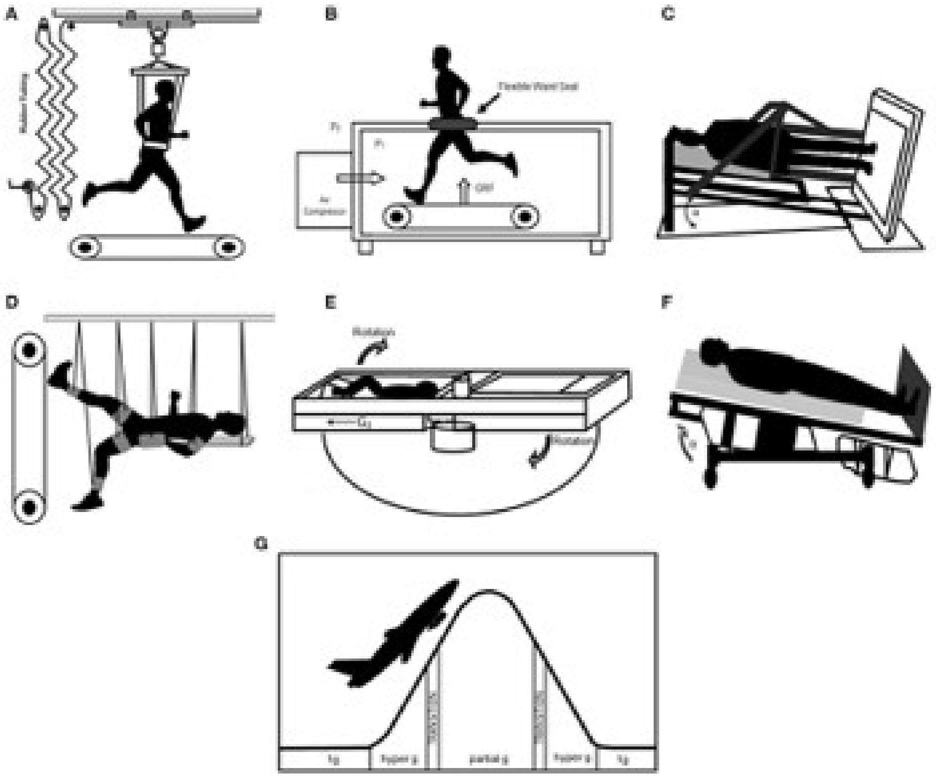

Figure 2-2 Visual representation of the hypogravity simulators used in the literature to assess hypogravity biomechanics. **(A)** Vertical body weight support **(B)** Lower body positive pressure **(C)** Titled body weight support **(D)** Supine suspension system **(E)** Centrifugation **(F)** Hued-up tilt **(G)** Parabolic flight. Figure taken from Richter *et al.* (2017)

Research has shown that gait movements in hypogravity are associated with a decrease in magnitude and duration of exposure to mechanical loading. Similar to spaceflight, running in hypogravity is associated with reduced peak ground reaction forces and vertical force loading rate (Apte *et al.*, 2018; Richter *et al.*, 2017), and the decline in peak vertical ground reaction force with gravity appears to be linear (Ivanenko *et al.*, 2002). There is evidence that the reduced gravity conditions influence the trajectory of the ground reaction force centre of pressure (Ivanenko *et al.*, 2002) and reduced ranges of motion of the lower-limb joints in the sagittal plane (Cutuk *et al.*, 2006; Sylos-Labini *et al.*, 2013) during walking and running gait. The altered orientation of the force vector and joint kinematics likely contributes to the reduced net joint moments at the hip, knee, and ankle as hypogravity increases (Apte *et al.*, 2018). The apparent decrease in the amplitude of limb movements is also reflected in reduced internal work, a metric that describes the motion of the body segments relative to the centre of mass, as hypogravity decreases (Pavei *et al.*, 2015). Additional to the clear decrease in the magnitude, there is a decrease in the duration of exposure to mechanical load. Duty factor, a metric representing the percentage of the gait cycle the foot is in contact with ground, has been shown to decrease when walking and running in hypogravity (Donelan & Kram, 1997, 2000), due to a decreased stance phase duration and increased gait cycle duration (Richter *et al.*, 2017). This suggests the decrease in vertical ground reaction force impulses (Richter *et al.*, 2017) manifests as a consequence of decreased magnitudes and durations. Metrics of cumulative load, such as impulses, have been shown to be better indicators of disease progression in other clinical contexts (e.g. osteoarthritis Kean *et al.*, 2012). Even though magnitudes of terrestrial loads are possible to attain in spaceflight, as described above, it appears the duration of exposure is equally important for understanding mechanical loading when exercising in hypogravity. One study has measured knee joint forces *in vivo* using a force instrumented knee prosthetic whilst walking in hypogravity. Macias and colleagues (2012) performed a case-study of a single 83-year-old male whilst walking on a lower-body partial pressure treadmill, and demonstrated peak knee contact force increased with gravity (0.1 - 1 g) and walking velocity (0.67 - 1.34 $\text{m}\cdot\text{s}^{-1}$). Since muscle forces are the main contributor to joint contact forces (Sasaki & Neptune, 2010), the decreased loading in hypogravity likely influences muscle forces. However, research has shown that the behaviour of the MTU changes with gravity (Richter *et al.*, 2021b), and individual muscles within the same muscle group can provide different functions during an exercise (Jacobs *et al.*, 1996; van Ingen Schenau & Bobbert, 1993). This shows that further research is needed to understand the changes in loading of individual muscles with hypogravity. Furthermore, it is not feasible to use force-instrumented joint prosthetic in younger healthy adults. Alternative approaches are needed to estimate the internal joint loading conditions when exercising in hypogravity. Knowledge of the external loading during hypogravity exercise is beneficial as it highlights that ground-based emulators of hypogravity could be used to systematically reintroduce mechanical load to the astronaut to progressively overload the system. That being said, without information about the loading on specific muscles there is still an opportunity to better optimise exercise prescription by aligning the exercises with the target muscles that require rehabilitation.

It is important to highlight that the majority of studies that quantify biomechanics during hypogravity exercise have done so during gait. This is limited in understanding how the MSK system is loaded in hypogravity because astronauts perform a variety of exercises on the International Space Station (Loehr *et al.*, 2015). Additionally, with the aim of long-duration space missions to the Moon and Mars there is a need to understand how best to load the MSK system to mitigate against adaptations to unloading to ensure mission success and astronaut health. Jumping movements provide a promising mode of exercise due to their high peak loads and loading rates and the minimal requirement for equipment and time resources (Gruber *et al.*, 2019). A sled jumping protocol during bed-rest has shown promising results in mitigating against MSK adaptations to disuse (Kramer *et al.*, 2017; Kramer, Kümmel, *et al.*, 2018a, 2018b; Ritzmann *et al.*, 2018), with peak vertical forces reported to reach ~70% pf 1 g (Kramer *et al.*, 2010). Despite this still not reaching 1 g levels, the high forces associated with jumping mean this equates to similar forces as at slower running speeds in 1 g. However, a very recent study recorded peak ground reaction forces that were <50% of those reported in terrestrial jumping (Cleather *et al.*, PrePrint). Although, asking the astronaut to jump with stiffer limbs may be beneficial to increase the peak ground reaction forces (Kramer *et al.*, 2017). Additionally, vertical hopping has been shown to reproduce similar vertical ground reaction forces to 1 g with increased hop height (Weber *et al.*, 2019). The research on jumping movements in hypogravity suffers from the same limitations described for gait, in that to date external measures of loading have been used to describe the MSK loading profile. However, what this does demonstrate is that the focus on gait movements in hypogravity is limiting, and the potential for MSK loading from other exercise modes should be explored to optimise exercise prescription.

2.3 Musculoskeletal Modelling to Estimate Load

Musculoskeletal modelling is a branch of biomechanics that uses mathematical definitions to represent the physical system. A replica of the human body is constructed as a multi-body system comprising a series of rigid segments, joint definitions, and actuated via muscle models to generate movement. The additional information about the MTU, including lines of action, moment arms, and force generating characteristics, allows the user to estimate muscle forces that are otherwise infeasible *in vivo*. This section describes modelling elements that influence the estimation of muscle forces, including skeletal model elements, muscle models, and joint contact models.

2.3.1 Model Definition

All model development, including MSK models, begins with deciding on the complexity of which to describe the system of interest. For example, the metatarsophelangeal (MTP) joint is often assumed to form a rigid segment with the rear-foot in dynamic optimisations, but can improve the realism of joint mechanics when included (Falisse *et al.*, 2022). The intended use of the model should drive the decision making process (Pandy, 2001), informed by the research question the user is aiming to answer. For the determination of muscular outcomes (e.g. forces or MTU behaviour), as is the interest of this thesis, it is important to model joints and muscle physiology of the MSK system. Muscle forces have been shown to be sensitive to uncertainty in body segment inertial parameters (BSIP) (Myers *et al.*, 2015), MTU geometry (Serrancolí *et al.*, 2020), and skeletal geometry (Carbone *et al.*, 2012; Navacchia *et al.*, 2016; Smith *et al.*, 2016; Thelen *et al.*, 2014). The propagation of error from distal-to-proximal in net joint moment calculations appears to underpin the sensitivity of muscle forces to BSIP uncertainty, as hip moments, and consequently hip muscles, are more sensitive than the ankle and knee moments (Myers *et al.*, 2015). Skeletal geometries play an important role in the alignment of muscle forces that can influence the estimation of joint contact forces, particularly at the knee joint when medial-lateral compartment are loaded. For example, frontal-plane alignment of the tibiofemoral joint $\pm 2°$ alters the tibial compartment loading distribution (Thelen *et al.*, 2014). The MTU geometries describe the path taken by the massless elements, and can be modified with additional wrapping surfaces and via points to create a more realistic geometry from origin to insertion. This plays an important role in the definition of MTU moment arms about the joint, which directly influence the moment-generating capacity about a joint. As demonstrated by Serrancolí *et al.* (2020), this can influence the muscle forces and joint force estimations as greater moment arms allowed the ankle plantarflexors to generate similar moments about the knee and ankle joint but with less muscle force. This led to more accurate joint reaction force predictions in comparison to *in vivo* measured loads during walking. However, creation of subject-specific models that accurately represent the MSK system of the individual require medical imagine techniques (e.g. MRI or CT scans) that are not always accessible. Primarily because they require expert medical and anatomical expertise to collect and segment the images, and can require upwards of 10 hours to create a lower-limb model (Modenese *et al.*, 2018). While automated skeletal and muscular geometry algorithms are becoming available (e.g., Modenese & Kohout, 2020; Modenese & Renault, 2021), these are still limited to lower-limb models.

2.3.2 Muscle-Tendon Unit Forces

A key element of developing a modelling framework is to decide how the model is driven. The main types are kinematic or angle-driven (e.g., Bezodis *et al.*, 2015; Yeadon *et al.*, 1990), moment-driven (e.g., Fregly *et al.*, 2015; Wilson *et al.*, 2007), and muscle-driven (e.g., Falisse, Serrancolí, Dembia, Gillis, Jonkers, *et al.*, 2019; Haralabidis *et al.*, 2021; Lin & Pandy, 2017). Kinematic- and moment-driven approaches are relatively simple to formulate as only accelerations and moments, respectively, about each degree of freedom are required. However, the main limitation in the context of this thesis is that they can only estimate MSK loading to the level of net joint moments, which is comparable to the literature already available in hypogravity exercise. Muscle-driven approaches allow for the estimation of muscle forces by modelling the geometry and force-generating elements of the muscle. Therefore, providing a more precise estimation of MSK loading not otherwise possible in traditional biomechanical analyses.

The purpose of a muscle model is to represent the physiological behaviour of the MTU. Representation of the MTU is typically based upon three force-generating elements: an active contractile element, a passive parallel elastic component, and a passive series elastic component (van den Bogert *et al.*, 2011; van den Bogert *et al.*, 1998; Zajac, 1989). The parallel and series elastic components, representative of the elastic tissue surrounding the muscle and the tendon tissue, respectively, are normally modelled as spring-elements that produce force as a function of length beyond a given point (De Groote *et al.*, 2016; Millard *et al.*, 2013; Zajac, 1989). The contractile element aims to represent the behaviour of the muscle fibres, specifically the force-length and force-velocity relationships that emerge due to cross-bridge dynamics (van den Bogert *et al.*, 1998; van den Bogert & Nigg, 2006; Zajac, 1989). An activation model (representative of the calcium concentration within the muscle) interacts with the force-length-velocity relationship to scale the force-generated by this element according to the active state (Zajac, 1989). The transmission of the MTU force to the tendon is then modelled as a function of the moment arm about each DOF. The two main muscle models used in MSK modelling are those originally described by Archibald Hill (Hill, 1938) and Sir Andrew Huxley (Huxley, 1957). The remainder of this subsection will briefly overview these two models and evaluate their use in MSK modelling frameworks.

Hill-Type Muscle Model

The Hill-type muscle model is a phenomenological representation of the muscle, and does not attempt to represent the mechanisms of muscle force production (i.e. actin and myosin cross-bridge dynamics). Rather it is a *black box* model that outputs a force as a function of active state, muscle length, and muscle velocity. The main criticism of the Hill-type model is that it assumes instantaneous force production based upon given inputs to the model (e.g. active state and length), and fails to account for history-dependent mechanisms of force production. Phenomena such as short-range stiffness after isometric contraction (Nichols & Houk, 1976) and force-enhancement following stretch (Herzog & Leonard, 2002) that occur due to state of the muscle prior to the moment of interest and type of contraction thereafter, leading to transient changes to the expected force produced by a muscle do not emerge using a a Hill-type model. This then require additional models to be added to represent these history-dependent characteristics (e.g., De Groote *et al.*, 2017; De Groote *et al.*, 2018), adding further complexity to the model formulation. Although, a particular strength of the Hill-type muscle model is the dimensionless formulation (Zajac, 1989). The parameters are scaled according to the specific muscle allowing all muscle models to be described by five parameters: maximum isometric force, optimal fibre length, pennation angle at optimal fibre length, maximum shortening velocity, and tendon slack length. These parameters govern certain aspects of the force-length-velocity relationships to capture the salient features of cross-bridge dynamics (Figure 2-3). The dimensionless formulation of this Hill-type model allows for the calibration of the MTU parameters depending on the muscle and individual being analysed. Additionally, the relative simplicity of the model lends itself to large-scale MSK modelling frameworks, and are the most regularly used in the analysis of human movement. Highly complex full-body MSK models with the lower-limbs actuated by upwards of 80 MTUs have been utilised in healthy (e.g., Lai *et al.*, 2017; Lin *et al.*, 2018) and pathological walking (e.g., Falisse *et al.*, 2020; Falisse, Serrancolí, Dembia, Gillis, Jonkers, *et al.*, 2019), running (e.g., Lai *et al.*, 2017), sprinting (e.g., Haralabidis *et al.*, 2021), and cycling (e.g., Lai *et al.*, 2017).

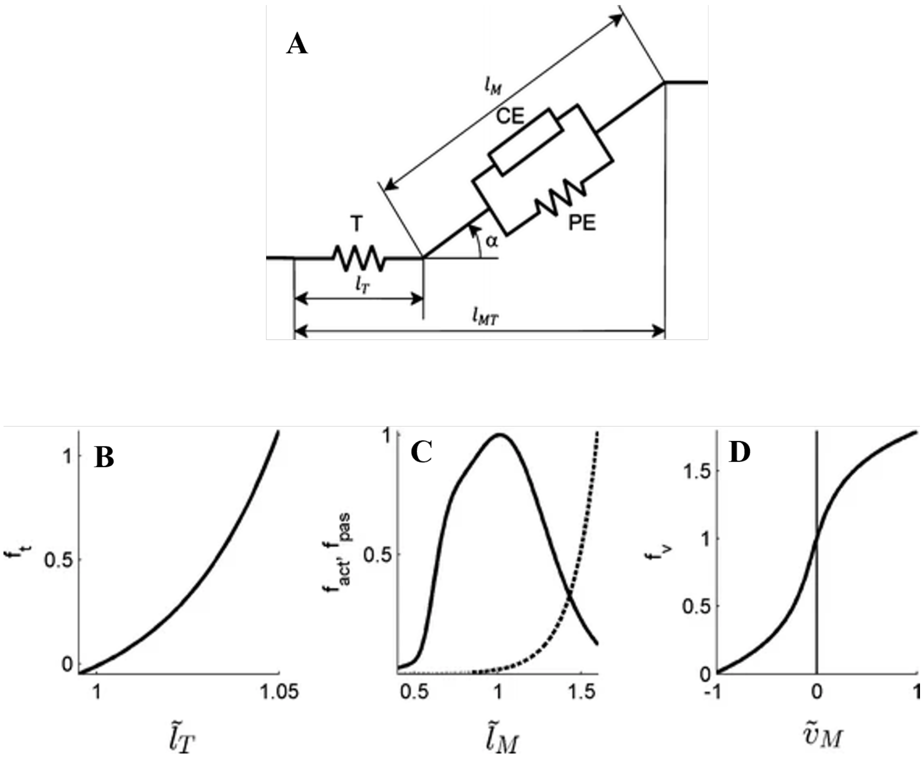

Figure 2-3 Schematic of the Hill-type muscle model (A), and the tendon-length (B), active (solid) and passive (dashed) muscle-length (C), and muscle-velocity (D) relationships of the dimensionless formulation. The muscle-tendon unit length (l_{MT}) is determined by the tendon (T) length (l_T) and the muscle length ($l_M l$) projected along the tendon (i.e. cosine of the pennation angle [α]). Figure taken and modified from De Groote *et al.* (2016).

The estimation of muscle forces is highly sensitive to the parameters that describe the Hill-type model. In particular, optimum fibre length and tendon slack length have consistently shown to be important in estimating accurate muscle forces and joint reaction forces (Ackland *et al.*, 2012; De Groote *et al.*, 2010; Myers *et al.*, 2015; Navacchia *et al.*, 2016; Redl *et al.*, 2007; Scovil & Ronsky, 2006; Serrancolí *et al.*, 2020). Both of these parameters influence the length of the muscle, which leads to different muscles being more sensitive to perturbations of these parameters than others. Indeed, muscles that primarily work on the ascending- or descending-limbs of the force-length relationship tend to be more sensitive to these parameters because, all else being equal, small changed can cause large force differences (Ackland *et al.*, 2012; Myers *et al.*, 2015). Maximum isometric force may be more important for more dynamic movements that require larger forces to be generated as it was found to be less important in walking (Ackland *et al.*, 2012; Redl *et al.*, 2007; Serrancolí *et al.*, 2020), but more important in running and maximum effort dynamometry (De Groote *et al.*, 2010; Scovil & Ronsky, 2006). Muscle forces are not as sensitive to the remaining parameters, but may play a role in assessing MTU behaviour. Pennation angle, which determines the proportion of muscle force projected along the tendon, has relatively little influence on muscle forces when $\leq 20°$ (Zajac, 1989), which is in the range of physiological measurement of human muscle. Increasing maximum shortening velocity allowed for faster maximum sprinting speeds to be achieved during predictive simulations (Miller *et al.*, 2012), but it was found to have little influence on muscle force estimations in the above studies. For highly dynamic movements, like sprint or jumping, this parameter may have more influence on muscle forces. It is worth noting the influence of tendon stiffness, which is not a parameter of the dimensionless formulation, is influential in MTU dynamics. A more compliant tendon leads to an increase in tendon length for a given applied force (i.e. the gradient of Figure 2-3B decreases), which impacts the muscle length and velocity (Falisse *et al.*, 2022; Narici & Maganaris, 2007).

Given the substantial muscular adaptations in response to spaceflight, the estimation of muscle forces using MTU parameters that are not adjust to the individual will impact the physiological realism of muscle force and joint force estimations. However, there is not currently any research that has attempted to describe muscle adaptations in terms of Hill-type muscle model parameters. In other contexts, authors have used medical imaging and known physiological relationships (i.e. PCSA) (e.g., Modenese & Renault, 2021; Valente *et al.*, 2017; Valente *et al.*, 2014), and computational methods (Falisse *et al.*, 2017; Modenese *et al.*, 2016; Serrancolí *et al.*, 2020) to estimate subject-specific parameters for their purpose. As discussed above, access to medical imagining is financially and time resource heavy, and requires a level of expertise to utilise properly. While computational methods can be difficult to implement and require ground-truth data to guide the parameter optimisation algorithm. Therefore, more research is needed to understand whether the Hill-type muscle model can be used to model adaptations to unloading.

Huxley-type Cross-Bridge Model

The Huxley-type model attempts to more directly represent the fundamental structures of the sarcomere, by modelling the interaction between the actin and myosin filments (Figure 2-4). Specifically, it attempts to describe the rate of cross-bridge attachment and detachment as a function of the distance between the myosin head and the nearest eligible attachment site (Herzog, 2017). From a computational perspective, the Huxley-type muscle model is more intensive than the Hill-type model for two main reasons. First, the early formulations of the Huxley-type muscle model were described by a set of partial differential equations that are harder to solve than ordinary differential equations (ODE) used for the Hill-type muscle model. Although a method for discretising the formulation to represent the model contraction dynamics as three ODE has been presented and used in the literature (Lemaire *et al.*, 2016; Zahalak, 1981), this exceeds the one ODE require for the Hill-model. Secondly, the Huxley-type model is modelled by five-parameters that govern the cross-bridge binding rate functions (Vardy *et al.*, 2012), and can require additional parameters depending on the formulation. These formulations do not include the passive force generation equations, meaning that when these elements are added (e.g. Lemaire *et al.*, 2016; van Soest *et al.*, 2019) more parameters are required that further increase the model's complexity. While these formulations are able to produce similar force estimations to the Hill-type model in some circumstances, they required 10,000 more CPU time to complete a relatively simple MSK model driven by just six MUs (van Soest

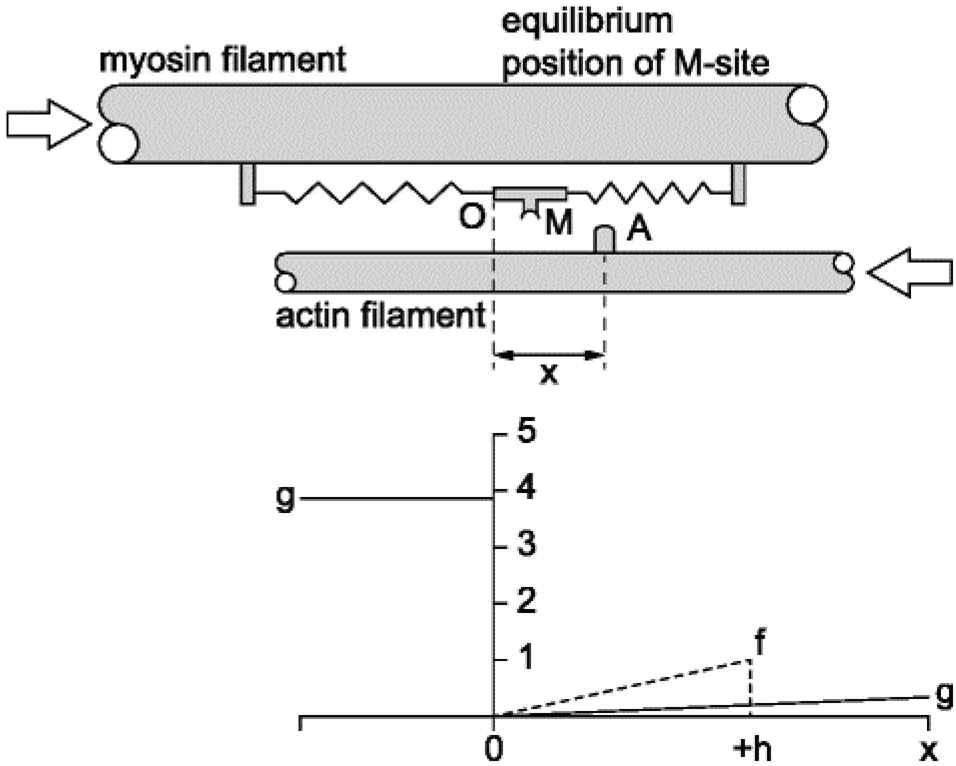

Figure 2-4 Schematic of the Huxley-type muscle model. The distance (x) between the myosin head (M) and actin bind site (A) determine the rate of attachment (f) an detachment (g). Figure taken from Herzog (2017).

et al., 2019). The added physiological realism of the model does not justify the substantial computational cost when attempting to estimate muscle and joint forces.

2.3.3 Joint Contact Force Estimation

Joint Reaction Forces

Joint reaction forces represent the resultant forces and moments transferred between two articulating bodies. The resultant forces are calculated based on Newtonian mechanics, whereby all known forces, including external forces, $F_{External}$, muscle forces, $F_{muscles}$, and adjacent segment reaction forces, JRF_{i+1}, are accounted for (e.q 2.2). Since muscle forces are the main contributor to joint contact forces (Sasaki & Neptune, 2010), once muscle forces are estimated using an optimisation (see 2.4) an estimate of joint loading can be obtained. The simple Newton-Euler formulation makes joint reaction force analyses efficient to implement within simulation frameworks (Dembia *et al.*, 2021; Serrancolí *et al.*, 2020), or as a *post hoc* analysis (DeMers *et al.*, 2014; Steele *et al.*, 2012). It is important to remember that the joint reaction forces are a cumulative quantity representing all the remaining unknown forces that are not modelled, such as ligaments, and do not represent bone-on-bone forces. Additionally, joint reaction analysis assumes rigid contact between surfaces, which misrepresents the nature of the deformation that occurs when biological surfaces interact.

$$JRF_i = M(q) \cdot \ddot{q} - (\sum F_{external} + \sum F_{muscles} + JRF_{i+1}) \tag{2.2}$$

Contact Models

An approach to overcome the limitation with joint reaction force analysis is to model the contact at the joint. Contact models attempt to more accurately represent the forces that occur when two compliant surfaces collide and undergo deformation (Sherman *et al.*, 2011; Skrinjar *et al.*, 2018). Two common types used in MSK modelling (Figure 2-5) are Hertzian and Elastic Foundation models. Hertzian-based models are represented by geometrical shapes, typically spheres in MSK applications (Figure 2-5A), and the force is estimated as the magnitude and velocity of penetration (Sherman *et al.*, 2011; Skrinjar *et al.*, 2018). This can misrepresent surfaces that are not well approximated as sphere-like at the point of contact. In contrast, elastic foundation models approximate the surface with a meshes that collectively form a *bed of springs* (Sherman *et al.*, 2011). The ability to arbitrarily represent the complex geometry of a joint surface lends itself to joint contact modelling and allow for estimation of the area of contact and contact pressures (Smith *et al.*, 2016). However, these models can be computational heavy due to the parameterisation of the contact geometries, and can be *stiff* with small changes in model kinematics leading to large changes in force estimations. Surrogate models have been used in dynamic optimisation in an attempt to reduce the computational requirements (e.g. Lin *et al.*, 2018), but these surrogate model still require creation against an elastic foundation model

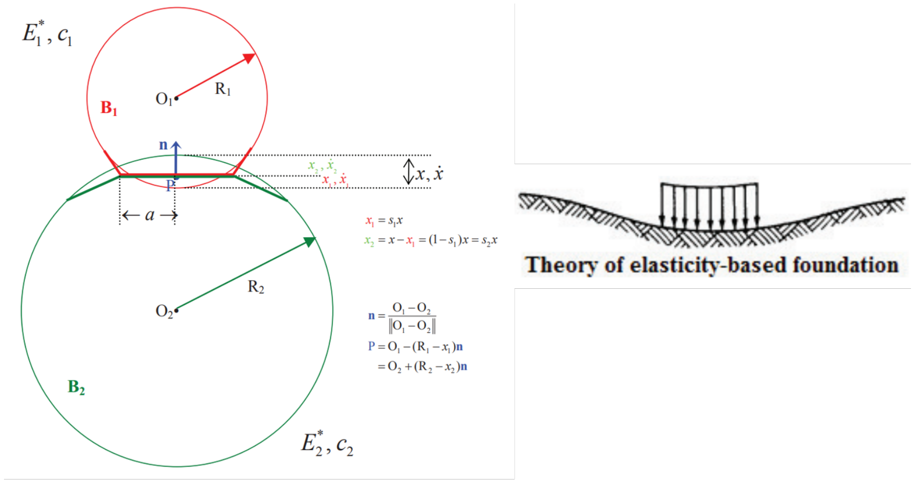

(A) (B)

Figure 2-5 Visual representation of contact geometries of the Hertian (A) and elastic foundation (B) contact geometries. Figures taken from Sherman *et al.* (2011).

before implementation (Lin *et al.*, 2010). Additionally, formulation of contact models in common MSK modelling software, such as OpenSim, are discontinuous, requiring the user to write bespoke continuous formulations to integrate them into gradient-based optimisations (e.g. Serrancolí *et al.*, 2019).

2.4 Optimisation to Solve the Muscle Redundancy Problem

The MSK system is an underdetermined system, with multiple muscles crossing a given degree of freedom (Figure 2-6). To allow for the estimation of internal loads (i.e. muscle and joint forces) using MSK models, the user must decide how to solve the muscle redundancy problem. Although there are various approaches described in the literature, they are all based on the same general optimisation approach (eq. 2.3):

$$\begin{aligned} &\text{minimize} && J = f(\star) \\ &\text{subject to} && \sum_{j=1}^{n} (F_{m,j} \cdot r_{m,k}) = \tau_k \\ &&& 0 \leq a_m \leq 1 \end{aligned} \tag{2.3}$$

where $F_{m,j}$ is the force of the j^{th} muscle, and $r_{m,k}$ and τ_k the moment arms and joint moments about the k^{th} joint, respectively. In other words, the optimisation minimises a user-defined cost function, J, whilst satisfying the constraint that the muscle moments (i.e. $F_m \cdot r_m$) match the net joint moments, and the muscle activations, a_m, are within the appropriate boundary. The cost function may vary between methods (i.e. denoted $\star$), but are commonly related to minimising the sum of a_m raised to the n^{th} power (Ackermann & van den Bogert, 2010). The multibody dynamics equations of motions that govern the skeletal dynamics of the modelled system are based upon Newton's second law of motion (eq. 2.4):

$$M(q) \cdot \ddot{q} = C(q, \dot{q}) + G(q) + F + \tau \tag{2.4}$$

where q, $\dot{q}$ and $\ddot{q}$ are the coordinate positions, velocities and accelerations vectors, $M(q)$ is the mass matrix, $C(q, \dot{q})$ the Coriolis and centrifugal forces, $G(q)$ is gravity, F is the vector of forces applied to the model (e.g. ground reaction forces), and τ the vector of coordinate forces and torques. The approach used to solve eq. 2.4 to calculate net joint moments can be used to categorised optimisation algorithms. This section overviews the different methods commonly employed in the literature, with a particular focus on their ability to estimate muscle forces and joint reaction forces.

2.4.1 Inverse Dynamics

When the kinematics and external forces (e.g ground reaction forces) are known it is possible to derive net joint moments (eq. 2.5). This is reflective of traditional biomechanical pipelines, where experimental measurement of biomechanics are used to quantify q, $\dot{q}$, $\ddot{q}$, and F, from which the joint moments (τ) and muscle forces that caused the movement can be derived. From this perspective, inverse

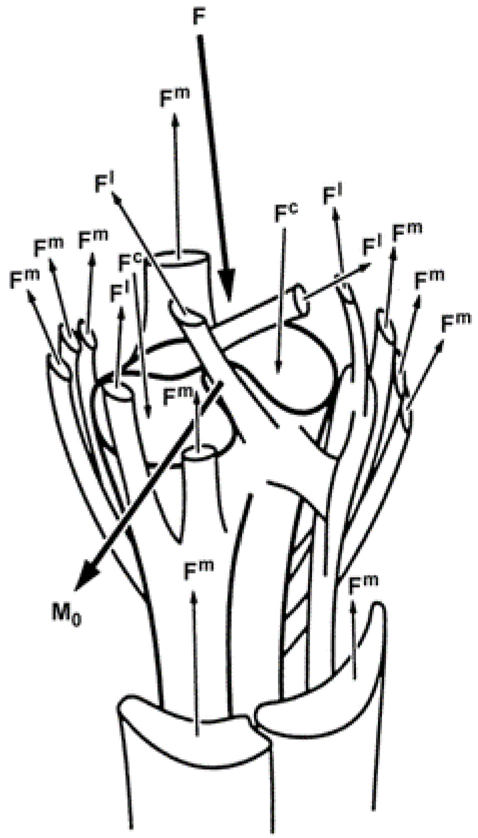

Figure 2-6 Visual representation of the muscle redundancy of the musculoskeletal system. For a given joint, muscle muscle (F_m), and indeed ligaments (F_l) act culminate in a total force (F) to generate moment (M_0) and cause movement. Figure taken from Herzog (2017).

approaches should be viewed as an additional analyses to estimate the muscle forces, and subsequently joint forces, that must have been acting on the skeleton to cause the measured movement.

$$\tau = M(q) \cdot \ddot{q} - [C(q, \dot{q}) + G(q) + F] \tag{2.5}$$

Due to experimental error and modelling assumptions, the experimental kinematics and kinetics are rarely dynamically consistent, requiring residual forces and moments to be applied to the model to balance the equations of motion. The residual reduction algorithm has been developed to make minor adjustments to the MSK model inertial parameters and measured kinematics to drive residuals to zero (Thelen & Anderson, 2006), but dynamical consistency is not easily achievable in this way. Consequently, when relating muscle forces to the net moments, as described in sq. 2.3, the error in the net joint moment calculations are carried forward in to the optimisation. This impacts the physiological realism of muscle forces and subsequent joint force estimations. However, the focus upon return-to-Earth during this thesis better lends itself to an inverse approach as the aims are to estimate the internal MSK loads that will have occurred during movement in hypogravity. Therefore, the estimated muscle and joint reaction forces that were present during an observed motion is more appropriate than predicted motion that resembles, but is not the same, as observed motion.

Static Optimisation

Static optimisation solves the muscle redundancy problem at each time point as time-independent sub-problems. Consequently, static optimisations are extremely computationally efficient requiring less preparation time (i.e. additional user input), and five times less CPU time than computed muscle control (Lin *et al.*, 2012), and up to 1000 times less CPU time than dynamic optimisations (Anderson & Pandy, 2001b). However, the inability to relate time-dependent physiological properties of the neuromuscular system, namely muscle activation and contraction dynamics, can lead to non-physiological, instantaneous changes in muscle force estimations between time steps. While omitting activation dynamics and force-length-velocity dynamics has been shown to not substantially influence muscle force estimations during walking (Anderson

& Pandy, 2001b), in doing so the muscle forces cannot be compared against known MTU behaviour (e.g. operating ranges of the muscle fibres). This omission of muscle dynamics can lead to the favouring of muscles with large maximum isometric forces and less accurate estimations during highly ballistic movements (Lin *et al.*, 2012). Additionally, static optimisation assumes tendons are rigid and is not recommended for movements with complex MTU dynamics or known reliance on elastic energy storage-return mechanisms (Hicks *et al.*, 2015). Movements that are highly dynamic, such as faster running and jumping, are more likely to produce unrealistic muscle activation and force predictions.

Computed Muscle Control

Computed muscle control (CMC) combines proportional-derivative controllers and static optimisation to estimate a set of muscle forces that drive the model kinematics towards a desired trajectory (Thelen & Anderson, 2006). While CMC does integrate a forward dynamics step (see 2.4.2) below), essentially creating a *hybrid* inverse-forward framework, the optimisation method used to estimate muscle forces is a static optimisation algorithm (Thelen & Anderson, 2006). However, CMC builds on static optimisation by inverting the activation and contraction dynamics equations to estimate muscle excitations. The optimised muscle excitations are used to advance the model dynamics forward in time, which when combined with the PD controllers, produces MTU behaviours that are more physiologically realistic for the experimental kinematics. However, the computation of viable starting muscle states requires a period of initiation (0.03 s) forcing the users to start the analysis 0.03 s prior to the period of interest or loss the initial part of the movement. Additionally, although the framework does allow for small changes in model kinematics due to tracking error, the prescription of external forces (e.g. ground reaction forces) mean residual forces are not always eliminated. If residuals cannot be eliminated prior to input into CMC the muscle forces will not be dynamically consistent with the experimental data.

EMG-Informed

EMG-informed methods are a technique where experimentally collected electromyography (EMG), a measure of muscle excitation, are prescribed to the framework to inform the active state of the MTU model. Net joint moments are derived from experimental data and are tracked within an optimisation to estimate a set of muscle excitation profiles that reproduce the measured moments (Lloyd & Besier, 2003; Pizzolato *et al.*, 2015). A set calibration of trials is typically used to adjust MTU model parameters and excitation-activation dynamics model to the participant, which improves joint reaction force estimations (Hoang *et al.*, 2018). Although this reduces the number of trials available for analysis. One of the main advantages of EMG-informed optimisations are the more realistic estimation of co-contractions when compared to other optimisation methods (Pizzolato *et al.*, 2015). Co-contractions are a physiological response to provide increase joint stability (Neptune *et al.*, 1999), and can be misrepresented in other optimisations as a consequence of objective functions working to minimise muscular effort. However, it is impossible to collect EMG-signals from all muscles, requiring redistribution of the collected EMG-signals across the remaining modelled MUs based on physiological assumptions (e.g. nerve innervation Pizzolato *et al.*, 2015; Sartori *et al.*, 2012). The use of EMG data within the framework also limits the data available to the user to validate their estimated muscle forces. While the assumption is that this is less important because they are being informed by experimental data, there is a risk that the calibration of the muscle and activation dynamics models are overfit to the EMG data. Other approaches, such as using open source dataset like the Knee Grand Challenge (Fregly *et al.*, 2012), are necessary to validate the muscle forces. Additionally, as with other inverse approaches, residuals that are not eliminated are carried forward into the muscle force estimations, impacting the dynamical consistency of simulations. An approach to overcome this residual issue is to integrate an EMG-informed approach into forward dynamic optimal control frameworks (see below), where residuals can be constrained to zero to force dynamical consistency.

2.4.2 Forwards Dynamics

In contrast to inverse methods, forward dynamic methods take knowledge of the MTU (e.g. active state) and the initial state of the model dynamics (e.g. kinematics) as input to estimate the model's accelerations (eq. 2.6). Together with an integration scheme (e.g. Runge-Kutta) the algorithm advances the dynamics of the model forward in time to estimate the motion. Without using experimental data to inform the simulation *a priori* this allows for the prediction of new kinematics (e.g., Ackermann & van den Bogert, 2012; Anderson & Pandy, 2001a; Falisse *et al.*, 2022; Falisse, Serrancolí, Dembia, Gillis, Jonkers, *et al.*, 2019). More applicable to this thesis, forward dynamic frameworks have been formulated in an inverse sense (e.g., Haralabidis *et al.*, 2021; Serrancolí *et al.*, 2019; Veerkamp *et al.*, 2021), where experimental data are *tracked* by minimising the error with simulated data in the objective function. These data-tracking approaches provide information to the simulation to drive the inputs towards values that produce outputs representative of the experimentally collected data. This represents a 'best of both worlds' scenario whereby MSK loads are estimated for the observed motion, but are able to overcome some of the limited associated with traditional inverse methods. A discussed in the previous section, the focus on return-to-Earth within this thesis is better aligned with an inverse approach because it is possible to collect experimental data to inform the optimisation approach. Adopting a purely forward, predictive simulation framework would be better suited to long-duration spaceflight where it is not possible to collect experimental data, such as predicting human movement during exercise in alternative hypogravity environments (e.g. the Moon or Mars).

$$\ddot{q} = M(q)^{-1} \cdot [C(q, \dot{q}) + G(q) + F + \tau] \tag{2.6}$$

Optimal Control Theory

Optimal control theory lends itself to MSK modelling by defining control variables that control the motion of the MSK system (state variables) to optimise an objective function. The continuous optimal control problem is discretised into finite set of variables and constraints, which converts them into nonlinear programs that can be solved with open-source solvers (e.g., IPOPT, Wächter & Biegler, 2006). The system dynamics, including skeletal equations of motions, MTU contraction and activation dynamics, are represented as a series of ordinary differential equations (ODEs). There are two approaches to solve the optimal control problem - indirect and direct methods - based on the transcription methods used to discretise the problem. The distinction between the two methods is indirect methods require the definition of the necessary conditions for optimality prior to discretising the variable trajectories, whereas the direct methods discretises before optimising the variables to reach the optimality (Kelly, 2017). The direct method is better suited to large scale MSK modelling as knowledge of the optimal conditions and constraint functions are not required *a priori*, which can be difficult to determine with a large-set of design variables (Betts, 2010). The main benefit of this approach is that prior knowledge of the muscle's active state is not required to run a simulation. In biomechanics, there are two main algorithms that have been used to estimate muscle and joint forces, shooting and collocation, which will be described separately.

Shooting Methods

Shooting methods discretise the control variable trajectories, and integrate to propagate the system dynamics forwards in time (Betts, 2010). When this is performed across one time step it is called *single-shooting*. The simulation output is particularly sensitive to the inputs (i.e. the initial guess) and is subject to increasing integration error as the duration of the simulation is extended (Betts, 2010). This makes single-shooting problematic for large-scale MSK models with numerous degrees-of-freedom and MUs, that require integration. One approach to circumnavigate this issue is to discretise the control trajectory into smaller single-shooting optimisations, call *Multiple Shooting*, and enforce continuity constraints at the end of each interval. However, this can still be computationally intensive for full-body, muscle-driven models, with CPU times of up to 13 - 20 hours for gait simulations (Ong *et al.*, 2019).

Collocation Methods

Collocation methods differ from shooting methods by discretising the control and state trajectories, and approximating the integration scheme as piecewise polynomials. This has an advantage over shooting methods in that the system dynamics can be represented as a series of constraints, eliminating the requirement to integrate the control variables (Betts, 2010). This also allows for implicit formulation of the system dynamics further improving numerical efficiency (van den Bogert *et al.*, 2011). This can lead to robustness in framework as the simulation outcome is less sensitive to the initial guess (De Groote *et al.*, 2016). It is also possible to employ additional constraints to the framework to further improve the physiological realism of the muscle force estimations. For example, Haralabidis *et al.* (2021) performed data-tracking simulations whilst constraining pelvis residuals to zero, achieving dynamically consistent simulations that cannot be done with inverse simulations. The increase time required to formulate the simulation framework and for simulations to run is compensated for by improved confidence in the muscle and joint force estimations. With continued innovation of numerical methods, such as algorithmic differentiation that can reduce simulation time by up to 20-times with respect to finite differences (Falisse, Serrancolí, Dembia, Gillis, & De Groote, 2019), this disadvantage is becoming less prominent.

2.5 Summary

This section restates the thesis aims in light of the reviewed literature.

Aim 1: To create a *Biomechanical Handbook* of normative muscle and joint loading profiles when exercise is performed in different gravity levels.

The literature clearly highlights the significant physiological challenge spaceflight represents for the human body. The severe MSK adaptations that occur place the returning astronaut in a compromised functional state that requires rehabilitation for terrestrial gravity. However, our understanding of MSK loading while exercising in hypogravity is provided by measures of external loading (e.g. ground-reaction forces and net joint moments) that are unable to describe the mechanical loading placed on the internal structures of the body (i.e muscles and joints). Musculoskeletal modelling and simulations methods are an underused tool within the space science community. Authors have began to apply modelling techniques to evaluate in-flight exercise countermeasure devices, but have yet to integrate muscle-driven models into their pipelines. This prevents the estimation of internal MSK loading (i.e. muscle and joint forces), which would provide information at the level of the structures that undergo adaption. The creation of a *Biomechanical Handbook*, a resource that collates normative values for expected internal loading, would be a valuable tool for informing astronaut exercise prescription as specific exercises can be aligned with the individual adaptations experienced by the astronaut to personalise their rehabilitation. The development of such a resource is dependent on being able to accurately estimate muscle forces and joint forces. Optimal control methods, in particular direct collocation, represent the most appropriate tool for solving the muscle redundancy problem. Their numerical efficiency allow for the integration of full-body MSK models, modelling of activation and contraction dynamics, and dynamically consistent solutions that lead to the most physiologically realistic muscle forces. Developing a direct collocation framework that can quantify internal MSK load for a catalogue of exercises and a range of hypogravities is a key step in the creation of the *Biomechanical Handbook*.

Aim 2: To assess how muscular adaptations to unloading can be replicated with a Hill-type muscle model.

A substantial body of literature is available that describes the adaptations to the MTU during disuse. However, there has been little work done on understanding how Hill-type muscle model parameters change in response to these muscular adaptations. The Hill-type muscle model is the most used muscle model within MSK models due to their computational efficiency and ability to recreate salient features of force generation related to cross-bridge formation (i.e. force-length and force-velocity relationships). The accuracy of muscle and joint force estimations rely on the appropriate selection of muscle model parameters. It is therefore key to understand whether muscular adaptations to disuse can be modelled with the Hill-type muscle model. This will allow for astronaut-specific models to be created based on their MSK adaptations, allowing for more accurate estimations of their internal loading during exercise in- and post-spaceflight.

Chapter 3

The Biomechanical Handbook: a novel computational framework for the estimation of internal musculoskeletal loading in hypogravity

Pre-chapter Commentary

This chapter includes the validation of a computational framework for the estimation of joint reaction forces. Establishing that a generic musculoskeletal modelling approach can be used to describe internal loading (i.e. muscle and joint forces) is an important step for defining normative values for use in a Biomechanical Handbook. The computation framework is then applied to a hypogravity case-study to demonstrate the application of the Handbook to better inform astronaut rehabilitation. This chapter was modified due to the COVID-19 pandemic. Originally the aim was perform a similar biomechanical data collection to the case-study current included, but across more hypogravity conditions and movement types. This original plan forms the basis for the protocol described in chapter four. The framework validation would then have been included as an appendix rather than a main outcome of the chapter. The pandemic meant that I could not travel to the University of Milan for these data collections due to travel restrictions and human testing not being permitted.

Abstract

Spaceflight is associated with substantial and variable musculoskeletal (MSK) adaptations. Characterisation of muscle and joint loading profiles can provide key information to better align exercise prescription to astronaut MSK adaptations upon return-to-Earth. The aim was to validate the estimation of lower limb MSK loading using a computational framework, and to test its application to hypogravity scenarios, with the final view to create a Biomechanical Handbook that informs post-spaceflight rehabilitation. The validation of a direct collocation framework, integrated with an OpenSim MSK model, was carried out using the Knee Grand Challenge dataset. Simulated joint reaction forces were compared to *in vivo* knee contact forces from an instrumented prosthesis during a walking gait at four walking speeds. Once validated, the framework was applied to five emulated hypogravity conditions (0.17 g, 0.25g, 0.37 g, 0.50 g, 1 g) of single-leg hopping collected using a body weight support system (BWSS). The estimated quadriceps muscle forces were input into a muscle adaption model to predict the volume of exercise needed to avoid detrimental adaptations. Joint reaction forces were estimated with a mean error of 0.62 - 0.85 BW, and mean peak error of 1.24 $\pm$ 0.17 BW. As walking speed increased, peak joint reaction force increased and joint reaction impulse decreased. Single-leg hopping in hypogravity was associated with increased quadriceps muscle forces, and a shift in rectus femoris force as gravity approached 1 g. The volume of exercise needed to combat muscle adaptations decreased substantially with gravity. Musculoskeletal modelling with direct collocation optimisations provide a valid alternative to profile the loading of different activities when subject-specific modelling is not possible. Information from this approach can be used to compare MSK loading between exercises performed in hypogravity to create a biomechanical handbook resource and inform rehabilitation following unloading periods.

3.1 Introduction

Spaceflight presents a substantial physiological challenge to the human body. Astronauts can present with substantial muscular adaptations, such as atrophy and reduced strength, power, and endurance, in as little as 7 - 14 days of spaceflight (Winnard *et al.*, 2019). To complicate matters, substantial inter-individual variability has been reported in the literature (Fernandez-Gonzalo *et al.*, 2021; Scott *et al.*, 2021), both in terms of the magnitude and the nature of the muscular adaptations experienced by astronauts. For example, Widrick and colleagues (1999) reported a 2-fold variation in responses of muscle contractile properties following 17 days spaceflight. While, Rittweger *et al.* (2018) showed that astronauts may or may not present with muscle architectural adaptations (i.e. fibre length and pennation angle) alongside muscle atrophy following long-term spaceflight. Despite comprehensive post-spaceflight rehabilitation programs (Lambrecht *et al.*, 2017) some aspects of the musculoskeletal system may not return to pre-flight condition after 1-year (Kramer, Kümmel, *et al.*, 2018b). Therefore, the selection of specific exercises to align with the individual adaptations experienced by the astronaut to personalise their rehabilitation is key. This would require characterisation of the loading profiles and the MSK structures being loaded (i.e. individual muscles and joints) during spaceflight relevant exercises.

Musculoskeletal (MSK) modelling presents a powerful tool that can be used to characterise biomechanical loading. Information about skeletal anatomy and muscle-tendon unit (MTU) physiology, including geometry, contraction dynamics, and neural control, are used to replicate the MSK system to analyse human movement. When combined with optimisation techniques to predict activation patterns it is possible to estimate internal loading variables (e.g. muscle forces and joint reaction forces) that are otherwise not feasible *in vivo*. This information has been used in other clinical contexts to inform rehabilitation of patients. For example, MSK modeling has allowed researchers to identify alternative muscle activation strategies to reduce joint contact forces (DeMers *et al.*, 2014), and to distinguish between clinical populations based on their joint contact loading profiles (e.g. Saxby *et al.*, 2016; Wesseling *et al.*, 2018). Furthermore, Van Rossom and colleagues (2018) quantified the magnitude and location of tibiofemoral and patellofemoral contact forces for common rehabilitation exercises. As they suggest, this type of information can be used to grade exercises according to their biomechanical loading profile, which can be better aligned to the patient's injury and rehabilitation stage. This is particularly relevant given the recent shift in focus to plyometric hopping as an in-flight exercise countermeasure (Weber *et al.*, 2019). The proposed benefit of repetitive, short-duration but high-loading associated with plyometric hopping can be compared to other exercises (e.g. walking and running) to understand whether plyometric exercises represent a more efficient method for mitigating against and rehabilitating from MSK adaptations to spaceflight. The vision proposed in this study is to create a *Biomechanical Handbook* resource that presents normative MSK loading profiles of key rehabilitation exercises to match the exercise specific loading according to the astronaut's specific post-spaceflight MSK condition. This vision is extended by also using the biomechanical loading to predict the type of adaptations generated. For example, Wisdom and colleagues (2015) present a muscle adaption model that predicted the rate of change in muscle cross-sectional area (CSA) given the current CSA and degree of overload experienced by the muscle. Combining information about the astronauts muscle atrophy, loading profiles, with a muscle adaption model would allow for the hypertrophic potential of difference exercises to inform astronaut-specific programs.

The first MSK modelling challenge to create the *Biomechanical Handbook* is to obtain accurate estimations of the internal variables to ensure appropriate predictions can be made at different hypogravity levels. Computational approaches are typically a trade-off between numerical efficiency and realism of muscle physiology. Although, recent improvements in computational power and efficient numerical methodologies have allowed for increasingly more complex models to be used that have begun to address this issue. In particular, dynamic optimisation methods have been developed that attempt to model muscle excitation-activation and contraction dynamics to provide a more physiologically consistent representation of muscle behaviour. These approaches have been shown to estimate more physiological MTU behaviour than static optimisations that solve independent problems at each time step (De Groote *et al.*, 2016; Lin *et al.*, 2012). Additionally, static optimisation problems neglect tendon compliance, which influences the estimated MTU behaviour during a simulation. While estimated muscle forces may be similar between static and dynamic optimisations during walking, the rigid tendon assumption may lead to overestimated activations due to the muscle working within less efficient force-length ranges (De Groote *et al.*, 2016). For more dynamic movements, that require higher muscle activations to perform the task, and movements that are known to stretch the tendon, such as plyometric hopping, the estimated muscles forces and MTU behaviour from static optimisation may be altered. For the Biomechanical Handbook, which may include a variety of different movements, modelling activation and contraction dynamics is important. However, the introduction of muscle activation and contraction dynamics leads to stiff equations that are difficult to solve due to large changes in the estimated states for small changes in the controls. These problems were initial solved using direct shooting, a numerical method that optimises for the control variables before integrating the dynamic equations to determine the state variables. Time-marching in the manor leads to long computational time, illustrated by 10,000 CPU hours required to solve a walking task (Anderson & Pandy, 2001a). In contrast, direct collocation, a increasingly popular method in the biomechanics literature (Ackermann & van den Bogert, 2012; Falisse, Serrancolí, Dembia, Gillis, Jonkers, *et al.*, 2019; Haralabidis *et al.*, 2021; Lin & Pandy, 2017; Lin *et al.*, 2018; Porsa *et al.*, 2016) removes the need for explicit integration by optimising for all variable simultaneously and formulating the system dynamics as a set of constraints. This leads to a sparse and tractable problem that, alongside hardware improvements, has seen computational times reduce to less than 3 hours for a similar walking simulation to the that reported by Anderson and Pandy (Lin & Pandy, 2017). The introduction of algorithmic differentiation, an efficient numerical approach for evaluating function derivative, further reduces computational time by up to 20-times over traditional finite difference approaches when combined with direct collocation (Falisse, Serrancolí, Dembia, Gillis, & De Groote, 2019). Additionally, dynamic optimisation approaches can be formulated in an inverse sense, whereby skeletal kinematics (e.g., joint translations and angles) are either prescribed or tracked within the formulation, or in a forward sense to predict new motion. Previous research has used both approaches to calibrate their frameworks using data-tracking before performing predictive simulations to address *what if?* scenarios that are not possible *in vivo* (e.g., Falisse, Serrancolí, Dembia, Gillis, Jonkers, *et al.*, 2019). The ability to analyse known kinematics (i.e., inverse dynamics) and predict new kinematics (i.e., forward dynamics) lends itself to spaceflight research, where biomechanical data are available post-spaceflight but is limited during spaceflight.

In addition to improve computational approaches, personalisation of MSK modelling elements to achieve high fidelity representations of the individual under observation has been shown to improve muscle force estimations. It is common to scale segment lengths and inertial parameters, and MTU parameters based on the anthropometrics of the participant to provide low-level model personalisation. This creates a generic MSK model that requires minimal extra data to generate, but this does not account for physiological and anatomical differences between people. Instead, collection and segmentation of medical images (e.g. magnetic resonance imaging [MRI] and computed tomography [CT]) allows for model personalisation (Modenese *et al.*, 2018), which has been shown to lead to more physiologically plausible MTU behaviour (Akhundov *et al.*, 2022) and more accurate joint contact force estimations (Kainz *et al.*, 2021). Another personalisation approach is mainly focused on tackling the uncertainty in MTU parameter estimation, and it has regularly been shown to impact the accuracy of simulation outcomes (Ackland *et al.*, 2012; Navacchia *et al.*, 2016; Scovil & Ronsky, 2006; Serrancolí *et al.*, 2020; Valente *et al.*, 2014). Such challenges has led authors to calibrate MTU parameters using optimisation to further personalise the MSK model to the participant (Falisse *et al.*, 2017; Pizzolato *et al.*, 2015; Reinbolt *et al.*, 2008; Serrancolí *et al.*, 2020). While model personalisation clearly improves MSK load estimations, the financial resources and expertise needed to collect medical images makes this approach less accessible. Additionally, creation of subject-specific models from medical imagining can take up to 10 hours to complete (Modenese *et al.*, 2018). While fast, automated algorithms for the creation of subject-specific skeletal and muscular geometries are becoming available (e.g. STAPLE, Modenese & Kohout, 2020; Modenese & Renault, 2021), these are currently limited to lower-limb models and do not overcome the need for resources to collect medical imaging data. In the context of space science, a subject-specific approach would require the creation of multiple models throughout the astronauts rehabilitation due to the substantial recovery of physiological systems (Kramer, Kümmel, *et al.*, 2018b), which is a significant undertaking without understanding how it may benefit practice. Assessing whether a generic MSK modelling approach is a valid alternative for comparing the MSK loading between exercises and gravity levels would allow for the analysis of exercise in hypogravity in contexts where subject-specific approaches are not viable. The benefit of the Biomechanical Handbook can be shown using a generic approach to provide justification for undertaking a subject-specific approach.

Therefore, it is pragmatic to initially test the Biomechanical Handbook concept by relying upon the use of generic MSK models. Evaluating the accuracy of MSK loading estimations when combining generic modelling with efficient dynamic optimisation methods is a necessary first step for reliably profiling the loading of a given exercise. Once a generic approach has been demonstrate it provides a platform from which more subject-specific modelling approaches can be built from. To this end, the aim of this study was to validate a direct collocation optimal control framework, integrated with a generic OpenSim MSK model, by quantifying the error in estimated joint reaction forces (JRF). The second aim was to demonstrate the development and application of a Biomechanical Handbook to predict the exercise regime needed to avoid detrimental adaptations during unloading periods. This was achieved by applying the framework to a staged hypogravity ($\leq$1 g) case-study of single-leg vertical hopping where different gravity conditions were emulated.

3.2 Methods

3.2.1 Experimental Data

Knee Grand Challenge Data Description

Synchronised marker trajectories, ground reaction forces (GRF), eTibia implant forces, and electromyography (EMG) data of a single male participant (88 years, 1.68 m, 66.7 kg) walking at four different speeds on a treadmill were extracted (slow = 0.8 m·s^{-1}, set = 1.0 m·s^{-1}, self-selected [ss] = 1.2 m·s^{-1}, fast = 1.4

m·s^{-1}) from the "Fourth Grand Challenge Competition to predict *in vivo* knee loads" (Fregly *et al.*, 2012). Maximum EMG trials were also extracted for data processing. These data were chosen as they provide a comprehensive repository of synchronised biomechanical data, including *in vivo* joint contact forces via the force instrumented knee prosthetic. The accuracy of the framework for estimating joint reaction forces, and indirectly muscle forces, can then be established because the experimental biomechanical data are intrinsically linked to the joint contact forces.

Table 3.1 Summary of the walking trials extracted for analysis

	Slow	Set	Self-Selected	Fast
Speed (m·s^{-1})	0.8	1.0	1.2	1.4
Steps Extracted	12	11	15	12

Body Weight Support Case Study

A case study from a single male (29 years, 1.82 m, 79.9 kg) performing single-leg vertical hopping was collected whilst attached to a body weight support system (BWSS) that emulated different gravity scenarios. This case-study was used to demonstrate how the quantification of MSK loading profiles can be used to develop the Biomechanical Handbook, which can predict what type of exercise should be done to avoid detrimental adaptations during unloading periods. The participant was attached to the vertical BWSS via a modified harness under four emulated hypogravity conditions (0.17 g, 0.25 g, 0.37 g, 0.50 g). The experimental set-up was replicated under terrestrial gravity (1 g) without the BWSS nor harness to provide a full spectrum of gravity conditions. The BWSS constituted a series of elastic bungee cords originating on a manually adjusted electric winch, and inserting onto the participant's harness. A ceiling-mounted pulley aligned the system above a single static force-platform (9287BA, Kistler Instruments Corporation, Switzerland). The line-of-action was in excess of 17 m to minimise vertical fluctuations in the body weight support force (Pavei *et al.*, 2015). A full-body marker set (200 Hz, Vicon MX, Oxford Metrics, UK), GRFs (2000 Hz), BWSS force via an in-series load-cell (2000 Hz, REP Transducers, TS

300 kg), and seven lower-limb EMG (2000 Hz, Trigno, Delsys Inc., Boston, MA, US) were collected. Five hops were extracted per condition for analysis.

Data Processing

A custom MATLAB (version R2017b, MathWorks Inc, USA) script was written to format the data for the simulation framework. Trials were cropped 25 frames prior to right foot touchdown (implant side and hopping side) to 25 following the consecutive right foot touchdown to allow resampling of the data before inclusion within the simulation framework. For the Knee Grand Challenge dataset, this yielded 50 steps of the right foot across the four walking speeds (Table 3.1). Inverse kinematics was performed via the OpenSim-Matlab API (version 3.3, Delp *et al.*, 2007) to obtain joint angles and translations from the marker trajectories. Inverse kinematic results, GRF, and, for where applicable, body weight support forces from the load cell were filtered at 6 Hz with a low-pass 2^{nd} order Butterworth filter. Inverse dynamics analysis was performed to obtain net joint moments and forces. For the hypogravity case study, body weight support forces were applied vertically to the pelvis centre of mass. Third-order B-splines were then used to resample the data, and to calculate velocities and accelerations of the inverse kinematics data. The resampled kinematics, net joint moments and GRF were used as experimental data within the simulation framework. The EMG data from each trial were band-pass filtered [10 Hz, 300 Hz], full-wave rectified, and low-pass filtered (6 Hz) to create a linear envelope. The linear envelope was normalised to the maximum value for each muscle across all maximum EMG and dynamic trials.

3.2.2 Simulation Framework

Musculoskeletal Model

Skeletal motion was modelled as rigid body dynamics using Newtonian mechanics, with compliant Hunt-Crossley contacts to model the foot-ground interaction. A generic full-body MSK model was utilised in this framework (Figure 3-1, Lai *et al.*, 2017). The model consisted of 23-segments – ground, pelvis, torso, and, bilaterally, femur, patella, tibia-fibula, talus, calcaneus, toe, humerus, radius, ulna and hand – and 37 degrees of freedom. Pelvis translation and rotation

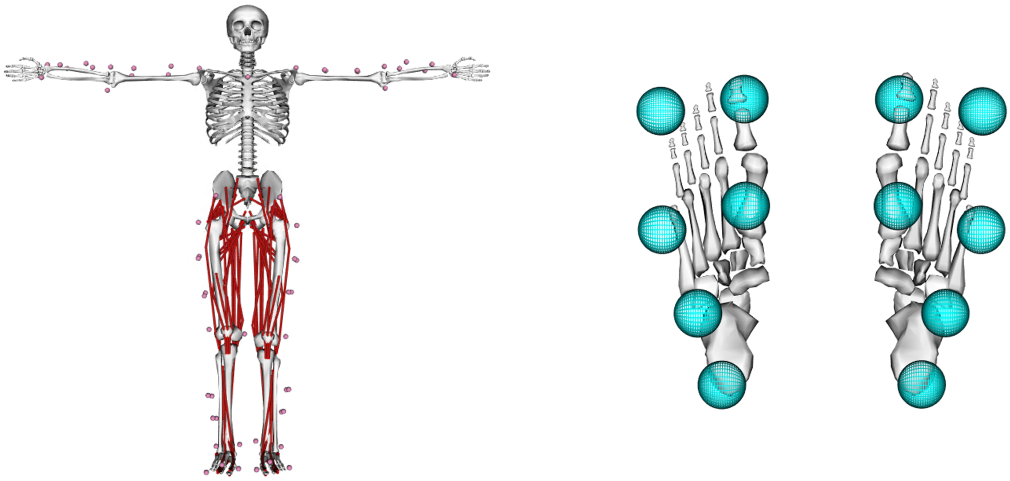

Figure 3-1 The generic musculosckeletal model used in this study (left). Pink spheres represent marker locations, and red string elements the muscle-tendon unit geometries. Dorsal view of the contact spheres placed on the model with respect to the foot segments (right).

with respect to the ground were modelled as a six degrees-of-freedom (DOF) joint. The torso-pelvis, shoulder, and hip joints were modelled as three DOF ball-and-socket joints, the wrists as two DOF universal joints, whilst ankle, subtalar, elbow, radioulnar and metatarsophalangeal (MTP) joints as one DOF hinge joints. The wrist and MTP joints were locked at 0°. The tibiofemoral joint (knee) was modelled as a 1-DOF hinge joint, with a 0-140° flexion range. The remaining tibia rotations and translations relative to the femur, and the sagittal plane patellofemoral joint motion (i.e. anteroposterior and vertical translation, and rotation about the mediolateral axis), were defined by polynomials as a function of knee flexion. Polynomial coefficients were calculated according to the SimmSpline functions defined in the model after scaling. The hip, knee, ankle, and subtalar DOF will be actuated by 80 Hill-type MTU, with the MTPs, torso and upper body driven by 19 ideal torque actuators. Idealised torques driving the non-muscle actuated DOF are described as a function of activation and maximum torque. The foot-ground interaction was modelled with six-spheres per foot – four attached to the calcaneus and two to the toe segments. Hunt-Crossley equations, modified to be twice continuously differentiable (Serrancolí *et al.*, 2019), were used to calculate the forces at each of the six spheres as a function of ground penetration and penetration velocity.

Three-element Hill-type muscle model formulations were used in this framework (Zajac, 1989). Briefly, the MTU consisted of a contractile component, a passive elastic component parallel to the contractile component, and a series passive elastic component. Active (force-length and force-velocity) and passive (parallel and series) force generation were modelled via the dimensionless equations presented by De Groote *et al.* (2016). The dimensionless equations were described by five parameters: maximum isometric force, optimum fibre length, pennation angle at optimum fibre length, maximum shortening velocity, and tendon slack length. Lengths, shortening velocities, and moment arms of MTUs were defined as a function of joint positions and velocities (Falisse, Serrancolí, Dembia, Gillis, Jonkers, *et al.*, 2019; Van den Bogert *et al.*, 2013). Polynomial coefficients were determined for the scaled muscle lengths, velocities and moment arms, extracted using OpenSim's Muscle Analysis with the model positioned across a range that exceeded the expected experimental data. Raasch's activation model (Raasch *et al.*, 1997) was used to model excitation-activation dynamics of the MTUs, with modifications by De Groote *et al.* (2009).

The model was scaled to the participant's anthropometrics using OpenSim's scaling tool (Delp *et al.*, 2007). Segment dimension-specific scaling factors were computed as the ratio between virtual and experimental distances of pairs of anatomical markers. The scale factors are used to scale segment lengths, widths, and depths, while the inertial parameters were scaled to the participant's mass assuming the mass distribution was preserved. Total MTU lengths were adjusted during scaling such that the ratio of optimal fibre length to tendon slack length was maintained. The MTU maximum isometric forces were scaled according physiological cross-sectional area (Lieber & Fridén, 2000), where muscle volumes were estimated for the participant's height and mass (Handsfield *et al.*, 2014) and a specific tension of 60 $N{\cdot}cm^2$ as done previously (Rajagopal *et al.*, 2016). Maximum shortening velocities were assumed to be ten times the optimal fibre lengths, and the tendon force-length curves had a gradient of 35 at 4% strain as done in a similar simulation framework (Falisse, Serrancolí, Dembia, Gillis, Jonkers, *et al.*, 2019). Pennation angles at optimum fibre length from the unscaled model were retained.

Optimal Control Problem

A muscle-driven, data-tracking simulation framework was formulated as an optimal control problem (OCP). A direct collocation method was then used to discretise the OCP into non-linear programs (NLPs) to track experimental kinematics, net joint moments, and GRFs for a single movement cycle. A single-movement cycle was defined as one right-foot step for the walking trials, and one contact and subsequent flight phase for single-leg hopping. The goal of the simulation was to minimise a cost function (eq. 3.1) to estimate muscle activations for a given movement whilst optimising for a set of state, x, control, u, and parameter variables, p, for a single-movement cycle. The framework is designed to track the experimental data with zero pelvis residuals to elicit a dynamically consistent solution, before estimating the JRFs from the simulated muscle activations. The aim was to estimate JRFs similar in shape and magnitude to knee joint contact forces measured by the eTibia implant. This was a key step to allow for the assessment of joint loading related variables for the proposed Biomechanical Handbook.

Foot-ground contact sphere stiffness and damping (constant across all spheres) and their 3D position were optimised as parameters within the OCP (p_{CM}). The remaining parameters were kept constant according to previous work (Falisse, Serrancolí, Dembia, Gillis, Jonkers, *et al.*, 2019), with the sphere radii set to 0.02 m. The state (x) and control (u) variables will be selected to allow efficient numerical formulation of the MSK system. The skeletal dynamics will be described by the model's kinematics. The state variables, q and $\dot{q}$, which correspond to the positions and velocities of the 37 DOF, respectively, will be controlled by their accelerations, $u_{\ddot{q}}$. Muscle activations, a_m, and normalised tendon forces, $\tilde{F}_t$, are introduced to describe the muscle model state, with their first time derivatives, u_{a_m} and $u_{\tilde{F}_t}$, introduced as control variables (De Groote *et al.*, 2016). The states of idealised torque actuators are described by their activations, a_τ, and controlled by their excitation, u_{e_τ}. Control variables are introduced for the GRFs, u_{GRF}, as done previously (Serrancolí *et al.*, 2019). This improves the convergence rate as the foot-ground contact sphere forces are subject to large fluctuations for small adjustments to the skeletal dynamics. Reserve actuators are added to muscle-driven DOF as control variables, u_{res}, that describe the instantaneous moment being produced, to help convergence of the simulations.

Cost Function

The cost function (J, eq. 3.1) was formulated with a gait performance and muscle sharing criterion (eq. 3.2), data tracking terms (eq. 3.3) and control variable minimisation terms (eq.3.4). Each term was weighted ($w_{1\text{-}3} = [0.01, 1, 10]$) via manual tuning to elicit accurate tracking and physiologically realistic simulations, and were kept constant once calibrated. Increased weight was placed on net joint moment tracking to ensure muscle forces were recreating accurate joint moments, and thus to give valid JRF estimations. Less emphasis was placed on tracking the vertical pelvis position to allow the simulation to move the model vertically to supplement the GRF tracking. To prevent large changes in kinematics and muscle activations and tendon forces between time points, increased weight was placed on minimising their control variables (i.e. $u_{\ddot{q}}$, u_{a_m} and $u_{\tilde{F}_t}$).

$$J = J_{effort} + J_{tracking} + J_{DynCon} \tag{3.1}$$

Muscle redundancy was solved by minimising the sum of muscle activations squared. Muscle activations were multiplied by their muscle volume expressed as a percentage, P_{V_j}, of all muscles according to Handsfield and colleagues (2014) to penalise the use of larger muscles.

$$J_{effort} = w_2 \sum_{j=1}^{80} \int_{t0}^{tf} \left(P_{V_j} \cdot a_j\right)^2 \ dt \tag{3.2}$$

Tracking terms were formulated to minimise the sum of squared error between the simulated (i.e. $\hat{q}$, $\hat{u}_{GRF}$, and $\hat{\tau}$) and experimental data (i.e. q, u_{GRF}, and τ). Each term was scaled to maintain equal weight within the cost function despite the different orders of magnitude. Coordinate angles and translations were scaled by 2° (s_{rot}) and 0.02 m (s_{tr}), respectively. The scale factors for the net joint moments ($s_\tau = 28.6$) and $\hat{u}_{GRF}$ (s_{GRF} = [5.1, 50, 5.1, 5.1, 50, 5.1]) were then derived as the moment and force values required to perform 1 unit of work given for the corresponding scale factor for the kinematics. The anteropostior and mediolateral forces were further scaled by 9.81 to account for gravity.

$$
\begin{aligned}
J_{tracking} = {} & w_2 \sum_{i=1}^{34} \int_{t0}^{tf} \left(\frac{q_i - \hat{q}_i}{s_{rot}} \right)^2 dt \\
& + w_1 \sum_{i=1}^{3} \int_{t0}^{tf} \left(\frac{q_{i,\ trans} - \hat{q}_{i,\ trans}}{s_{tr}} \right)^2 dt \\
& + w_2 \sum_{n=1}^{6} \int_{t0}^{tf} \left(\frac{GRF_n - \hat{u}_{GRF_n}}{s_{GRF}} \right)^2 dt \\
& + w_3 \sum_{i=1}^{31} \int_{t0}^{tf} \left(\frac{\tau_k - \hat{\tau}_k}{s_{\tau}} \right)^2 dt
\end{aligned} \tag{3.3}
$$

Minimisation of control and reserve actuator variables was included to improve the physiological realism of the solutions as done previously (Falisse, Serrancolí, Dembia, Gillis, Jonkers, *et al.*, 2019; Haralabidis *et al.*, 2021). The control variables were normalised with their corresponding upper bounds (s_{Bound}, see *Direct Collocation* below). The u_{res} were scaled ($s_{res} = 2$) and minimised in the cost function to penalise their use within the framework.

$$
\begin{aligned}
J_{Control} = {} & w_2 \sum_{i=1}^{37} \int_{t0}^{tf} \left(\frac{u_{\ddot{q}_i}}{s_{Bound}} \right)^2 dt \\
& + w_3 \sum_{j=1}^{80} \int_{t0}^{tf} \left(\frac{u_{\tilde{F}_{t_j}}}{s_{Bound}} \right)^2 dt \\
& + w_3 \sum_{j=1}^{80} \int_{t0}^{tf} \left(\frac{u_{a_{m_j}}}{s_{Bound}} \right)^2 dt \\
& + w_2 \sum_{m=1}^{12} \int_{t0}^{tf} \left(\frac{u_{res_j}}{s_{res}} \right)^2 dt
\end{aligned} \tag{3.4}
$$

Direct Collocation

A direct collocation method was used to convert the OCP into a NLP using *Legendre-Gauss-Radau* quadrature. The framework was implemented in MATLAB (version R2017b, MathWorks Inc, USA) and CasADi (Andersson *et al.*, 2019), and was solved using IPOPT (Wächter & Biegler, 2006). A modified

OpenSim and SimBody release was utilised to allow for algorithmic differentiation of function derivatives (Falisse, Serrancolí, Dembia, Gillis, & De Groote, 2019). Net joint forces and moments via inverse dynamics, and Hunt-Crossley forces will be estimated at each mesh point as a function of model kinematics (i.e. q, $\dot{q}$, and $\ddot{q}$), external force (i.e. u_{GRF}, and, where applicable, body weight support forces), and foot-ground contact model parameters (i.e. p_{CM})..

Foot-ground contact model parameters will be included as static parameters¸ $p = [p_{CM}]$. The state ($x = [q, \dot{q}, a_m, \tilde{F}_t, a_\tau]$) and control ($u = [\ddot{q}, u_{a_m}, u_{\tilde{F}_t}, u_{GRF}, u_{e_\tau})$ trajectories were discretised into with 50 equally spaced mesh intervals (Ackermann & van den Bogert, 2010). The mesh was refined during initial testing whereby the number of points was varied - 20, 40, 50, 80, and 100 - across four trials (one per walking speed). Fifty points were needed to achieve optimal solutions for all four walking speeds, with minimal additional improvement in tracking and joint reaction force estimation as the number of points increased. Given the increased computational demand required for a more refined mesh, 50 points was chosen. Between mesh points the state trajectories were transcribed into three-point intervals (collocation points) approximated with third-order polynomials, while the control variables were kept constant. The cost function is evaluated as the time integral between the start and end of the movement cycle, evaluated at each collocation point. State, control and static variables will be bounded and then scaled within the NLP such that each variable fell between -1 to 1 to improve the numerical conditioning of the NLPs (Betts, 2010). Kinematic variables (i.e. q, $\dot{q}$, and $\ddot{q}$) and u_{GRF} were bounded between minimum and maximum experimental values, but further extended by the range. The contact model spheres were initially positioned according to Falisse *et al.* (2019), and allowed to deviated ± 0.025 m. The stiffness and damping coefficients were bounded between $1e^5$ - $1e^7$ and 0.5 - 10, respectively, to align with similar previous research (Falisse, Serrancolí, Dembia, Gillis, Jonkers, *et al.*, 2019; Haralabidis *et al.*, 2021; Lin & Pandy, 2017). These parameters were included in the framework after initial testing whereby three simulations were performed across four trials (one per walking speed). The foot-ground model parameters were either: (1) taken from the literature (Falisse, Serrancolí, Dembia, Gillis, Jonkers, *et al.*, 2019), (2) only the stiffness and damping parameters were optimised, or

(3) the stiffness, damping and sphere positions were optimised. Optimising for stiffness, damping and sphere positions resulted in smoother experimental data tracking compared with when contact parameters were not optimised, and lower estimated joint reaction force error relative to the eTibia when sphere positions were not optimised. The remaining variables were bounded according to Falisse *et al.* (2019).

A series of dynamic constraints are imposed at each collocation point to maintain system dynamics. Scaled variables were included in the constraint equations. The skeletal dynamics and activation dynamics are imposed as implicit constraints via first-order differential equations (eq. 3.5 - 3.8). The excitation-activation dynamics of the idealised torque actuators were formulated explicitly as linear first-order approximations given an electromechanical delay (emd = 35 ms) (eq. 3.9, Falisse, Serrancolí, Dembia, Gillis, Jonkers, *et al.*, 2019).

$$\frac{dq}{dt} - \dot{q} = 0 \tag{3.5}$$

$$\frac{d\dot{q}}{dt} - u_{\ddot{q}} = 0 \tag{3.6}$$

$$\frac{da_m}{dt} - u_{\dot{a}_m} = 0 \tag{3.7}$$

$$\frac{d\tilde{F}_t}{dt} - u_{\dot{\tilde{F}}_t} = 0 \tag{3.8}$$

$$\frac{da_\tau}{dt} = \frac{u_{e_\tau} - a_\tau}{emd} \tag{3.9}$$

Path constraints were imposed at the beginning of each mesh interval to achieve physiologically appropriate solutions. The muscle forces were related to the net joint moments of the muscle-driven DOF (τ_m) via implicit constraints according to their polynomial-computed moment arms and the reserve actuators (eq. 3.10). The polynomials created to relate joint kinematics (i.e., q and $\dot{q}$) to the MTU lengths, velocities, and moment arms were evaulated at each mesh point. The torque-driven DOF (τ_T) were scaled and related to the a_τ via implicit constraints (eq. 3.10). An additional constraint enforced dynamical consistency by enforcing pelvis residuals to be zero (τ_{Pelvis}, eq. 3.12). The u_{GRF} were implicitly constrained to match the DLL calculated forces for foot-ground interaction (F_{HC}, eq. 3.13). The Hill-equilibrium condition (F_c) was implicitly imposed by enforcing the muscle forces projected along the tendon to match the tendon forces (eq. 3.14). Raasch's activation model was imposed on the muscle activations via two inequality constraints based on the activation ($t_a = 0.015$ s) and deactivation ($t_d = 0.06$ s) time constants (eq. 3.15 - 3.16, De Groote *et al.*, 2009).

$$\sum(\tilde{F}_t \cdot MA) + u_{res} - \tau_m = 0 \tag{3.10}$$

$$a_\tau - \frac{\tau_T}{s_T} = 0 \tag{3.11}$$

$$\tau_{pelvis} = 0 \tag{3.12}$$

$$u_{GRF} - F_{HC} = 0 \tag{3.13}$$

$$F_c(a_m, \tilde{F}_t, u_{a_m}, u_{\tilde{F}_t}, q, \dot{q}) - F_t = 0 \tag{3.14}$$

$$u_{\dot{a}_m} + \frac{a_m}{t_a} \leq \frac{1}{t_a} \tag{3.15}$$

$$u_{\dot{a}_m} + \frac{a_m}{t_d} \geq 0 \tag{3.16}$$

A continuity constraint was imposed on the state variables at the end of each mesh interval to ensure consistency between the consecutive mesh points, such that the end of the previous interval must equal the start of the next.

Initial Guess

Two initial guesses were formulated, and the solution with the lowest cost function value used in further analysis. A data-informed initial guess was generated by extracting experimental data for kinematics (i.e. q, $\dot{q}$, and $\ddot{q}$) and GRFs. The remaining state and control variables were set to their corresponding lower bounds. A second guess was generated where all variables were set to zero, or, where the bounds did not cross zero, their corresponding lower bound. For both guesses, the contact sphere parameters were set to the same values. The stiffness and damping coefficients were set to 1e^6 N·m^{-2} and 2 s·m^{-1}, respectively. The same initial guess as Falisse *et al.* (2019) was used for the sphere positions.

3.2.3 Data Analysis

Simulation performance was assessed by calculating maximum errors and root mean squared errors (RMSE) between experimental and simulated data.

Acceptable tracking errors were determined based on recommendations by Hicks et al. (2015). Reserve actuators were considered acceptable if they did not contribute more than $5N \cdot m$ or 10% to overall net joint moments. Optimised muscle activations were extracted and compared to experimental EMG for magnitude and timing.

Knee Grand Challenge Data

Simulated knee JRFs were estimated using OpenSim's Analysis Tool. The contact sphere forces were applied as external forces to the body using the optimised sphere positions as points of application. Actuator forces for the model were given as optimised tendon forces and inverse dynamics ID torques for the muscle-driven and torque-drive actuators, respectively. The vertical JRF exerted on the right tibia by the right femur, expressed in the tibia frame, was compared to the eTibia. All values were normalised to body weight. Confidence intervals (95%) were calculated to compare differences in simulated peak JRFs between walking speeds. The R^2 and RMSE were used to explore the shape and error magnitude, respectively, between the simulated JRFs and experimental eTibia forces. The joint reaction impulse (JRI), the time integral of JRF, for the knee JRF and eTibia were also compared. The JRI captures information about magnitude and duration of JRF loads, that can be used as indicative of cumulative load based on a movement cycle (e.g. per step taken). A *per unit cycle analysis* is more informative than peak force alone (Miller *et al.*, 2014), thus determining the accuracy of JRI estimations provide a more complete estimation joint loading profiles. The bias in estimating the peak JRF was explored via a Bland-Altman analyses, where mean bias, bias standard deviations, and 95% limits of agreement were calculated (Bland & Altman, 2010). To evaluate the estimation of JRF at the hip additional instrumented prosthetic data were obtained from a public online database[1]. These data include participants with a force instrumented hip or knee prosthetic walking overground at a self-selected pace. The 25^{th} and 75^{th} percentiles from normative data for the hip (Bergmann *et al.*, 2016) and knee (Bergmann *et al.*, 2014) were extracted and the R^2 and RMSE calculate.

[1]www.orthoload.com

Body-Weight Support Case Study

Quadriceps muscle forces were extracted and were input into a muscle adaption model (eq. 3.17, Wisdom *et al.*, 2015). The adaptation model estimates the rate of change in cross-sectional area (CSA) of a muscle based on the degree of overload experienced, the muscle's current CSA, a physiological maximum possible CSA, and a minimum load threshold required to trigger adaption. The switch factor, $F - F_0$, determines the rate of change in CSA, $\dot{A}(t)$, when $F > F_0$. The model assumes muscle adapts in response to overload by addition of sarcomere in parallel, and CSA increases in an exponential fashion before converging to a new homeostatic equilibrium. The quadriceps force, F, was taken as the cumulative active and parallel passive forces from the Rectus Femoris (RF), Vastus Lateralis (VL), Vastus Intermedius (VI), and Vastus Medialis (VM) muscles, normalised to their summed maximum isometric force parameters contained within the scaled OpenSim model. The physiological threshold, F_0, was taken as 0.2 to replicate 20% one-repetition maximum, which is sufficient to elicit hypertrophic benefits to resistance training under the right conditions despite the low-load (Schoenfeld, 2013). The baseline CSA, A, physiological limiting value for CSA, A^{max}, and shape parameters, τ and δ, that determined the model shape were determined based on data from DeFreitas *et al.* (2011). These data included thigh lean mass CSA determined via peripheral quantitative CT (pQCT) during a resistance-training intervention given to healthy, untrained, young adult men, which was considered appropriate for the case study participant. The number of repetitions required to generate hypertrophy will be estimated based on a minimal worthwhile increase in CSA of 3.37%. DeFreitas and colleagues (2011) defined the minimal worthwhile increase based on the calculations of Weir (2005).

$$\dot{A}(t) = \frac{1}{\tau}\left(\frac{A^{max} - A}{A^{max} - 1}\right)^{\delta} F - F^{0} \tag{3.17}$$

Using the same target repetitions per set (12) and sessions per week (3) as DeFreitas *et al.* 2011, the number of sets required to meet the worthwhile increase was calculated.

3.3 Results

Knee Grand Challenge Data

Of the 50 trials, 47 converged to an optimal solution from at least one initial guess and were used in the analysis. Experimental data were closely tracked during all simulations. Example tracking results are presented for self-selected walking for brevity (Figure 3-2 - 3-4), but reflect the other walking speeds. The other walking speeds can be viewed in the supplementary material (see appendix A). Kinematics were tracked to within 3° across all trials (maximum error: 2.91°, RMSE: 0.94°). Maximum pelvis angles, and non-vertical translation tracking errors were within 1.85 ° and 0.04 m, respectively. The vertical translation, which was allowed to vary more to facilitate GRF tracking, did not exceed 0.065 m across all trials. Vertical GRF were tracked to within a maximum error of 0.35 BW and RMSE of 0.08 BW, whilst the anteroposterior and mediolateral GRF components were tracked to within 5 N and 2 N, respectively. Net joint moments were tracked within 0.43 N·m·kg^{-1} across all trials. Reserve moments did not provide substantial assistance to the model, with peak moments not exceeding 2.61 N·m across all DOF. Left and right hip rotation (mean = 1.07 ± 0.29 N·m) required more assistance than the other DoF (mean = 0.40 ± 0.16 N·m). For the right knee, one trial required a maximum reserve of 1.80 N·m with the remainder remaining below 1 N·m (mean = 0.58 ± 0.15 N·m). Muscle activations showed qualitatively similar profiles to the EMG data in terms of the magnitude, timing and consistency across all trials for the majority of muscles.

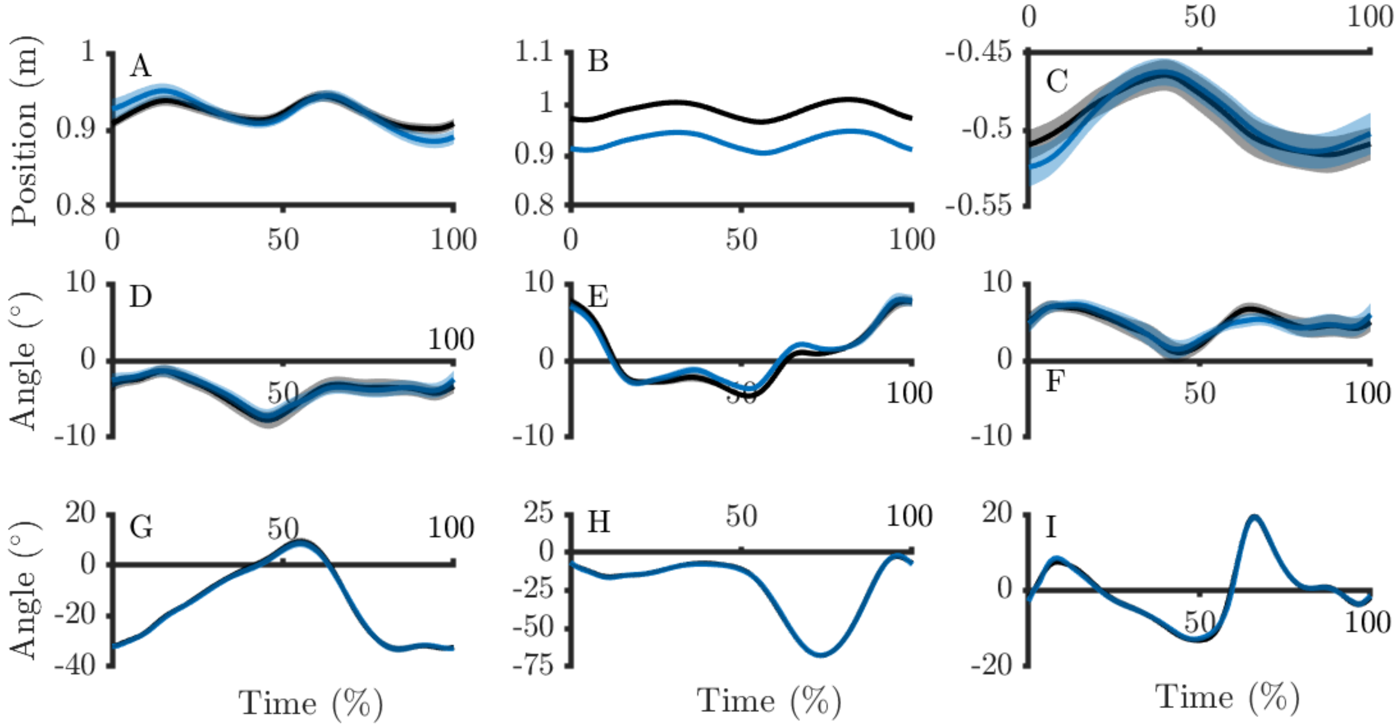

Figure 3-2 Pelvis translation (A: A-P, B: Vertical, & C: M-L) and rotation (D: tilt, E: lateral title, & F: rotation), and sagittal plane angle (G: Hip, H: Knee, I: Ankle) tracking at self-selected (1.2 m·s^{-1}) walking speed. Backward tilt, right lateral tilt, anti-clockwise, extension, plantar flexion were defined as positive. Blue = simulated, black = experimental.

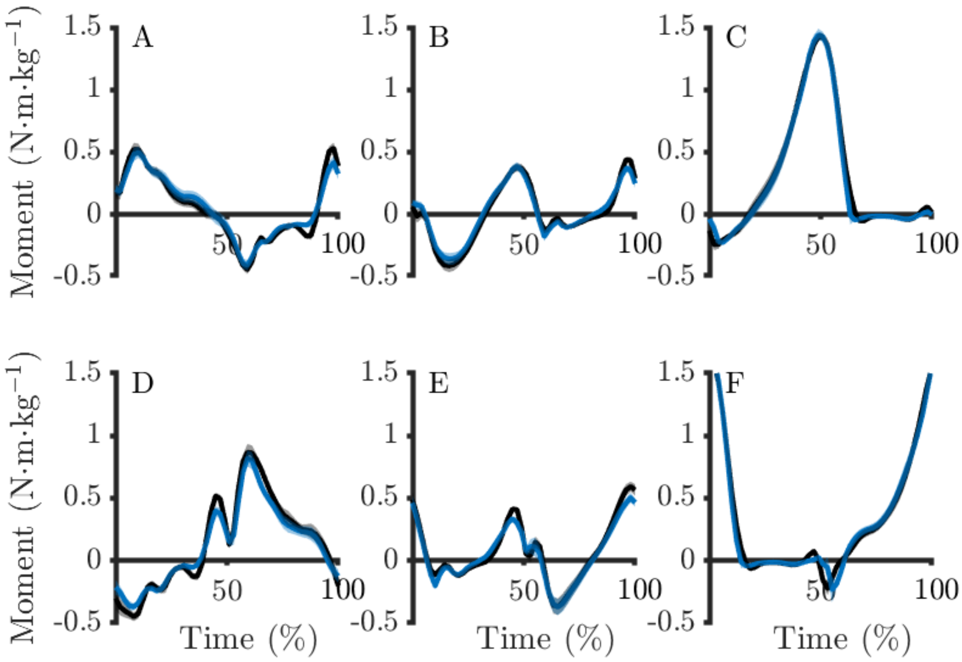

Figure 3-3 Right (A - C) and left (D - F) net joint moment tracking for hip extension (A & D), knee flexion (B & E) and ankle plantarflexion (C & F) during self-selected walking speed (1.2 m·s^{-1}). Extension and plantar flexion were defined as positive. Blue = simulated, black = experimental.

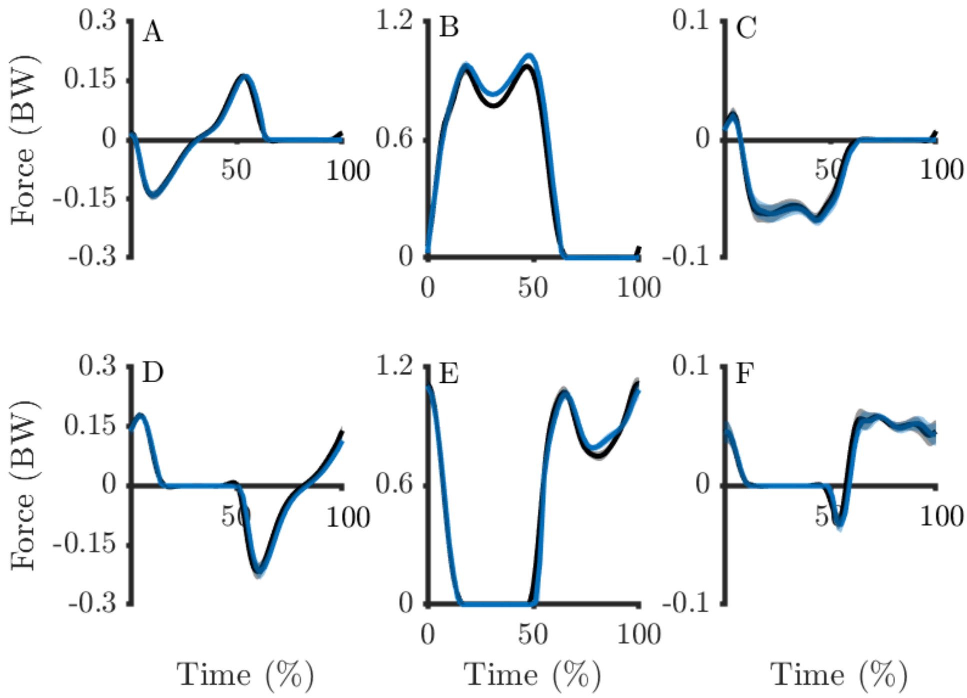

Figure 3-4 Normalised A-P (A & D), vertical (B & E) and M-L (C & F) GRF tracking of the right (A-C) and left (D-F) steps for the self-selected walking speed (1.2 m·s^{-1}). Blue = simulated, black = experimental.

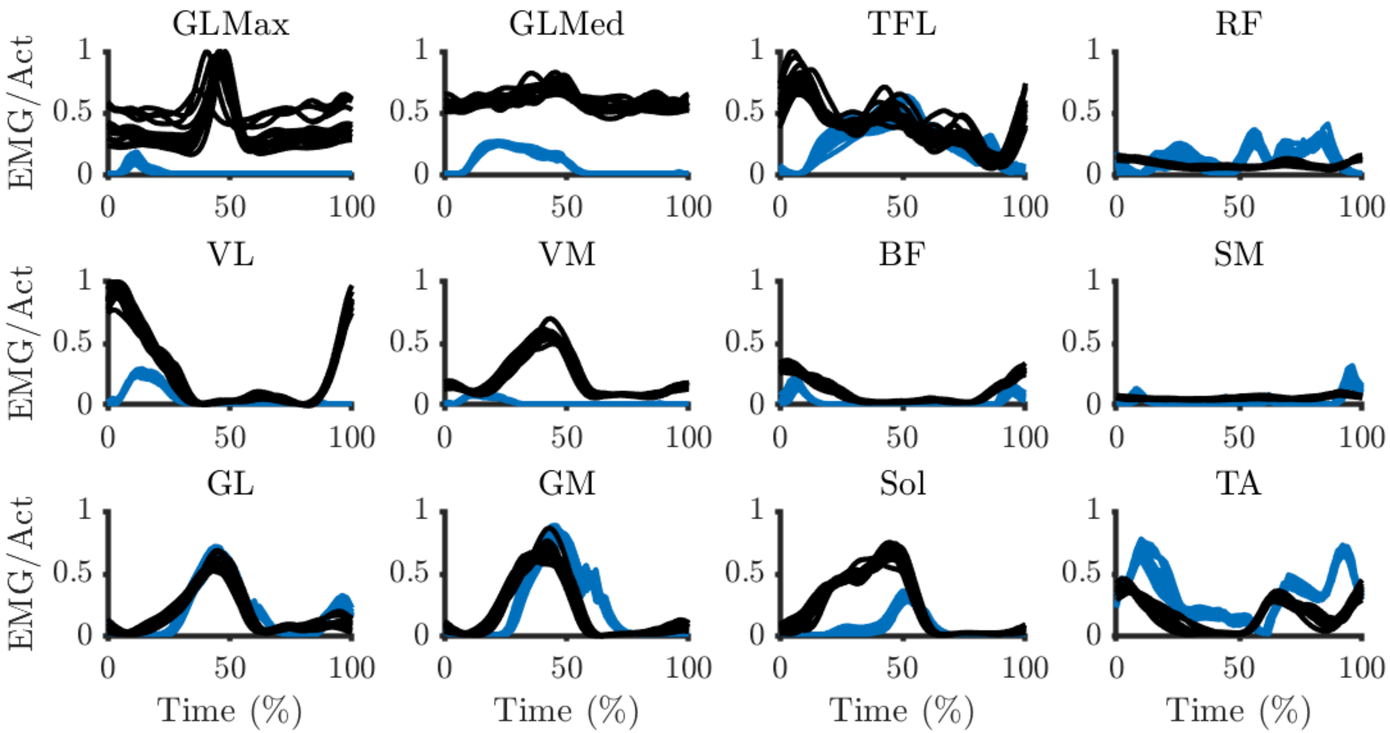

Figure 3-5 Comparison between simulated muscle activations (blue) and experimental EMG (black) during self-selected walking (1.2 m·s^{-1}). GLMax = gluteus maximus, GLMed = gluteus medius, TFL = tensor fascia latae, RF = rectus femoris, VL = vastus lateralis, VM = vastus medius, BF = biceps femoris, SM = semimembranosus, GL = gastrocnemius lateralis, GM = gastrocnemius mediaslis, Sol = soleus, TA = tibialis anterior.

The estimated JRF came within 0.62 - 0.85 BW across all trials, and were able to reflect the double peak profile measured with the eTibia (Figure 3-6). The R^2 values ranged between 0.65 - 0.9, however, as speed increased the shape agreement deteriorated (Figure 3-7). This was reflected in the RMSE results that also increased as walking speed increased The largest error in the JRF estimations corresponded to the second peak around 50 % of stance, which was overestimated by 1.23 ± 0.17 BW (Figure 3-8A). Although, the framework was able to detect significant increases in peak JRF with walking speed (slow = 3.17 ± 0.22 BW [CI: 3.13 - 3.21 BW]; set = 3.27 ± 0.23 BW [CI: 3.22 - 3.32 BW]; ss = 3.44 ± 0.17 BW [CI: 3.42 - 3.46 BW]; fast = 3.60 ± 0.12 BW [CI: 3.58 - 3.63 BW]). The limits of agreement estimate that peak joint forces can be estimated within 0.85 - 1.62 BW 95% of the time irrespective of walking speed. However, it is important to note that there was uneven distribution of data points about the mean value, indicating that estimated peak JRFs were overestimated to a greater extent when eTibia values were higher. This is reflected in mean error values for each walking speed, with higher speeds having higher peak JRF errors (slow = 1.06 ± 0.16 BW; set = 1.26 ± 0.14 BW; ss = 1.33 ± 0.11 BW; fast = 1.28 ± 0.13 BW). Similarly, the JRI were overestimated by 0.75 ± 0.10 BW·s across walking speeds, however, the error decreased as walking speed increased (Figure 3-8B).

When compared to the Orthoload data set, the estimated knee JRFs showed similar shape (R^2 = 0.84 ± 0.02) and magnitudes (RMSE = 0.50 ± 0.03 BW). Although, the peak joint force was still overestimated (Figure 3-9B). Hip joint forces were well estimated (R^2 = 0.89 ± 0.02, RMSE = 0.59 ± 0.02 BW), but there was qualitative differences between the Orthoload and simulated data (Figure 3-9A). Specifically, the simulated data did not capture the nadir between the two peaks that was present in the hip Orthoload data.

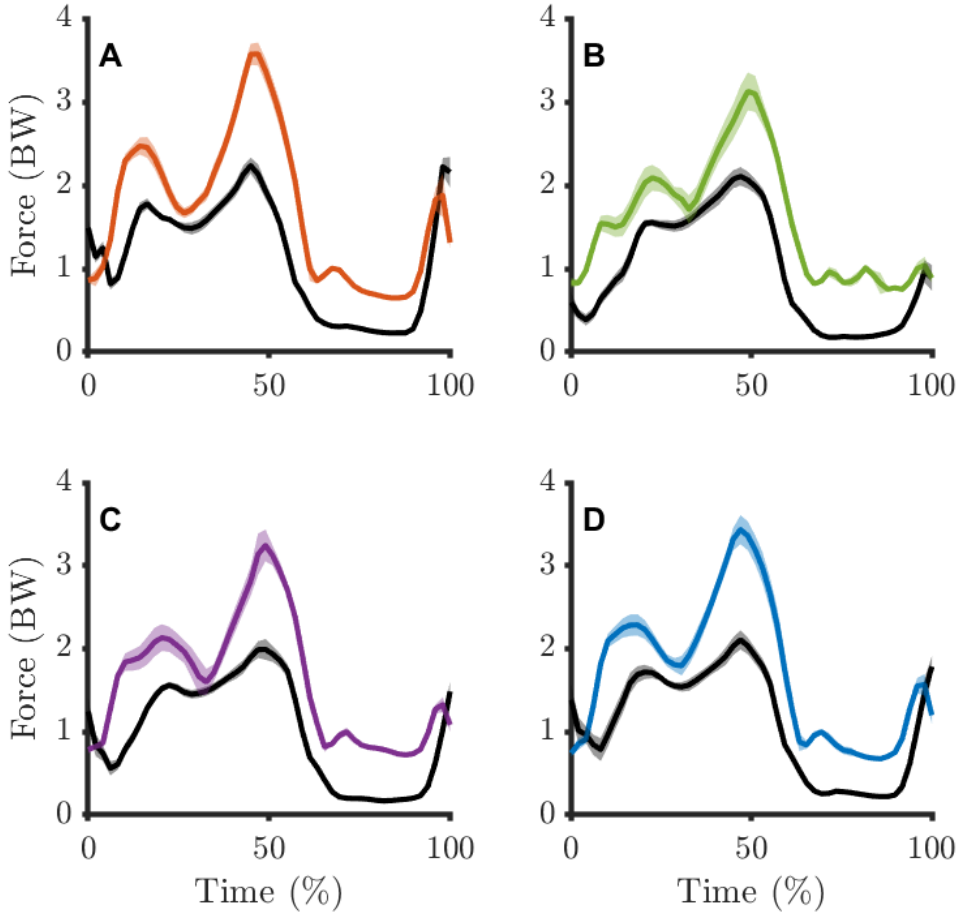

Figure 3-6 Vertical joint reaction forces (blue) and eTibia forces (black) for fast (1.4 m·s^{-1}, A), slow (0.8 m·s^{-1}, B), set (1.0 m·s^{-1}, C) and self-selected (1.2 m·s^{-1}, D) walking speeds. Mean and standard deviation are represented by the thick lines and shaded area, respectively.

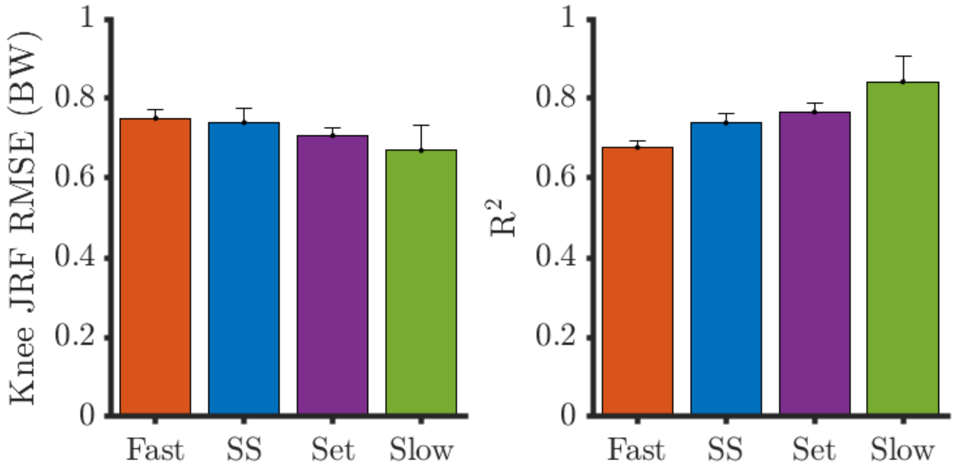

Figure 3-7 Mean root mean squared error (A) and R^2 (B) in the joint reaction force (JRF) estimations for each walking speed relative to the eTibia.

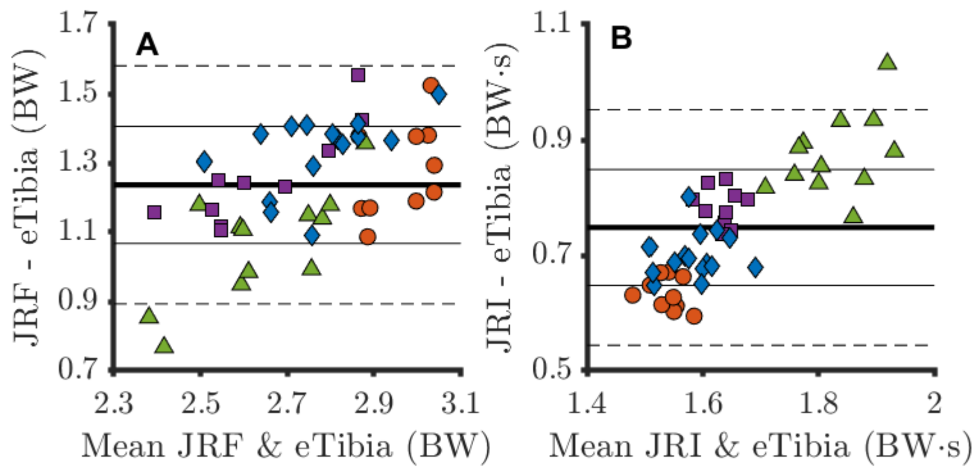

Figure 3-8 Bland-Altman analysis of the simulated peak vertical joint reaction forces (A) and impulses (B) versus the eTibia at fast (1.4 m·s^{-1}, circles), slow (0.8 m·s^{-1}, triangles), set (1.0 m·s^{-1}, squares) and self-selected (1.2 m·s^{-1}, diamonds) walking speeds. Agreement is described by the mean (bold line), standard deviation (solid line), and 95 % limits of agreement (dashed lines).

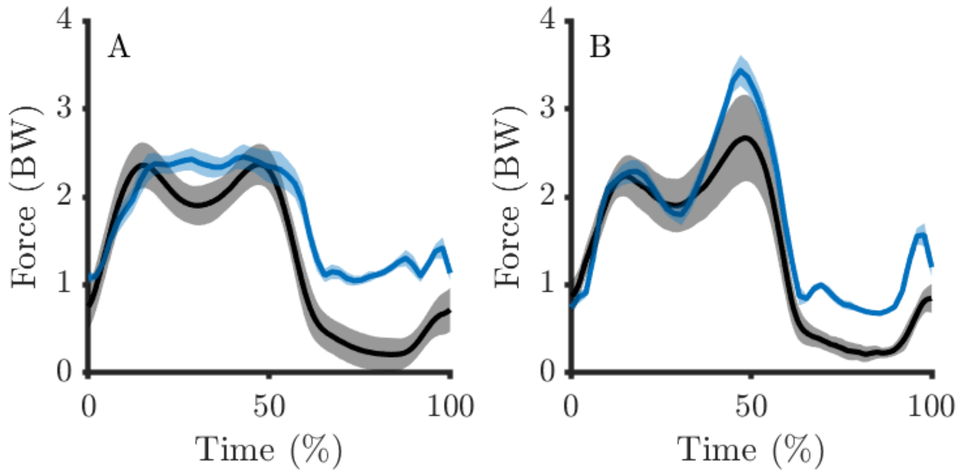

Figure 3-9 Estimate hip (A) and knee (B) vertical joint reaction forces (blue) at a self-selected walking speed (1.2 m·s^{-1}) and the Orthoload data set (black).

Body-Weight Support Case Study

All 5 trials per gravity condition optimised for both initial guesses. Kinematics were tracked to within a maximum error of 3.8° and 0.08 m across all DoF and trials. After removing the pelvis vertical translation (0.08 m), the maximum tracking error fell below 0.02 m. Maximum tracking error across all GRF components and net joint moments were within 0.08 BW and 0.81 N·m·kg^{-1}, respectively. Tracking figures can be viewed in the supplementary material (appendix A). Summed muscle forces of the quadriceps muscles monotonically increased between 0.17 g and 1.0 g (Figure 3-10). There were two distinct patterns in how the muscle forces were distributed amongst the quadriceps between hypogravity (0.17 - 0.50 g) and terrestrial gravity (1 g). In hypogravity, the RF was the main contributor to quadriceps muscle force. However, at 1.0 g the Vasti muscles, particularly the VL, became more dominant, with the RF contributing less force at 1.0 g than at any of the other gravity levels. The estimated repetitions required to elicit a 3.37% increase in muscle CSA monotonically decreased as gravity increased (0.16 g = 1426 ± 99; 0.25 g = 1334 ± 138; 0.37 g = 1164 ± 130; 0.50 g = 1025 ± 184; 1.00 g = 252 ± 14).

Hypothetical training volumes demonstrate that the number of estimated repetitions decreased as gravity level increased. The model estimate that between

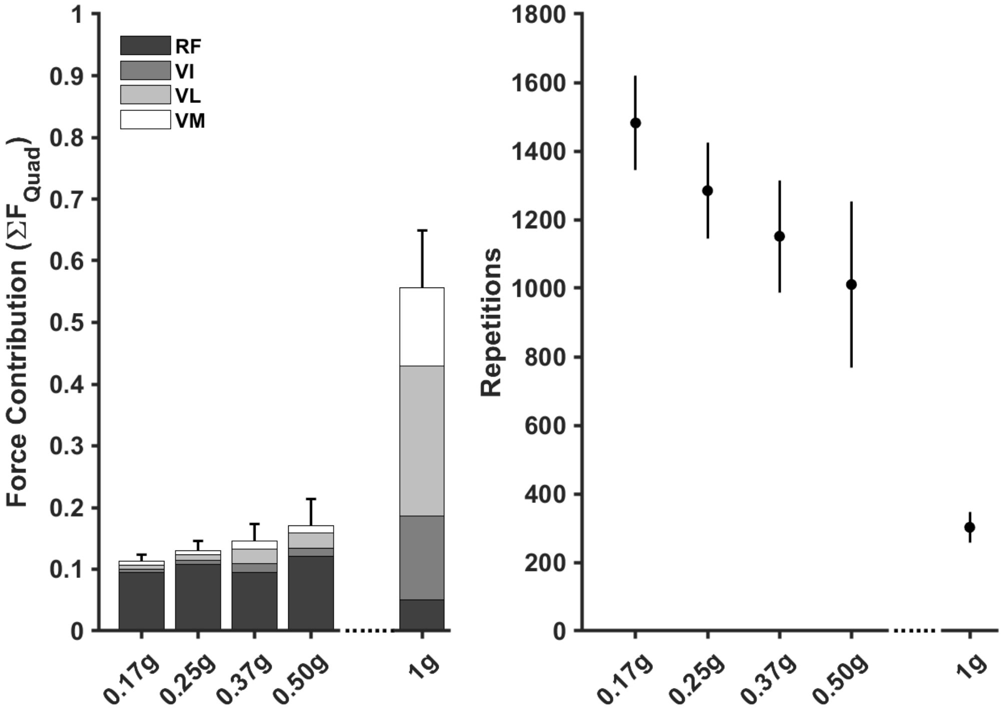

Figure 3-10 Normalised knee extensor muscle forces, stacked to represent the Quadricep muscle group, for each gravity condition (left) were used to estimate repetitions required (mean ± 95% CI) to elicit a 3.37% increase in cross-sectional area (right). RF = Rectus Femoris, VI = Vastus Intermedialis, VL = Vastus Lateralis, VM = Vastus Medias

40 - 29 sets would need to be completed per session as gravity increased from 0.17 g to 0.50 g to achieve a 3.37% increase in CSA. In contrast, only 7 sets would be needed to be completed at 1.0 g.

3.4 Discussion

The first aim of this study was to validate a direct collocation framework for the estimation of JRFs against experimental measured joint contact forces. Our results demonstrate that the simulation framework can estimate knee JRFs to within 0.62 - 0.85 BW (RMSE) across four walking speeds, and captured increased joint loading as walking speed increased. Furthermore, although faster walking speeds were associated with increased error in the JRFs, this increased error appeared to be less influential than step time when estimating JRIs. The second aim was to test the applicability of the framework to hypogravity conditions by comparing the individual quadriceps muscle forces and estimated volume of exercise needed to combat detrimental adaptations at different emulated hypogravity levels. A gravity-dependent organisation of quadricep muscle forces was shown to meet the increasing external demands, with the vasti muscles increasing the force output as gravity increased but the rectus femoris contributing less force as gravity increased from 0.5 g to 1 g. When applied to a muscle adaption model, it was demonstrated that the volume of single-legged hops required in hypogravity is decreased substantially with gravity and a very large number of hops is required to combat adaptations at lower hypogravity levels. This is key information that can be used to identify the appropriate gravity level to use for a specific individual (e.g. 1 g), and identify which muscle groups would be mainly targeted in this condition.

Framework Validation

Our framework was able to estimate JRFs similar in magnitude and shape to experimental knee contact forces measured via instrumented joint implants. At self-selected walking speeds, the framework also estimated knee and hip JRFs with an RMSE of 0.50 BW and 0.6 BW, respectively, of the Orthoload data. Additionally, faster gait speeds are known to increase joint contact forces (Lerner *et al.*, 2014), and we have shown our framework was able to capture this increase. The error in the knee JRF estimations (0.62 - 0.85 BW) and R^2 (0.65 - 0.9) compares well to similar validation studies, with authors reporting values between 0.49 - 0.92 BW and 0.45 - 0.89, respectively (Brandon *et al.*, 2011; Hast & Piazza, 2011; Kinney *et al.*, 2013; Knowlton *et al.*, 2012; Manal & Buchanan, 2012b; Manal *et al.*, 2010; Moissenet *et al.*, 2011). In comparison to a similar data-tracking direct collocation framework, our results are less accurate with estimated joint contact forces reported between 0.24 - 0.32 BW for two participants (Lin *et al.*, 2018). However, Lin and colleagues (2018) estimated joint contact forces using a surrogate model constructed against a elastic foundation model, allowing for a more precise estimation of articular contact forces. Joint reaction forces, as used in this study, represent the net forces remaining to balance Newton's second law of motion once all known forces have been removed (e.g. inertial forces, GRFs and muscle forces). In our case, this would include structures not included within the generic model (e.g. ligaments), which explains the difference found relative to Lin *et al.*. Altogether, combining direct collocation with a generic MSK model was able to capture magnitude differences between walking speeds, which is a key step in the vision for the Biomechanical Handbook, as it allows for comparisons of the biomechanical loading between different exercises and gravity levels. However, it is acknowledged that the framework did not outperform other, less complex algorithms for solving the muscle redundancy problem so that joint reaction forces could be estimated. That being said, save for the Lin *et al.* (2017) study that has been discussed, the previous studies all incorporate some element of subject-specificity or additional complexity into their model, including imaging informed bone geometries (e.g., Thelen *et al.*, 2013) and EMG-assisted simulations (e.g., Manal & Buchanan, 2012a), or a more complex knee model (Brandon *et al.*, 2011; Moissenet *et al.*, 2011), or the joint reaction forces tracking within the framework (e.g., Serrancolí *et al.*, 2020). The purely generic approach taken within this study allows for the framework to be used when only marker trajectories and ground reaction forces are available, which is common practice in biomechanical studies. Additionally, data-tracking simulations using direct collocation have been used as a first step in initialising the framework before performing predictive simulations (e.g., Haralabidis, Unpublished Doctoral Thesis). Given the experimental, equipment, and time constraints associated with spaceflight, the flexibility to predict human movement in space justifies the continued use of the direct collocation approach described in this work.

The comparison of simulated JRF with the eTibia indirectly demonstrates our framework was able to estimate physiologically plausible muscle forces. Muscle forces have a large influence on JRF estimations (DeMers *et al.*, 2014; Steele *et al.*, 2012), thus showing good agreement with the *in vivo* eTibia gave confidence to our muscle force estimations. However, it is important to acknowledge the differences observed between the simulated activations and EMG data. Since the active state of the muscle is not a direct simulation of the EMG signal, it is common practice for authors to scrutinise the onset and offset of muscle activations rather than the magnitude (Hicks *et al.*, 2015; Lund *et al.*, 2012).

Following this approach, the framework estimates the timings of activations well for the grastrocnemii, soleus, tibialis anterior and biceps femoris long head muscles. Simulations frameworks commonly estimate some, but not all, muscle activations within the model - regularly the triceps surae muscles as found in this study - with modest to poor agreement with the remaining muscles (Heintz & Gutierrez-Farewik, 2007; Prilutsky & Zatsiorsky, 2002; Żuk *et al.*, 2018). The inability to measure muscle forces *in vivo* for validation of estimate muscle activations was the main justification of using the eTibia data for this study; the muscle forces are the main contributors to joint reaction forces meaning the cumulative influence of the muscles can be scrutinised via the eTibia comparison. Also, it is difficult to directly measure pattern and magnitude due to normalisation and data collection errors. For example, the age of the participant from the "Grand knee challenge" data set may have influenced the linear envelope of the EMG due to overestimation of the maximum isometric force. Age-related muscle weakness is a well known phenomenon (Moreland *et al.*, 2004), and will not have been captured when calibrating the maximum isometric forces to the participants height and mass. Overestimating the maximum isometric force in this manor would allow the muscle models to generate the same active force at a lower lever of activation. This was observed in our data, where all but the tibialis anterior had comparable or lower muscle activations compared to the EMG data. Therefore, calibrating the maximum isometric force is likely to better align the muscle activations to the EMG data, but would not necessary alter the absolute forces been estimated by the framework.

Framework Validation and Model Personalisation

Although mean error in the JRF estimations was comparable to previous literature, the magnitude of error was not uniform across the step cycle. Specifically, the peak error in the JRFs was 1.23 BW and corresponded to the second peak in the data at ~50% of stance. This is important for characterising load profiles for a biomechanical handbook, because peak values are often extracted to define the load on the joints (e.g. Van Rossom *et al.*, 2018). Overestimating the peak knee JRF is common in studies that do not calibrate MTU parameters and muscle moment arm geometries (DeMers *et al.*, 2014; Marra *et al.*, 2015; Serrancolí *et al.*, 2020; Thelen *et al.*, 2013). In particular, Serrancolí and colleagues (2020) showed that when moment arms are not calibrated the gastrocnemius muscles contribute a large proportion to the knee JRFs. Muscle-tendon unit calibration reduced the second peak through increasing the moment arms of these muscles so they could produce the same joint moment with a reduced muscle force. Having not calibrated the moment arm geometries, it is possible that the mechanical advantage about each joint required the muscles to produce more force to balance the net joint moments. This would explain the increased error in the JRF estimations as the walking speed increased. To illustrate this point, we found that in our data that between self-selected and fast walking the gastronemius medialis contributed ~100 N more force but only ~1.5 N·m more torque to the knee. That being said, the peak JRF reported by this study (2.80 - 3.79 BW) fall well within the wide range of peak knee force values that have been previously estimated during walking gait (1.8 - 8.1 BW) (Fregly *et al.*, 2012). Furthermore, the study that used the most similar generic model to that used here estimated the peak JRF with a 1.7 BW error (DeMers *et al.*, 2014), which exceeds our estimate by almost 0.5 BW on average. De Mers *et al.* (2014) used a static optimisation algorithm, which, while computationally efficient, tends to favour muscles with large maximum isometric forces and does not model muscle activation dynamics. This can lead to non-physiological activation changes between time points and non-physiological muscle force estimations (Lin *et al.*, 2012). This highlights direct collocation provides additional benefit to JRF estimations when using generic MSK models.

JRF Impulse

Impulse is an important factor in describing tissue loading as it captures the magnitude and the duration of application. Our results demonstrate that knee JRI decreased with faster walking speeds, and the error relative to the eTibia impulse also decreased as speed increased. This indicated that the difference in step duration offset the increase in knee joint forces. This is analogous to comparing walking to running where running is associated with substantially higher peak JRFs but comparable impulse per unit distance due to reduced step times (Miller, 2017; Miller *et al.*, 2014). Additionally, the decreased error in the JRI as walking speed increased despite JRF RSME increasing over the same speeds suggests that the reduced step duration may be more influential than JRF magnitude. For example, if the increase in RMSE, because it represents the mean error, had increased more between walking speeds then it would be expected that the JRI error would have remained constant or increased. The importance of JRI to the biomechanical handbook is highlighted by other clinical contexts, where net impulse variables have been shown to better distinguish between populations than peak variables alone (e.g. Kean *et al.*, 2012). Astronaut exercise prescription involves a wide range of exercise modes (Lambrecht *et al.*, 2017; Loehr *et al.*, 2015), that will vary in magnitude and duration of loading. The results give confidence that the comparisons can be made between exercise of different loading durations, as the error in the JRF estimations was not more influential than duration in this study.

The Biomechanical Handbook

Having established our framework was able to provide physiological muscle force and acceptable JRF and JRI estimations, it suggests that a more generic modelling approach is accurate enough to differentiate between load profiles and inform the creation of a biomechanical handbook. The estimation of joint loading could be used to better align the MSK condition of the astronaut upon return-to-Earth to the expected loading on the MSK system for a given exercise. To demonstrate this, the results from the body-weight support case-study highlighted that the quadriceps muscle force increased monotonically to meet the increasing knee extension moment as gravity increased. This aligns with previous research that has shown net joint moments increase when walking with progressively less body weight support (i.e. increasing gravity) (Apte *et al.*, 2018). The normal conclusion from this level of analysis would be that increasing gravity leads to increased loading on the knee musculature. More interestingly, the application of the muscle adaption model provided the biomechanical handbook with an extra dimension. Hypothetical training volumes required to stimulate substantial muscle hypertrophy post-spaceflight and to avoid detrimental adaptations during spaceflight can now be predicted. The feasibility of completing these training volumes within a realistic time frame can then be evaluated. From these data, for this participant, is was shown that single-leg hopping in hypogravity (0.17 g - 0.50 g) would require more than 29 sets of 12 repetitions based on a training schedule of three times per weak.

This is not feasible without risking overused injury. Additionally, the framework showed that while the vasti muscles did monotonically increase their force output with increased gravity, the rectus femoris muscle force was lowest at 1 g. Taken together, this suggests that single-leg hopping in 1 g had the potential to provide an appropriate training stimulus to induce hypertrophy, but with the caveat that the rectus femoris may not receive the same load at the vasti muscles. This suggests that single-leg hopping in 1 g may not be an appropriate exercise mode for stimulating hypertrophy in the rectus femoris, which would not have been captured using net joint moments to describe the loading profile of single-leg hopping. Future research should look to repeat this work with a catalogue of exercises and in various hypogravity conditions to allow for them to be graded and aligned with the astronauts post-spaceflight condition.

The fact that the rectus femoris contributed less muscle force at 1 g than at all hypogravity levels, including 0.17 g, was initially a surprising outcome. It is logical to assume that the 6-fold increase in gravitational forces would require more contribution from the rectus femoris, even if the increase across the quadricep muscles was not uniform as gravity increased. Further analysis into the rectus femoris revealed a shift in RF muscle behaviour between 0.5 g and 1 g (See supplementary material: appendix A). Specifically, the biarticular rectus femoris was being lengthened to a greater extent than the monoarticular vasti, due to increased hip flexion at 1 g, which moved the rectus femoris into the descending-limb of the force-length relationship. From a computational perspective, this made the rectus femoris more expensive in the cost function due to greater activation being required to achieve the same force output, thus encouraging the optimisation to prioritise the vasti muscles to solve the problem. From a physiological perspective, there is evidence that biarticular muscles work to transfer power between joints while the monoarticular muscles work to produce larger active forces (Jacobs *et al.*, 1996; van Ingen Schenau & Bobbert, 1993). This may explain the shift to prioritising the vasti muscles as greater active force became more necessary in 1 g. As this was the first study to estimate quadriceps muscle forces when exercising in hypogravity, further work is needed to understand the roles of biarticular muscles in this context to ensure their loading profiles are accurately represented for hypogravity exercise.

Limitations

It is important to recognise the limitations of the muscle adaption model presented in this study. Mainly, the model does not capture the complexity of tissue remodelling. The model assumes the muscle can only increase in size, and does not capture the decrease in CSA that likely occurs when mechanical stimuli are removed (e.g. during sleep). That been said, the model's parameters are calibrated against a 12-week training program, and will indirectly reflect the periods of rest within the shape of the relationship. Additionally, our understanding of the mechanisms of muscle hypertrophy are not fully understood. The model used here is based on the assumption that the muscle adapts in response to mechanical tension, and does not account for muscle damage and metabolic stress as mechanisms for hypertrophy (Schoenfeld, 2010). Therefore, estimated repetitions should not be taken as an absolute value, but rather for comparison between exercises and to supplement the users own philosophy and experiences. As our understanding of muscle adaptation theory evolves with further research and higher fidelity adaptation models are developed, the muscle forces that can be extracted from MSK modelling, as presented here, can continue to inform the biomechanical handbook. It should also be recognised that the underlyding MSK model was primarily developed based on male participants, validated against a single male and single female participant, scaled to a male participant, and the Knee Grand Challenge data and the vertical hopping case study data were collected from a single male participants, respectively. The results of this study need to be replicated for female derived data to have full confidence in the applicability of the result to women.

Conclusion

A direct collocation simulation framework, integrated with a generic MSK model, was validated in this study against *in vivo* knee contact forces measured via a force-instrumented joint prosthetic. The results demonstrated that the framework was able to estimate physiological JRFs with an error similar to previous research. Importantly, the JRF estimations were able to capture salient features of joint loading, including the double-peak pattern and significant increases of JRF as walking speed increased. This highlights that when subject-specific modelling approaches are not feasible, due to resource constraints, generic MSK modelling can be used to compare loading profiles of exercises for biomechanical handbook-type resources. The applied case-study on hypogravity showed that the biomechanical handbook can provide useful estimation of muscle contributions and exercise volume to avoid detrimental adaptations. More specifically, during single-leg hopping, it was highlighted that while total quadriceps muscle force increased with gravity, the rectus femoris did not follow the same pattern. Future work should look to extend this approach to a catalogue of hypogravity exercise contexts to allow tailoring of astronaut rehabilitation to their MSK condition.

Chapter 4

Movement in Low gravity environments (MoLo) experiment series – The MoLo-Milano Study Protocol

Pre-chapter Commentary

In this chapter an experimental protocol is presented that builds on the Biomechanical Handbook concept presented in the previous chapter. The computation framework will be applied to a wider variety of exercises and gravity levels to quantify the internal loading. This is important for the Biomechanical Handbook as it allows for comparison between exercise contexts to better align them with the astronaut's musculoskeletal condition. Additionally, it was assumed in the previous chapter that the loading between exercises and gravities will be greater than between walking speeds. The increased catalogue of exercises also allows for this assumption to be scrutinised. Therefore, this protocol provides a blueprint for the creation of the Biomechanical Handbook. The protocol described within this chapter was originally intended to form the main data collection for this thesis. The impact of the COVID-19 pandemic meant that travel to the University of Milan was not possible during the time frame of this thesis. I wanted to include the protocol to give context to the case-study described in chapter three by highlighting that a more comprehensive biomechanical data collection was planned to inform the creation of Biomechanical Handbook

Abstract

Exposure to prolonged periods in microgravity is associated with deconditioning of the musculoskeletal system due to chronic changes in mechanical stimulation. Given astronauts will operate on the Lunar surface, it is critical to quantify both the external (e.g., ground reaction forces) and internal (e.g., joint reaction forces) loads during a catalogue of exercises in variable gravity levels. This information can be used to inform the creation of a *Biomechanical Handbook* resource to inform exercise countermeasures during and after spaceflight. The aim was to create a comprehensive Biomechanical Handbook of normative muscle and joint reaction loading profiles by integrating a hypogravity biomechanical data set of gait and jumping into a computational framework. A total of 26 healthy participants will be recruited for this cross-sectional study. Participants will perform gait (walking, running and skipping) and jumping (vertical hopping, vertical countermovement jumping, drop landing) trials at different simulated hypogravity-levels (1g, 0.7g, 0.5g, 0.38g, 0.27g, 0.16g) in a randomized order. Body motion, centre of mass, ground reaction forces, muscle architecture and tendon length will be recorded via a motion capture system, force platforms, wireless EMG, and ultrasound, respectively. A computational approach is adopted to calculate centre of mass movement and estimate lower-limb muscle forces and joint contact forces by tracking the *in vivo* data. This information will provide key information regarding expected internal musculoskeletal loading whilst exercising in hypogravity to inform the creation of a Biomechanical Handbook. This resource can be used to make comparisons between exercise and hypogravity contexts to align expected loading with the individual's musculoskeletal condition.

4.1 Introduction

The exposure to prolonged periods in microgravity is associated with deconditioning of the musculoskeletal system (Lang *et al.*, 2017; Stavnichuk *et al.*, 2020b; Winnard *et al.*, 2019), including bone mineral density loss, muscle atrophy, and muscle weakness (Korth, 2015), and substantial inter-individual variability (Scott *et al.*, 2021). Such changes are due to the fact that musculoskeletal tissues are mechanosensitive (Goodman *et al.*, 2015), precipitating shifts in remodelling if exposed to chronic changes in mechanical stimulation. Given the European Space Agency (ESA) astronauts will, as part of the Artemis programme, operate on the Lunar surface it is critical to quantify both the external (e.g. ground reaction forces) and internal (e.g. joint reaction forces and muscle-tendon forces) loads associated with locomotor and plyometric activities performed in variable gravity levels (g). Such knowledge can be used to create a *Biomechanical Handbook* resource that presents normative musculoskeletal (MSK) loading profiles of key rehabilitation exercises to match the exercise specific loading according to the astronaut's specific post-spaceflight MSK condition. This is similar to the approach used by Van Rossom and colleagues (2018), who quantified the magnitude and location of tibiofemoral and patellofemoral contact forces for common rehabilitation exercises. They proposed to use this type of information to grade exercises according to their biomechanical loading profile, to better align the patient's injury and rehabilitation stage with exercise prescription.

There is a substantial body of research demonstrating the association between (simulated) hypogravity and the reduction of external kinetics. For instance, studies conducted in the L.O.O.P. (Locomotion on Other Planets) Ground Based Facility of the University of Milan demonstrated reduced external and internal work when running and skipping in simulated hypogravity using a vertical body weight support, compared to the 1g condition (Pavei *et al.*, 2015; Pavei & Minetti, 2016). Furthermore, hip, knee and ankle net joint moments have been shown to monotonically decrease when walking in simulated hypogravity (Apte *et al.*, 2018). Similarly, peak vertical ground-reaction force (GRF) was reported to positively relate to simulated gravity level (0.16g, 0.27g, 0.38g, and 0.7g) during sub-maximal plyometric hopping (Weber *et al.*, 2019). However, during walking with 30% body weight support (i.e. 0.7g) muscle-tendon (fascicle–series elastic element) behaviour of the gastrocnemius was preserved during walking (Richter *et al.*, 2021b), but not running (Richter *et al.*, 2021a). Whether, this is the case for lower g levels or other exercise modes is at present unknown. On the International Space Station (ISS), gravity replacement load systems are employed during inflight exercise to combat decreases in external kinetics. Whilst comprehensive external kinetics data is lacking, the GRFs and joint kinetics experienced at 1g are neither replicated on the T2 treadmill (De Witt & Ploutz-Snyder, 2014; Genc *et al.*, 2010; McCrory *et al.*, 2004), or the Advance Resistive Exercise Device (ARED) (Fregly *et al.*, 2015). This inability to provide 1g-equivalent musculoskeletal loading whilst exercising in microgravity on the ISS presumably contributes to crew returning to Earth with compromised functional capacity (Petersen *et al.*, 2016). Whether this would be the case in constant Lunar hypogravity is unknown.

To close this knowledge gap it is critical to understand how hypogravity-induced decrements in external kinetics during movement are associated with changes in internal joint forces (e.g. the ones experienced at joint, muscle-tendon and bone level). For instance, with the same external loading, joint contact forces driving bone remodelling can diverge as they are significantly modulated by the muscle forces generated during the movement (DeMers *et al.*, 2014). Also, muscle adaptation models (e.g. Wisdom *et al.*, 2015) use muscle activation or forces as inputs to investigate whether internal forces associated with movement are sufficient to maintain or promote musculoskeletal homeostasis. In computational biomechanics, joint reaction forces and muscle-tendon forces can be estimated from joint kinematics and external load measurement using musculoskeletal or finite element modelling approaches. When combined with muscle adaptation models it is possible to estimate a hypothetical exercise volume that elicits a meaningful increase in muscle size, to better bridge the gap between theoretical musculoskeletal models and practice. However, currently there is no compelling evidence for the application of such approaches in hypogravity. Musculoskeletal modelling approaches have instead been applied to microgravity to simulate squatting using the Advanced Resistance Exercise Device (Fregly *et al.*, 2015) and to inform design of a lower extremity resistive device to replicate 1g mechanical loading (Han *et al.*, 2020). The only computational study focusing on hypogravity sought to predict locomotive strategies (Ackermann & van den Bogert, 2012) but did not provide any insight on the internal loads experienced during locomotion or plyometric exercises.

Recent research has highlighted plyometric-type exercise as an effective and efficient way of loading the musculoskeletal system – thereby mitigating the de-conditioning including loss of lean mass, bone mineral density and bone mineral content (Kramer *et al.*, 2017), and functional performance (Kramer, Kümmel, *et al.*, 2018a) associated with unloading. The generation of high external forces, as seen during plyometric movements, is considered a key component in the mechano-stimulation of remodeling in both bone (Frost, 1987, 2003), and muscle (Schoenfeld, 2010). Interestingly, there is evidence that peak ground reaction forces comparable to 1g can be achieved in simulated hypogravity (0.16g, 0.27g, 0.38g, and 0.7g) when performing sub-maximal hopping (Weber *et al.*, 2019). Unfortunately, hop height was constrained by the experimental facility used, and thus whether similar relationships are evident during maximal hops and other forms of explosive jumping (e.g. countermovement jumping and drop landing) is currently unknown. In fact, the only ground-based analogue that currently allows to explore such relationships is the L.O.O.P. It is also critical that muscle-tendon and joint reaction forces are evaluated to determine their potential role in musculoskeletal regulation. The L.O.O.P allows simultaneous measurement of 3D kinematics, ground reaction forces, and muscle-tendon imaging during both locomotion and maximal ballistic (jumping) movements in high fidelity (i.e., constant off-loading) simulated hypogravity.

Thus, by using the L.O.O.P. we aim to inform the creation of a *Biomechanical Handbook* via: i) the collection of a unique dataset of body kinematics, ground reaction forces, muscle activation, and muscle-tendon behaviour at incremental hypogravity levels (1g, 0.7g, 0.5g, 0.38g, 0.27g, 0.16g), and ii) integrate musculoskeletal models and optimal control frameworks to estimate the musculoskeletal loading at the muscle and joint level during locomotion activities and maximal plyometric exercise.

4.2 Materials and Methods

Study Design

This study will be of a cross-sectional study design. Participants will be asked to make two visits to the University of Milan, where the first visit will be used to familiarise participants with the vertical body weight support system and the performance of walking, running, hopping, and skipping using the L.O.O.P. GBF. During the second visit, participants will perform locomotion (i.e., walking, running and skipping) trials and, after a 1 hour break, plyometric (i.e., vertical hopping, vertical countermovement jumping, and drop landing) trials at a range of different simulated hypogravity levels (1g, 0.7g, 0.5g, 0.38g, 0.27g, 0.16g) in a randomized order.

Ethics Approval

The study received ethical approval form the Research Ethics Approval Committee for Health of the University of Bath, the Ethics Committee of the University of Milan, and was approved by the European Space Agency Medical Board. All participants will be asked to give written informed consent in accordance with the Declaration of Helsinki after having received written and oral explanation of the study and after having given the opportunity to ask any additional question they might have about the study.

Study Population

Twenty-six healthy participants (13 males and 13 females) will be included. All participants will be recruited through a combination of convenience sampling and snowball sampling. Initial contact will be made via word of mouth in line with the usual processes of the University of Milan. Thereafter, recruitment via word of mouth from previous volunteers will run in parallel.

To be eligible for inclusion, volunteers can either be male or female and must meet the following eligibility criteria:

Inclusion:

- Adults between the age of 18 and 64 years.
- Being physically active, defined as at least 30 minutes of moderate-to-vigorous physical activity three times per week.
- Individuals who have the ability to understand the explanations and instruction related to the present study, either in English or Italian.

Exclusion:

- Unable to walk, run, or jump without an assistive device or the help of another person.
- Any current lower-limb injury that prevents the participant from performing high impact movements such as jumping.
- Any injury or condition that prevents the wearing of a safety harness, required for the body weight support system.
- Any other (severe) visual, neurological, cardiovascular, or musculoskeletal impairment that impedes the proposed procedures.

Sample Size

Sample size calculations were performed using data from a pilot data collection of a single male (29 years, 1.82 m, 79.9 kg) performing single-leg vertical hopping whilst attached to the same body weight support system for a range of hypogravity conditions (0.16g, 0.25g, 0.37g, 0.50g, 1g). The same set-up and analysis, including the simulation framework, was performed on these data as is planned in this protocol (see below). Mean and standard deviations of peak hip, knee, and ankle vertical joint reaction forces, and peak gastronemius lateralis and medialis, and vastus lateralis muscle-tendon unit forces were extracted for sample size calculations. These variables represent the main outcome variables of this protocol, and, therefore, it is important to appropriately power the analyses of these variables. For the ultrasound variables, the gastronemius medialis fascicle lengths and pennation angles were extracted from Richter and colleagues (2021b).

This study was identified due to the use of a similar body weight support system, and a comparable ultrasound set-up to that proposed in this protocol. Sample size calculations require an estimation of minimal detectable difference, based on the variance in the variable being powered for statistical analysis. The sample size calculation from a single participant is not perfect, as the variability within the single participant cannot be scrutinised relative to a group of participants. However, this will be the first study to investigate the influence of gravity on internal MSK loading (e.g., muscle forces and joint reaction forces) and the pilot data represents the only data available to inform variance in the outcome variables. A *Post Hoc* power analysis will be conducted after study completion to re-evaluate the sample size used.

Mean and standard deviation values were extracted and Cohen's D effect sizes were calculated. The effect sizes were used to calculate the appropriate sample size using G*Power (Faul *et al.*, 2007) based on a two-tailed, repeated measures t-test, where $p = 0.05$. From the calculations, a sample size of 26 participants was identified. This value achieved at least 80% power for the ultrasound variables, and at least 95% power for the remaining variables.

Experimental Set-up

The objectives of the study requires the use of the validated body weight support system. The L.O.O.P GBF of the University of Milan (Pavei *et al.*, 2015; Pavei & Minetti, 2016) uniquely allows for the offset of gravity whilst simultaneously recording 3D kinematics, ground reaction forces, and electromyography during locomotion activities and plyometric exercises.

L.O.O.P Ground Based Facility

The L.O.O.P. facility is located within a narrow (3 x 3 m) and tall (17 m) space inside the Human Physiology building of the University of Milan where the calibrated bungee cords provide body suspension (Pavei *et al.*, 2015; Pavei & Minetti, 2016), which will be combined with a motorized treadmill (Bertec, Columbus, USA) provided by the German Aerospace Center (DLR). The suspension device consists of two bungee cords (Exploring Outdoor srl, Italy) with a resting length of 4 m and a stiffness of 92.7 $N \cdot m^{-1}$. These bungee cords are linked in-series with an inextensible short cable (Dyneema SK78, diameter 4 mm, length 1.2 m, Gottifrede & Maffioli, Italy), working on the upper pulley. One end of the bungee cords is fixed to the wall, while the other is connected to a force transducer (TS 300kg, AEP Transducers, Modena, Italy) placed in series with a body harness. The mobile pulley can be raised or lowered by means of a suspension cable which is connected to a motorized winch (E.C.E, 750 W, Italy) allowing for the unloading of the body to a set hypogravity level (1g, 0.7g, 0.5g, 0.38g, 0.27g, 0.16g) according to bungee force measured via the transducer.

What discriminates this hypogravity simulator from other simulators is that the upper pulley is located high above the subject (16 m), which reduces the horizontal forces that could be generated due to the small fore-aft and lateral displacements during locomotion on the treadmill. For example, at simulated Lunar gravity (0.16g), a horizontal movement of 0.03 m with respect to the pulley results in an additional horizontal force of 0.92 N, representing 0.4% - 0.7% of the peak push-off force during terrestrial (1g) stance respectively (Nilsson & Thorstensson, 1989). Additionally, the height of the shaft allows the use of only one pulley to accommodate for the 20 m (when extended, 2 x 10 m) bungee cords, which limits friction and displacement, independent of vertical force (Pavei *et al.*, 2015). However, it is important to note that, although this set-up provides accurate reproduction of hypogravity by applying near constant vertical forces to the body's centre of mass, the swinging limbs are still under the effect of 1g.

Study Hardware

Motion Capture Set-up

The L.O.O.P. is equipped with a three dimensional motion capture system consisting of a total of 20 cameras (MX Cameras, Vicon Motion Systems Ltd, Oxford, UK) measuring marker trajectories at a frequency of 200 Hz. A CAST marker set (Cappozzo *et al.*, 1995) consisting of 37 retro-reflective markers placed on anatomical locations and eight four-marker rigid-clusters will be used. The anatomical markers will define segments for the pelvis, head-trunk, and bilaterally the thigh, shank, foot, toes, upper-arm, and forearm.

Motorize Treadmill

A split-belt instrumented treadmill (total walking surface: 1.75 x 1m; speed range: 0.00 – 5.83 m·s^{-1}; Bertec, Columbus, USA) records ground reaction forces (F) and moments (M) from each belt (Fx, Fy, Fz, Mx, My, Mz) at a sampling rate of 2000 Hz which will be integrated within the 3D-Motion Analysis System.

Surface Electromyography Set-up

Sixteen wireless electromyography (EMg) sensors (Trigno Sensor, Delsys, US) will be positioned according to SENIAM guidelines[1] to assess the myoelectrical activity of the gluteus maximus, rectus femoris, vastus lateralis, biceps femoris (lateral hamstrings), semitendinosus (medial hamstrings), tibialis anterior, m. gastrocnemius and soleus bilaterally. Recording areas will be shaved, abraded, and cleaned with an alcohol wipe/swab prior to electrode placement. EMG signals will be high-pass filtered, full-wave rectified, and low-pass filtered using a zero-lag second-order Butterworth filter. Signals will be normalised to each participant's maximum excitation, defined as the maximum value recorded across all dynamic trials for each muscle according to SENIAM guidelines.

Ultrasonography Set-up

Real-time B-mode ultrasound (Prosound α7, ALOKA, Tokyo, Japan) captured at 73 Hz using a T-shaped 6cm linear array transducer (13 MHz), placed in a custom-made cast and secured with elastic Velcro, will be positioned over both the m. gastrocnemius mid-belly to determine fascicle length and pennation angles (Richter *et al.*, 2021b), and over the myotendinous junction to determine tendon length (Stäudle *et al.*, 2020; Werkhausen *et al.*, 2019). The ultrasound recordings will be time-synchronized via a rectangular TTL pulse generated by a hand switch recorded on the electrocardiography channel of the ultrasound device and the MyoResearch software (Noraxon USA Inc., Scottsdale, Arizona, USA). A semi-automated tracking algorithm (UltraTrack Software, Farris & Lichtwark, 2016) will be used to quantify the muscle fascicle length and pennation angles during the stance phase. The ultrasound tracking procedures are well established and have been used in previous studies (Werkhausen *et al.*, 2021).

[1] https://www.seniam.org/

Data Collection Protocol

Each participant will be given time to perform a self-selected warm-up, consisting of light aerobic exercises and dynamic mobility before completing the experimental protocol. Prior to dynamic trials, static calibrations will be collected with participants quietly standing within the motion capture volume and on the force instrumented treadmill. All dynamic movements will be performed in a random order for a given hypogravity before moving to the next condition, the order of the simulated hypogravity conditions (1g, 0.7g, 0.5g, 0.38g, 0.27g, 0.16g) will also be randomised.

First, all locomotion trials will be performed continuously for one minute in a randomized order for all hypogravity conditions and consist of:

- Three walking speeds: 0.56 $m{\cdot}s^{-1}$, 1.11 $m{\cdot}s^{-1}$, and 1.39 $m{\cdot}s^{-1}$.
- Five running speeds: 1.39 $m{\cdot}s^{-1}$, 1.94 $m{\cdot}s^{-1}$, 2.50 $m{\cdot}s^{-1}$, 3.06 $m{\cdot}s^{-1}$, and 3.61 $m{\cdot}s^{-1}$.
- Two skipping speeds: 1.94 $m{\cdot}s^{-1}$ and 2.50 $m{\cdot}s^{-1}$

These speeds were identified in order to enable the same gait at different hypogravity levels and match the speeds used in previous studies (Pavei *et al.*, 2015; Pavei & Minetti, 2016), which allows to analyse the behaviour of the muscle-tendon unit and joint internal load in relation to the cost of transport curve.

After a one hour break to reduce the influence of fatigue, all plyometric trials will be completed for all hypogravity conditions in a randomized order:

- Vertical hopping will be performed in a single ramp-up-ramp-down trial consisting of 30 consecutive hops building from very shallow to maximum jump height and back to shallow ones (Weber *et al.*, 2019). Audio and visual feedback will be provided.
- Three maximum effort vertical countermovement jumps will be performed.
- Three drop-landings will be performed.

Self-selected rest periods will be allowed between the different trials and gravity conditions to mitigate potential fatigue, and any discomfort association with the harness.

Outcome Measures

For each locomotion and plyometric trial, 3D kinematics, ground reaction forces, electromyography and ultrasound will be simultaneously recorded.

Antropometrics

For each participant, age (years), body weight (kg), height (m) and leg length (m) will be collected.

Biomechanical Outcome Parameters

Primary outcome parameters will be joint reaction forces for the hip, knee and ankle to quantify joint loading, estimated through a direct collocation data-tracking simulation framework (see 'Planned Data Analysis') implementing several secondary outcomes. Secondary outcome parameters include ground reaction forces extracted from the force instrumented treadmill thus providing data on external forces acting on participants during movement. Ground reaction forces will also be used to identify gait events (i.e., single and double support phase, flight time, contact time) and for segmenting dynamic trials into single cycles for further analysis. Additionally, the generic musculoskeletal model will be scaled to each participant's anthropometrics and mass using 3D-marker trajectories and the participant's mass recorded during the static calibration trials. OpenSim's (Delp *et al.*, 2007; Seth *et al.*, 2018) inverse kinematics and inverse dynamics algorithms will be used to gain information about the model's pose (i.e., positions and angles of the degrees of freedom, m or °) and velocities (i.e., the time derivative of the positions/angles, $m \cdot s^{-1}$ or $° \cdot s^{-1}$), and net joint kinetics (i.e., net joint moments and forces, N·m or N) for each dynamic trial.

Muscle Structure & Function Outcome

During the different locomotion trials and plyometric exercises, ultrasound images from the muscle belly and myotendinous junction will be analysed to collect information on tendon strain, muscle fascicle length (the distance between the insertion of the fascicles into the superficial and the deep aponeuroses, mm), pennation angle (the angle between the fascicle and the deep aponeurosis, °), and fascicle velocity (the time derivative of the fascicle length, mm·s^{-1}).

Planned Data Analysis

Musculoskeletal Modelling and Simulation

Skeletal motion was modelled as rigid body dynamics using Newtonian mechanics, with compliant Hunt-Crossley contacts to model the foot-ground interaction. The collected data will be used as input into optimal control problems (OCPs). This framework uses a direct collocation method to track experimental kinematics, net joint moments, and ground reaction forces for a single movement cycle. A movement cycle being defined as two successive heel contacts of the right foot for the locomotion trials, and one contact and subsequent flight phase for the jumping exercises. The goal of the simulation is to minimise a cost function, consisting of a muscle-sharing term, data tracking terms and control variable minimisation terms, to estimate muscle activations for a given moment. The framework is designed to track the experimental data with zero pelvis residuals to elicit a dynamically consistent solution, before estimating the joint reaction forces from the simulated muscle activations. A generic OpenSim musculoskeletal model that has been validated for high knee flexion movement will be used within the framework (Figure 4-1, Lai *et al.*, 2017). The model consists of 23-segments – ground, pelvis, torso, and, bilaterally, femur, patella, tibia-fibula, talus, calcaneus, toe, humerus, radius, ulna and hand – and 37 degrees of freedom (DOF). Pelvis translation and rotation with respect to the ground are modelled as a six DOF joint. The torso-pelvis, shoulder, and hip joints are modelled as three DOF ball-and-socket joints, the wrists as two DOF universal joints, whilst ankle, subtalar, elbow, radioulnar and metatarsophalangeal (MTP) joints are modelled as one DOF hinge joints. The MTP and wrist joints are locked at 0°. The tibiofemoral joint (knee) is modelled as a 1-DOF hinge joint, with a 0-140° flexion range. The remaining tibia rotations and translations relative to the femur, and the sagittal plane patellofemoral joint motion (i.e. anteroposterior and vertical translation, and rotation about the mediolateral axis), are defined

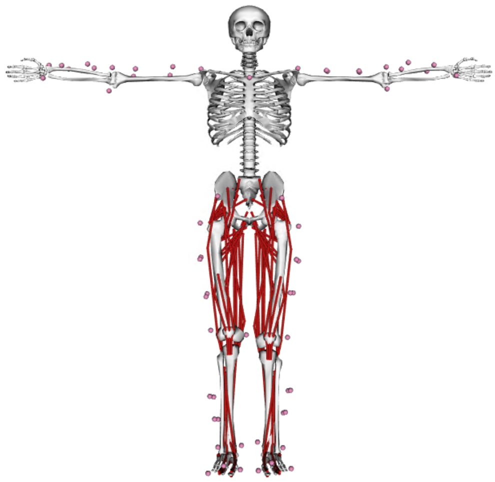

Figure 4-1 The generic musculosckeletal model used in this study. Pink spheres represent marker locations, and red string elements the muscle-tendon unit geometries.

by polynomials as a function of knee flexion. The hip, knee, ankle, and subtalar DOF are actuated by 80 Hill-type MTU, with the torso and upper body driven by 17 ideal torque actuators. The generic musculoskeletal model will be linearly scaled within OpenSim. Scale factors will be calculated from experimental marker data to scale anthropometrics (i.e. segment length, width and depth), inertial parameters (i.e. segment masses and moments of inertia), muscle-tendon unit model parameters and geometries (i.e. maximum isometric forces, optimal fibre length, pennation angle at optimum fibre length, tendon slack length, attachment sites and moment arms) to each participant. The lower-limbs are driven by 80 Hill-type muscle models (Zajac, 1989) Polynomials will be constructed to describe the muscle-tendon unit lengths, velocities and moment arms, estimated for a wide rage of joint angles using OpenSim's muscle analysis tool, as a function of joint angle and joint angular velocity (Falisse, Serrancolí, Dembia, Gillis, & De Groote, 2019; Van den Bogert *et al.*, 2013). The remaining 25 coordinates are driven by torque actuators. Twelve sphere elements (six per foot) will be added to model the foot-ground interaction. Hunt-Crossley equations, modified to be twice continuous (Serrancolí *et al.*, 2019), will be used to calculate the forces at each sphere (two attached to the toes, four to the calcaneus) as a function of ground penetration and penetration velocity.

Foot-ground contact sphere stiffness and damping (constant across all spheres) and their position coordinates will be included as static parameters within the optimisation (p_{cm}). The remaining friction, radii and transition velocity parameters will be kept constant. The state variables, q and $\dot{q}$, which correspond to the positions and velocities of each DOF, respectively, will be controlled by the coordinate accelerations, $u_{\ddot{q}}$. Muscle-tendon unit contraction and activation dynamics will be formulated according to De Groote *et al.* (2016) and Raach's model (De Groote *et al.*, 2009; Raasch *et al.*, 1997), respectively. Muscle activations, a_m, and normalised tendon forces, $\tilde{F}_t$, are introduced to describe the MTU state, with their first time derivatives, u_{a_m} and $u_{\tilde{F}_t}$, introduced as control variables (De Groote *et al.*, 2016). The state of idealised torque actuators are described by their activations, a_τ, and controlled by their excitation, u_τ. Control variables are introduced for the ground reaction forces, u_{GRF}, as done previously (Serrancolí *et al.*, 2019). This improves the convergence rate as the foot-ground contact sphere forces are subject to large fluctuations for small adjustments to the skeletal kienamtics. Reserve actuators may be added to muscle-driven DOF as control variables, u_{res}, that described the instantaneous moment being produced, to help convergence of the simulations.

The objective function will be formulated to minimise muscular effort and error between simulated and experimental data. Additional terms will be included to achieve physiologically realistic simulations. Muscle-sharing will be achieved through minimisation of the summed muscle activations squared. Squared activations are weighted by muscle volume to replicate a minimisation of muscular effort simulation (Ackermann & van den Bogert, 2010). This approach has been successfully used in submaximal (Lin & Pandy, 2017) and maximal effort simulations (Haralabidis *et al.*, 2021) and is deemed appropriate for all the movements in the protocol. Data-tracking terms were formulated as the squared error between experimental and simulated data for kinematics (angles and positions), ground reaction forces, and net joint moments. Tracking terms will be scaled to ensure terms are of numerically similar magnitudes within the objective function. Minimising the sum of squared terms will be included for reserve actuators (where appropriate) and control variables ($u_{\ddot{q}}$, u_{a_m}, $u_{\tilde{F}_t}$) (Falisse, Serrancolí, Dembia, Gillis, Jonkers, *et al.*, 2019; Haralabidis *et al.*, 2021).

The validity of the simulations will be assessed through comparison with the experimental data, and the cost function weights modified to achieve accurate data-tracking and physiologically realistic simulations. The objective function, including weightings, will be kept constant once calibrated.

The framework (Figure 4-2) is implemented in MATLAB (Mathworks INC., USA) using CasADi (Andersson *et al.*, 2019), and is solved using IPOPT (Wächter & Biegler, 2006). A modified version of OpenSim and SimBody will be used to allow for algorithmic differentiation. Algorithmic differentiation allows for efficient and truncation-free evaluation of derivatives required by a NLP, which can lead to an almost 20-fold decrease in simulation time (Falisse, Serrancolí, Dembia, Gillis, & De Groote, 2019). The OCPs will be transcribed into nonlinear programs (NLP) via a direct collocation method. The state ($\mathrm{x} = [q,\ \dot{q},\ a_m,\ \tilde{F}_t,\ a_\tau]$) and control ($\mathrm{u} = [\ddot{q},\ \mathrm{u}_{a_m},\ \mathrm{u}_{\tilde{F}_t},\ \mathrm{u}_{GRF},\ \mathrm{u}_\tau,\ \mathrm{u}_{res}]$) trajectories will be initially discretised into 50 equally spaced time intervals (Ackermann & van den Bogert, 2010). The number of intervals will be tested following data collections to whether more or less are needed to achieve appropriate simulation outcomes. The state trajectories were further discretised into three-point intervals (collocation points) between time points using Legendre-Gauss-Radau quadrature, and approximated with third-order polynomials.

The skeletal dynamics and activation dynamics are imposed as implicit constraints at each collocation point as first-order differential equations (De Groote *et al.*, 2009). Explicit dynamic constraints are imposed on the excitation-activation dynamics of the idealised torque actuators as electromechanical delayed linear approximations (Falisse, Serrancolí, Dembia, Gillis, Jonkers, *et al.*, 2019). Path constraints are imposed at the beginning of each interval to achieve physiologically appropriate solutions. The muscle forces are related to the experimental net joint moments via implicit constraints according to their polynomial-computed moment arms and the reserve actuators. Additional constraints imposed dynamical consistency by setting pelvis residuals to zero. The u_{GRF} controls will be related to the foot-ground contact model as implicit constraints. Raasch's model was imposed on the muscle activations via two inequality path constraints based on the time of activation (0.015 s) and deactivation (0.06 s) of u_{a_m} (De Groote *et al.*, 2009). The Hill-equilibrium condition is implicitly imposed by enforcing the muscle forces projected along the tendon to match the tendon forces. Continuity of the state variables between the end of collocation interval and the next time step will be enforced via implicit constraints. All variables will be scaled and bounded between -1 and 1 to ensure numerically similar magnitudes between optimised variables (Betts, 2010). The scale factors will be determined with a similar approach to Falisse *et al.* (2019). These scale factors differ from those used to scale variables within the cost function.

Best practise guidelines will be used after each simulation to assess tracking accuracy and physiological realism of the results (e.g., Hicks *et al.*, 2015). Tracking accuracy will be quantified via maximum and root mean squared error (RMSE) between simulated and experimental kinematics, GRFs and NJT. Simulated muscle activations will be qualitatively compared to the EMG in terms of timing and magnitude of the signals. Additionally, fascicle lengths and velocities, and pennation angles from the ultrasound images will be compared to the simulated muscle-tendon unit behaviour. Once validate, simulated kinematics, GRFs and muscle-tendon unit forces will be used to calculate joint reaction forces using OpenSim. Muscle-tendon unit forces will be input into a muscle adaption model (Wisdom *et al.*, 2015). The adaptation model estimates the rate of change in cross-section area (CSA) of a muscle based on the degree of overload experienced, the muscle's current CSA, a physiological maximum possible CSA, and a minimum load threshold required to trigger adaption. The model assumes muscle adapts in response to overload by addition of sarcomere in parallel, and CSA increases in an exponential fashion before converging to a new homeostatic equilibrium. Contractile element and parallel elastic element forces will be summed and normalised to their maximum isometric force defined in the OpenSim model before being input into the adaptation model. These two elements are assumed to represent the load experience by the muscle belly that will lead to CSA adaptations (i.e. not the tendonous regions). A minimum load threshold of 0.2 will be used to replicate 20% one-repetition maximum, which is sufficient to elicit hypertrophic benefits to resistance training under the right conditions despite the low-load (Schoenfeld, 2013). The remaining parameters will be informed by Wisdom *et al.* (2015). The number of repetitions required to

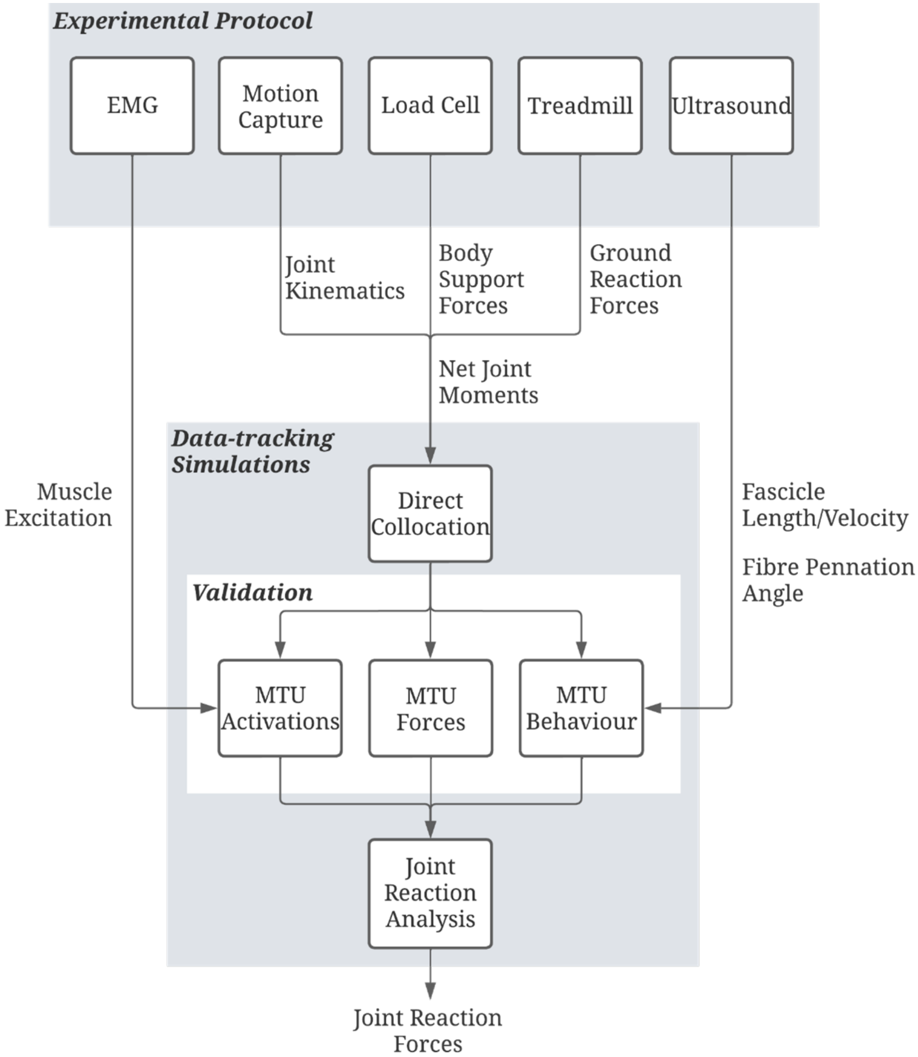

Figure 4-2 A schematic of the data workflow to obtain the main outcome measure, joint reaction forces. Experimental data are fed into the direct collocation optimal control framework to perform data-tracking simulations. Experimental EMG and ultrasound data are compared to simulated muscle-tendon unit (MTU) activations and behaviour, respectively, to validate the simulated MTU outcomes. The MTU outcomes are then used to inform a joint reaction analysis to calculate the joint reaction forces as a function of simulated kinematics, external loads, (ground reaction and support forces), and MTU forces. EMG = electromyography

generate hypertrophy will be estimated based on a minimal worthwhile increase in CSA of 3.37%. The minimal worthwhile increase is taken from the same study the model was originally validated against (DeFreitas *et al.*, 2011) based on the minimal worthwhile change calculations of Weir (2005).

Statistical Analysis

All data will be analysed using SPSS Software (IBM Corp. Released 2020, IBM SPSS Statistics for Windows, Version 27.0, Armonk, NY). The level of significance will be set at p = 0.05. At first, normality of the data will be assessed using the Kolmogorov-Smirnov test, QQ plots and histograms. In case of normally distributed data, these will be presented as mean (SD), non-normally distributed data will be presented as median (IQR).

The effect of simulated gravity (1, 0.7, 0.5, 0.38, 0.27 and 0.16g) upon lower limb internal kinetics (i.e., joint reaction forces) when walking, running, and skipping at speeds ranging between 0.53 - 3.6 m·s^{-1} will be determined by a Two-Way Repeated Measures ANOVA with:

- Independent variables: six simulated gravity conditions; 10 locomotion trials
- Dependent variables: Joint reaction forces of the hip, knee, and ankle

The effect of simulated gravity (1g, 0.7g, 0.5g, 0.38g, 0.27g, 0.16g) upon lower limb internal kinetics (i.e., joint reaction forces) during candidate plyometric movement (i.e., maximal ankle hopping, maximal effort countermovement jumping, and drop landing) will be determined by a One-Way Repeated Measures ANOVA with:

- Independent variables: six simulated gravity conditions
- Dependent variables: Joint reaction forces of the hip, knee and ankle

In case the assumption of sphericity been violated (i.e., Mauchly's test statistic is significant [$p < 0.05$]), the Geisser-Greenhouse correction will be used to determine the effect of the independent variables on the dependent variables. If a significant effect of the simulated gravity condition, the locomotion trial, or the interaction between simulated gravity condition and locomotion trial is found, Bonferroni corrected post-hoc t-tests will be employed. If data has a non-normal distribution the non-parametric Friedman test with Dunn's post-test will be used. A *post hoc* power analysis will be conducted with the final sample, Cohen's d effect sizes, a two-tailed test, and $p = 0.05$ to calculate the statistical power achieved.

Data Management

Protection of all personal information collected throughout the experiment is ensured to meet the requirements of GDPR regulations. Several agreements between all institutions involved have been documented:

- Data will be collected by the L.O.O.P. GBF personnel on an encrypted laptop and stored on a secure server, anonymized, backed up and then shared according to a data sharing agreement to the partners using an encrypted file sharing system. Therefore, all data files will be named with a key identifier that L.O.O.P. personnel will define, and have responsibility to manage.

- The 'raw' kinematics, kinetics, and electromyography data will be saved as .C3D files whilst ultrasound data will be saved in DICOM format. Both sets of files will be temporarily stored on encrypted data capture laptops. All files will be pseudonymised with a numeric code and kept separate from all other study data in a password protected folder.

- The ‘raw’ data will be uploaded on the same day of the data collection to a shared drive on a secure server by L.O.O.P. personnel. Access will be shared with the researchers from other institutions. A secured connection will be used to upload and download raw data from the shared drive. All academic partners will be able to access and download the data from this shared area and perform the analysis or calculation independently.

- As a number of institutions will be involved in the project, a data sharing agreement between institutions will be obtained but only pseudonymised data will be shared.

4.3 Conclusion

A comprehensive protocol is presented for the collection of a biomechanical dataset that aims to inform the creation of a *Biomechanical Handbook*. The data gathered from this study will also provide first insights into the internal musculoskeletal loads for movement in various levels of simulated hypogravity, including Moon (0.16g) and Mars (0.38g) gravities. By integrating experimental data and a musculoskeletal model with a data-tracking direct collocation optimal control framework, the muscle and joint reaction forces will be estimated for a catalogue of exercises, including gait and jumping movements, to profile the expected musculoskeletal loads in a range of hypogravity conditions. Furthermore, passing optimised muscle forces into a muscle adaption model will allow for the estimation of hypothetical training volumes that will elicit a meaningful change in muscle size in response to the loading profile. This provides novel information that can be used to assess the feasibility of exercises programs before being prescribed. For example, taking a common training program design (e.g. 12 repetitions per set, 3 sessions per week) it is possible to estimate how many sets per session are required, which gives insight into whether it would be possible to complete in a reasonable time frame (e.g. 1 week). Documenting this information within a Biomechanical Handbook allows for the better alignment exercise programs, in terms of structures that are loaded and the potential hypertrophic benefit, to the individual's musculoskeletal condition. For example, an astronaut who presents with a more atrophied rectus femoris relative to the vasti muscle, an exercise and gravity level can be selected that targets hypertrophy of the rectus femoris. This will benefit post-spaceflight rehabilitation by providing an evidence-based resource for practitioners to inform exercise program design.

Chapter 5

Optimal Fibre length and Maximum Isometric Force are the most influential parameters when modelling muscular adaptations to unloading using Hill-Type muscle models

Pre-chapter Commentary

This chapter investigates modelling muscular adaptations to disuse using a Hill-type muscle model. Appropriately adjusting muscle model parameters is key in musculoskeletal modelling to achieve accurate simulation outcomes. I realised the need for this study because previous literature had focused on adjusting model parameters to capture differences between people, such as anatomical or genetic differences, rather than changes to the muscle due to disuse. In this context, anatomical and genetic influences remain relatively constant, and the importance of model parameters for representing muscle adaptations to disuse needed to be understood to achieve physiological simulations. This information can be used to inform astronaut-specific musculoskeletal models to better inform future studies in this domain. Due to the COVID-19 pandemic is was not possible to collect experimental data pre- and post-disuse (e.g. bedrest or spaceflight), and the European Space Agency (who match-funded this research) did not have a data-sharing policy at the time of the study that would have provided access to astronaut data. Therefore, it was adapted by using previously reported data from the literature.

Abstract

Spaceflight is associated with severe muscular adaptations with substantial inter-individual variability. A Hill-type muscle model is a common method to replicate muscle physiology in musculoskeletal simulations, but little is known about how the underlying parameters can be adjusted to model adaptations to unloading. The aim of this study was to determine how Hill-type muscle model parameters can be adjusted to model disuse muscular adaptations. Isokinetic dynamometer data were used to perform tracking simulations at two knee extension angular velocities ($30°{\cdot}s^{-1}$ and $180°{\cdot}s^{-1}$). The activation and contraction dynamics were solved using an optimal control approach and direct collocation algorithm. A Monte Carlo sampling technique was used to perturb muscle model parameters within physiological boundaries to create theoretical populations characterised by feasible adapted muscle parameters. Knee flexor and non-knee muscle optimal fibre lengths were significant predictors of successful simulation. Optimal fibre length could not be shortened by more than 67% and 61% for the knee flexors and non-knee muscle, respectively. The parameters that were not found to be important, particularly maximum isometric force, were discussed. The Hill-type muscle model successfully replicated muscular adaptations due to unloading, and recreated salient features of muscle behaviour associated with spaceflight, such as altered force-length behaviour. Future researchers should carefully adjust the optimal fibre lengths of their muscle-models when trying to model adaptations to unloading, particularly muscles that primarily operate in the ascending and descending limbs of the force-length relationship.

5.1 Introduction

Spaceflight remains an exciting and key objective both for international space agencies and commercial companies (e.g. Virgin Galactic and Blue Origin). Attenuation of musculoskeletal (MSK) adaptations to spaceflight, including skeletal muscle mass and strength (Winnard *et al.*, 2019), remains a priority to maintain astronaut and passenger health and performance during and following spaceflight. Computational MSK modelling approaches have been identified as a key next step in understanding how exercise in hypogravity can mitigate against and rehabilitate these adaptations (Lang *et al.*, 2017). Accurately replicating the MSK system, including muscle activation and contraction dynamics, allows for the estimation of internal loads that are otherwise not possible to measure *in vivo*. This information is key to profile the loading related to a specific exercise mode, and better align exercise prescription with the individuals MSK adaptations. This is particularly relevant for post-spaceflight rehabilitation when the functional capacity of an astronaut is most compromised due to the reintroduction of gravitational forces (Berg *et al.*, 1997; English *et al.*, 2020).

Simulation of human movement is made possible by coupling equations of motions governing the rigid-body system with equations that replicate muscle activation and muscle contraction dynamics. However, the physiological realism of the estimated muscle forces is determined by the choice of muscle model and muscle parameters used. Hill-type models are widely used in muscle-driven simulations due to their ability to describe features of muscle force generation with relative computational efficiency (van den Bogert *et al.*, 1998; Winters, 1990). While an alternative model, the Huxley-type model, can achieve similar muscle force estimations to the Hill-type model in certain circumstances , they can require up to 10,000 more CPU time in relatively simple MSK models (van Soest *et al.*, 2019) The force generating capacity of the Hill model is described by five main muscle-tendon unit (MTU) parameters: maximum isometric force, optimal fibre length, pennation angle at optimal fibre length, tendon slack length, and maximum shortening velocity. Tendon stiffness is often included as the elongation of the tendon, which would occur to a greater extent with a more compliant tendon, influence fibre length and velocity (Narici & De Boer, 2011). This consequently influences the force-length-velocity contraction dynamics of the MTU. The parameters that describe the Hill-muscle have a large influence on muscle behaviour (Ackland *et al.*, 2012) and estimated muscle forces and joint contact forces (Ackland *et al.*, 2012; De Groote *et al.*, 2010; Serrancolí *et al.*, 2020; Valente *et al.*, 2014) during dynamic optimisations. Therefore, an appropriate estimation and use of MTU parameters is needed to generate physiologically plausible simulations and interpret their outcome. How best to do this to replicate muscular adaptations to unloading has currently not been addressed and represents an important area of study to integrate MSK modelling into space science.

From an experimental perspective, a substantial body of research has been conducted that describes the nature of muscular adaptations to unloading following spaceflight and ground-based analogues (e.g. bed rest). A systematic review of bed rest studies highlighted that, without exercise intervention, muscle atrophy (volume and cross-section area) and weakening can present within as little as 14 days (Winnard *et al.*, 2019). These adaptations are not uniform between muscle groups, with the anti-gravity extensor muscle groups of the legs typically experiencing greater adaptations than flexor groups (Gopalakrishnan *et al.*, 2010; Kramer *et al.*, 2017) and the arm muscles (Gopalakrishnan *et al.*, 2010; Rittweger *et al.*, 2005). Although muscular size and strength are closely linked, the degree of weakening tends to exceed the degree of muscle atrophy following unloading (Alkner & Tesch, 2004). This highlights that additional factors, such as architectural adaptations (i.e. fibre length and pennation angle) and fibre type composition, contribute to the decline in muscular function following unloading. Indeed, shorter and less pennate muscle fibres have been reported alongside reduced muscular strength following spaceflight (Koryak, 2019) and bed rest (De Boer *et al.*, 2008; Reeves *et al.*, 2002). Further evidence of the complexity inherent to muscle adaptations, are i) a preferential shift from type I to type II fibres has been observed following disuse (Trappe *et al.*, 2004), ii) the inter-individual variation reported in the literature (Fernandez-Gonzalo *et al.*, 2021; Scott *et al.*, 2021), which also complicates the adjustment of muscle model parameters. For example, muscle fibre CSA and peak isometric fibre force ranged between 49 - 106% and 30 - 90%, respectively, across eight astronauts from a single study (Fitts *et al.*, 2010). Additionally, *in vitro* analyses of single-fibre shortening velocities have been reported to decrease by 44% (Fitts *et al.*, 2010) or to increase two-fold (Yamashita-Goto *et al.*, 2001) following long-term disuse. The appropriateness of the Hill-muscle model for modelling adaptations to unloading is contingent on the ability to measure muscle parameters *in vivo* to personalise the model or identify clear strategies for adjusting parameters depending on the profile of adaptations being modelled.

Therefore, modelling approaches can become a very useful tool to investigate how the muscles adapt during unloading, but specific Hill-type muscle model parameters must be adjusted to ensure realism, and validly model different adaptations. The aim of this study was to identify Hill-type muscle model parameters that are the most important to feasibly model muscular adaptations. A stochastic sampling approach was adopted to randomly sample Hill-type muscle model parameter perturbations to estimate a distribution of feasible combinations for modelling muscular adaptations to unloading.

5.2 Methods

5.2.1 Reference Data

The following case study was derived from data presented in the literature. Knee net joint moments recorded at 30° knee flexion during a $30°{\cdot}s^{-1}$ and a $180°{\cdot}s^{-1}$ angular velocity dynamometry task, pre and post 90-days bed rest, were used as ground truth data (Alkner *et al.*, 2016). These data were combined with normative knee net joint moment profiles of young, healthy adults for the same isokinetic task for flexion angles between 90° to 0° flexion (Knapik *et al.*, 1983). Values were adjusted proportionally and interpolated to construct complete knee extensor moment profiles before and after 90 days bed rest at both angular velocities (see appendix B). These data were used as reference knee net joint moments within the simulation framework.

5.2.2 Simulation Framework

Skeletal motion was modelled as rigid body dynamics using Newtonian mechanics. Optimal control problems (OCP) were formulated to solve the activation and contraction dynamics of the MTU. Only the MTU dynamics were optimised in this framework. During isokinetic dynamometry testing, the joint kinematics (positions and velocities) are constrained by the sitting posture and the dynamometer arm. Consequently, we prescribed this information to remove optimisation variables from the OCP that would solve the skeletal dynamics. Similarly, this allowed for the reference net joint moments described above to be used to relate the MTU forces to the kinematics. The goal of the simulation was to minimise a cost function (eq. 5.1), subject to MTU activation and contraction dynamics. Through the systematic perturbation of MTU parameters to replicate unloading induced adaptations, our objective was to identify a hypothetical population of MTU parameters that represented feasible solutions to the problem. These were then used to describe feasible (i.e. optimal solutions) and infeasible (i.e. non-optimal solutions) approaches to use Hill-type MTUs to model muscular adaptations to unloading.

A generic full-body MSK model was modified before utilisation within the framework (Figure 5-1, Lai *et al.*, 2017). The model was linearly scaled in OpenSim to an adult male, who had similar anthropometrics to the pre-flight reference data (model participant: 28 years, 79.9 kg, 1.82 m; reference data: 32 $\pm$ 4 yrs, 72 $\pm$ 5 kg, 1.73 $\pm$ 0.03 m). The torso, both arms, and left leg segments were removed to leave a right-leg only model (assumed to be the tested leg) leaving seven segments (pelvis, femur, patella, tibia-fibula, talus, calcaneus and toes) and 13 degrees of freedom (6 pelvis, 3 hip, and 1 knee, ankle, subtalar and MTP). The model was positioned to replicate a sitting posture. Right knee angles were varied from 90° to 0° flexion at $30°\cdot s^{-1}$ and $180°\cdot s^{-1}$. Right hip flexion was set to 90°, with the remaining coordinates set to neutral. During initial testing of the muscle-driven simulations, large parallel elastic component (PEC) forces were observed for the knee flexors as knee flexion angle approached 0°. Consequently, the pelvis was positioned with 30° backwards tilt, and hip flexion adjusted to maintain a femur position parallel with the ground plane. This was to allow the musculature to work at more realistic normalised fibre-length during the simulations. This also corresponds to high hip flexion condition in other knee extension dynamometry studies (60 - 70 deg, De Groote *et al.*, 2010). The model was actuated by 40 Hill-type MTU with the equations governing active (force-length and force-velocity) and passive (parallel and series) force generation according to De Groote *et al.* (2016). The lengths, velocities and moment arms of the MTUs were described by polynomials as a function of joint angle and joint angular velocity (Falisse, Serrancolí, Dembia, Gillis, & De Groote, 2019; Van den Bogert *et al.*, 2013). The polynomials were constructed against a wide rage of joint angles using OpenSim's muscle analysis tool. MTU activation and contraction dynamics were formulated as first-order differential equations (De Groote *et al.*, 2016; Zajac, 1989). Normalised tendon force, $\tilde{F}_t$, and activation, a, were used to describe the state of the MTUs, with their first time derivatives introduced as control variables ($u_{\tilde{F}_t}$ and u_a, respectively). This allowed for first-order dynamic constraints to be imposed, which were formulated implicitly to improve the numerical conditioning of the problem (van den Bogert *et al.*, 2011). The Hill-equilibrium condition was formulated as a path constraint to ensure $\tilde{F}_t$ equalled the projected normalised muscle force. Raasch's activation dynamics equations were enforce as path constraints (De Groote *et al.*, 2009; Raasch *et al.*, 1997). These constraints were expressed as linear inequality constraints with activation and deactivation time constants of 0.015 ms and 0.06 ms, respectively (Falisse, Serrancolí, Dembia, Gillis, Jonkers, *et al.*, 2019). The muscle forces about the knee joint were related to the reference knee joint moment data via an equality path constraint according to their polynomial-computed moment arms and reserve moments added at the knee. The moments about the hip and ankle joints were not constrained since participants were strapped in position, thus any moment produced by the muscles would be counteracted by the dynamometer chair. An additional control variable, u_{res}, was introduced at each muscle-driven DOF for the reserve actuator that described the instantaneous moment being produced. The MTU state and control variables were bounded and scaled based on Falisse and colleagues (2019) before evaluation in the cost function and constraint equations. Reserve actuators were bounded between ±25 to allow a maximum instantaneous moment contribution of 25 N·m, and scaled between ±1.

A cost function, J, was constructed to solve the muscle redundancy problem through minimising the sum of squared activations (J_{Effort}), sum of squared of the reserve actuators ($J_{Reserves}$), and the MTU control variables ($J_{Control}$).

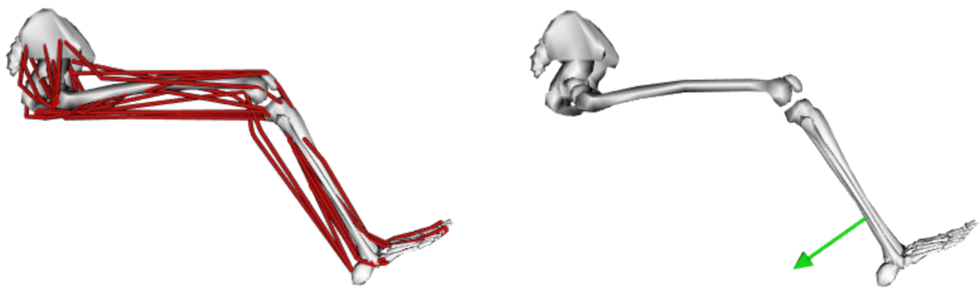

Figure 5-1 The modified generic musculosckeletal model (Lai *et al.*, 2017) used in this study. The force applied to the tibia by the dynamometer arm (green arrow) was applied in the tibia reference frame at 75% of the tibia's length.

Despite primarily been used as a surrogate for efficient muscular effort, the sum of muscle activations squared has been successfully used in sprinting simulations (Haralabidis *et al.*, 2021) and was deemed appropriate to use for this maximal knee extension task. Minimisation of control terms was included to improve convergence of the simulation given the implicit formulation of the OCP by penalising large, non-physiological changes in the state variables. The OCP was formulated to minimise the u_{res} so that simulations could be identified where reserve actuators did not provide assistance to the muscle forces above a given threshold. The reserve and control variable terms were scaled before inclusion in the cost function.

$$J = J_{Effort} + J_{Reserves} + J_{Controls} \tag{5.1}$$

$$J_{Effort} = \sum_{j=1}^{40} \int_{t0}^{tf} \left(P_{V_j} \cdot a_j\right)^2 \; dt \tag{5.2}$$

$$J_{Reserves} = \sum_{i=1}^{6} \int_{t0}^{tf} \left(u_{res}\right)^2 \; dt \tag{5.3}$$

$$\begin{aligned} J_{Control} = & \sum_{j=1}^{40} \int_{t0}^{tf} \left(u_{\tilde{F}_{tj}}\right)^2 \; dt \\ & + \sum_{j=1}^{40} \int_{t0}^{tf} \left(u_{\dot{a}_j}\right)^2 \; dt \end{aligned} \tag{5.4}$$

The OCPs were transcribed into non-linear programme (NLP) programs via a direct collocation technique. The state (x = [a, $\tilde{F}_t$]) and control (u = [u_a, $u_{\tilde{F}_t}$]) trajectories were discretised into 50 equally spaced time intervals using Legendre-Gauss-Radau quadrature. The state trajectories were further discretised into four-point intervals between time points, and approximated with third-order polynomials. The dynamic constraints were imposed at each collocation point, with path constraints imposed at the beginning of each mesh interval. Additional continuity constraints were imposed to ensure state variables at the end of each collocation interval matched those at the next node point. The NLP was formulated in MATLAB using CasADi (v3.4.2, Andersson *et al.*, 2019), to allow algorithmic differentiation to be used, and were solved using IPOPT (Wächter & Biegler, 2006).

5.2.3 Monte Carlo Framework

A Monte Carlo sampling technique was used to explore MTU adaptations to unloading. For a single MTU, five parameters were identified as inputs for the analysis: maximum isometric force (F^{MAX}), optimal fibre length (l^0), penntion angle at l^0 (θ^0), maximum shortening velocity (V^{MAX}), and tendon compliance (k_t). Tendon slack length was not included for two reasons: i) there is a lack of evidence available describing how tendon length adapts to unloading, and ii) a mechanism for adaptation to a change in loading (e.g. a change tissue architecture) was not identified to justify it's inclusion. In contrast, the tendon has been shown to become more compliant (or less stiff) during unloading (Kubo *et al.*, 2004b), which will influence muscle contractions as tendon elongation directly impacts fibre length and velocity (Narici & Maganaris, 2007). Therefore, it was deemed necessary to include tendon compliance to fully understand how Hill-models can replicate adaptations to unloading. Further explanation of how the boundaries were constructed is provided in the supplementary material (see appendix B).

The Monte Carlo was formulated to select parameter perturbations within literature informed boundaries. These boundaries were defined based on spaceflight and ground-based unloading studies to reflect the inter-individual variability that is reported following unloading (Scott *et al.*, 2021), and where necessary, derived based on assumptions about muscle physiology (Lieber &

Table 5.1 Boundaries used to perturb the Hill-type muscle model parameters within the Monte Carlo analysis. Values are expressed as a percentage change relative to baseline (i.e. unperturbed = 100%)

Parameter	Perturbation Boundaries (%)
Maximum Isometric Force	40 - 100
Optimal Fibre Length (OFL)	60 - 100
Pennation Angle at OFL	75 - 100
Maximum Shortening Velocity	50 - 200
Tendon Compliance	40 - 100

Fridén, 2000). The perturbation boundaries are shown in Table 5.1. Each simulation would then represent an individual returning to Earth after a hypothetical exposure to microgravity (∼0 g), with all feasible simulations representing a hypothetical population of muscle model parameter combinations that are physiologically meaningful. This would allow for the identification of parameters most important for modelling muscle adaptations and their relative variability in unloading scenarios. Simulations were deemed feasible when it converged to an optimal solution and when reserve actuators did not contribute above a predefined threshold. This threshold was determined as when reserve actuators did not contribute more than 9% of the reference net joint moment data for the post-unloading condition (Figure 5-2). The 9% threshold was based on the test-retest reliability of a commercially available dynamometer (Li *et al.*, 1996). All other solutions were defined as infeasible.

The 40 MTUs defined in the generic model were grouped as flexors, extensors, and non-knee muscles according to their moment arms about the knee coordinate. This reduced the number of parameters to perturb from 200 to 15, with five parameters per muscle group. A set of uniformly distributed values between 0 and 1 were randomly generated in MATLAB. These values were used to derive percentage perturbation for each input parameter. The baseline values for the MTU parameters were taken from the scaled MSK model used to derive the reference knee net joint moment data in OpenSim (see appendix B). Tendon

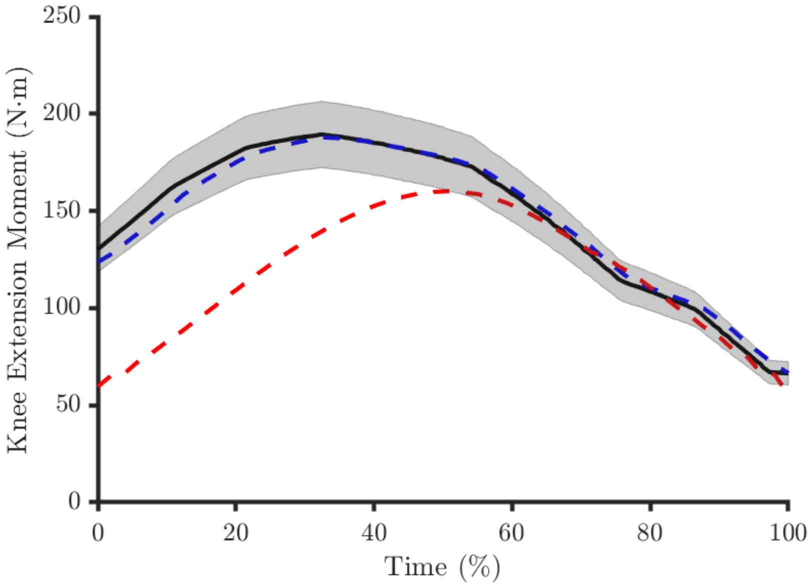

Figure 5-2 The muscle forces had to produce a net knee joint moment within 9% of the reference experimental data (solid black line and shaded area). The solution was considered feasible if this was achieved across the entire movement period (blue dashed line) and infeasible if this was violated at one or more time points (red dashed line).

stiffness and maximum shortening velocity values were set to 35 at 4% strain and 10 $l^0 \cdot s^{-1}$, respectively (Falisse, Serrancolí, Dembia, Gillis, Jonkers, *et al.*, 2019). A uniform distribution was used to allow for equal probability of perturbations to be sampled across the defined perturbation boundaries. Two Monte Carlo simulations were performed: one for the $30° \cdot s^{-1}$ condition and one for the $180° \cdot s^{-1}$ condition.

5.2.4 Data Analysis

All feasible and infeasible solutions were used in further analysis for angular velocity conditions. The parameter perturbations represented the main outcome measure, and, due to the uniform distribution of the Monte Carlo sampling, data were expressed as median ± inter-quartile range (IQR). Medians, inter-quartile ranges, and kernel densities were explored between feasible and infeasible solutions to identify patterns in the muscle model parameters.

Statistical Analysis

A step-wise logistic regression model was created for each Monte Carlo condition. Parameter perturbations were centred about zero (i.e. unperturbed), and expressed as a percentage to allow regression coefficients to describe odds ratio changes per 1% perturbation of a given parameter. A logit function was used to link the covariates (i.e. the muscle model parameter perturbations and interaction terms) to the log-odds of a simulation being successful, and a maximum likelihood estimation was used to fit the regression model. Terms were added to the model where the adjusted McFadden's pseudo R^2 was increased by 2.5%. This threshold was chosen as the best balance between maintaining model simplicity (i.e. fewest necessary predictor variables), and accuracy in classifying parameters as feasible and infeasible (see appendix B). Regression coefficients were transformed into odds ratios, and confidence intervals for the odds ratios were calculated. Confidence intervals that did not cross 1 (i.e. equal odds between feasible and infeasible solutions) were used to identify significant regression terms ($p < 0.01$).

5.3 Results

The distribution of perturbations highlighted differences between the feasible and infeasible solutions for knee flexion and non-knee muscle optimal fibre lengths, and knee extension maximum isometric forces (Figures 5-3 - 5-4). Feasible solutions were more densely populated nearer to baseline for these three parameters (Figure 5-5), which is reflected in the descriptive statistics. On average, feasible solutions tended to occur when OFLs were not shortened to much for both the knee flexors ($30°·s^{-1}$: feasible = 89.2 ± 5.8%, infeasible = 70.8 ± 6.2%; $180°·s^{-1}$: feasible = 89.4 ± 5.7%, infeasible = 71.1 ± 6.3) and the non-knee muscles ($30°·s^{-1}$: feasible = 83.7 ± 8.5%, infeasible = 75.8 ± 10.5%; $180°·s^{-1}$: feasible = 83.6 ± 8.6%, infeasible = 76.4 ± 10.6%). In fact, a maximum level of perturbation was observed for these parameters, as all simulations were categorised as infeasible when the OFL were shortened beyond 67% and 61% of baseline for the knee flexors and non-knee muscles, respectively (Table 5.2). Feasible solutions were obtainable across the entire spectrum of perturbation values for the remaining muscle parameters. The density of feasible and infeasible solutions were qualitatively similar and evenly spread across the perturbation ranges for the remaining solutions (see appendix B).

Both logistic regression models were exclusively comprised of OFL parameters (Table 5.3). Optimal fibres length of the knee flexor and non-knee muscles were the strongest predictors of achieving feasible simulations. For every percentage the OFL parameters were shortened the odds ratios increased by 22% ($30°\cdot s^{-1}$) and 22% ($180°\cdot s^{-1}$) for the knee flexors OFL, and 9% ($30°\cdot s^{-1}$) and 9% ($180°\cdot s^{-1}$) for the non-knee OFL. The intercept values from both models demonstrated that when the other predictor variables were zero (i.e. the baseline parameters were used) the odds ratio of a feasible solution was substantial. The adjusted R^2 values for the final models were 0.59 and 0.58 for the $30°\cdot s^{-1}$ and $180°\cdot s^{-1}$ conditions, respectively.

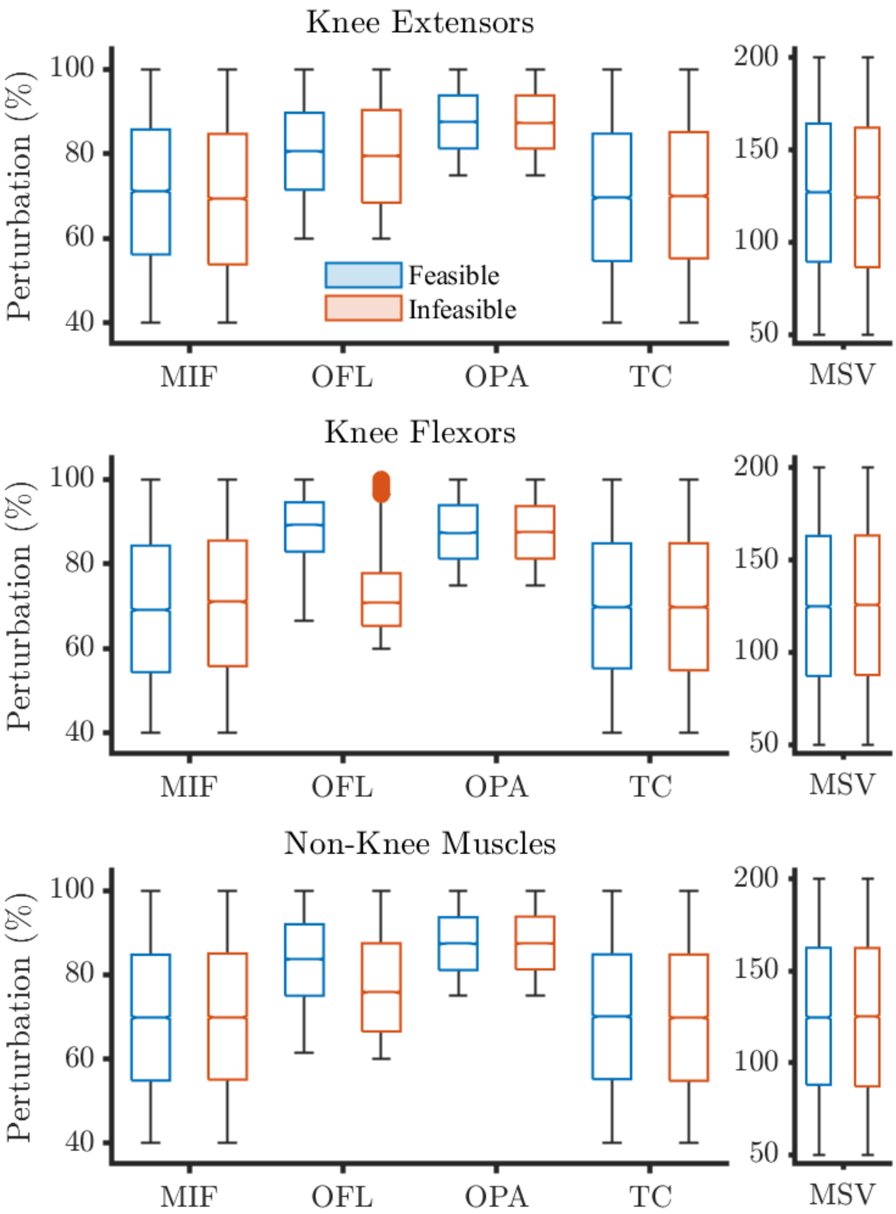

Figure 5-3 Sampling distributions of parameter perturbations for feasible and infeasible solutions for the $30°{\cdot}s^{-1}$ condition. Values expressed as percentages where 100% describes baseline. MIF = maximum isometric force; OFL = optimal fibre length; OPA = Pennation angle at OFL; TC = tendon compliance; MSV = maximum shortening velocity.

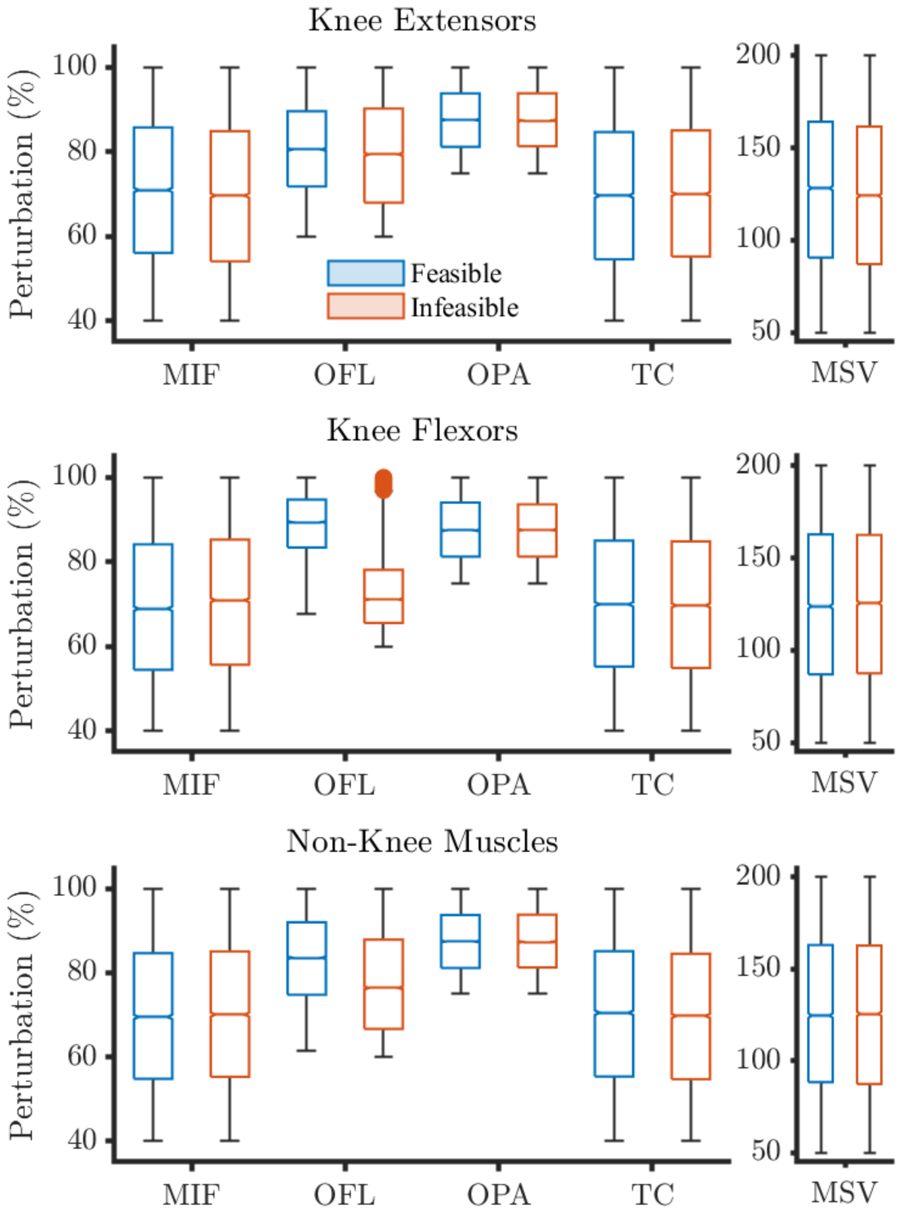

Figure 5-4 Sampling distributions of parameter perturbations for feasible and infeasible solutions for the 180°·s^{-1} condition. Values expressed as percentages where 100% describes baseline. MIF = maximum isometric force; OFL = optimal fibre length; OPA = Pennation angle at OFL; TC = tendon compliance; MSV = maximum shortening velocity.

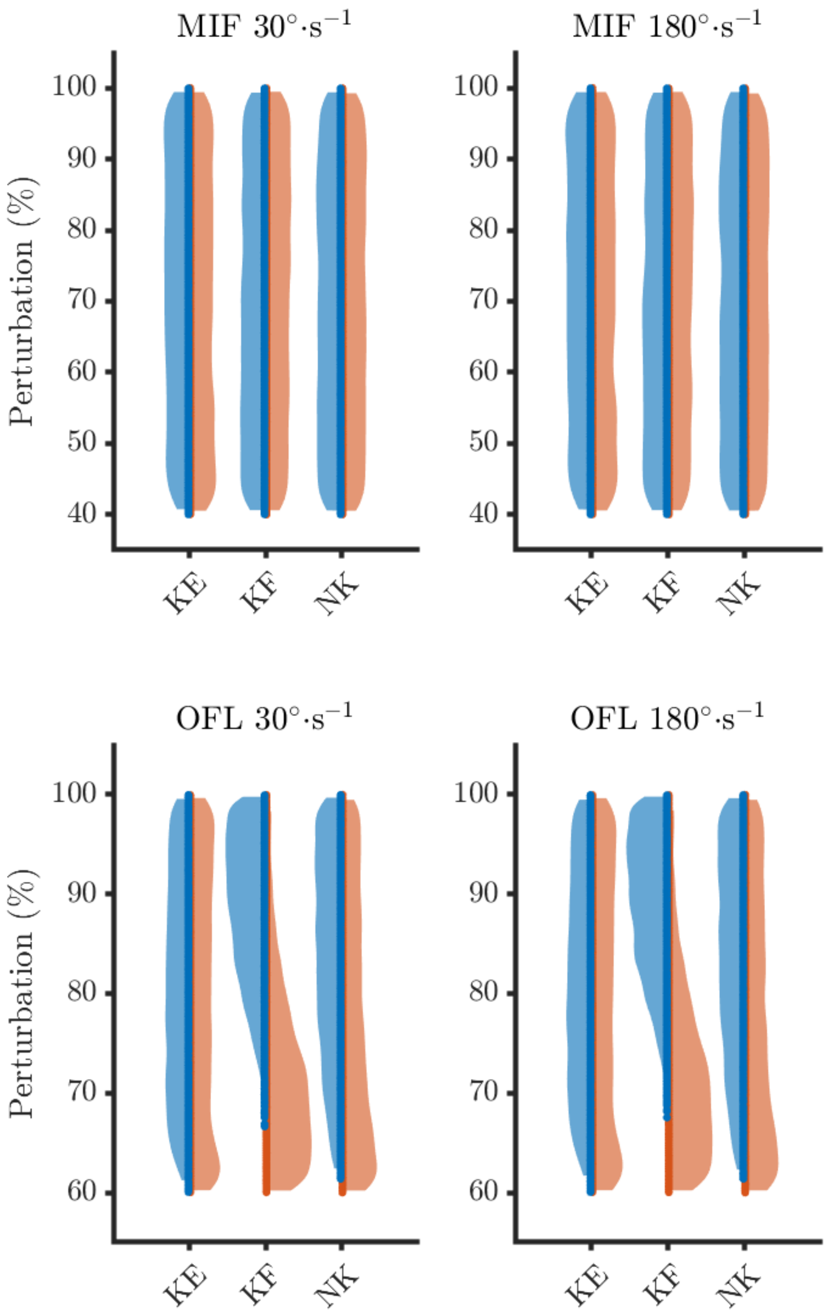

Figure 5-5 Sampling density of maximum isometric forces (MIF) and optimal fibre length (OFL) for the feasible (blue) and infeasible (orange) solutions. KE = knee extensors; KF = knee flexors; NK = non-knee muscles.

Table 5.2 The distribution of parameter perturbations expressed as a percentage change relative to baseline (i.e. 100%) for feasible solutions

		$30°{\cdot}s^{-1}$					$180°{\cdot}s^{-1}$				
		Median	IQR	95% CI	Min	Max	Median	IQR	95% CI	Min	Max
Knee Extensors	MIF	71.2	14.8	70.6 - 71.7	40.0	100.0	71.0	15.0	70.3 - 71.6	40.0	100.0
	OFL	80.6	9.1	80.2 - 80.8	60.0	100.0	80.6	8.9	80.1 - 81.0	60.0	100.0
	OPA	87.6	6.3	87.3 - 87.8	75.0	100.0	87.6	6.3	87.3 - 87.8	75.0	100.0
	MSV	127.3	37.4	126.1 - 128.3	50.0	200.0	128.2	36.8	126.6 - 129.6	50.0	200.0
	TC	69.6	15.1	69.1 - 70.1	40.0	100.0	69.6	15.1	68.9 - 70.2	40.0	100.0
Knee Flexors	MIF	69.1	15.0	68.6 - 69.6	40.0	100.0	68.9	14.9	68.3 - 69.5	40.0	100.0
	OFL	89.2	5.8	89.0 - 89.3	66.7	100.0	89.4	5.7	89.2 - 89.6	67.4	100.0
	OPA	87.4	6.3	87.2 - 87.7	75.0	100.0	87.5	6.4	87.2 - 87.8	75.0	100.0
	MSV	124.7	37.9	123.2 - 125.9	50.0	200.0	123.8	37.9	122.2 - 125.5	50.0	200.0
	TC	69.9	14.8	69.4 - 70.4	40.0	100.0	70.0	14.9	69.4 - 70.6	40.0	100.0
Non-Knee Muscles	MIF	69.8	15.0	69.4 - 70.3	40.0	100.0	69.5	14.9	68.8 - 70.1	40.0	100.0
	OFL	83.7	8.5	83.5 - 84.0	61.4	100.0	83.6	8.6	83.3 - 83.9	61.4	100.0
	OPA	87.4	6.3	87.2 - 87.6	75.0	100.0	87.4	6.3	87.1 - 87.8	75.0	100.0
	MSV	124.6	37.2	123.3 - 125.8	50.0	200.0	124.6	37.3	123.1 - 126.1	50.0	200.0
	TC	70.1	14.8	69.6 - 70.6	40.0	100.0	70.5	14.9	69.8 - 71.1	40.0	100.0

MIF = maximal isometric force, OFL = optimal fibre length, OPA = pennation angle at OFL,
TC = tendon compliance, MSV = maximum shortening velocity, CI = confidence interval,
Min & Max = minimum and maximum perturbations that led to feasible solutions

Table 5.3 Included parameters in the logistic regression models with coefficients expressed as odds ratios and odds ratio 99% confidence intervals.

	Log Odds	Odds Ratio	Confident Interval
$30°\cdot s^{-1}$			
Intercept	6.16	475.46	(375.68 - 601.74)
KF OFL	0.22	1.25	(1.24 - 1.26)
NK OFL	0.10	1.10	(1.10 - 1.11)
$180°\cdot s^{-1}$			
Intercept	5.82	336.11	(251.77 - 448.70)
KF OFL	0.22	1.25	(1.24 - 1.26)
NK OFL	0.09	1.09	(1.09 - 1.10)

OFL = Optimal fibre length
KF = knee flexors, NK = non-knee muscles

5.4 Discussion

The aim of this study was to understand how Hill-type muscle model parameters can be adjusted to reflect unloading-induced muscular adaptations. To do so, kinematics and kinetics data of knee flexion-extension performed on a dynamometer, post-spaceflight, were retrieved from the literature and used for the analysis. A Monte Carlo sampling technique was used to randomly perturb muscle model parameters and understand their importance in modelling muscular adaptations to disuse. The findings showed that the Hill-type muscle model can be used to model physiological muscular adaptations providing that adjustments to the knee flexor and non-knee muscle optimal fibre lengths, and the knee extensor maximum isometric forces, are appropriate.

Modelling Muscle adaptations to Unloading

The results demonstrate it was possible to replicate the changes in functional outcomes due to muscular adaptations to unloading by adjusting Hill-type muscle model parameters. The simulations that were optimal solution represent feasible parameter sets for reproducing the post-disuse knee joint torque. The likelihood of attaining such optimal solution was most influenced by the knee flexor and non-knee muscle optimal fibre lengths. Specifically, shortening the optimal fibre lengths reduced the odd ratios for both the $30°{\cdot}s^{-1}$ and $180°{\cdot}s^{-1}$ conditions. This supports previous studies that have highlighted that it is important to calibrate optimal fibre length to obtain valid simulation outcomes (Ackland *et al.*, 2012; De Groote *et al.*, 2010; Redl *et al.*, 2007; Scovil & Ronsky, 2006; Serrancolí *et al.*, 2020). It was surprising that maximum isometric force was not included within the step-wise regression models given the maximum effort nature of the dynamometer task. There is debate within the literature as to whether simulation results are (De Groote *et al.*, 2010; Scovil & Ronsky, 2006) or are not sensitive (Ackland *et al.*, 2012; Redl *et al.*, 2007) to maximum isometric force. Those studies that found maximum isometric force was an important MTU parameter were investigating movements that required high force output. For example, Scovil and Ronsky (2006) found that simulations of running were sensitive to maximum isometric force but walking simulations were not. While in the most similar study to this, where the sensitivity of net joint moments to MTU parameters was assessed during maximal isometric and isokinetic knee extension dynamometry tasks, it was suggested that sensitivity to optimal fibre length and maximum isometric force was substantial for some muscles (De Groote *et al.*, 2010). On face value, it is possible that the maximum isometric forces were not perturbed enough to prevent the muscles being able to balance the net joint moments. However, given the boundaries were informed by the disuse literature and the lower boundary represented 40% of the unperturbed values, this is difficult to envisage. Alternatively, this finding may be an artifact of the muscle sharing term aiming to minimise the muscle activations. We observed that the knee flexors, particularly the hamstring muscles, were on average not activated above 20% and spent the majority of the movement below 10% of maximum activation. Minimal active force generation from the knee flexors will have made it easier for the knee extensors to balance the net knee joint moment, reducing the need for large maximum isometric forces. The minimising of muscle activations means the simulations assumed minimal co-activation. However, antagonist co-activation is a known phenomenon, particularly for joint stability (Neptune *et al.*, 1999), and can be considerable in the hamstrings during isokinetic knee extension dynamometry (e.g., Osternig *et al.*, 1986). One approach that can better represent co-contraction is EMG-informed modelling (e.g., Pizzolato *et al.*, 2015). Future research should consider alternative muscle sharing terms within the cost function or EMG-informed modelling (e.g., Pizzolato *et al.*, 2015) to better represent co-activation.

Validity of Parameter Perturbations

Without other similar modelling studies for comparison, the logical question is then whether the adjustments presented in this study represent 'appropriate' adaptations to the MTU parameters to model unloading adaptations. Maximum isometric force is commonly assumed to be proportional to physiological cross-sectional area, and regularly scaled in MSK models based on this assumption (e.g., Rajagopal *et al.*, 2016). The maximum perturbation allowed for MIF within the Monte Carlo was determined using this method, and is therefore reflective of literature data that would be used to scale MIF in a MSK model. To discuss optimal fibre length, it is important to consider what is being modelled by this parameter. For a single sarcomere, the optimal length represents the point at which the maximum number of cross-bridges can be formed due to overlap of actin and myosin filaments (Gordon *et al.*, 1966; van den Bogert *et al.*, 1998). However, sarcomeres are not necessarily uniformity spaced within a fiber (Huxley & Peachey, 1961; Llewellyn *et al.*, 2008; Moo *et al.*, 2016), meaning it is plausible to assume that architectural adaptations to unloading will alter the fiber length at which the maximum number of cross-bridges can be formed. Indeed, there is consistent evidence of muscle CSA (Winnard *et al.*, 2019) and fascicle length changes (De Boer *et al.*, 2008; Koryak, 2019; Reeves *et al.*, 2002; Rittweger *et al.*, 2018) after unloading, which suggest a loss of sarcomeres both in parallel and series formation. This can manifest in reduced functional capacity, with astronauts presenting with reduced sit-and-reach performance upon return-to-Earth relative to pre-flight (Laughlin *et al.*, 2015), likely due to a more flexed resting posture in microgravity (i.e. $\sim$0g) (Han Kim *et al.*, 2019; Simons, 1964). Sit-and-reach performance is often used to indicate lower-back and hamstring flexibility, which supports the finding that OFL of the knee flexors and non-knee muscles were significant in the regression model but knee extensors were not. It has been hypothesised that reduced serial sarcomeres would result in a right-shift on the force-length curve at equivalent MTU lengths because the sarcomere would be lengthened to achieve the same fascicle length (Narici & Maganaris, 2007). The results of this study showed that shortening the OFL, indicative of serial sarcomere loss, recreated the right-shift on the force-length curve. Further, feasible solutions were observed when OFLs were unchanged or shortened within a muscle-group, albeit to different levels of tolerance. The ability to recreate features of muscle contraction dynamics and align with literature measured outcomes (i.e. reduced flexibility) provide evidence that shortening OFL is a likely physiological adaptation to unloading. This suggests that using post-spaceflight assessment processes to determine fascicle length (e.g. using ultrasound) would allow for identifying whether adjustment of OFL is necessary to appropriately use the Hill-type model to recreate muscular adaptations to unloading.

Having established that optimal fibre length is a realistic adaptation, the next question is whether it is physiologically plausible that optimal fibre-length can shorten by as much as 21% in the knee flexors. No feasible solutions were observed when perturbing the OFL beyond 79% and 76% of baseline values for the knee flexors and non-knee muscles, respectively, suggesting there is a physiological limit that cannot be exceeded. Assuming that structural adaptations alone govern the change in OFL (i.e. fascicle length is directly proportional to OFL), the most perturbed value reported in this study falls within fascicle length changes reported following bed rest and spaceflight (-26 - 0%, De Boer *et al.*, 2008; Koryak, 2019; Reeves *et al.*, 2002; Rittweger *et al.*, 2018). Although it is important to note that only one study reported fascicle length changes in excess of -10% (-5 to -26%, Koryak, 2019). These results suggest that there should be inter-individual variation in OFL and that OFL shortening will not be excessive in the majority of individuals. The study results support these suggestions as feasible solutions were achieved between -21% - 0% for the knee flexor muscles and -24% - 0% for the non-knee muscles, but with a higher density of feasible solutions at lower levels of perturbation for both muscle groups. However, whether salient features of an astronauts post-spaceflight movement patterns can be captured is difficult to ascertain because there is a sparsity of biomechanical data available and few previous modelling studies to compare OFL adjustments used to model adaptations to the muscular system. Drawing from another clinical population, the more flexed posture of the hip and knee joints in microgravity is analogous, albeit less extreme, to the crouched gait position reported in Cerebral Palsy children (Wren *et al.*, 2005). Crouch gait occurs, in part, due to muscle contractures (i.e. muscle shortening) of the iliopsoas and hamstring musculature (Delp *et al.*, 1996; Schutte *et al.*, 1997). Shortening OFL, in isolation or alongside lengthening tendon slack length, has been a common approach for simulating contractures in this context. Predictive simulations have shown that crouch gait emerges when the OFL of the correct hip and knee flexor muscles is shortened between -40% to -50% (Falisse *et al.*, 2020; Mehrabi *et al.*, 2019). Given crouch gait represented an extreme context for which OFL adjustments may be necessary to model adaptations of the underlying pathology, it seems reasonable that to model adaptations to unloading did not reach this magnitude of shortening. The challenge for future research is to determine whether the characteristics of an astronauts movement, such as during gait, are captured with the MTU parameter adjustments outlined in this study.

Similar to maximum isometric force, maximum shortening velocity, pennation angle at OFL nor tendon compliance were found to be important parameters for modelling adaptations to disuse. Given the six-fold change in angular velocity between conditions, it is perhaps initially surprising that MSV was not more influential at $180°{\cdot}s^{-1}$ where MTU length changes may occur more rapidly. Increasing MSV allows muscles to generate greater forces at similar contractile component (CC) shortening velocities. Compliance of the series elastic component (SEC) can facilitate CC-SEC dynamics by permitting the CC to work at comparable shortening velocities even when MTU shortening velocities may be different (Miller *et al.*, 2012). The Monte Carlo could only perturb tendon stiffness by making the tendon more compliant, and it is possible that the more compliant tendon allowed for the CC to work within similar force-velocity regions. However, since optimal solutions were found across the entire range of the MSV and TC perturbations, it appears that the baseline TC value was sufficient to allow the CC to work in an appropriate region of the force-velocity relationship. Pennation angle was not found to be influential in this study, likely because it was only allowed to decrease when perturbed. Decreasing the pennation angle increases the proportion of the muscle forces (active and passive) projected along the tendon, meaning perturbing this parameter was reducing the muscle force requirements to achieve the same joint moment contribution. However, this does align with previous observations about Hill-type formulations, which generally consider pennation angle to have relatively little influence on muscle forces when $\leq 20°$ (Zajac, 1989). Of the 40 muscles in the model, 35 had an baseline OPA of $\leq 20°$, which would only become smaller once perturbed during the Monte Carlo. These results suggest that to model adaptations to unloading, it is more important to appropriately calibrate MIF and OFL to model the architectural adaptations to the muscle. However, it may still be necessary to adjust these parameters to investigate MTU behaviour changes following spaceflight. The complexity of the muscular system allows other parameters within the same muscle model (Miller *et al.*, 2012), or forces from other muscles (van der Krogt *et al.*, 2012), to compensate for perturbations to a given parameter. It is likely that the adaptations to maximum shortening velocity, pennation angle at OFL and tendon compliance are specific to the individual, and future researchers should consider their unique research questions when deciding which parameters to adjust alongside MIF and OFL.

Limitations

There are limitations of the approach taken in this study that should be recognised when interpreting the results. In the absence of experimental data, the reference net joint moments derived for the knee extension task do not have corresponding EMG data to validate muscle activations. Salient features of muscle activity, such as post-disuse presenting with decreased activations (Kramer, Kümmel, *et al.*, 2018a) and a tendency for greater activity from vastus lateralis relative to the rectus femoris (Salzman *et al.*, 1993), were captured by the simulations. The shape and magnitude of the activations cannot be further verified, and thus it cannot be ruled out that muscle activation amplitude did not compensate for parameter alterations. Additionally, neural adaptations were omitted from the study as the main focus was on modelling the muscular adaptations of the MSK system to disuse. Alterations to the neural dynamics of the muscle have been shown through reduced amplitude of EMG (Berg *et al.*, 1997; Kramer, Kümmel, *et al.*, 2018a), greater torque generation via supramaximal stimulation than voluntary contraction (Koryak, 2014), and altered firing frequency and fibre conduction velocity (Mulder *et al.*, 2009). The activation dynamics of the muscle were not altered between the pre- and post-conditions, and it is likely this would influence the estimated muscle forces. However, muscle force estimations are relatively insensitive to the time of activation and deactivation (Scovil & Ronsky, 2006), and it is expected there would have been minimal influence on the conclusions of this study. Furthermore, to reduce the complexity of the Monte Carlo it was assumed the nature of adaptations within muscles groups was uniform. However, heterogeneity within muscle groups in how the muscles adapt has been observed in the literature (e.g., LeBlanc, Lin, *et al.*, 2000). It is unclear whether muscles within a muscle group were more sensitive to the parameter perturbations than others, which prevents conclusions being drawn as to whether muscle parameters within the same group can be adjusted differently. It should also be recognised that the underlyding MSK model was primarily developed based on male participants, validated against a single male and single female participant, scaled to a male participant, and the reference isokinetic knee moment data were derived from a sample of male participants. The results of this study need to be replicated for female derived data to have full confidence in the applicability of the result to women. Finally, tendon slack length was not included in the Monte Carlo analysis because there was not any evidence to show a change with unloading, nor a physiological mechanism that might explain how this parameter might adapt to a change in (un)loading conditions (see appendix B). However, it is recognised that tendon slack length is regularly cited as being an important parameter for determining muscle forces in computational approches (e.g, Hicks *et al.*, 2015; Serrancolí *et al.*, 2020). The recommendation would be that for modelling adaptations to unloading using the Hill-type muscle model, pre-spaceflight tendon slack length (e.g. after calibration using computational approaches) should not be changed.

Conclusions

It has been shown that the Hill-type muscle model is capable of modelling muscular adaptations to unloading. It is important to carefully adjust optimal fibre length, particularly for muscles working within the ascending and descending limbs of the force-length relationship, to obtain feasible simulation results.

Shortening the optimal fibre length appears to align with observations that spaceflight is associated with a more flexed posture, but extreme shortening can influence the ability to obtain realistic simulation results. Future work should consider investigating more movements (e.g. gait or jumping movements) and alternative muscle sharing terms within the objective function to further understand how the Hill-type-muscle model can be used to represent adaptations to disuse.

Chapter 6

General Discussion

The overarching purpose of this thesis was to inform hypogravity exercise prescription by applying musculoskeletal (MSK) modelling and optimal control simulation methods to hypogravity exercise contexts. The aims were to i) create a *Biomechanical Handbook* of normative muscle and joint loading profiles when exercise is performed in different gravity levels, and ii) to assess how muscular adaptations to unloading can be replicated with a Hill-type muscle model. Until now, despite the clear benefits to the space science community, MSK modelling has been a surprisingly underutilised tool in hypogravity exercise research. Even beyond the aims of this thesis, the resource limitations placed on the collection of experimental data during spaceflight (e.g. space, equipment, expertise, and financial cost) lends itself to MSK modelling and simulation methods that can provide an effective solution to such challenges, with the only caveat of being able to validly replicate the context under investigation. In this thesis, this approach has been validated and used, for the first time, to quantify the internal loading on muscles and joint structures in different hypogravity scenarios. This is a key step as the exposure to hypogravity, and indeed other disuse paradigms, is associated with a plethora of MSK adaptations that compromise the functional capacity of the individual. The ability to estimate the internal MSK loading enables the investigation of which exercises, or more generically external loads, might trigger remodelling processes to maintain tissue integrity. Prior to this work, the loading profiles of these exercises were informed by external loads (i.e. ground reaction forces) or net joint moments that do not directly represent the stress placed on specific MSK structures. A more accurate and direct characterisation of how MSK tissues are loaded during hypogravity exercise allows for better alignment of expected stress to the structures that need rehabilitation. Additionally, in this thesis, the applicability of the Hill-type muscle model for replicating adaptations due to unloading was investigated. The Hill-type muscle model is the most common muscle model used in computational biomechanics because of it's ability to replicate muscle mechanics with relatively few parameters and high computational efficiency. The work of this thesis shows that known adaptations to spaceflight and bed rest can be successfully modelled and replicated by adjusting the Hill-type muscle model parameters. This provides an extremely valuable example of how MSK modelling and simulation approaches can contribute to space science.

6.1 Summary of Studies

The thesis began by presenting a vision for the creation of a *Biomechanical Handbook* resource that presents normative MSK loading profiles of key rehabilitation exercises. This was presented in the first study (Chapter 3), and was structured in two parts. First, a comprehensive open source biomechanical data repository, including *in vivo* measured knee contact forces via a force-instrumented joint prosthetic (eTibia), was used to validate the framework. Taking the eTibia data as ground-truth knee contact forces, the first part of the study sought to establish the accuracy of joint reaction force estimations, and indirectly physiological realism of muscle forces, when integrating a generic MSK modelling approach with a numerically efficient optimal control algorithm (direct collocation). A publicly available MSK model was scaled to the repository participant's anthropometrics, and combined with joint kinematics (derived from three-dimensional marker trajectories), ground reaction forces, net joint moments (calculated via inverse dynamics analysis) and electromyography (EMG) data and input into the framework to perform data-tracking simulations. The main outcomes were that the error in the joint reaction forces was within an expected tolerance, and performed comparably to similar generic modelling approaches. Additionally, the framework was able to capture salient features of joint loading, including showing an increase in joint reaction forces and a decrease in joint reaction impulses (a measure of magnitude and duration of loading) as walking speed increased. The novel contribution from this approach was that direct collocation, combined with a generic MSK modelling approach, can estimate MSK loading profiles during human movement with enough accuracy to compare the loading experienced between different exercises. This was a key step to enable the creation of a biomechanical handbook that includes normative values for expected loading profiles between gravity levels and different exercises. Additionally, although automatic algorithms for the segmentation of medical imaging data to create subject-specific models are being developed, these approaches still require financial resources and expertise to collect and process. This is not a viable approach during post-spaceflight rehabilitation because the recovery of the MSK system likely requires the creation of personalised models at multiple time points for the model to still be *subject-specific*. A generic approach is also more accessible to agencies and intuitions that do not have the financial, time, or intellectual resources to undertake a subject-specific approach. This is particularly relevant with the emergence of powerful simulations tools, such as OpenSim's MoCo (Dembia *et al.*, 2021) and SCONE (Geijtenbeek, 2019), that have made trajectory optimisation methods (i.e. direct collocation and shooting methods) more accessible to the wider biomechanics community who may not have access to subject-specific modelling methods. By demonstrating the benefit a Biomechanical Handbook it provides a platform for space agencies to integrate subject-specific modelling approaches into their astronaut monitoring to supplement findings using a generic approach.

The second part of the study saw the simulation framework applied to an experimentally simulated set of hypogravity scenarios, which involved a single participant performing a single-leg hopping task whilst attached to a body weight support system. It was found that although total quadriceps femoris muscle force (sum of all four muscles) increased as gravity increased, the individual contributions, particularly from the rectus femoris, was not consistent across gravity conditions. This highlighted the benefit of MSK modelling to exercise in hypogravity as it demonstrated that force contributions at the individual muscle level did not follow the same pattern as more 'external' (or less accurate) estimations of MSK loading (e.g. ground reaction forces or net joint moments). The most novel aspect of this study was the integration of a muscle adaptation model to the MSK simulations, which bridges the gap between theoretical simulations and application to practice. The adaptation model, which estimated the increase of muscle cross-section area as a function of overload, allowed, for the first time, the estimation of hypothetical training volumes (i.e. repetitions) required to elicit a meaningful muscle hypertrophy. This can provide additional benefit, from a space science perspective, to assess the appropriateness of different exercises paradigms, such as single-leg hopping, to avoid detrimental adaptations. The study not only provides information of how the MSK structures are being loaded, but also assesses the feasibility of the time frame required to achieve the overload. For example, the estimated repetitions can be broken down into typical training parameters (e.g. repetitions per set and sets per session), which can be used to assess whether the number of session per week are feasible to achieve. From this, more information is provided to the practitioner to determine which gravity level is best aligned with the participant's MSK condition. This information can be used to develop a *Biomechanical Handbook*, a resource that documents expected loading profiles and training volumes of rehabilitation exercises to better align exercise programs to the individual's MSK condition.

To this end, Chapter 4 features an experimental protocol that expanded on the Biomechanical Handbook concept described in Chapter 3. Through the collection and analysis of a comprehensive catalogue of gait and jumping movements in hypogravity, this protocol provides a blueprint for making the Biomechanical Handbook a reality. Within the protocol there is a description of a comprehensive biomechanical data collection in an array of hypogravity conditions, including Lunar ($\sim$0.17 g) and Martian ($\sim$0.38 g) gravity. Marker trajectories, ground reaction forces and EMG data will be collected for a combination of gait movements common in hypogravity (i.e. walking, running and skipping) and jumping/plyometric movements common in rehabilitation/training (i.e. hopping, vertical countermovement jumps, and drop landings). The same data-tracking simulation framework outlined in Chapter 3 is presented as a method to estimate the MSK loading profiles (i.e. muscle forces and joint reaction forces) and training volumes (i.e. via the muscle adaptation model) for the catalogue of movements under investigation. Additionally, two ultrasonography probes on the gastronemius muscle belly and Achilles tendon junction will provide valuable insight into the muscle-tendon unit (MTU) behaviour when exercising in hypogravity. Fibre lengths, velocities, pennation angle and tendon lengths will be captured to provide insight in and of themselves, but will also provide opportunity to validate the simulated physiological behaviour outcomes of the muscle models used in the MSK model. The proposed work builds upon the case-study presented in study one by extending the *Biomechanical Handbook* idea to a wider variety of gait and rehabilitation movements. This allows for comparison between different exercises at the same gravity level, the same exercises at different gravity levels, and different exercises at different gravity levels to optimise exercise prescription. A secondary novel contribution of this approach is the comparison of different exercises at the same gravity level, as has the potential to identify optimum exercises for loading MSK structures in different gravity conditions. For example, with space agencies planning for long-distance space missions to the Moon and Mars, knowledge of expected loading profiles when performing different exercises in these environments can provide insight into best practices for mitigating against muscular adaptations to unloading.

The third study, presented in Chapter 5, outlines a Monte Carlo sampling framework to investigate the fidelity of Hill-type muscle models, a common model used in MSK simulation, in replicating the functional outcomes due to the severe adaptations reported after disuse. Post-spaceflight knee moment data of isokinetic knee extension tasks (i.e. two angular velocities) was retrieved from the literature and used in a simulation framework to replicate the movements and internal loading generated by an individual in a muscular adapted state. A modified version of the direct collocation framework presented in Chapters 3 & 4 was developed and used to solve for the MTU activation and contraction dynamics with skeletal dynamics of the knee angle prescribed based on the isokinetic condition. A Monte Carlo sampling technique was utilised to randomly perturb the muscle model parameters within literature defined boundaries, where each simulation represented a hypothetical individual who has been exposed to microgravity ($\sim$0 g). The optimal solutions found by the framework ensured the physiologically plausibility of the simulated data through computational and physiological criteria (i.e. acceptable knee extensor moment values). This allowed for a hypothetical population of Hill-type muscle model parameters to be generated that were representative of specific muscle adaptations. It was shown that if the optimal fibre lengths are adjusted correctly, the Hill-type muscle model is able to recreate muscular adaptations.

6.2 Limitations and Future Work

Astronaut Specific Loading Profiles

The use of generic MSK models was championed in this thesis, particularly during Chapter 3, as it was argued that access to resources required for model personalisation is limited. As mentioned, the creation of subject-specific models is not a trivial task, and automatic segmentation algorithms do not overcome the issues related to the collection of medical imaging data. The creation of a biomechanical resource outlining the expected MSK loads during exercise in hypogravity provides a valuable insight for these contexts. However, it is recognised that the load profiles may not reflect those of an astronaut who presents with muscular adaptations. Data collected during the Monte Carlo in chapter five demonstrated that adjustment of Hill-type muscle model parameters led to altered muscle-tendon behaviour despite producing the same net joint moment about the knee. This finding is confirmed in the literature, with van Der Krogt *et al.* (2012) demonstrating that when maximum isometric forces are reduced to simulated muscle weakness other muscles will regularly compensate with increased activation and force output. This might lead to exercise prescriptions during rehabilitation that are either insufficient to stimulate adaptations, leading to longer rehabilitation times, or that exceed the astronaut's capacity to perform, placing them at risk of injury. Chapter 3 provided an approach for addressing this issue by demonstrating a vision for a biomechanical handbook to inform astronaut rehabilitation. The scientific protocol outlined in Chapter 4 expands on this vision by presenting a catalogue of exercise paradigms performed in a range of hypogravities to broaden the application of the biomechanical handbook. These data would capture the biomechanical changes to movement strategies (i.e. kinematics and kinetics) and neural changes (i.e. EMG) that can be used to calibrate the MTU parameters of the muscle models, as has been done previously (e.g., Falisse *et al.*, 2017), to run data-tracking simulations. Repeating this approach with a large enough sample would also allow for loading profiles to be defined according to the astronaut-specific adaptations. Given the limited sample of astronauts, bed rest studies would provide an alternative population to sample from to statistically power these analyses. This would supplement the work presented in Chapter 3 with generic and astronaut-specific loading profiles to be incorporated into the Biomechanical Handbook resource, and allow for researchers and practitioners to inform their work based on the information available to them.

Predictive Simulations of Astronaut "Pre-habilitation"

It is often said that *prevention is the best cure.* The focus on optimising rehabilitation is necessary because although there are substantial exercise countermeasures, and indeed non-exercise countermeasures, in place during spaceflight (Loehr *et al.*, 2015), astronauts still present with MSK adaptations that impair their terrestrial function. However, in an ideal world the MSK adaptations would be completely mitigated against via in-flight exercise, so-called *pre-habilitation*, as there would be minimal impact on their reintegration into society and the substantial resources needed for rehabilitation (e.g., time, finances, and labour). Building upon the work Chapter 5, if the Hill-type muscle model can be used to model different, astronaut-specific adaptations, and astronauts can then be categorised according to emerging muscular adaptations during spaceflight, interventions can be applied to mitigate against further deterioration. These hypothetical sub-populations of Hill-type muscle model parameter combinations that represent astronaut-specific MSK models can be created according to their specific muscular adaptations. These could be used to inform predictive simulations to assess the efficacy of hypothetical training interventions to alter the course of their MSK health. There are two main challenges for future research. Firstly, what self-administered monitoring tools can be introduced during spaceflight that relate muscular adaptations *in vivo* to Hill-type muscle model parameters. In a recent perspective article, Fregly (2021) outlined a blueprint from improving impact of MSK modelling and simulation frameworks in real world clinical applications. Within this review Fregly highlights the importance of appropriately assessing the needs of the clinical populations. Could one of the current exercise devices on the International Space Station be used to assess muscular function to predict parameter adjustments relative to a subject-specific pre-flight model? Or could a new tool, such as ultrasound, be used to directly measure adaptations to muscle architecture? Secondly, determining what optimisation principles successfully predict the maintenance of MSK health during exercise in spaceflight. One approach could be to marry the outcomes of a predictive simulation with the muscle adaptation model concept presented in Chapter 3. This could be used to design an in-flight training intervention where, instead of predicting repetitions to elicit an increase in muscle size, the adaptation model is modified to predict the repetitions required to prevent a decrease in muscle size.

Another approach for predictive simulations is to estimate MSK loading in *what if?* scenarios. Currently, there is a gap between the required MSK loading during spaceflight to stimulate tissue remodelling to maintain homeostasis, and what is currently possible to perform on the International Space Station. For example, currently on the International Space Station limited exercise modes are available and limited time available for exercise. With further space missions on the horizon (i.e. to the Moon and Mars) these factors could be even more constrained. In theory, an inverse MSK modelling approach would be possible in-flight if biomechanical data can be collected. However, operational resources, such as shuttle payload, room on the space station, and astronaut expertise, make this option difficult as the accuracy of the data collected may be compromised. Development of predictive simulations would allow for the exploration of equipment design and alternative exercises with the current equipment, which could be used to improve in-flight exercise programs. This concept has been demonstrated by Fregly and colleagues (Fregly *et al.*, 2015) who modelled the advance resistive exercise device (a multi-purpose resistance exercise device on the International Space Station) in 1 g and in microgravity. They showed that modifying foot position forward and backward during a back squat exercise altered the net joint moments of the lower-limb, and could reproduce similar magnitudes to those measured in 1 g. In a similar vein, formulating predictive simulations to replicate the expected loading profile of terrestrial movement would allow exploration of equipment design and movement modifications to improve in-flight exercise. For example, another exercise device currently on the International Space Station is a Treadmill with vibration isolation (TVIS) that, through a harness, provides gravity replacement loads to the astronaut via bungee cords (McCrory *et al.*, 2004). Different exercises could be simulated using the TVIS in its current state to evaluate whether other movements might provide a more quality training stimulus than walking or running. Plyometric hopping has recently shown promise in an experimental study where ground reaction forces in 1 g could be replicated in hypogravity if hopping height was sufficient (Weber *et al.*, 2019). Alternatively, the design of this system could be optimised by including the parameters of the bungee cords (i.e. stiffness and resting length) as design variables and/or adding new elements to create a new model for the gravity replacement load system (e.g. damping or active motor resistance).

Longitudinal Study Designs

Building on the previous point, the recovery of MSK tissue during post-spaceflight rehabilitation can take longer than the original space mission, potentially taking three years to return to pre-flight condition in some individuals (Sibonga *et al.*, 2007). This further complicates the landscape as inter-individual variability in MSK adaptations following disuse as it appears to emerge in the recovery of tissue during rehabilitation. The experimental protocol outlined in Chapter 4 is a cross-sectional design meaning the loading profiles defined in this study would represent the MSK condition at that point in time. Defining MSK load profiles using cross-sectional study designs are arguably not sensitive enough for a spaceflight rehabilitation context, as it is impossible to identify those who recovery less quickly. Longitudinal study designs have been combined with MSK modelling previously to identify patients who do and do not respond to post-surgery rehabilitation (Killen *et al.*, 2020; Wesseling *et al.*, 2018). Capturing the propensity for the biological system's adaptability over time is what distinguished them from mechanical systems, and is fundamental to improving clinical impact of MSK modelling (Fregly, 2021). Employing a longitudinal design during astronaut rehabilitation would allow for observing the pattern of change in MSK loading profiles over time in those who do and do not recover. This has two potential benefits: i) it adds an extra-dimension to the Biomechanical Handbook by including stage of rehabilitation to supplement the grading of exercises according to hypogravity and an astronaut's MSK condition, and ii) further analyses could be incorporated into the study design to identify mechanisms that explain the inter-individual variability in recovery.

6.3 Conclusion

The concept of a *Biomechanical Handbook* was presented and applied to a hypogravity context. This was achieved thanks to the validation of a data-tracking, direct collocation optimal control framework, which allowed for the estimation of muscle forces and joint reaction forces. The novel contribution of this resource is the ability to inform astronaut rehabilitation by quantifying internal loading profiles (i.e. muscle and joint forces), which was also estimated for the first time during hypogravity movement. In doing so it provides a more accurate representation of MSK loading than previous work (i.e. from net joint moments), and a method for which to grade hypogravity rehabilitation exercises according to the astronaut's MSK condition. Combining adaptation models, such as the muscle adaptation model presented here, with the outcomes of MSK modelling was shown to have added benefit that could be used to optimise exercise prescription.

Future directions have been contemplated to continue the novel contributions made in this thesis, with particular focus on how MSK modelling and computer simulations can have an impact on the space science community. In particular, the challenge facing future research centres around how to address the large inter-individual variability in astronaut adaptations and recovery during rehabilitation. The generic approaches utilised in this thesis provide a useful resource for contexts where access to model personlisation is limited, but likely do not capture the astronaut-specific biomechanical consequences of their adapted MSK condition. Acknowledging this, the final study of this thesis provided insight into how muscular adaptations can be modelled using a common muscle model used in computational biomechanics. This gives future research a platform to inform the adjustment of muscle model parameters to improve estimation of MSK in astronauts.

Musculoskeletal modelling is an underutilised tool in space science, and as the push towards personalised medicine continues in other clinical contexts, this thesis provides a timely contribution to astronaut rehabilitation. The capacity to estimate internal loading (i.e. muscle force and joint forces) will help to inform practice by allowing practitioners to supplement their experience with information on the loading on key GRF structures, and allow for astronaut-specific adaptations to be aligned with the expected loading profiles. Additionally, the identification of strategies for adjusting MTU parameters depending on the adaptations being modelled will be invaluable for future simulation studies to ensure the accuracy and validity of their outcomes. This places space science within the domain of computational biomechanics, ready to benefit from developments in clinical practice as GRF modelling continues to be embraced as part of clinical rehabilitation pipelines.

Appendix A

Appendix to Chapter 3

A.1 Knee Grand Challenge Data

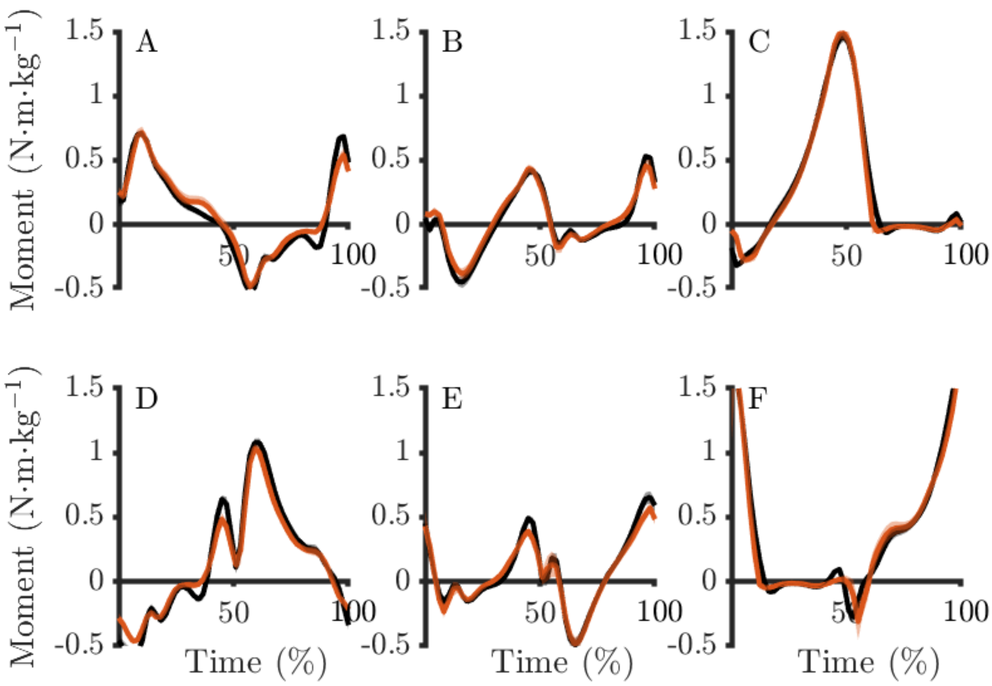

Figure A-1 Right (A - C) and left (D - F) net joint moment tracking for hip extension (A & D), knee flexion (B & E) and ankle plnatarflexion (C & F) during the fastest walking speed (1.4 $m \cdot s^{-1}$). Extension and plantar flexion were defined as positive. Coloured = simulated, black = experimental.

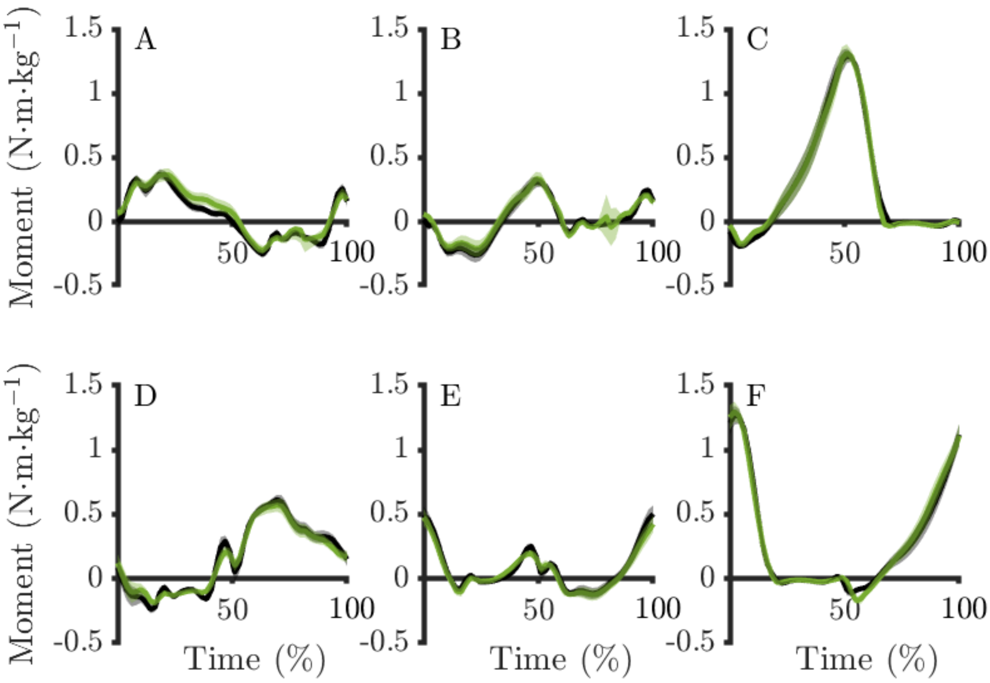

Figure A-2 Right (A - C) and left (D - F) net joint moment tracking for hip extension (A & D), knee flexion (B & E) and ankle plnatarflexion (C & F) during the slowest walking speed (0.8 $m \cdot s^{-1}$). Extension and plantar flexion were defined as positive. Coloured = simulated, black = experimental.

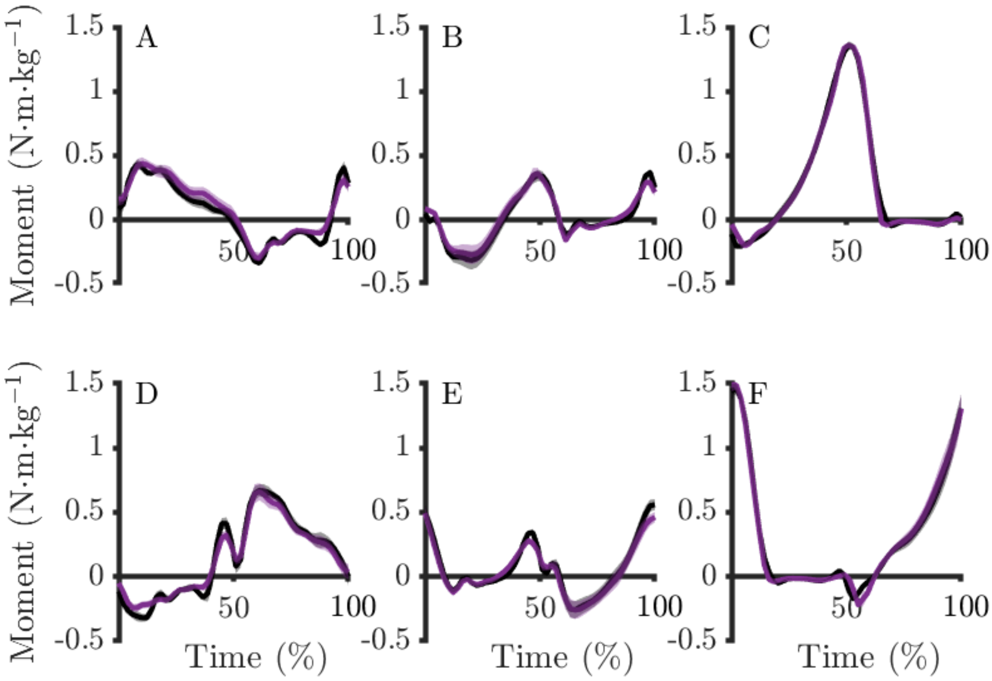

Figure A-3 Right (A - C) and left (D - F) net joint moment tracking for hip extension (A & D), knee flexion (B & E) and ankle plnatarflexion (C & F) during the set walking speed (1.0 $m \cdot s^{-1}$). Extension and plantar flexion were defined as positive. Coloured = simulated, black = experimental.

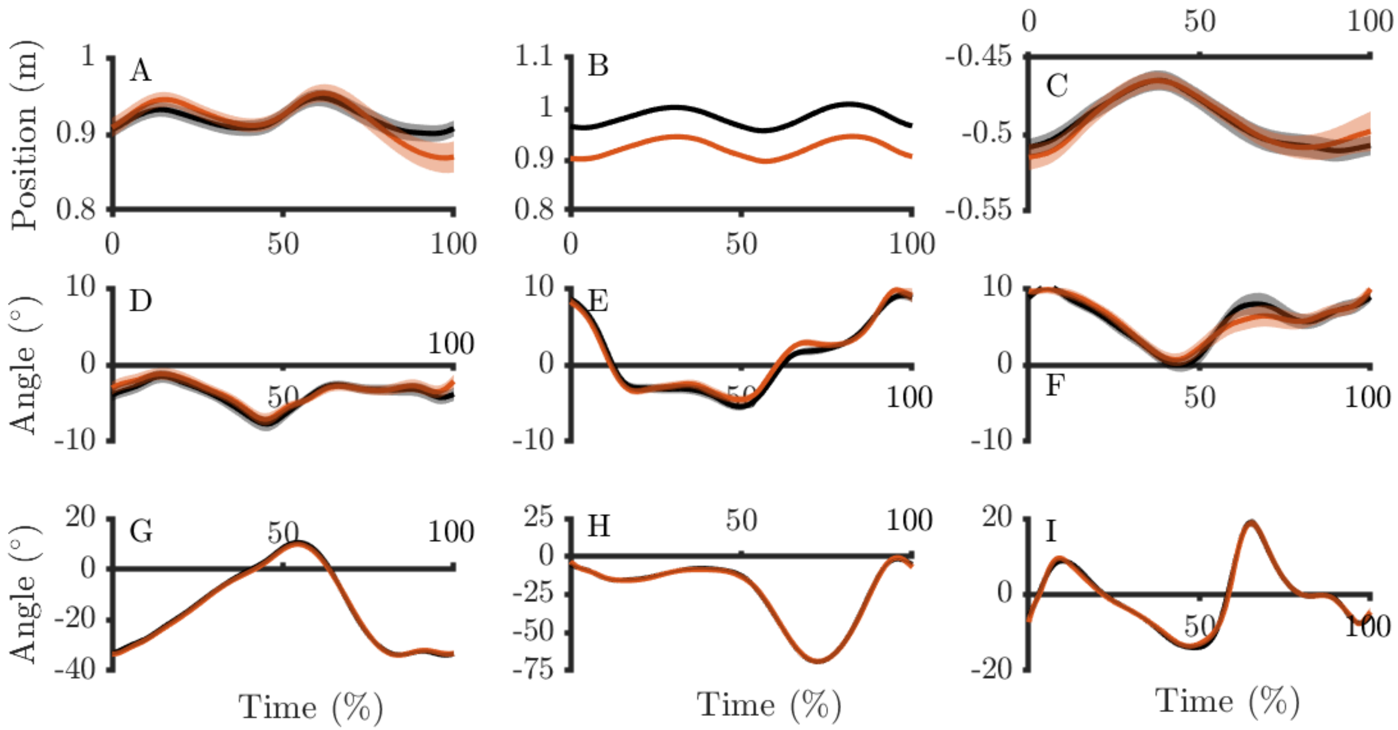

Figure A-4 Pelvis translation (A: A-P, B: Vertical, & C: M-L) and rotation (D: tilt, E: lateral title, & F: rotation), and sagittal plane angle (G: Hip, H: Knee, I: Ankle) tracking at the fastest walking speed (1.4 $m \cdot s^{-1}$) walking speed. Backward tilt, right lateral tilt, anti-clockwise, extension, plantar flexion were defined as positive. Coloured = simulated, black = experimental.

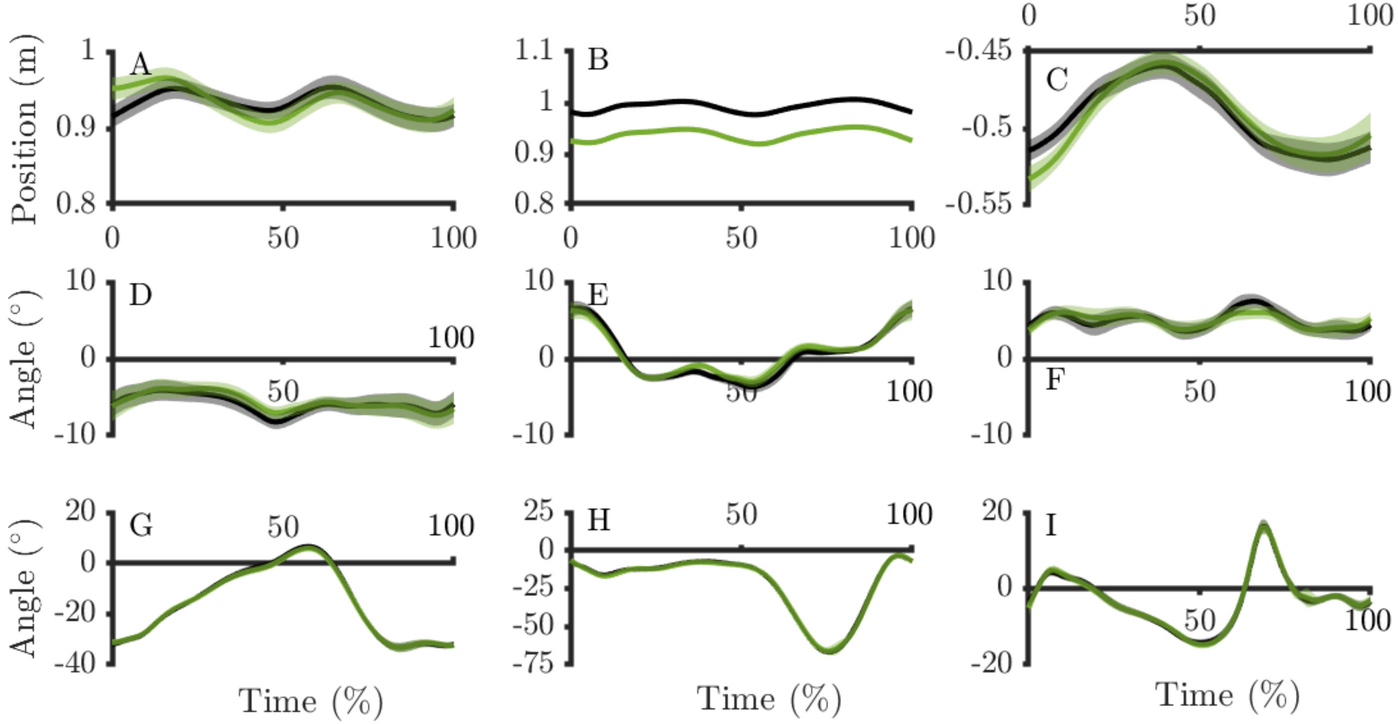

Figure A-5 Pelvis translation (A: A-P, B: Vertical, & C: M-L) and rotation (D: tilt, E: lateral title, & F: rotation), and sagittal plane angle (G: Hip, H: Knee, I: Ankle) tracking at the slowest walking speed (0.8 $m \cdot s^{-1}$) walking speed. Backward tilt, right lateral tilt, anti-clockwise, extension, plantar flexion were defined as positive. Coloured = simulated, black = experimental.

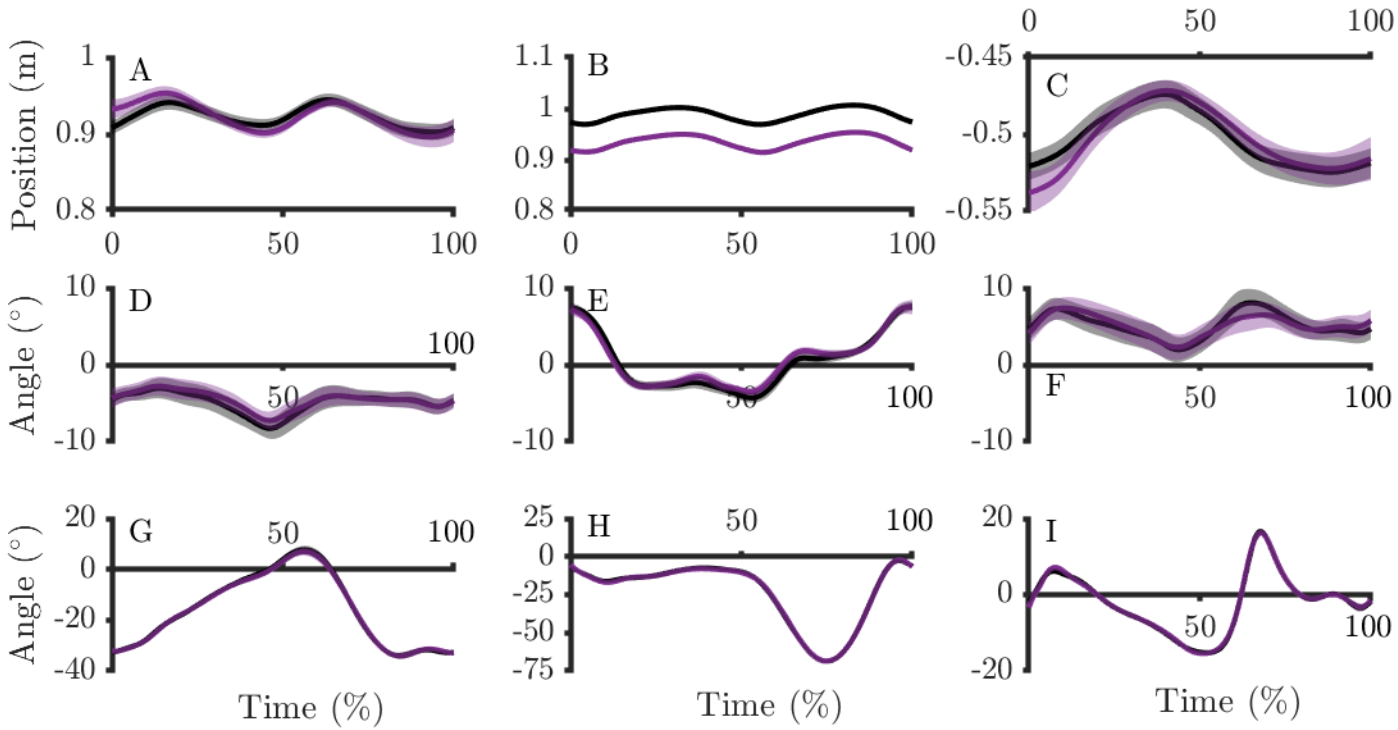

Figure A-6 Pelvis translation (A: A-P, B: Vertical, & C: M-L) and rotation (D: tilt, E: lateral title, & F: rotation), and sagittal plane angle (G: Hip, H: Knee, I: Ankle) tracking at the set walking speed (1.0 $m \cdot s^{-1}$) walking speed. Backward tilt, right lateral tilt, anti-clockwise, extension, plantar flexion were defined as positive. Coloured = simulated, black = experimental.

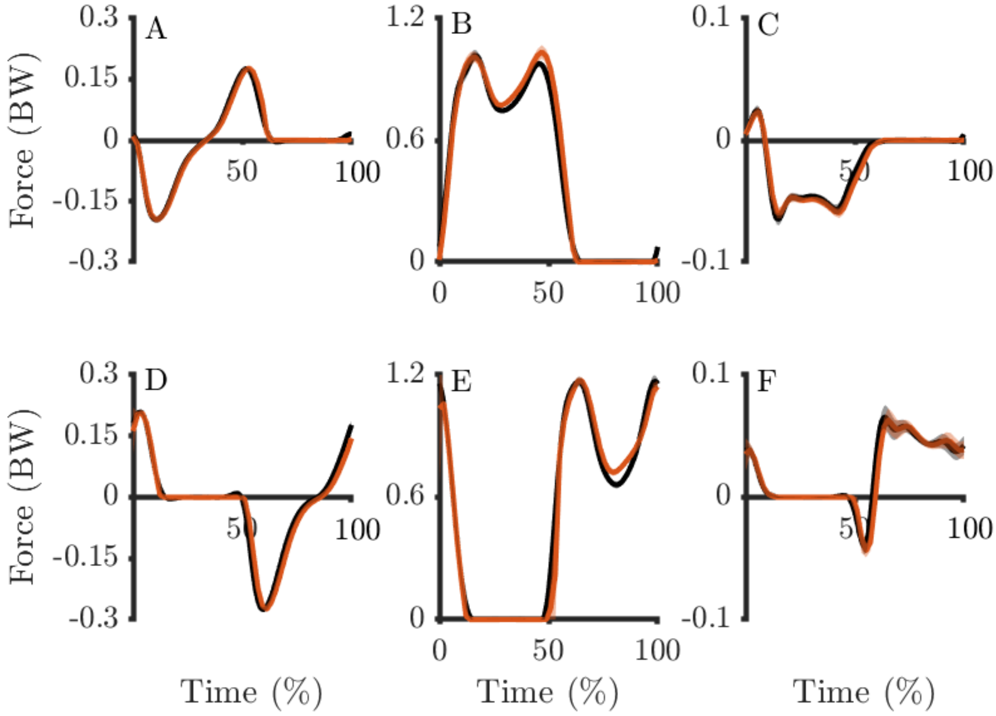

Figure A-7 Normalised A-P (A & D), vertical (B & E) and M-L (C & F) GRF tracking of the right (A-C) and left (D-F) steps for the fastest walking speed (1.4 m·s^{-1}). Coloured = simulated, black = experimental.

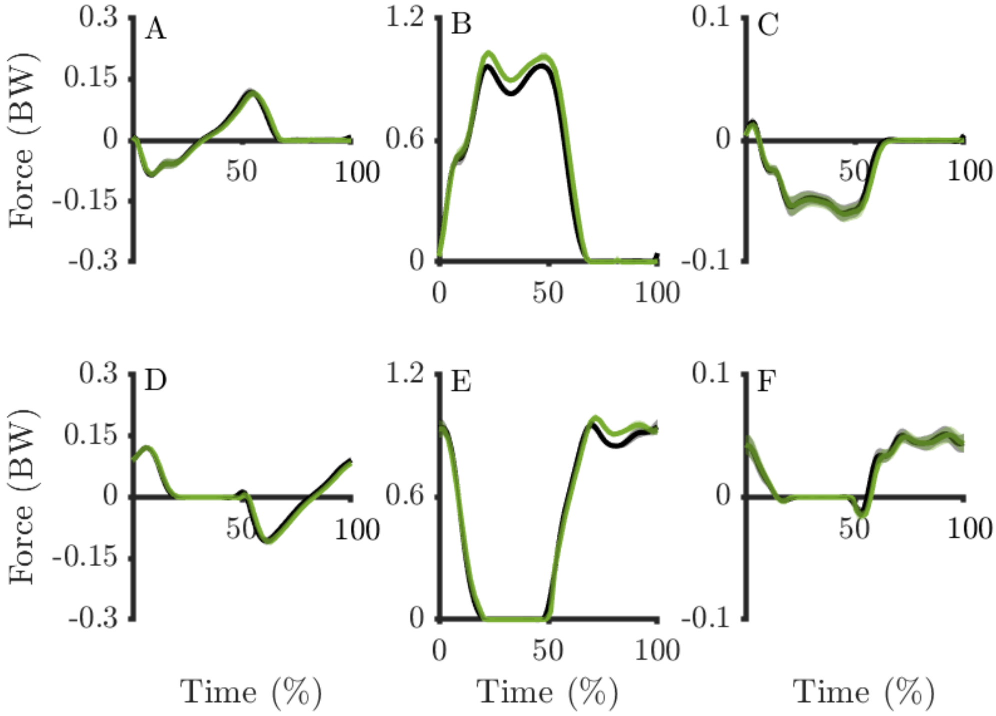

Figure A-8 Normalised A-P (A & D), vertical (B & E) and M-L (C & F) GRF tracking of the right (A-C) and left (D-F) steps for the slowest walking speed (0.8 m·s^{-1}). Coloured = simulated, black = experimental.

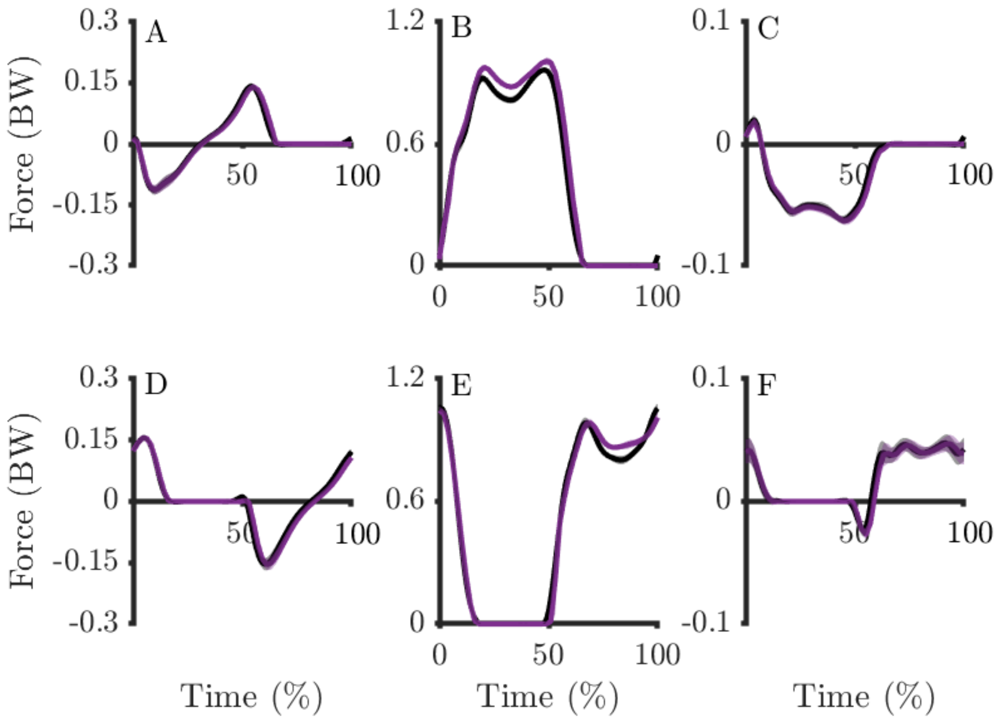

Figure A-9 Normalised A-P (A & D), vertical (B & E) and M-L (C & F) GRF tracking of the right (A-C) and left (D-F) steps for the set walking speed (1.0 m·s^{-1}). Coloured = simulated, black = experimental.

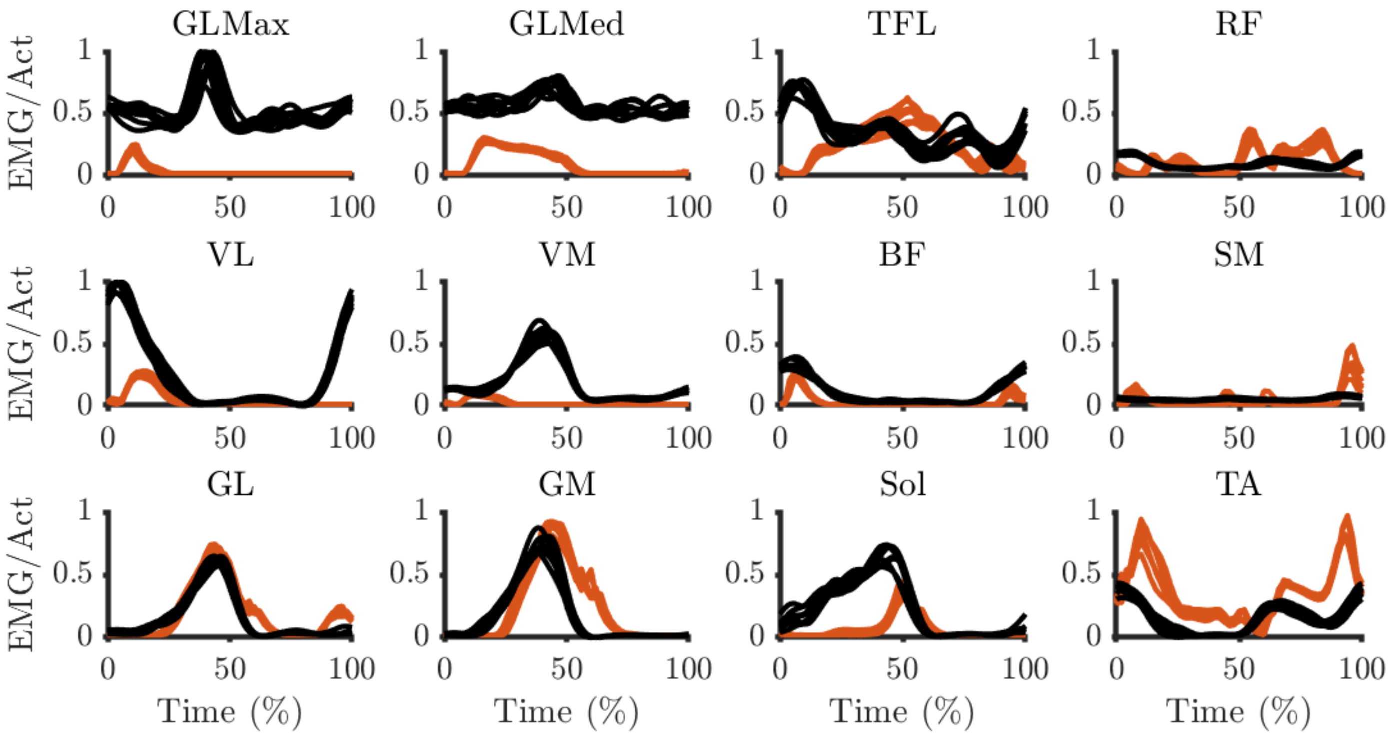

Figure A-10 Comparison between simulated muscle activations and experimental EMG during fast walking (1.4 m·s^{-1}). Coloured = simulated, black = experimental. GLMax = gluteus maximus, GLMed = gluteus medius, TFL = tensor fascia latae, RF = rectus femoris, VL = vastus lateralis, VM = vastus medius, BF = biceps femoris, SM = semimembranosus, GL = gastrocnemius lateralis, GM = gastrocnemius mediaslis, Sol = soleus, TA = tibialis anterior.

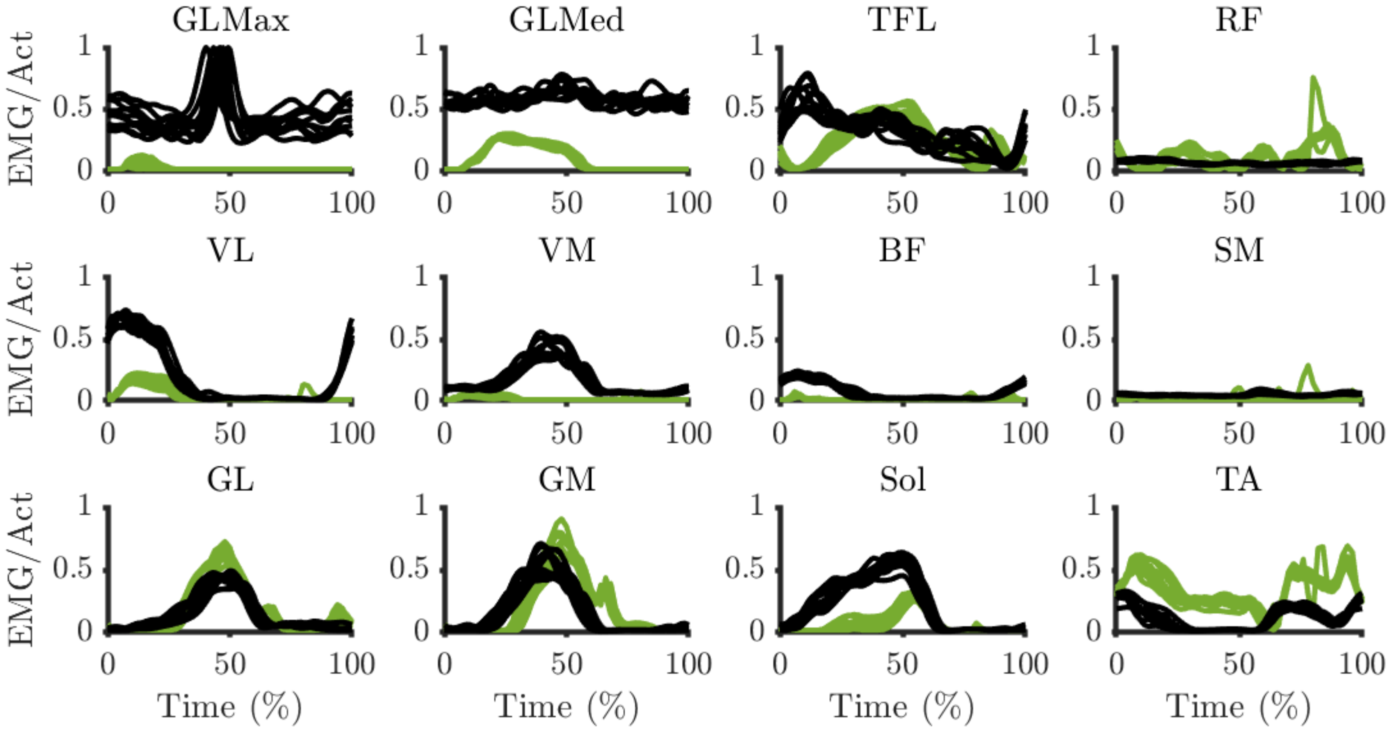

Figure A-11 Comparison between simulated muscle activations and experimental EMG during slow walking ($0.8\ \mathrm{m{\cdot}s^{-1}}$). Coloured = simulated, black = experimental. GLMax = gluteus maximus, GLMed = gluteus medius, TFL = tensor fascia latae, RF = rectus femoris, VL = vastus lateralis, VM = vastus medius, BF = biceps femoris, SM = semimembranosus, GL = gastrocnemius lateralis, GM = gastrocnemius mediaslis, Sol = soleus, TA = tibialis anterior.

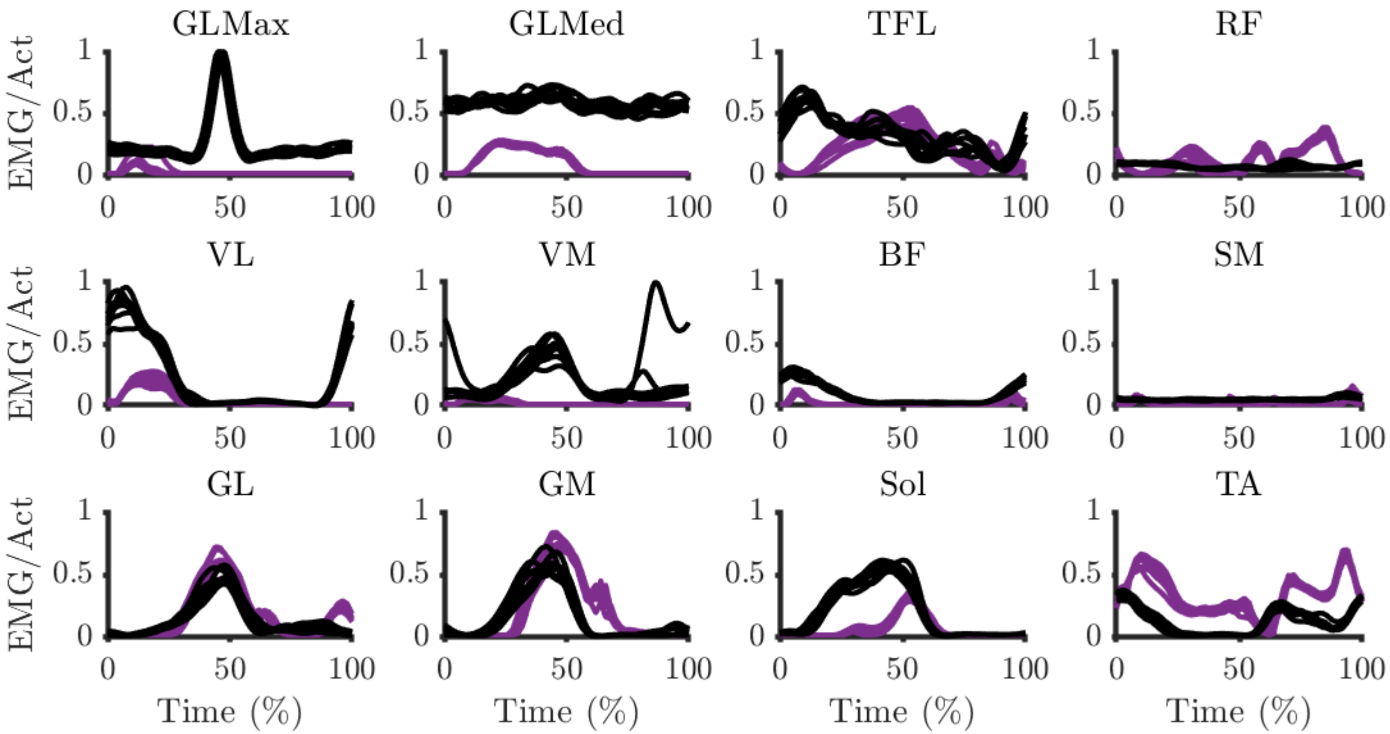

Figure A-12 Comparison between simulated muscle activations and experimental EMG during set speed walking (1.0 m·s^{-1}). Coloured = simulated, black = experimental. GLMax = gluteus maximus, GLMed = gluteus medius, TFL = tensor fascia latae, RF = rectus femoris, VL = vastus lateralis, VM = vastus medius, BF = biceps femoris, SM = semimembranosus, GL = gastrocnemius lateralis, GM = gastrocnemius mediaslis, Sol = soleus, TA = tibialis anterior.

A.2 Hypogravity Case Study

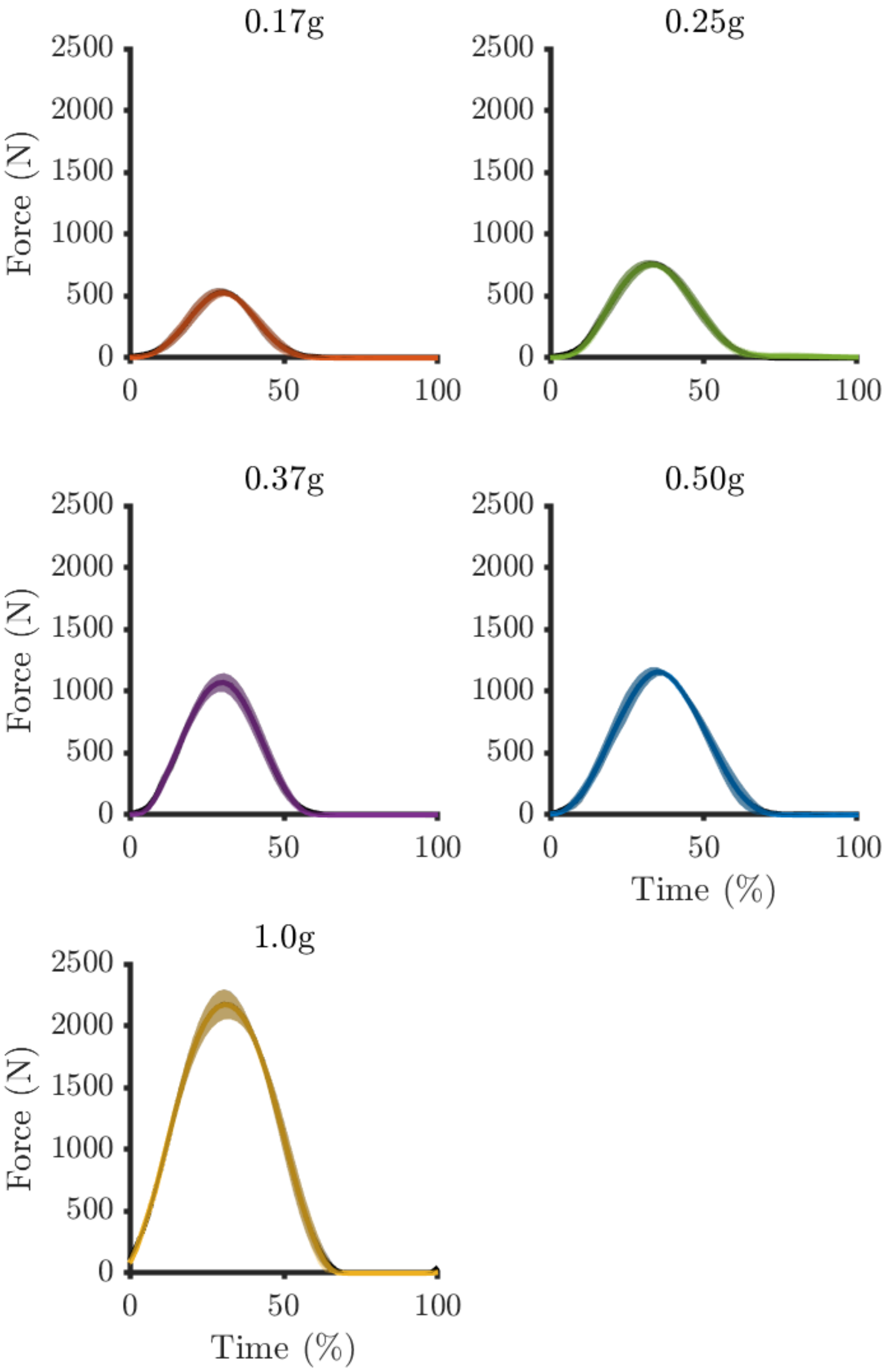

Figure A-13 Vertical ground reaction force tracking whilst hopping at different gravity levels. Coloured = simulated, black = experimental.

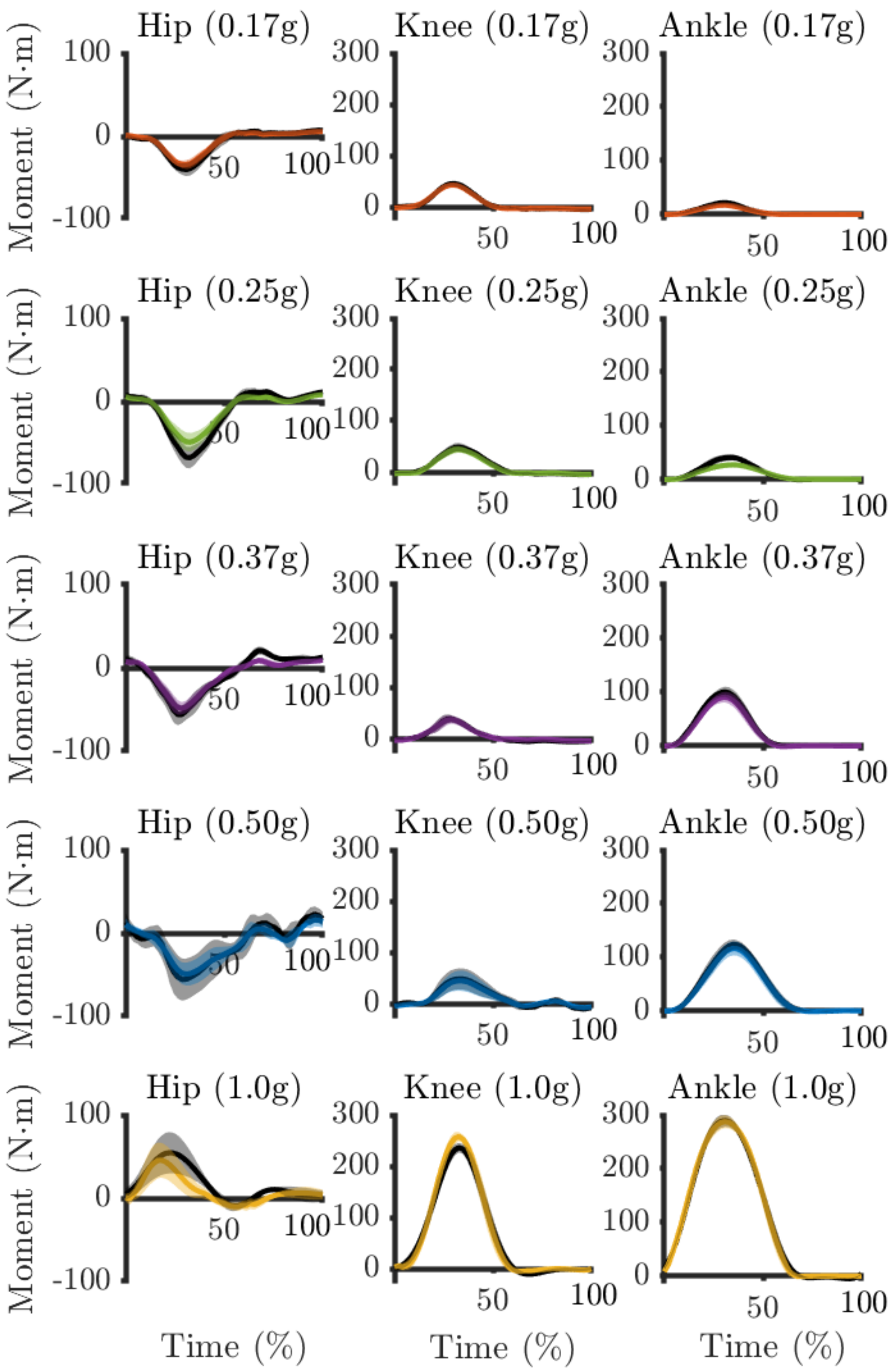

Figure A-14 Net joint moment tracking at the hip, knee, and ankle in the sagittal plane at different levels of gravity. Coloured = simulated, black = experimental.

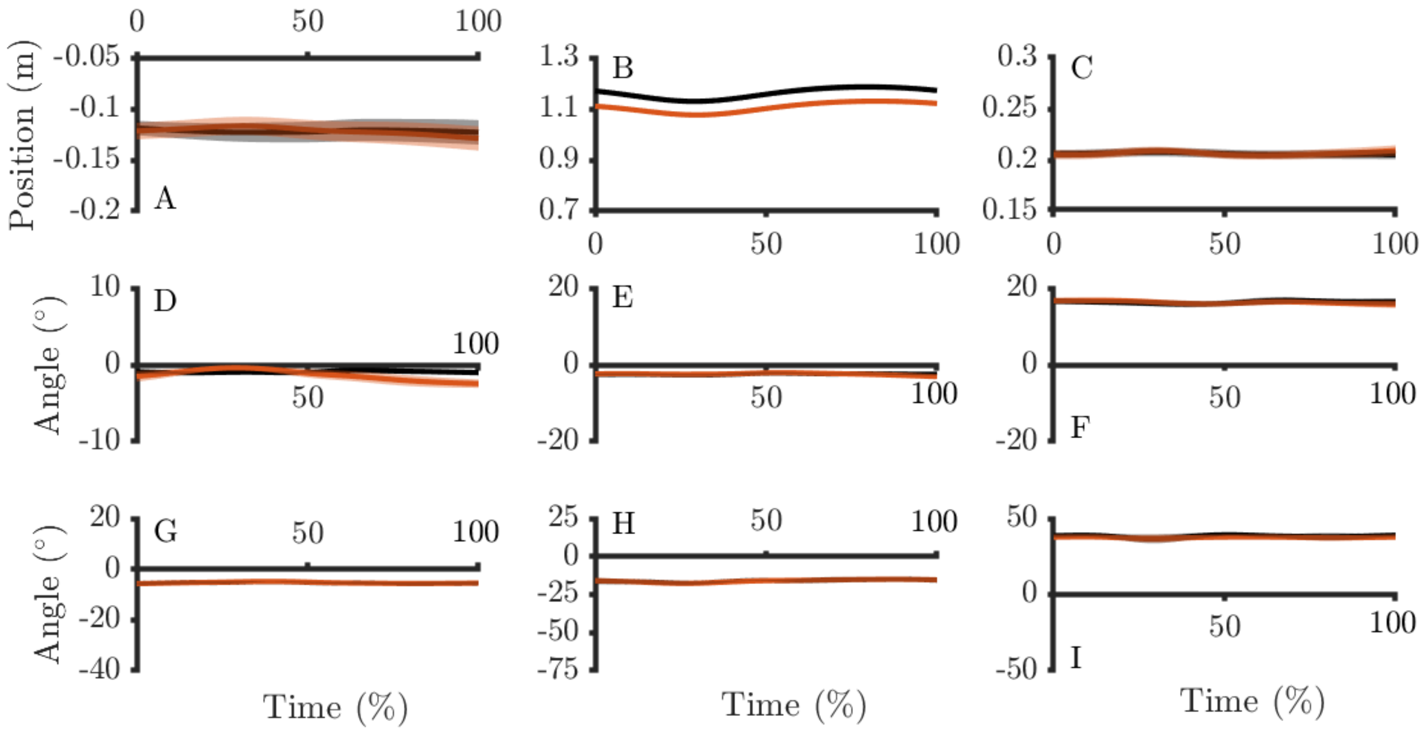

Figure A-15 Pelvis translation (A: A-P, B: Vertical, & C: M-L) and rotation (D: tilt, E: lateral title, & F: rotation), and sagittal plane angle (G: Hip, H: Knee, I: Ankle) tracking whilst hopping at 0.17 g hypogravity. Backward tilt, right lateral tilt, anti-clockwise, extension, plantar flexion were defined as positive. Coloured = simulated, black = experimental.

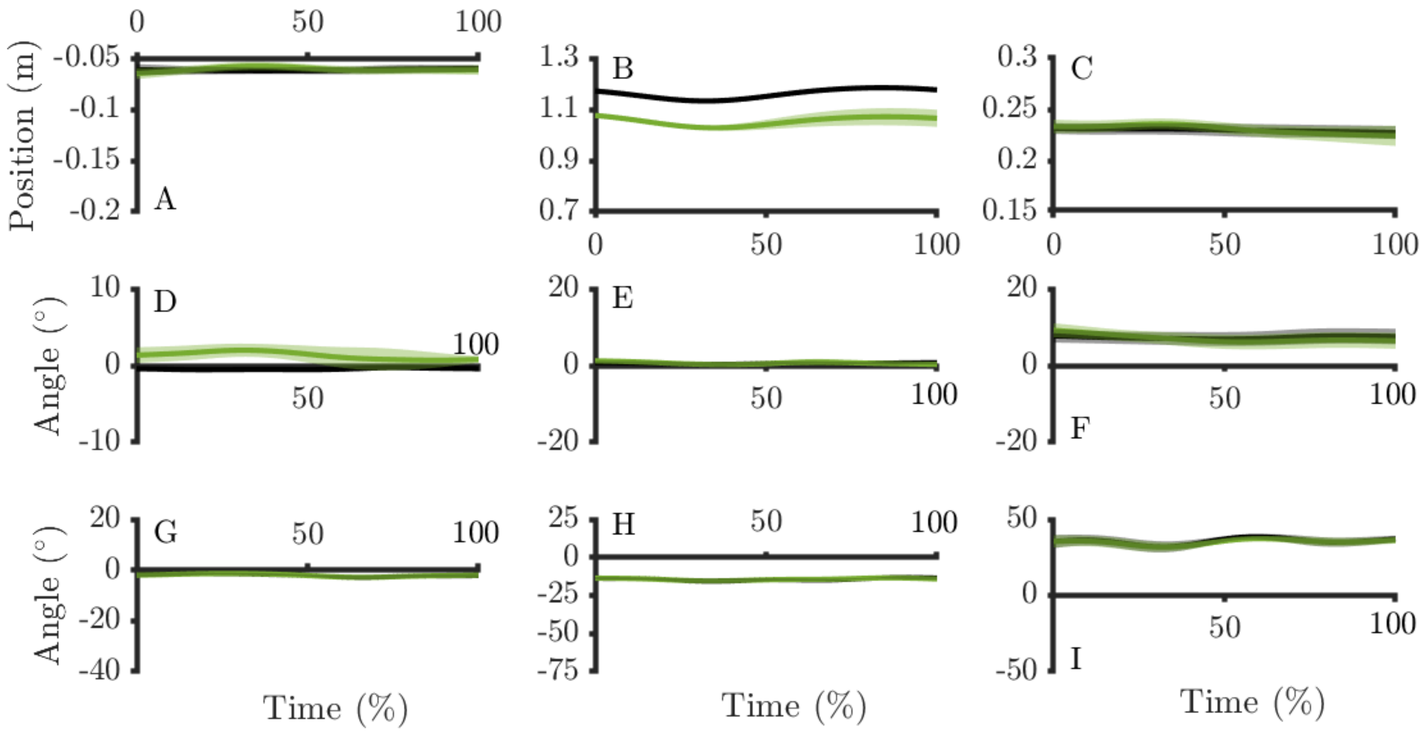

Figure A-16 Pelvis translation (A: A-P, B: Vertical, & C: M-L) and rotation (D: tilt, E: lateral title, & F: rotation), and sagittal plane angle (G: Hip, H: Knee, I: Ankle) tracking whilst hopping at 0.25 g hypogravity. Backward tilt, right lateral tilt, anti-clockwise, extension, plantar flexion were defined as positive. Coloured = simulated, black = experimental.

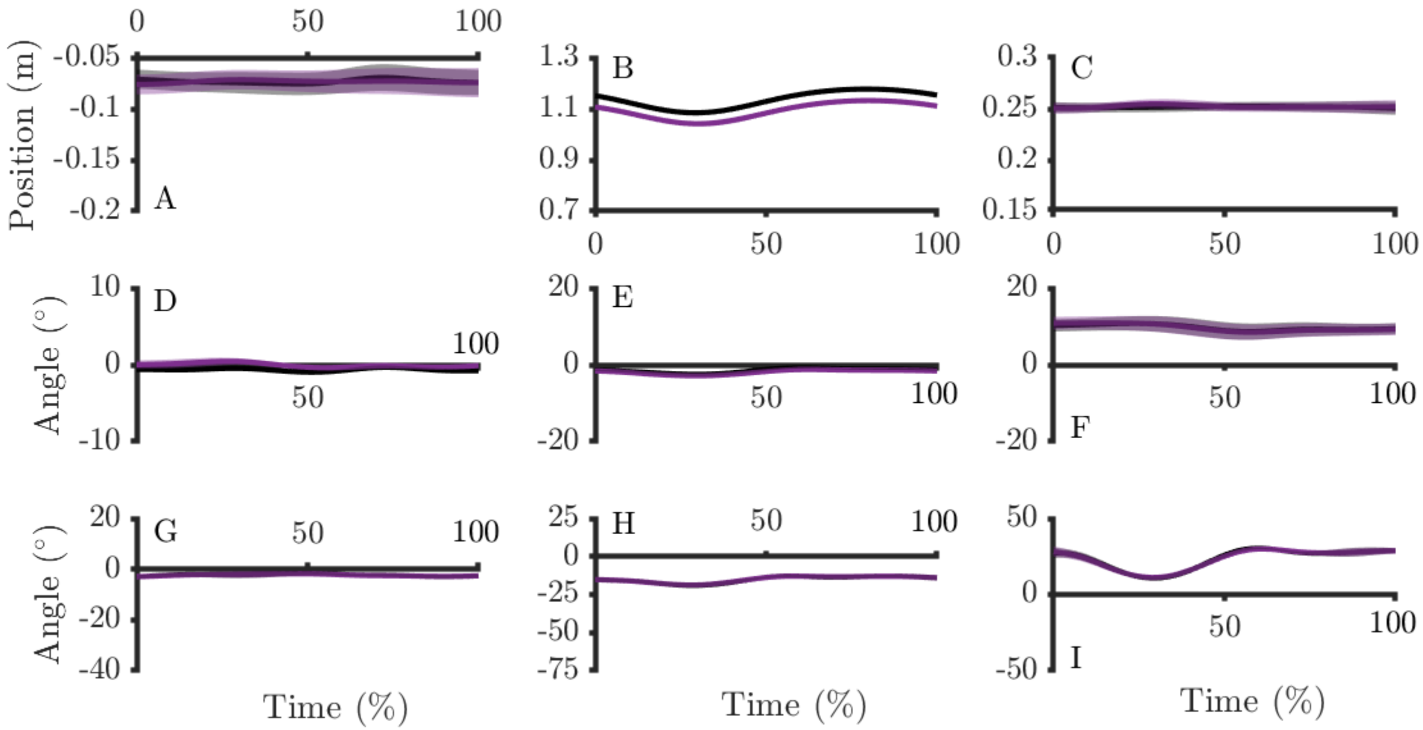

Figure A-17 Pelvis translation (A: A-P, B: Vertical, & C: M-L) and rotation (D: tilt, E: lateral title, & F: rotation), and sagittal plane angle (G: Hip, H: Knee, I: Ankle) tracking whilst hopping at 0.37 g hypogravity. Backward tilt, right lateral tilt, anti-clockwise, extension, plantar flexion were defined as positive. Coloured = simulated, black = experimental.

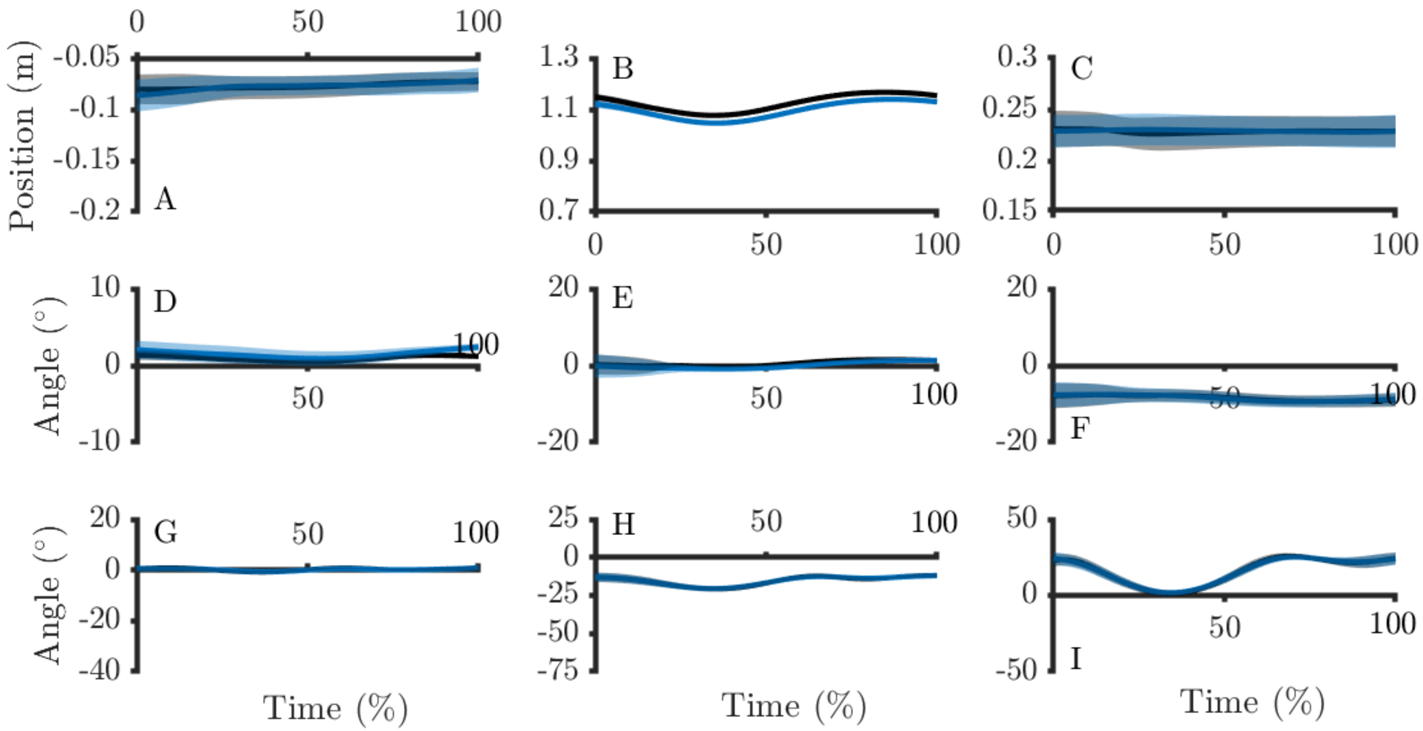

Figure A-18 Pelvis translation (A: A-P, B: Vertical, & C: M-L) and rotation (D: tilt, E: lateral title, & F: rotation), and sagittal plane angle (G: Hip, H: Knee, I: Ankle) tracking whilst hopping at 0.50 g hypogravity. Backward tilt, right lateral tilt, anti-clockwise, extension, plantar flexion were defined as positive. Coloured = simulated, black = experimental.

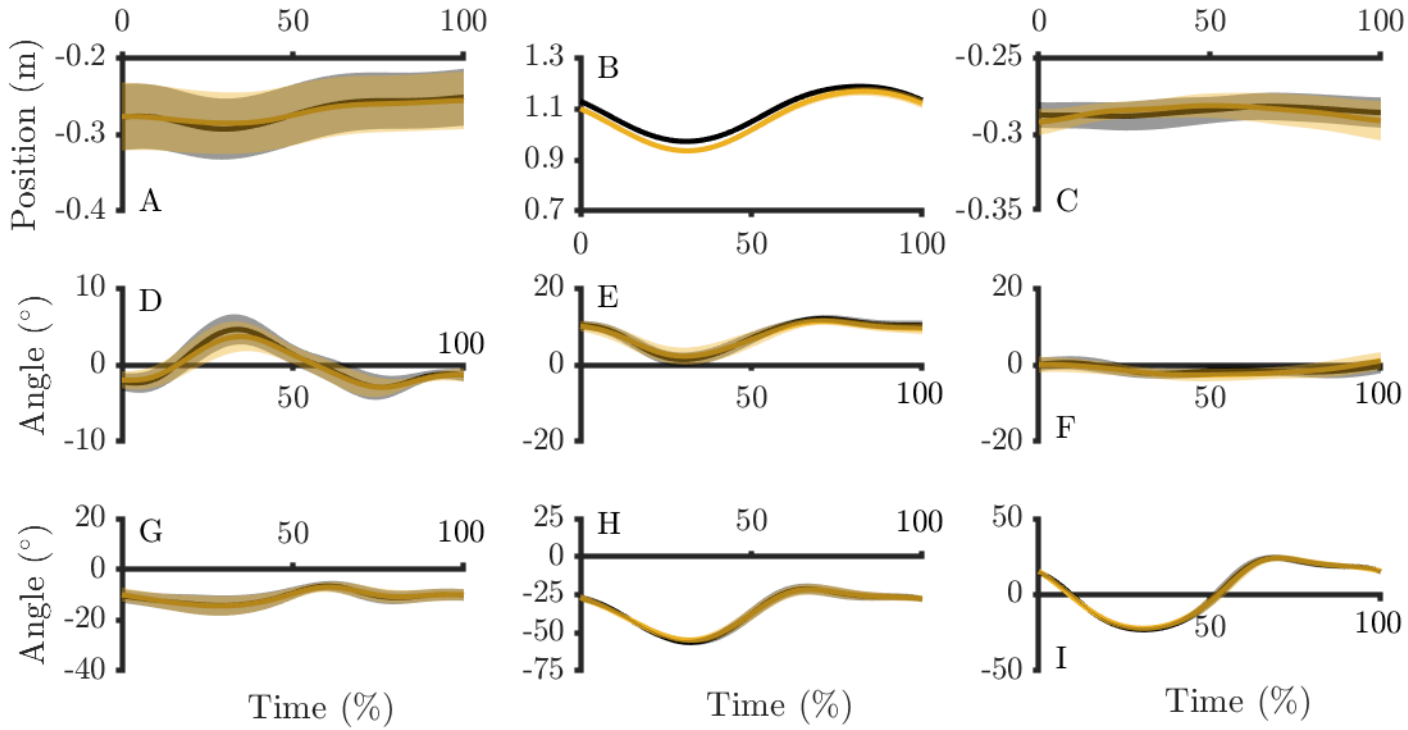

Figure A-19 Pelvis translation (A: A-P, B: Vertical, & C: M-L) and rotation (D: tilt, E: lateral title, & F: rotation), and sagittal plane angle (G: Hip, H: Knee, I: Ankle) tracking whilst hopping at 1 g hypogravity. Backward tilt, right lateral tilt, anti-clockwise, extension, plantar flexion were defined as positive. Coloured = simulated, black = experimental.

Quadriceps Muscle-Tendon Unit Length

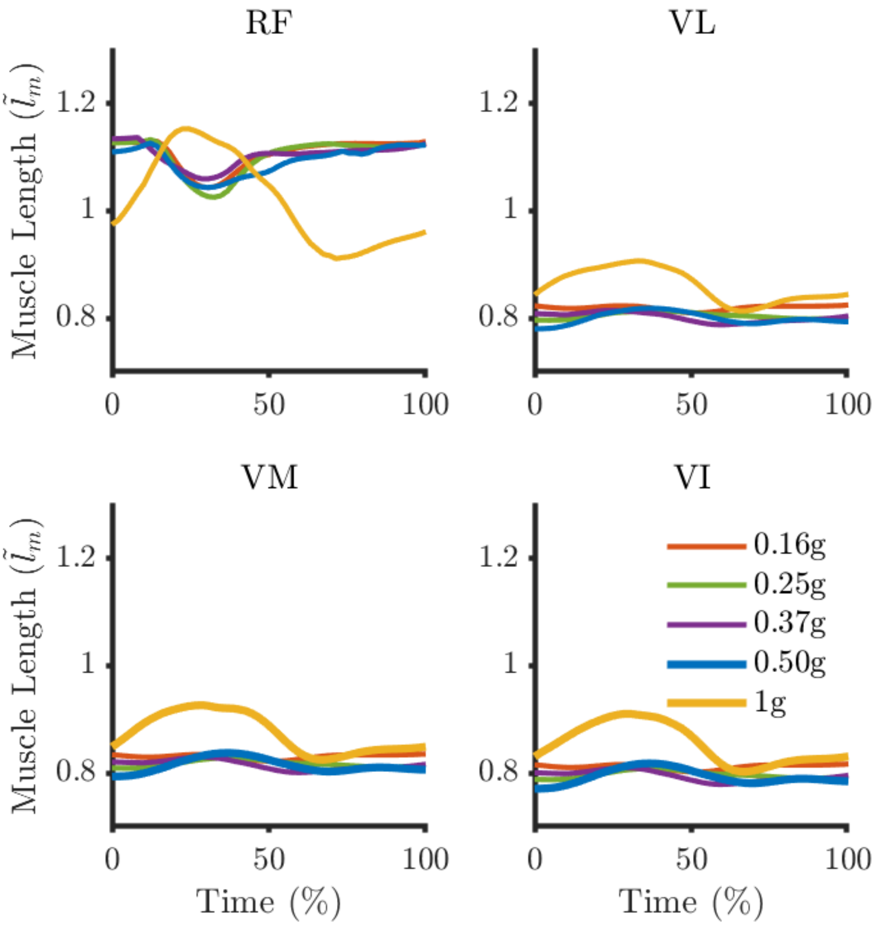

Figure A-20 Normalised muscle length of the four quadricep muscles across each gravity level during the hopping movement. RF = rectus femoris, VL = Vastus Lateralis, VM = Vastus Medialis, VI = Vastus Intermedius.

Appendix B

Appendix to Chapter 5

B.1 Baseline Parameters

Table B.1 Generic unperturbed muscle-tendon unit parameters of muscles with knee flexion moments arms, and the perturbation boundaries used during Monte Carlo sampling

	F^{Max} (N· m)	l^0 (m)	θ^0 (rad)	V^{max} ($l^0 \cdot s^{-1}$)	k_t (∇ at 4% strain)
Knee Extensors					
Rectus Femoris	2192	0.076	0.217	10.0	35
Vastus Intermedius	1697	0.117	0.063	10.0	35
Vastus Lateralis	5149	0.117	0.253	10.0	35
Vastus Medialis	2748	0.110	0.422	10.0	35
Knee Flexors					
Biceps Femoris SH	557	0.110	0.246	10.0	35
Biceps Femoris LH	1313	0.098	0.176	10.0	35
L. Gastrocnemus	1575	0.069	0.210	10.0	35
M. Gastrocnemus	3116	0.059	0.166	10.0	35
Gracilis	281	0.228	0.172	10.0	35
Sartorius	249	0.403	0.026	10.0	35
Semimembranosus	2201	0.086	0.255	10.0	35
Semitendinosus	591	0.193	0.241	10.0	35
Tensor Fasciae Latae	411	0.095	0.052	10.0	35
Perturbation Boundaries	0.40 - 1	0.60 - 1	0.75 - 1	0.50 - 2.00	0.4 - 1

Table B.2 Generic unperturbed muscle-tendon unit parameters of muscles without knee flexion moment arms, and the perturbation boundaries used during Monte Carlo sampling

	F^{Max} (N· m)	l^0 (m)	θ^0 (rad)	V^{max} ($l^0 \cdot s^{-1}$)	k_t (∇ at 4% strain)
Non-Knee Muscles					
Add. Brevis	626	0.112	0.115	10.0	35
Add. Longus	917	0.118	0.138	10.0	35
Add. Magnus Dist.	597	0.194	0.195	10.0	35
Add. Magnus Isch.	597	0.170	0.168	10.0	35
Add. Magnus Mid.	597	0.152	0.207	10.0	35
Add. Magnus Prox.	597	0.116	0.311	10.0	35
Ext. Digit. Long.	603	0.074	0.218	10.0	35
Ext. Hall. Long.	286	0.080	0.197	10.0	35
Fl. Digit. Long.	423	0.047	0.225	10.0	35
Fl. Hall. Long.	907	0.056	0.258	10.0	35
Glut. Max. Sup.	984	0.164	0.354	10.0	35
Glut. Max. Mid.	1406	0.172	0.367	10.0	35
Glut. Max. Inf.	948	0.185	0.382	10.0	35
Glut. Med. Sup.	1093	0.081	0.317	10.0	35
Glut. Med. Mid.	765	0.083	0.317	10.0	35
Glut. Med. Inf.	871	0.085	0.317	10.0	35
Glut. Mini. Ant.	374	0.081	0.175	10.0	35
Glut. Mini. Mid.	394	0.067	0.000	10.0	35
Glut. Mini. Post.	447	0.046	0.017	10.0	35
Perturbation Boundaries	0.40 - 1	0.60 - 1	0.75 - 1	0.50 - 2.00	0.4 - 1

Table B.2 continued

	F^{Max} (N· m)	l^0 (m)	θ^0 (rad)	V^{max} ($l^0 \cdot s^{-1}$)	k_t (∇ at 4% strain)
Non-Knee Muscles					
Iliacus	1021	0.116	0.280	10.0	35
Peronceus Brevis	521	0.049	0.205	10.0	35
Peronceus Longus	1115	0.055	0.248	10.0	35
Piriformis	1029	0.029	0.175	10.0	35
Psoas	1427	0.126	0.216	10.0	35
Soleus	6194	0.048	0.381	10.0	35
Tibialis Anterior	1227	0.074	0.195	10.0	35
Tibialis Posterior	1730	0.041	0.226	10.0	35
Perturbation Boundaries	0.40 - 1	0.60 - 1	0.75 - 1	0.50 - 2.00	0.4 - 1

B.2 Parameter Perturbation Boundaries

The literature was used to inform the boundaries used to perturb the MTU parameters within the Monte Carlo framework.

Maximum Isometric Force

A body of literature described the change in muscle forces via involuntary stimulation methods. Ten studies reported *in vitro* maximally stimulated muscle-fibre force following spaceflight (Fitts *et al.*, 2010; Widrick *et al.*, 2001; Widrick *et al.*, 1999), bed rest (Trappe *et al.*, 2008; Trappe *et al.*, 2007; Trappe *et al.*, 2004; Widrick *et al.*, 1998; Widrick *et al.*, 1997; Yamashita-Goto *et al.*, 2001), and unilateral lower-limb support (Widrick *et al.*, 2002). The greatest decline in peak fibre-force was reported at -52% following bed rest (Trappe *et al.*, 2007). It was assumed that losses at the fibre-level manifested in an equivalent change in force loss at the whole muscle-level.

Alternatively, Koryak (Koryak, 1995, 1998, 1999, 2010, 2014, 2015) presented a series of studies assessing the change in involuntary maximal contraction of a muscle group following titanic supramaximal stimulation. Maximum muscle force was estimated to decrease by as much as -36.7% from these studies. Involuntary stimulation removes neurological influences on muscle force generation, giving an indication of maximum force generating capacity.

A common approach for estimating the maximum isometric force, and indeed when developing musculoskeletal models (e.g. Rajagopal *et al.*, 2016), is to assume it is proportional to physiological cross-sectional area and specific tension (σ^m) (eq. B.1) (Lieber & Fridén, 2000).

$$F^{Max} = \sigma^m \cdot PCSA \tag{B.1}$$

Specific tension is consistently reported to decline with disuse, with the largest decrease reported as -27%, -45% and -55% following spaceflight (Rittweger *et al.*, 2018), bed rest (Larsson *et al.*, 1996) and immobilisation (D'Antona *et al.*, 2003), respectively. Using a combination of medical imaging methods (MRI and ultrasound), research have reported decreases between -16% and -5% for PCSA (Akima *et al.*, 2001; Akima *et al.*, 1997; Akima, Kubo, Kanehisa, *et al.*, 2000; Funato *et al.*, 1997; Kawakami *et al.*, 2001; Kawakami *et al.*, 2000). Using the literature data, the fractional change in specific tension and PCSA were multiplied together to estimate the decrease in maximum isometric force that would occur. A substantial body of literature exists reporting muscle size changes (volume and cross-sectional area) that could be used to derive PCSA based on muscle fibre length and pennation angle (Lieber & Fridén, 2000). The calculated maximum decrease in maximum isometric force (-58.8%) agreed well with the *in vitro* maximal stimulation studies (-52%). Since maximal stimulation is a more direct measure of maximum force generation, this value was preferred for defining the maximal boundary for perturbing maximum isometric force. Therefore, the maximum isometric force was perturbed between 40% and 100% of the generic model.

Muscle Fibre Length at Optimum

Quantifying optimal fibre length is difficult to measure *in vivo*. Optimal fibre length represents a theoretical fascicle length whereby the greatest volume of cross-bridges can be formed across all sarcomere. Research has shown that muscle has the capacity to add and remove sarcomere in series in response to overstretch and understretch (Lieber & Fridén, 2000; Williams & Goldspink, 1978), and that sarcomere lengths are not uniform across the fascicle (Moo *et al.*, 2016). This provides a physiological mechanism that that would underpin a change in fascicle length, and alter the optimal fibre length as the capacity for cross-bridge formation has been altered. Therefore, studies that reported muscle fascicle length using ultrasonography in either a resting posture or voluntary isometric contraction were used. Seven studies were identified that reported resting fibre changes following spaceflight (Koryak, 2019; Rittweger *et al.*, 2018), bed rest (De Boer *et al.*, 2008; Reeves *et al.*, 2002), and unilateral lower-limb support (Campbell *et al.*, 2013; De Boer *et al.*, 2007; Seynnes *et al.*, 2008). From these studies, the muscle fibre shortened between -26% and 0% depending on the muscle group. These values were used, and slightly extended to account for the non-uniform sarcomere lengths across the fascicle, to6 define the perturbation range between 60% and 100% of the generic model.

Pennation Angle at Optimal Fibre Length

Similar to optimal fibre length, pennation angle has been reported via ultrasonography at rest and not directly measured due to methodological issues with measuring optimal fibre length. By definition, the pennation angle at optimal fibre length will change when optimal fibre length changes. Additionally, architecturally a decrease in sarcomere in series is believed to be indicative of a decrease in pennation angle (Lieber & Fridén, 2000). Given the known decrease in muscle CSA with disuse, there is evidence that pennation angle will decrease even when optima fibre length does not change. Therefore, pennation angle changes at rest were deemed appropriate to inform the perturbation boundaries. Ten studies were identified reporting muscle fascicle pennation angle changes following spaceflight (Koryak, 2019; Rittweger *et al.*, 2018), bed rest (De Boer *et al.*, 2008; Kawakami *et al.*, 2001; Kawakami *et al.*, 2000; Reeves *et al.*, 2002), immobilisation (Psatha *et al.*, 2012), and unilateral lower-limb support (Campbell *et al.*, 2013; De Boer *et al.*, 2007; Seynnes *et al.*, 2008). Of the eleven studies identified, all of them reported pennation angle decreased by at least -1.4% (Kawakami *et al.*, 2001; Kawakami *et al.*, 2000), and as much as -23.2% (Rittweger *et al.*, 2018). Although one study reported that one of their two participants had increased pennation angle following spaceflight, but this only modest (3.3 - 3.7%, Rittweger *et al.*, 2018). From these values the perturbation ranges was set between 75% and 100% of baseline values.

Maximum Shortening Velocity

Maximum shortening velocity has exclusively been determined using *in vitro* analysis of single-muscle fibres via a slack test procedure. Eleven studies were identified reporting shortening velocity following spaceflight (Fitts *et al.*, 2010; Widrick *et al.*, 2001; Widrick *et al.*, 1999), bed rest (Trappe *et al.*, 2008; Trappe *et al.*, 2004; Widrick *et al.*, 1998; Widrick *et al.*, 1997; Yamashita-Goto *et al.*, 2001), immobilisation (D'Antona *et al.*, 2003), and unilateral lower-limb support (Widrick *et al.*, 2002). A wide range of values are reported with shortening velocity reported to decline by as much as -44% (Fitts *et al.*, 2010), but increase by as much as 100% (Yamashita-Goto *et al.*, 2001). From an architectural perspective, all else being equal, shortening muscle fascicle length would reduce the maximum shortening velocity (Lieber & Fridén, 2000; Narici & De Boer, 2011). However, disuse is associated with a shirt towards faster fibre-types (i.e. type I to type II, Fitts *et al.*, 2010; Trappe *et al.*, 2004), which shows fibre shortening velocity is not purely influenced by muscle architecture following disuse. Therefore, it was deemed reasonable to assume maximum shortening velocity may decrease or increase, and thus the perturbation boundaries were set to between 50% - 200% of the baseline value.

Tendon Slack Length

There is a paucity of literature investigating tendon slack length changes in response to unloading. Rather, authors reported tendon length changes from the distal insertion to the myotendinous junctions whilst resting and under tension. The confounding issue with this approach for inferring slack length changes is that when under tension the change in tendon length is influenced by the mechanical properties of the tendon. Since tendon stiffness has been shown to decrease with unloading (see below), then is impossible to deconstruct tendon length into the influence of slack length and mechanical property adaptations. That being said, only three studies were found that reported tendon length changes following an unloading paradigm, with unloaded tendon length either decreasing by <2% (Kinugasa *et al.*, 2010) or remaining unchanged (Couppé *et al.*, 2012; Reeves *et al.*, 2005). Loading studies (i.e. training interventions) have reported cross-sectional area changes in the tendon, which is believed to relate to tendon stiffness, but not slack length (Tardioli *et al.*, 2012). Furthermore, a systematic review of chronic stretching interventions was unable to identify any studies that measured tendon slack length changes (Freitas *et al.*, 2018). Therefore, there were no studies identified that reported a substantial change in tendon slack length, or indeed resting length, in healthy young adults.

In the absence of direct measurement of tendon slack length, the literature was searched for evidence of a physiological rationale that would lead to a change in tendon slack even if it was not measured, similar to the sarcomerogenesis in response to overstretch in muscle. The architecture of tendon is such that the dimensions of the tendon are influenced by the organisation of tendon collagen (Kastelic *et al.*, 1978). Evidence has shown that remodelling of collagen is minimal in the Achilles tendon after maturation (Heinemeier *et al.*, 2013), suggesting the length of the tendon is unlikely to change during adulthood. Given the lack of evidence of direct or indirect measurement of tendon length changing in response to unloading, and the lack of physiological mechanisms that might support the change in tendon slack length, it was decided that the evidence does not support perturbing tendon slack length in the Monte Carlo simulations. However, it is recognised that tendon slack length is regularly cited as being the most important parameter for determining muscle forces during simulation (e.g, Hicks *et al.*, 2015; Serrancolí *et al.*, 2020). The recommendation from the evidence would be that to model adaptations to unloading using the Hill-type muscle model pre-spaceflight tendon slack length (e.g. after calibration using computational approaches) should not be changed.

Tendon Compliance

Tendon compliance is not a main parameter for Hill-type muscle modelling, but plays a important role in muscle-tendon unit (MTU) contraction dynamics

(Zajac, 1989). The stiffness of a tendon determines the elongation experienced under a given load, which influences the MTU in two main ways. The linear region of a tendon is typically modelled as a linear-spring, meaning the force output from the series elastic element is directly influenced by it's stiffness and elongation from rest (i.e. tendon slack length). Additionally, the MTU operates as one entity with the length of the tendon influencing the length of the contractile element (i.e the muscle) such that while the MTU length may be unchanged the muscle and tendon lengths may be different. This impacts contraction dynamics, and indirectly, the activation dynamics, as the muscle can operate in a different region of the force-length curve. Indeed, muscle activation, fibre length, and metabolic power have been shown to be sensitive to tendon compliance during simulated walking and running (Orselli *et al.*, 2017; Uchida *et al.*, 2016). The aim of this study was to understand how to model the muscle adaptations of unloading using a Hill-type muscle model. It is clear that tendon compliance is important in determining the force-length-velocity dynamics as it influences the length and shortening velocity of the contractile element. Consequently, given there is a body of research that consistently demonstrates that tendons become more compliant when unloaded it was necessary to include this parameter in the analysis. There were six studies identified that reported stiffness of the Achilles or Patella tendons as an outcome following bed rest (Kubo *et al.*, 2004a; Kubo *et al.*, 2000; Kubo *et al.*, 2004b; Reeves *et al.*, 2005) and unilateral lower-limb support (Couppé *et al.*, 2012; De Boer *et al.*, 2007). From these studies, the tendon became between 13.7% - 32.5% more compliant in approximately 20 days (Couppé *et al.*, 2012; De Boer *et al.*, 2007; Kubo *et al.*, 2004a; Kubo *et al.*, 2000; Kubo *et al.*, 2004b), and increased to 58% more compliant by 90 days (Reeves *et al.*, 2005). Tendon compliance was therefore perturbed between 40% - 100% of the baseline compliance in the model.

B.3 Calibrating Logistic Regression

A key consideration when using a step-wise regression is defining the criteria for additional additional terms to the model. The influence the addition of a new term had on the logistic regression model fit was assessed. Six thresholds were tested (0.1%, 1%, 2.5%, 5%, 7.5%, 10%) that defined the increase in adjusted

R^2 required for a new term to be added. The aim was to determine a threshold for adding terms into the logistic regression that best combined the model fit with the fewest independent variables (i.e. model simplicity). Interaction terms were allowed to be added to the model. The adjusted R^2, that adjusts the R^2 to account for the number of independent variables, was used to explore the variance explained by each model. The receiver operator characteristic curve (ROC) was used to explore the ability of the model to correctly classify the simulations as feasible and infeasible solutions. The false positive rate (FPR) at 90% sensitivity (i.e. 0.9 true positive rate [TPR]), the sensitivity at 0.1 false positive rate (i.e. false positive accepted 10% of the time), and the area under the curve (AUC) were extracted for comparison.

As expected, the more strict the threshold (i.e. the greater the increase in the variance explained required to add terms to the model) the number of terms and model fit decreased within the regression model (Table B.3). The classifier performance was also impacted, with the TPR decreasing and FPR increasing at the same sensitivity thresholds. There was a clear drop off in all the metrics and the ROC curve (Figure B-1) between 5% and 7.5%, indicating the model was too simple. A threshold of 2.5% was deemed the best trade-off between required terms, and model performance. This was based on two points. First, the additional of two terms between 2.5% and 5% thresholds improved the variance explained by 9% whereas 13 terms were needed for only an 8% increase with a 0.1% threshold. Second, the addition of more terms did not have a substantial impact on the shape of ROC nor the AUC. This meant the model with a 2.5% threshold was categorising simulations with similar accuracy to the models with additional terms.

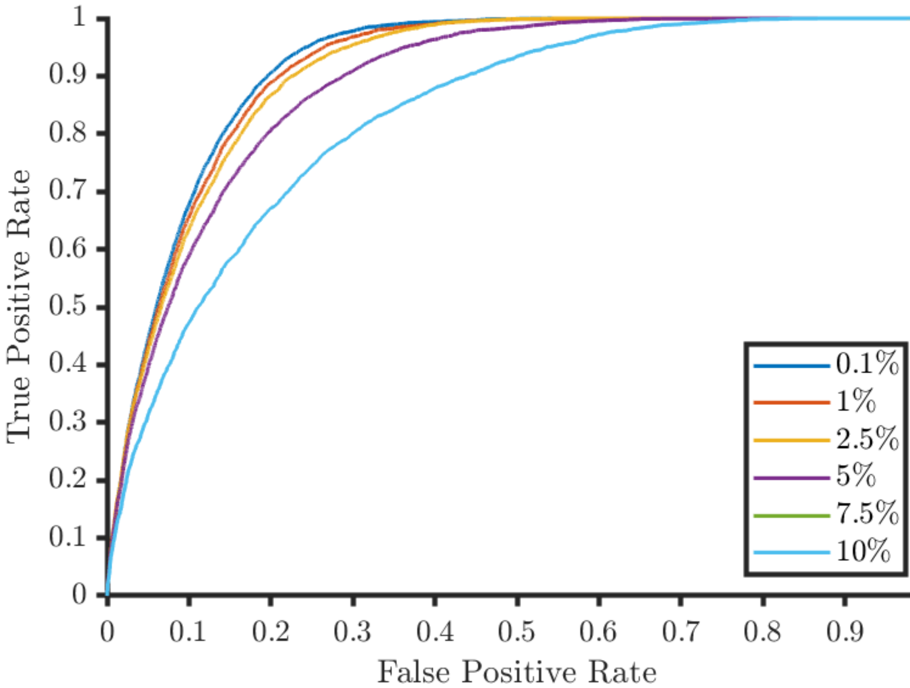

Figure B-1 The receiver operator characteristic curves for each step-wise logistic regression as the the threshold required to add terms to the model was manipulated.

Table B.3 Comparison of model fit and classifier performance with different thresholds for adding new independent variables to the step-wise logistic regression

Measure	0.1%	1%	2.5%	5%	7.5%	10%
Terms	21	11	8	6	3	3
Adjusted R^2	0.62	0.58	0.54	0.45	0.25	0.25
FPR at 0.9	0.12	0.14	0.17	0.25	0.44	0.44
TRP at 0.1	0.87	0.83	0.79	0.70	0.47	0.47
AUC	0.96	0.95	0.94	0.91	0.83	0.83

FPR at 0.9 = false positive rate at 0.9 true positive rate, TRP at 0.1 = true positive rate at 0.1 false positive rate.

B.4 Additional Results

Muscle Activations

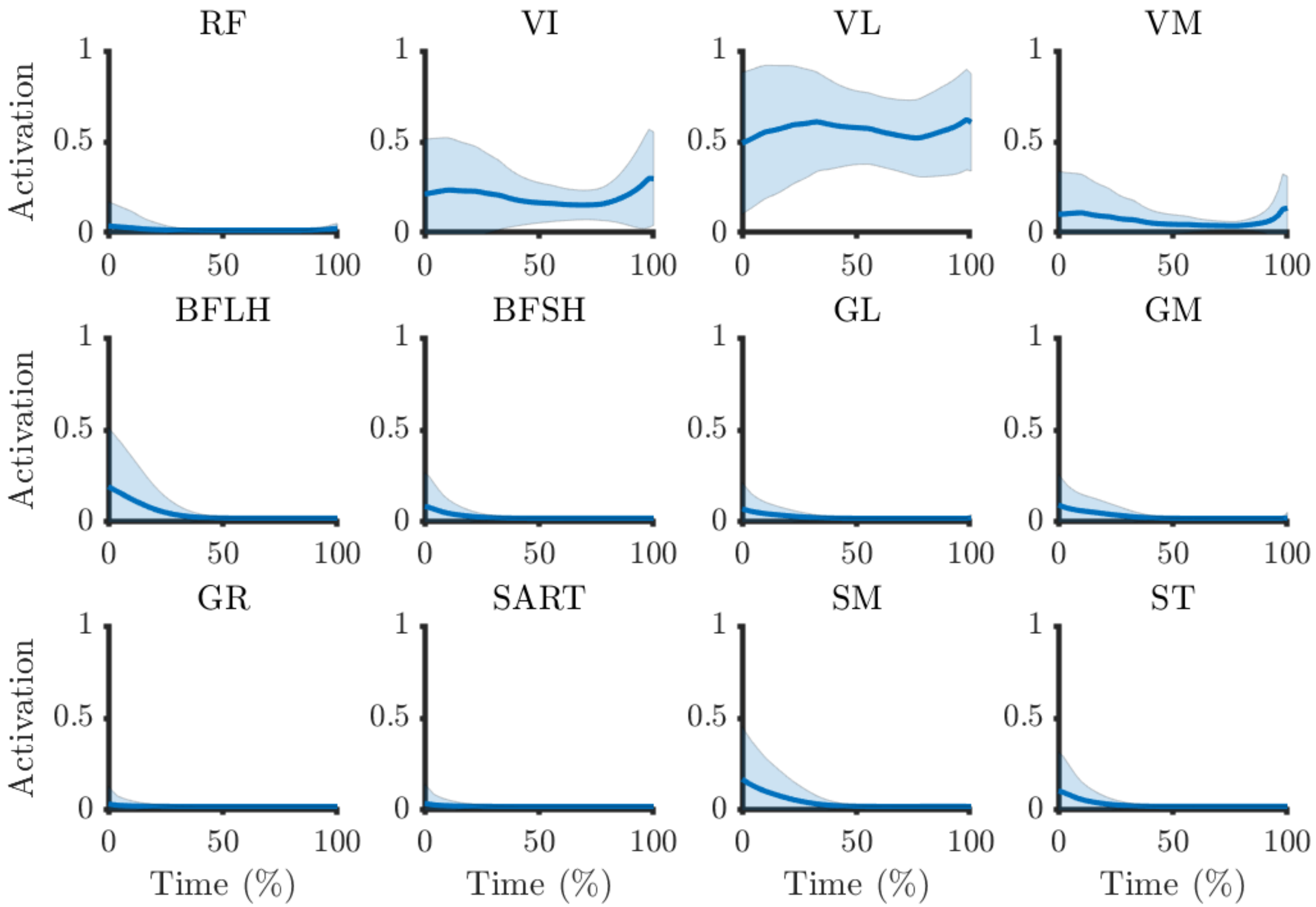

Figure B-2 Mean (solid line) and standard deviation (shaded area) muscle activations from the feasible solutions for the knee musculature during the $30°{\cdot}s^{-1}$ condition. RF = rectus femoris, VI = vastus intermedius, VL = vastus lateralis, VM = vastus medialis BFLH = biceps femoris long head, BFSH = biceps femoris long head, GL = gastroc. lateralis, GM = gastrco. medialis, GR = gracilis, SART = sartorius, SM = semimembranosus, ST = semitendinosus.

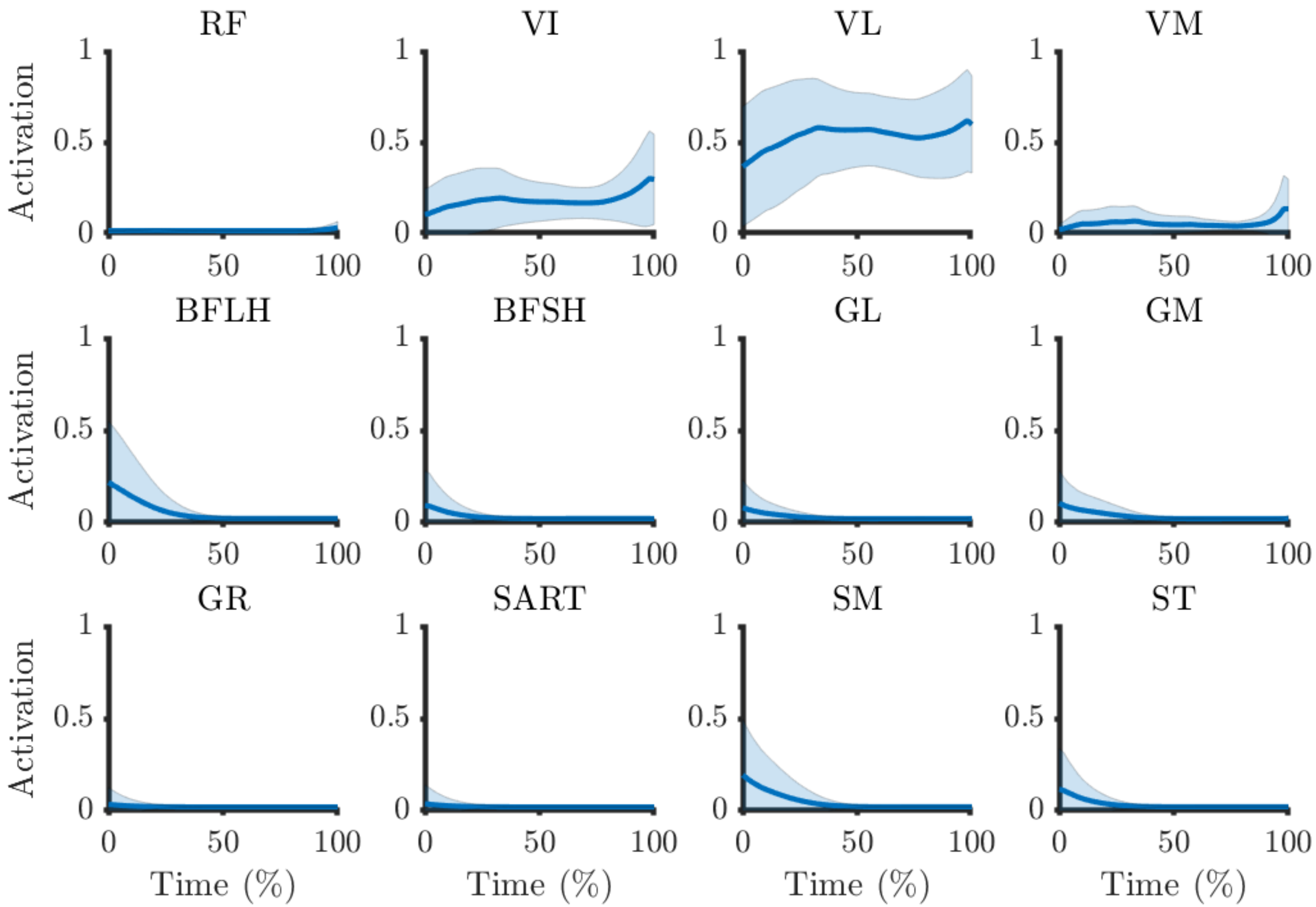

Figure B-3 Mean (solid line) and standard deviation (shaded area) muscle activations from the feasible solutions for the knee musculature during the 180°·s^{-1} condition. RF = rectus femoris, VI = vastus intermedius, VL = vastus lateralis, VM = vastus medialis BFLH = biceps femoris long head, BFSH = biceps femoris long head, GL = gastroc. lateralis, GM = gastrco. medialis, GR = gracilis, SART = sartorius, SM = semimembranosus, ST = semitendinosus.

Population Densities

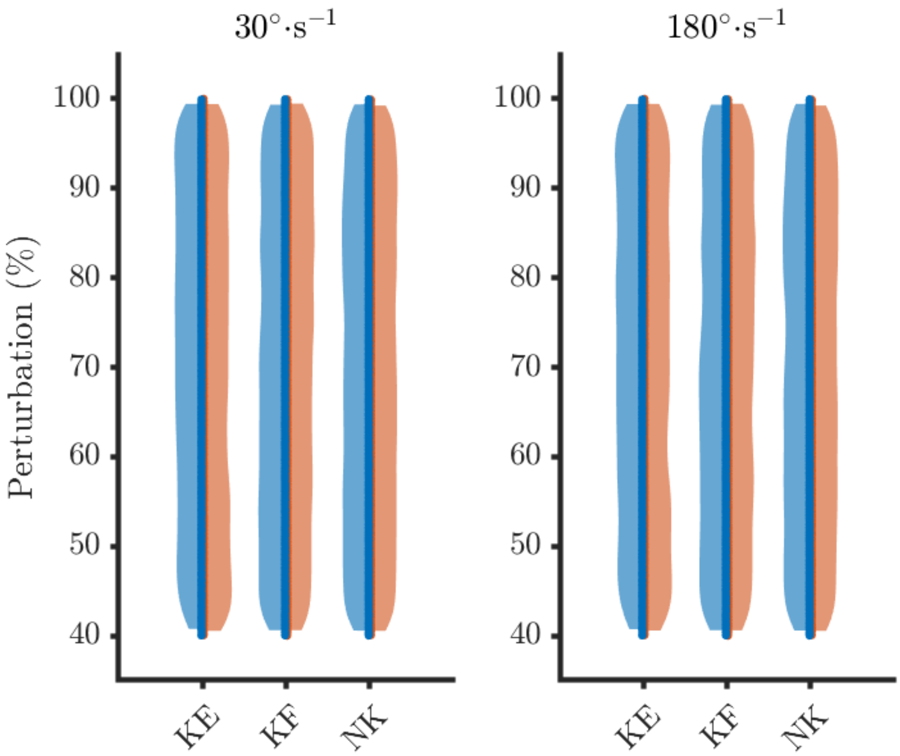

Figure B-4 Sampling density of maximum isometric force for the feasible (blue) and infeasible (orange) solutions. KE = knee extensors; KF = knee flexors; NK = non-knee muscles.

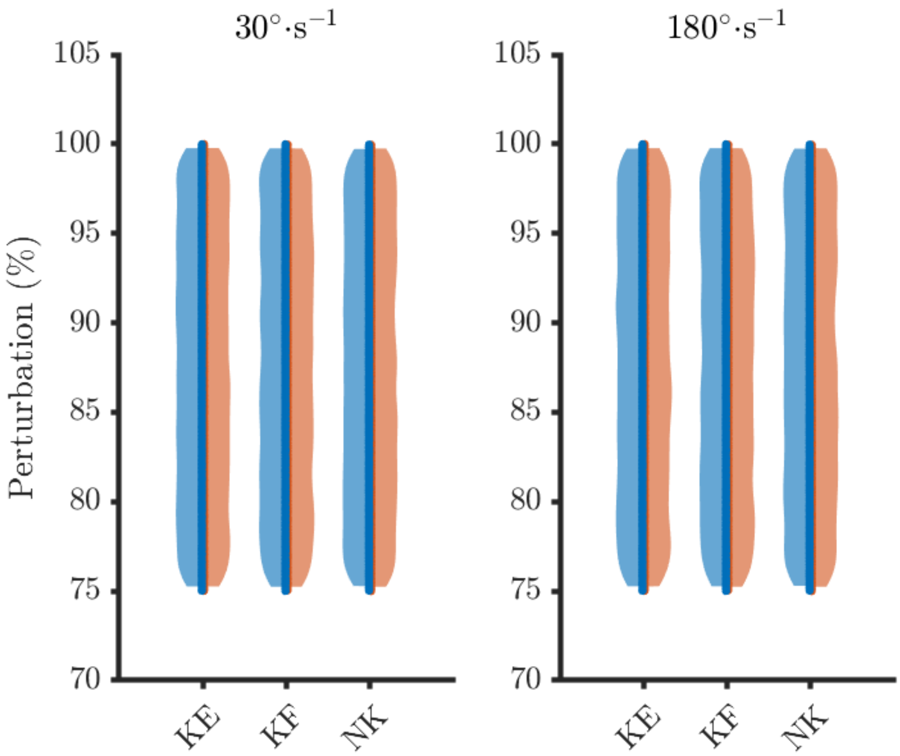

Figure B-5 Sampling density of pennation angle at optimum fibre length for the feasible (blue) and infeasible (orange) solutions. KE = knee extensors; KF = knee flexors; NK = non-knee muscles.

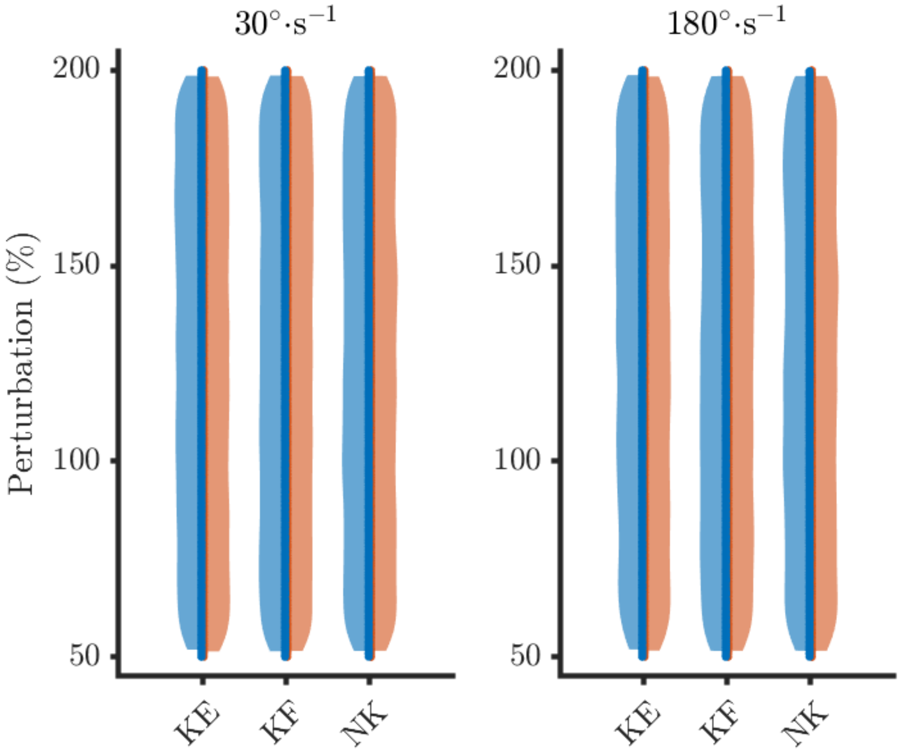

Figure B-6 Sampling density of maximum shortening velocity for the feasible (blue) and infeasible (orange) solutions. KE = knee extensors; KF = knee flexors; NK = non-knee muscles.

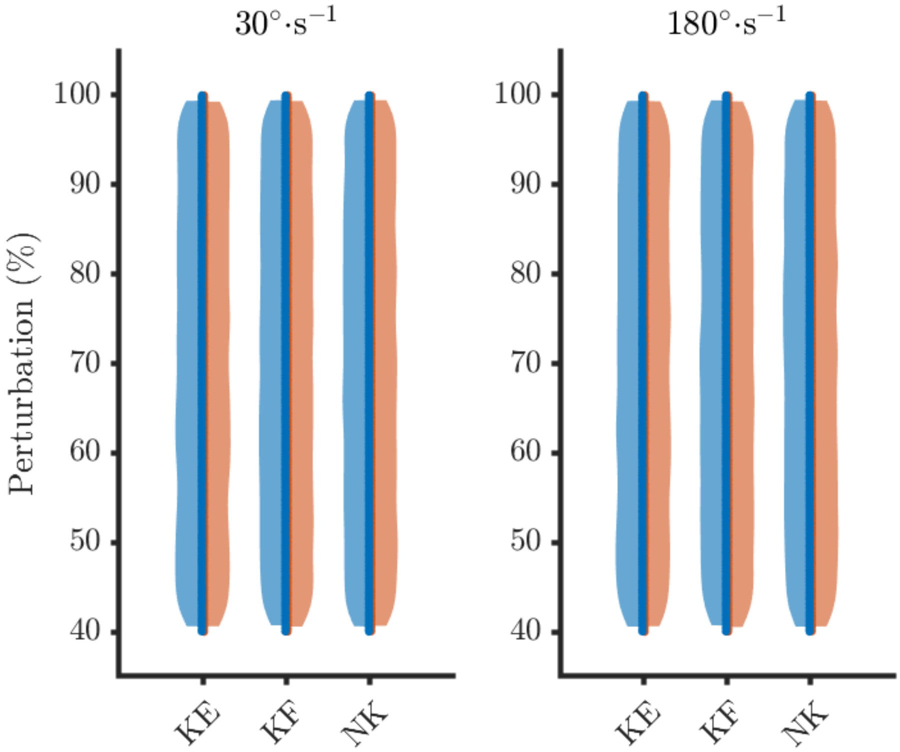

Figure B-7 Sampling density of tendon compliance for the feasible (blue) and infeasible (orange) solutions. KE = knee extensors; KF = knee flexors; NK = non-knee muscles.

References

Ackermann, M., & van den Bogert, A. J. (2010). Optimality principles for model-based prediction of human gait. *Journal of Biomechanics*, *43*(6), 1055–1060.

Ackermann, M., & van den Bogert, A. J. (2012). Predictive simulation of gait at low gravity reveals skipping as the preferred locomotion strategy. *Journal of Biomechanics*, *45*(7), 1293–1298.

Ackland, D. C., Lin, Y.-C., & Pandy, M. G. (2012). Sensitivity of model predictions of muscle function to changes in moment arms and muscle–tendon properties: A monte-carlo analysis. *Journal of Biomechanics*, *45*(8), 1463–1471.

Akhundov, R., Saxby, D. J., Diamond, L. E., Edwards, S., Clausen, P., Dooley, K., Blyton, S., & Snodgrass, S. J. (2022). Is subject-specific musculoskeletal modelling worth the extra effort or is generic modelling worth the shortcut? *PLOS ONE*, *17*(1), e0262936.

Akima, H., Kubo, K., Imai, M., Kanehisa, H., Suzuki, Y., Gunji, A., & Fukunaga, T. (2001). Inactivity and muscle: Effect of resistance training during bed rest on muscle size in the lower limb. *Acta Physiologica Scandinavica*, *172*(4), 269–278.

Akima, H., Kuno, S., Suzuki, Y., Gunji, A., & Fukunaga, T. (1997). Effects of 20 days of bed rest on physiological cross-sectional area of human thigh and leg muscles evaluated by magnetic resonance imaging. *Journal of Gravitational Physiology*, *4*(1), S15–21.

Akima, H., Kubo, K., Kanehisa, H., Suzuki, Y., Gunji, A., & Fukunaga, T. (2000). Leg-press resistance training during 20 days of 6 head-down-tilt bed rest prevents muscle deconditioning. *European Journal of Applied Physiology*, *82*(1), 30–38.

Akima, H., Kawakami, Y., Kubo, K., Sekiguchi, C., Ohshima, H., Miyamoto, A., & Fukunaga, T. (2000). Effect of short-duration spaceflight on thigh and leg muscle volume. *Medicine and Science in Sports and Exercise*, *32*(10), 1743–1747.

Alkner, B. A., Norrbrand, L., & Tesch, P. A. (2016). Neuromuscular adaptations following 90 days bed rest with or without resistance exercise. *Aerospace Medicine and Human Performance*, *87*(7), 610–617.

Alkner, B. A., & Tesch, P. A. (2004). Knee extensor and plantar flexor muscle size and function following 90 days of bed rest with or without resistance exercise. *European Journal of Applied Physiology*, *93*(3), 294–305.

Ammann, P., & Rizzoli, R. (2003). Bone strength and its determinants. *Osteoporosis International*, *14*(3), 13–18.

Anderson, F. C., & Pandy, M. G. (2001a). Dynamic optimization of human walking. *Journal of Biomechanical Engineering*, *123*(5), 381–390.

Anderson, F. C., & Pandy, M. G. (2001b). Static and dynamic optimization solutions for gait are practically equivalent. *Journal of Biomechanics*, *34*(2), 153–161.

Andersson, J. A., Gillis, J., Horn, G., Rawlings, J. B., & Diehl, M. (2019). Casadi: A software framework for nonlinear optimization and optimal control. *Mathematical Programming Computation*, *11*(1), 1–36.

Apte, S., Plooij, M., & Vallery, H. (2018). Influence of body weight unloading on human gait characteristics: A systematic review. *Journal of Neuroengineering and Rehabilitation*, *15*(1), 1–18.

Bamman, M. M., Clarke, M. S. F., Feeback, D. L., Talmadge, R. J., Stevens, B. R., Lieberman, S. A., & Greenisen, M. C. (1998). Impact of resistance exercise during bed rest on skeletal muscle sarcopenia and myosin isoform distribution. *Journal of Applied Physiology*, *84*(1), 157–163.

Berg, H. E., Dudley, G. A., Haggmark, T., Ohlsen, H., & Tesch, P. A. (1991). Effects of lower limb unloading on skeletal muscle mass and function in humans. *Journal of Applied Physiology*, *70*(4), 1882–1885.

Berg, H. E., Eiken, O., Miklavcic, L., & Mekjavic, I. B. (2007). Hip, thigh and calf muscle atrophy and bone loss after 5-week bedrest inactivity. *European Journal of Applied Physiology*, *99*(3), 283–289.

Berg, H. E., Larsson, L., & Tesch, P. (1997). Lower limb skeletal muscle function after 6 wk of bed rest. *Journal of Applied Physiology*, *82*(1), 182–8.

Bergmann, G., Bender, A., Dymke, J., Duda, G., & Damm, P. (2016). Standardized loads acting in hip implants. *PLOS ONE*, *11*(5), 1–23.

Bergmann, G., Bender, A., Graichen, F., Dymke, J., Rohlmann, A., Trepczynski, A., Heller, M. O., & Kutzner, I. (2014). Standardized loads acting in knee implants. *PLOS ONE*, *9*(1), 1–12.

Betts, J. T. (2010). *Practical methods for optimal control and estimation using nonlinear programming* (Second Eds.). Society for Industrial; Applied Mathematics.

Bezodis, N. E., Trewartha, G., & Salo, A. I. T. (2015). Understanding the effect of touchdown distance and ankle joint kinematics on sprint acceleration performance through computer simulation. *Sports Biomechanics*, *14*(2), 232–245.

Bland, J. M., & Altman, D. G. (2010). Statistical methods for assessing agreement between two methods of clinical measurement. *International Journal of Nursing Studies*, *47*(8), 931–936.

Blottner, D., Salanova, M., Püttmann, B., Schiffl, G., Felsenberg, D., Buehring, B., & Rittweger, J. (2006). Human skeletal muscle structure and function preserved by vibration muscle exercise following 55 days of bed rest. *European Journal of Applied Physiology*, *97*(3), 261–271.

Blue Origin. (2021). Virgin galactic successfully completes first fully crewed spaceflight. *www.blueorigin.com*. Retrieved September 3, 2021, from https://www.blueorigin.com/news/first-human-flight-updates

Brandon, S. C. E., Thelen, D. G., & Deluzio, K. J. (2011). *A weighted objective function reduces estimates of medial and lateral knee joint contact loads during gait* (Vol. Parts A & B).

Bruce, S., Newton, D., & Woledge, R. (1989). Effect of age on voluntary force and cross-sectional area of human adductor pollicis muscle. *Quarterly Journal of Experimental Physiology: Translation and Integration*, *74*(3), 359–362.

Caiozzo, V. J., Haddad, F., Baker, M. J., Herrick, R. E., Prietto, N., & Baldwin, K. M. (1996). Microgravity-induced transformations of myosin isoforms and contractile properties of skeletal muscle. *Journal of Applied Physiology*, *81*(1), 123–132.

Campbell, E.-L., Seynnes, O. R., Bottinelli, R., McPhee, J. S., Atherton, P., Jones, D., Butler-Browne, G., & Narici, M. V. (2013). Skeletal muscle adaptations to physical inactivity and subsequent retraining in young men. *Biogerontology*, *14*(3), 247–259.

Cappozzo, A., Catani, F., Della Croce, U., & Leardini, A. (1995). Position and orientation in space of bones during movement: Anatomical frame definition and determination. *Clinical Biomechanics*, *10*(4), 171–178.

Carbone, V., van der Krogt, M. M., Koopman, H. F., & Verdonschot, N. (2012). Sensitivity of subject-specific models to errors in musculo-skeletal geometry. *Journal of Biomechanics*, *45*(14), 2476–2480.

Cavanagh, P. R., Genc, K. O., Gopalakrishnan, R., Kuklis, M. M., Maender, C. C., & Rice, A. J. (2010). Foot forces during typical days on the international space station. *Journal of Biomechanics*, *43*(11), 2182–2188.

Cavanagh, P. R., Gopalakrishnan, R., Rice, A. J., Genc, K. O., Maender, C. C., Nystrom, P. G., Johnson, M. J., Kuklis, M. M., & Humphreys, B. T. (2009). An ambulatory biomechanical data collection system for use in space: Design and validation. *Aviation, Space, and Environmental Medicine*, *80*(10), 870–881.

Cervinka, T., Sievänen, H., Hyttinen, J., & Rittweger, J. (2014). Bone loss patterns in cortical, subcortical, and trabecular compartments during simulated microgravity. *Journal of Applied Physiology*, *117*(1), 80–88.

Christensen, B., Dyrberg, E., Aagaard, P., Enehjelm, S., Krogsgaard, M., Kjær, M., & Langberg, H. (2008). Effects of long-term immobilization and recovery on human triceps surae and collagen turnover in the achilles tendon in patients with healing ankle fracture. *Journal of Applied Physiology*, *105*(2), 420–426.

Cleather, D., Price, P. D., & Kennett, J. E. (PrePrint). Repeated horizontal jumping is a feasible exercise countermeasure for microgravity.

Convertino, V. A., & Tsiolkovsky, K. (1990). Physiological adaptations to weightlessness: Effects on exercise and work performance. *Exercise and Sport Sciences Reviews*, *18*(1), 119–166.

Couppé, C., Suetta, C., Kongsgaard, M., Justesen, L., Hvid, L., Aagaard, P., Kjær, M., & Magnusson, S. P. (2012). The effects of immobilization on the mechanical properties of the patellar tendon in younger and older men. *Clinical Biomechanics*, *27*(9), 949–954.

Cronin, N. J., Avela, J., Finni, T., & Peltonen, J. (2013). Differences in contractile behaviour between the soleus and medial gastrocnemius muscles during human walking. *Journal of Experimental Biology*, *216*(5), 909–914.

Crook, B. S., Collins, A. T., Lad, N. K., Spritzer, C. E., Wittstein, J. R., & DeFrate, L. E. (2021). Effect of walking on in vivo tibiofemoral cartilage strain in acl-deficient versus intact knees. *Journal of Biomechanics*, *116*, 110210.

Cutuk, A., Groppo, E. R., Quigley, E. J., White, K. W., Pedowitz, R. A., & Hargens, A. R. (2006). Ambulation in simulated fractional gravity using lower body positive pressure: Cardiovascular safety and gait analyses. *Journal of Applied Physiology*, *101*(3), 771–777.

D'Antona, G., Pellegrino, M. A., Adami, R., Rossi, R., Carlizzi, C. N., Canepari, M., Saltin, B., & Bottinelli, R. (2003). The effect of ageing and immobilization on structure and function of human skeletal muscle fibres. *The Journal of Physiology*, *552*(2), 499–511.

De Boer, M. D., Maganaris, C. N., Seynnes, O. R., Rennie, M. J., & Narici, M. V. (2007). Time course of muscular, neural and tendinous adaptations to 23 day unilateral lower-limb suspension in young men. *The Journal of Physiology*, *583*(3), 1079–1091.

De Boer, M. D., Seynnes, O. R., Di Prampero, P. E., Pišot, R., Mekjavić, I. B., Biolo, G., & Narici, M. V. (2008). Effect of 5 weeks horizontal bed rest on human muscle thickness and architecture of weight bearing and non-weight bearing muscles. *European Journal of Applied Physiology*, *104*(2), 401–407.

De Groote, F., Pipeleers, G., Jonkers, I., Demeulenaere, B., Patten, C., Swevers, J., & De Schutter, J. (2009). A physiology based inverse dynamic analysis of human gait: Potential and perspectives. *Computer Methods in Biomechanics and Biomedical Engineering*, *12*(5), 563–574.

De Groote, F., Allen, J. L., & Ting, L. H. (2017). Contribution of muscle short-range stiffness to initial changes in joint kinetics and kinematics during perturbations to standing balance: A simulation study. *Journal of Biomechanics*, *55*, 71–77.

De Groote, F., Blum, K. P., Horslen, B. C., & Ting, L. H. (2018). Interaction between muscle tone, short-range stiffness and increased sensory feedback gains explains key kinematic features of the pendulum test in spastic cerebral palsy: A simulation study. *PLoS One*, *13*(10), e0205763.

De Groote, F., Kinney, A. L., Rao, A. V., & Fregly, B. J. (2016). Evaluation of direct collocation optimal control problem formulations for solving the muscle redundancy problem. *Annals of Biomedical Engineering*, *44*(10), 2922–2936.

De Groote, F., Van Campen, A., Jonkers, I., & De Schutter, J. (2010). Sensitivity of dynamic simulations of gait and dynamometer experiments to hill muscle model parameters of knee flexors and extensors. *Journal of Biomechanics*, *43*(10), 1876–1883.

De Witt, J. K., & Ploutz-Snyder, L. L. (2014). Ground reaction forces during treadmill running in microgravity. *Journal of Biomechanics*, *47*(10), 2339–2347.

DeFreitas, J. M., Beck, T. W., Stock, M. S., Dillon, M. A., & Kasishke, P. R. (2011). An examination of the time course of training-induced skeletal muscle hypertrophy. *European Journal of Applied Physiology*, *111*(11), 2785–2790.

Delp, S. L., Anderson, F. C., Arnold, A. S., Loan, P., Habib, A., John, C. T., Guendelman, E., & Thelen, D. G. (2007). Opensim: Open-source software to create and analyze dynamic simulations of movement. *IEEE Transactions on Biomedical Engineering*, *54*(11), 1940–1950.

Delp, S. L., Arnold, A. S., Speers, R. A., & Moore, C. A. (1996). Hamstrings and psoas lengths during normal and crouch gait: Implications for muscle-tendon surgery. *Journal of Orthopaedic Research*, *14*(1), 144–151.

Dembia, C. L., Bianco, N. A., Falisse, A., Hicks, J. L., & Delp, S. L. (2021). Opensim moco: Musculoskeletal optimal control. *PLOS Computational Biology*, *16*(12), 1–21.

DeMers, M. S., Pal, S., & Delp, S. L. (2014). Changes in tibiofemoral forces due to variations in muscle activity during walking. *Journal of Orthopaedic Research*, *32*(6), 769–776.

Dirks, M. L., Wall, B. T., van de Valk, B., Holloway, T. M., Holloway, G. P., Chabowski, A., Goossens, G. H., & van Loon, L. J. (2016). One Week of Bed Rest Leads to Substantial Muscle Atrophy and Induces Whole-Body Insulin Resistance in the Absence of Skeletal Muscle Lipid Accumulation. *Diabetes*, *65*(10), 2862–2875.

Donelan, J. M., & Kram, R. (1997). The effect of reduced gravity on the kinematics of human walking: A test of the dynamic similarity hypothesis for locomotion. *The Journal of Experimental Biology*, *200*(24), 3193–3201.

Donelan, J. M., & Kram, R. (2000). Exploring dynamic similarity in human running using simulated reduced gravity. *Journal of Experimental Biology*, *203*(16), 2405–2415.

Edgerton, V. R., Zhou, M. Y., Ohira, Y., Klitgaard, H., Jiang, B., Bell, G., Harris, B., Saltin, B., Gollnick, P. D., Roy, R. R., & et al., a. (1995). Human fiber size and enzymatic properties after 5 and 11 days of spaceflight. *Journal of Applied Physiology*, *78*(5), 1733–1739.

English, K. L., Downs, M., Goetchius, E., Buxton, R., Ryder, J. W., Ploutz-Snyder, R., Guilliams, M., Scott, J. M., & Ploutz-Snyder, L. L. (2020). High intensity training during spaceflight: Results from the nasa sprint study. *NPJ Microgravity*, *6*(1), 1–9.

English, K. L., Lee, S., Loehr, J. A., Ploutz-Snyder, R. J., & Ploutz-Snyder, L. L. (2015). Isokinetic strength changes following long-duration spaceflight on the iss. *Aerospace Medicine and Human Performance*, *86*(12), A68–A77.

Eurpoean Space Agency. (2022). Lunar exploration – esa's missions. *www.esa.int*. Retrieved January 1, 2022, from https://www.esa.int/Education/Teach_with_the_Moon/Lunar_Exploration_ESA_s_missions

Falisse, A., Afschrift, M., & De Groote, F. (2022). Modeling toes contributes to realistic stance knee mechanics in three-dimensional predictive simulations of walking. *PLOS ONE*, *17*(1), e0256311.

Falisse, A., Pitto, L., Kainz, H., Hoang, H., Wesseling, M., Van Rossom, S., Papageorgiou, E., Bar-On, L., Hallemans, A., Desloovere, K., et al. (2020). Physics-based simulations to predict the differential effects of motor control and musculoskeletal deficits on gait dysfunction in cerebral palsy: A retrospective case study. *Frontiers in Human Neuroscience*, *14*, 40.

Falisse, A., Serrancolí, G., Dembia, C. L., Gillis, J., & De Groote, F. (2019). Algorithmic differentiation improves the computational efficiency of opensim-based trajectory optimization of human movement. *PLOS ONE*, *14*(10), 1–19.

Falisse, A., Serrancolí, G., Dembia, C. L., Gillis, J., Jonkers, I., & De Groote, F. (2019). Rapid predictive simulations with complex musculoskeletal models suggest that diverse healthy and pathological human gaits can emerge from similar control strategies. *Journal of the Royal Society Interface*, *16*(157), 20190402.

Falisse, A., Van Rossom, S., Jonkers, I., & De Groote, F. (2017). Emg-driven optimal estimation of subject-specific hill model muscle–tendon parameters of the knee joint actuators. *IEEE Transactions on Biomedical Engineering*, *64*(9), 2253–2262.

Farris, D. J., & Lichtwark, G. A. (2016). Ultratrack: Software for semi-automated tracking of muscle fascicles in sequences of b-mode ultrasound images. *Computer Methods and Programs in Biomedicine*, *128*, 111–118.

Faul, F., Erdfelder, E., Lang, A.-G., & Buchner, A. (2007). G* power 3: A flexible statistical power analysis program for the social, behavioral, and biomedical sciences. *Behavior Research Methods*, *39*(2), 175–191.

Fernandez-Gonzalo, R., McDonnell, A. C., Simpson, E. J., MacDonald, I. A., Rullman, E., & Mekjavic, I. B. (2021). Substantial and reproducible individual variability in skeletal muscle outcomes in the cross-over designed planica bed rest program. *Frontiers in Physiology*, *12*.

Ferrando, A. A., Stuart, C. A., Brunder, D. G., & Hillman, G. R. (1995). Magnetic resonance imaging quantitation of changes in muscle volume during 7 days of strict bed rest. *Aviation, Space, and Environmental Medicine*, *66*(10), 976–981.

Fitts, R. H., Trappe, S., Costill, D. L., Gallagher, P. M., Creer, A. C., Colloton, P. A., Peters, J. R., Romatowski, J. G., Bain, J. L., & Riley, D. A.

(2010). Prolonged space flight-induced alterations in the structure and function of human skeletal muscle fibres. *The Journal of Physiology*, *588*(18), 3567–3592.

Fregly, B. J. (2021). A conceptual blueprint for making neuromusculoskeletal models clinically useful. *Applied Sciences*, *11*(5), 2037.

Fregly, B. J., Besier, T. F., Lloyd, D. G., Delp, S. L., Banks, S. A., Pandy, M. G., & D'lima, D. D. (2012). Grand challenge competition to predict in vivo knee loads. *Journal of Orthopaedic Research*, *30*(4), 503–513.

Fregly, B. J., Fregly, C. D., & Kim, B. T. (2015). Computational prediction of muscle moments during ared squat exercise on the international space station [121005]. *Journal of Biomechanical Engineering*, *137*(12).

Freitas, S. R., Mendes, B., Le Sant, G., Andrade, R. J., Nordez, A., & Milanovic, Z. (2018). Can chronic stretching change the muscle-tendon mechanical properties? a review. *Scandinavian Journal of Medicine & Science in Sports*, *28*(3), 794–806.

Frost, H. M. (1987). Bone "mass" and the "mechanostat": A proposal. *The Anatomical Record*, *219*(1), 1–9.

Frost, H. M. (2003). Bone's mechanostat: A 2003 update. *The Anatomical Record. Part A, Discoveries in Molecular, Cellular, and Evolutionary Biology*, *275*(2), 1081–101.

Funato, K., Matsuo, A., Yata, H., Akima, H., Suzuki, Y., Gunji, A., & Fukunaga, T. (1997). Changes in force-velocity and power output of upper and lower extremity musculature in young subjects following 20 days bed rest. *Journal of Gravitational Physiology*, *4*(1), S22–30.

Gallagher, P., Trappe, S., Harber, M., Creer, A., Mazzetti, S., Trappe, T., Alkner, B., & Tesch, P. (2005). Effects of 84-days of bedrest and resistance training on single muscle fibre myosin heavy chain distribution in human vastus lateralis and soleus muscles. *Acta Physiologica Scandinavica*, *185*(1), 61–69.

Gazenko, O. G., Genin, A. M., & Egorov, A. D. (1981). Summary of medical investigations in the ussr manned space missions. *Acta Astronautica*, *8*(9-10), 907–917.

Geijtenbeek, T. (2019). Scone: Open source software for predictive simulation of biological motion. *Journal of Open Source Software*, *4*(38), 1421.

Genc, K., Gopalakrishnan, R., Kuklis, M., Maender, C., Rice, A., Bowersox, K., & Cavanagh, P. (2010). Foot forces during exercise on the international space station. *Journal of Biomechanics*, *43*(15), 3020–3027.

Gisler, M., & Sornette, D. (2009). Exuberant innovations: The apollo program. *Society*, *46*(1), 55–68.

Goldberg, A. L., Etlinger, J. D., Goldspink, D. F., & Jablecki, C. (1975). Mechanism of work-induced hypertrophy of skeletal muscle. *Medicine and Science in Sports*, *7*(3), 185–198.

Goodman, C. A., Hornberger, T. A., & Robling, A. G. (2015). Bone and skeletal muscle: Key players in mechanotransduction and potential overlapping mechanisms. *Bone*, *80*, 24–36.

Gopalakrishnan, R., Genc, K. O., Rice, A. J., Lee, S., Evans, H. J., Maender, C. C., Ilaslan, H., & Cavanagh, P. R. (2010). Muscle volume, strength, endurance, and exercise loads during 6-month missions in space. *Aviation, Space, and Environmental Medicine*, *81*(2), 91–104.

Gordon, A., Huxley, A. F., & Julian, F. (1966). The variation in isometric tension with sarcomere length in vertebrate muscle fibres. *The Journal of Physiology*, *184*(1), 170–192.

Greenisen, M. C., Hayes, J. C., Siconolfi, S. F., & Moore, A. D. (1999). *Functional performance evaluation* (C. F. Sawin, G. R. Taylor, W. L. Smith, & J. T. Brown, Eds.;). National Aeronautics and Space Administration, USA.

Gruber, M., Kramer, A., Mulder, E., & Rittweger, J. (2019). The importance of impact loading and the stretch shortening cycle for spaceflight countermeasures. *Frontiers in Physiology*, *10*, 311.

Hamner, S. R., & Delp, S. L. (2013). Muscle contributions to fore-aft and vertical body mass center accelerations over a range of running speeds. *Journal of Biomechanics*, *46*(4), 780–787.

Han, J. I., Choi, H. S., & Baek, Y. S. (2020). Simulation of a lower extremity assistive device for resistance training in a microgravity environment. *Applied Sciences*, *10*(3), 1160.

Han Kim, K., Young, K. S., & Rajulu, S. L. (2019). Neutral body posture in spaceflight. *Proceedings of the Human Factors and Ergonomics Society Annual Meeting*, *63*(1), 992–996.

Handsfield, G. G., Meyer, C. H., Hart, J. M., Abel, M. F., & Blemker, S. S. (2014). Relationships of 35 lower limb muscles to height and body mass quantified using MRI. *Journal of Biomechanics*, *47*(3), 631–638.

Haralabidis, N. (Unpublished Doctoral Thesis). Tracking and predictive simulations of sprinting: A direct collocation optimal control approach. *Unpublished Doctoral Thesis*.

Haralabidis, N., Serrancolí, G., Colyer, S., Bezodis, I., Salo, A., & Cazzola, D. (2021). Three-dimensional data-tracking simulations of sprinting using a direct collocation optimal control approach. *PeerJ*, *9*, e10975.

Hasselman, C. T., Best, T. M., Hughes IV, C., Martinez, S., & Garrett Jr, W. E. (1995). An explanation for various rectus femoris strain injuries using previously undescribed muscle architecture. *The American Journal of Sports Medicine*, *23*(4), 493–499.

Hast, M. W., & Piazza, S. J. (2011). *Dual-joint modeling for estimation of total knee replacement contact forces during locomotion* (Vol. Parts A & B).

Heinemeier, K. M., Schjerling, P., Heinemeier, J., Magnusson, S. P., & Kjaer, M. (2013). Lack of tissue renewal in human adult achilles tendon is revealed by nuclear bomb 14c. *The FASEB Journal*, *27*(5), 2074–2079.

Heintz, S., & Gutierrez-Farewik, E. M. (2007). Static optimization of muscle forces during gait in comparison to emg-to-force processing approach. *Gait & Posture*, *26*(2), 279–288.

Herzog, W., & Leonard, T. R. (2002). Force enhancement following stretching of skeletal muscle: a new mechanism. *Journal of Experimental Biology*, *205*(9), 1275–1283.

Herzog, W. (2017). Skeletal muscle mechanics: Questions, problems and possible solutions. *Journal of Neuroengineering and Rehabilitation*, *14*(1), 1–17.

Hicks, J. L., Uchida, T. K., Seth, A., Rajagopal, A., & Delp, S. L. (2015). Is my model good enough? best practices for verification and validation of musculoskeletal models and simulations of movement [020905]. *Journal of Biomechanical Engineering*, *137*(2).

Hill, A. V. (1938). The heat of shortening and the dynamic constants of muscle. *Proceedings of the Royal Society of London. Series B-Biological Sciences*, *126*(843), 136–195.

Hinterwimmer, S., Krammer, M., Krötz, M., Glaser, C., Baumgart, R., Reiser, M., & Eckstein, F. (2004). Cartilage atrophy in the knees of patients after seven weeks of partial load bearing. *Arthritis & Rheumatism*, *50*(8), 2516–2520.

Hoang, H. X., Pizzolato, C., Diamond, L. E., & Lloyd, D. G. (2018). Subject-specific calibration of neuromuscular parameters enables neuromusculoskeletal models to estimate physiologically plausible hip joint contact forces in healthy adults. *Journal of Biomechanics*, *80*, 111–120.

Huxley, A. F. (1957). Muscle structure and theories of contraction. *Biophysical Chemistry*, *7*, 255–318.

Huxley, A., & Peachey, L. (1961). The maximum length for contraction in vertebrate striated muscle. *The Journal of Physiology*, *156*(1), 150.

Hvid, L. G., Brocca, L., Ørtenblad, N., Suetta, C., Aagaard, P., Kjaer, M., Bottinelli, R., & Pellegrino, M. A. (2017). Myosin content of single muscle fibers following short-term disuse and active recovery in young and old healthy men. *Experimental Gerontology*, *87*, 100–107.

Ivanenko, Y. P., Grasso, R., Macellari, V., & Lacquaniti, F. (2002). Control of foot trajectory in human locomotion: Role of ground contact forces in simulated reduced gravity. *Journal of Neurophysiology*, *87*(6), 3070–3089.

Jacobs, R., Bobbert, M. F., & van Ingen Schenau, G. J. (1996). Mechanical output from individual muscles during explosive leg extensions: The role of biarticular muscles. *Journal of Biomechanics*, *29*(4), 513–523.

Kainz, H., Wesseling, M., & Jonkers, I. (2021). Generic scaled versus subject-specific models for the calculation of musculoskeletal loading in cerebral palsy gait: Effect of personalized musculoskeletal geometry outweighs the effect of personalized neural control. *Clinical Biomechanics*, *87*, 105402.

Kastelic, J., Galeski, A., & Baer, E. (1978). The multicomposite structure of tendon. *Connective Tissue Research*, *6*(1), 11–23.

Kawakami, Y., Abe, T., & Fukunaga, T. (1993). Muscle-fiber pennation angles are greater in hypertrophied than in normal muscles. *Journal of Applied Physiology*, *74*(6), 2740–2744.

Kawakami, Y., Akima, H., Kubo, K., Muraoka, Y., Hasegawa, H., Kouzaki, M., Imai, M., Suzuki, Y., Gunji, A., Kanehisa, H., et al. (2001). Changes in muscle size, architecture, and neural activation after 20 days of bed rest with and without resistance exercise. *European Journal of Applied Physiology*, *84*(1), 7–12.

Kawakami, Y., Muraoka, Y., Kubo, K., Suzuki, Y., & Fukunaga, T. (2000). Changes in muscle size and architecture following 20 days of bed rest. *Journal of Gravitational Physiology*, *7*(3), 53–59.

Kean, C. O., Hinman, R. S., Bowles, K. A., Cicuttini, F., Davies-Tuck, M., & Bennell, K. L. (2012). Comparison of peak knee adduction moment and knee adduction moment impulse in distinguishing between severities of knee osteoarthritis. *Clinical Biomechanics*, *27*(5), 520–523.

Kelly, M. (2017). An introduction to trajectory optimization: How to do your own direct collocation. *SIAM Review*, *59*(4), 849–904.

Keyak, J., Koyama, A., LeBlanc, A., Lu, Y., & Lang, T. (2009). Reduction in proximal femoral strength due to long-duration spaceflight. *Bone*, *44*(3), 449–453.

Killen, B. A., Falisse, A., De Groote, F., & Jonkers, I. (2020). In silico-enhanced treatment and rehabilitation planning for patients with musculoskeletal disorders: Can musculoskeletal modelling and dynamic simulations really impact current clinical practice? *Applied Sciences*, *10*(20), 7255.

Kinney, A. L., Besier, T. F., D'Lima, D. D., & Fregly, B. J. (2013). Update on Grand Challenge Competition to Predict in Vivo Knee Loads [021012]. *Journal of Biomechanical Engineering*, *135*(2).

Kinugasa, R., Hodgson, J. A., Edgerton, V. R., Shin, D. D., & Sinha, S. (2010). Reduction in tendon elasticity from unloading is unrelated to its hypertrophy. *Journal of Applied Physiology*, *109*(3), 870–877.

Knapik, J. J., Wright, J. E., Mawdsley, R. H., & Braun, J. (1983). Isometric, Isotonic, and Isokinetic Torque Variations in Four Muscle Groups Through a Range of Joint Motion. *Physical Therapy*, *63*(6), 938–947.

Knowlton, C. B., Wimmer, M. A., & Lundberg, H. J. (2012). *Grand challenge competition: A parametric numerical model to predict in vivo medial and lateral knee forces in walking gaits* (Vol. ASME 2012 Summer Bioengineering Conference, Parts A and B).

Korhonen, R., Wong, M., Arokoski, J., Lindgren, R., Helminen, H., Hunziker, E., & Jurvelin, J. (2002). Importance of the superficial tissue layer for the indentation stiffness of articular cartilage. *Medical Engineering & Physics*, *24*(2), 99–108.

Korth, D. W. (2015). Exercise countermeasure hardware evolution on iss: The first decade. *Aerospace, Medicine, and Human Performance*, *86*(12), A7–A13.

Koryak, Y. (1995). Contractile properties of the human triceps surae muscle during simulated weightlessness. *European Journal of Applied Physiology and Occupational Physiology*, *70*(4), 344–350.

Koryak, Y. (1998). Effect of 120 days of bed-rest with and without countermeasures on the mechanical properties of the triceps surae muscle in young women. *European Journal of Applied Physiology and Occupational Physiology*, *78*(2), 128–135.

Koryak, Y. (1999). The effects of long-term simulated microgravity on neuromuscular performance in men and women. *European Journal of Applied Physiology and Occupational Physiology*, *79*(2), 168–175.

Koryak, Y. (2010). Mechanical responses of the human triceps surae after passive stretching training of the plantarflexors in conditions modulating weightlessness. *Journal of Human Kinetics*, *24*(2010), 19–34.

Koryak, Y. (2014). Influence of simulated microgravity on mechanical properties in the human triceps surae muscle in vivo. i: Effect of 120 days of bed-rest without physical training on human muscle musculo-tendinous stiffness and contractile properties in young women. *European Journal of Applied Physiology*, *114*(5), 1025–1036.

Koryak, Y. (2015). Influence of simulated microgravity on mechanical properties in the human triceps surae muscle in vivo. *Central European Journal of Sport Sciences and Medicine*, *3*(11), 125–143.

Koryak, Y. (2019). Changes in human skeletal muscle architecture and function induced by extended spaceflight. *Journal of Biomechanics*, *97*, 109408.

Kramer, A., Gollhofer, A., Armbrecht, G., Felsenberg, D., & Gruber, M. (2017). How to prevent the detrimental effects of two months of bed-rest on muscle, bone and cardiovascular system: An rct. *Scientific Reports*, *7*(1), 1–10.

Kramer, A., Kümmel, J., Gollhofer, A., Armbrecht, G., Ritzmann, R., Belavy, D., Felsenberg, D., & Gruber, M. (2018a). Plyometrics can preserve peak power during 2 months of physical inactivity: An rct including a one-year follow-up. *Frontiers in Physiology*, *9*, 633.

Kramer, A., Kümmel, J., Gollhofer, A., Armbrecht, G., Ritzmann, R., Belavy, D., Felsenberg, D., & Gruber, M. (2018b). Plyometrics can preserve peak power during 2 months of physical inactivity: An rct including a one-year follow-up. *Frontiers in Physiology*, *9*, 633.

Kramer, A., Ritzmann, R., Gollhofer, A., Gehring, D., & Gruber, M. (2010). A new sledge jump system that allows almost natural reactive jumps. *Journal of Biomechanics*, *43*(14), 2672–2677.

Kubo, K., Akima, H., Ushiyama, J., Tabata, I., Fukuoka, H., Kanehisa, H., & Fukunaga, T. (2004a). Effects of 20 days of bed rest on the viscoelastic properties of tendon structures in lower limb muscles. *British Journal of Sports Medicine*, *38*(3), 324–330.

Kubo, K., Akima, H., Kouzaki, M., Ito, M., Kawakami, Y., Kanehisa, H., & Fukunaga, T. (2000). Changes in the elastic properties of tendon structures following 20 days bed-rest in humans. *European Journal of Applied Physiology*, *83*(6), 463–468.

Kubo, K., Akima, H., Ushiyama, J., Tabata, I., Fukuoka, H., Kanehisa, H., & Fukunaga, T. (2004b). Effects of resistance training during bed rest on the viscoelastic properties of tendon structures in the lower limb. *Scandinavian Journal of Medicine & Science in Sports*, *14*(5), 296–302.

Kwok, A. T., Mohamed, N. S., Plate, J. F., Yammani, R. R., Rosas, S., Bateman, T. A., Livingston, E., Moore, J. E., Kerr, B. A., Lee, J., et al. (2021). Spaceflight and hind limb unloading induces an arthritic phenotype in knee articular cartilage and menisci of rodents. *Scientific Reports*, *11*(1), 1–17.

Lacquaniti, F., Ivanenko, Y. P., Sylos-Labini, F., La Scaleia, V., La Scaleia, B., Willems, P. A., & Zago, M. (2017). Human locomotion in hypogravity: From basic research to clinical applications. *Frontiers in Physiology*, *8*, 893.

Lai, A. K., Arnold, A. S., & Wakeling, J. M. (2017). Why are antagonist muscles co-activated in my simulation? a musculoskeletal model for analysing human locomotor tasks. *Annals of biomedical engineering*, *45*(12), 2762–2774.

Lambertz, D., Pérot, C., Kaspranski, R., & Goubel, F. (2001). Effects of long-term spaceflight on mechanical properties of muscles in humans. *Journal of Applied Physiology*, *90*(1), 179–188.

Lambrecht, G., Petersen, N., Weerts, G., Pruett, C., Evetts, S., Stokes, M., & Hides, J. (2017). The role of physiotherapy in the european space agency strategy for preparation and reconditioning of astronauts before and after long duration space flight. *Musculoskeletal Science and Practice*, *27*, S15–S22.

Lang, T., LeBlanc, A., Evans, H., Lu, Y., Genant, H., & Yu, A. (2004). Cortical and trabecular bone mineral loss from the spine and hip in long-duration spaceflight. *Journal of Bone and Mineral Research*, *19*(6), 1006–1012.

Lang, T., Van Loon, J. J. W. A., Bloomfield, S., Vico, L., Chopard, A., Rittweger, J., Kyparos, A., Blottner, D., Vuori, I., Gerzer, R., & Cavanagh, P. R. (2017). Towards human exploration of space: The theseus review series on muscle and bone research priorities. *NPJ Microgravity*, *3*(1), 1–8.

Larsson, L., Li, X., Berg, H. E., & Frontera, W. R. (1996). Effects of removal of weight-bearing function on contractility and myosin isoform composition in single human skeletal muscle cells. *Pflügers Archiv*, *432*(2), 320–328.

Laughlin, M. S., Guilliams, M. E., Nieschwitz, B. A., & Hoellen, D. (2015). Functional fitness testing results following long-duration iss missions. *Aerospace Medicine and Human Performance*, *86*(12), A87–A91.

LeBlanc, A., Rowe, R., Schneider, V., Evans, H., & Hedrick, T. (1995). Regional muscle loss after short duration spaceflight. *Aviation, Space, and Environmental Medicine*, *66*(12), 1151–1154.

LeBlanc, A., Schneider, V., Shackelford, L., West, S., Oganov, V., Bakulin, A., & Voronin, L. (2000). Bone mineral and lean tissue loss after long duration space flight. *Journal of Musculoskeletal & Neuronal Interactions*, *1*(2), 157–160.

LeBlanc, A., Lin, C., Shackelford, L., Sinitsyn, V., Evans, H., Belichenko, O., Schenkman, B., Kozlovskaya, I., Oganov, V., Bakulin, A., Hedrick, T., & Feeback, D. (2000). Muscle volume, mri relaxation times (t2), and body composition after spaceflight. *Journal of Applied Physiology*, *89*(6), 2158–2164.

Lemaire, K. K., Baan, G. C., Jaspers, R. T., & van Soest, A. K. (2016). Comparison of the validity of hill and huxley muscle–tendon complex models using experimental data obtained from rat m. soleus in situ. *Journal of Experimental Biology*, *219*(7), 977–987.

Lerner, Z. F., Haight, D. J., DeMers, M. S., Board, W. J., & Browning, R. C. (2014). The effects of walking speed on tibiofemoral loading estimated via musculoskeletal modeling. *Journal of Applied Biomechanics*, *30*(2), 197–205.

Li, R. C., Wu, Y., Maffulli, N., Chan, K. M., & Chan, J. L. (1996). Eccentric and concentric isokinetic knee flexion and extension: A reliability study using the cybex 6000 dynamometer. *British Journal of Sports Medicine*, *30*(2), 156–160.

Lieber, R. L., & Fridén, J. (2000). Functional and clinical significance of skeletal muscle architecture. *Muscle & Nerve*, *23*(11), 1647–1666.

Lin, Y.-C., Dorn, T. W., Schache, A. G., & Pandy, M. G. (2012). Comparison of different methods for estimating muscle forces in human movement. *Proceedings of the Institution of Mechanical Engineers, Part H: Journal of Engineering in Medicine*, *226*(2), 103–112.

Lin, Y.-C., Haftka, R. T., Queipo, N. V., & Fregly, B. J. (2010). Surrogate articular contact models for computationally efficient multibody dynamic simulations. *Medical Engineering & Physics*, *32*(6), 584–594.

Lin, Y.-C., & Pandy, M. G. (2017). Three-dimensional data-tracking dynamic optimization simulations of human locomotion generated by direct collocation. *Journal of Biomechanics*, *59*, 1–8.

Lin, Y.-C., Walter, J. P., & Pandy, M. G. (2018). Predictive simulations of neuromuscular coordination and joint-contact loading in human gait. *Annals of Biomedical Engineering*, *46*(8), 1216–1227.

Liphardt, A.-M., Mündermann, A., Koo, S., Bäcker, N., Andriacchi, T. P., Zange, J., Mester, J., & Heer, M. (2009). Vibration training intervention to maintain cartilage thickness and serum concentrations of cartilage oligometric matrix protein (comp) during immobilization. *Osteoarthritis and Cartilage*, *17*(12), 1598–1603.

Llewellyn, M. E., Barretto, R. P., Delp, S. L., & Schnitzer, M. J. (2008). Minimally invasive high-speed imaging of sarcomere contractile dynamics in mice and humans. *Nature*, *454*(7205), 784–788.

Lloyd, D. G., & Besier, T. F. (2003). An emg-driven musculoskeletal model to estimate muscle forces and knee joint moments in vivo. *Journal of Biomechanics*, *36*(6), 765–776.

Loehr, J. A., Guilliams, M. E., Petersen, N., Hirsch, N., Kawashima, S., & Ohshima, H. (2015). Physical training for long-duration spaceflight. *Aerospace Medicine and Human Performance*, *86*(12), A14–A23.

Lu, X., Mow, V., & Guo, X. (2009). Proteoglycans and mechanical behavior of condylar cartilage. *Journal of Dental Research*, *88*(3), 244–248.

Lund, M. E., de Zee, M., Andersen, M. S., & Rasmussen, J. (2012). On validation of multibody musculoskeletal models. *Proceedings of the Institution of Mechanical Engineers, Part H: Journal of Engineering in Medicine*, *226*(2), 82–94.

Macias, B. R., D'Lima, D. D., Cutuk, A., Patil, S., Steklov, N., Neuschwander, T. B., Meuche, S., Colwell, C. W., & Hargens, A. R. (2012). Leg intramuscular pressures and in vivo knee forces during lower body positive and negative pressure treadmill exercise. *Journal of Applied Physiology*, *113*(1), 31–38.

Manal, K., & Buchanan, T. S. (2012a). Predictions of condylar contact during normal and medial thrust gait. *ASME 2012 Summer Bioengineering Conference*, *ASME 2012 Summer Bioengineering Conference, Parts A and B*, 197–198.

Manal, K., & Buchanan, T. S. (2012b). *Predictions of condylar contact during normal and medial thrust gait* (Vol. Parts A & B).

Manal, K., Innocenti, B., Labey, L., & Buchanan, T. S. (2010). *Condylar contact during normal walking and lateral trunk sway gait: An emg-driven modeling approach to estimate articular loading* (Vol. ASME 2010 Summer Bioengineering Conference, Parts A and B).

Marra, M. A., Vanheule, V., Fluit, R., Koopman, B. H. F. J. M., Rasmussen, J., Verdonschot, N., & Andersen, M. S. (2015). A subject-specific musculoskeletal modeling framework to predict in vivo mechanics of total knee arthroplasty [020904]. *Journal of Biomechanical Engineering*, *137*(2).

Martin, M. L., Travouillon, K. J., Fleming, P. A., & Warburton, N. M. (2020). Review of the methods used for calculating physiological cross-sectional area (pcsa) for ecological questions. *Journal of Morphology*, *281*(7), 778–789.

McCrory, J. L., Derr, J., & Cavanagh, P. R. (2004). Locomotion in simulated zero gravity: Ground reaction forces. *Aviation, Space, and Environmental Medicine*, *75*(3), 203–210.

Mehrabi, N., Schwartz, M. H., & Steele, K. M. (2019). Can altered muscle synergies control unimpaired gait? *Journal of Biomechanics*, *90*, 84–91.

Mendoza-Pinto, C., Garcıéa-Carrasco, M., Juárez-Melchor, D., Munguıéa-Realpozo, P., Etchegaray-Morales, I., Santiago-Martıén, N., Ayón-Aguilar, J., & Méndez-Martıénez, S. (2021). A retrospective analysis of longitudinal changes in bone mineral density in women with systemic lupus erythematosus. *Calcified Tissue International*, 1–9.

Millard, M., Uchida, T., Seth, A., & Delp, S. L. (2013). Flexing computational muscle: Modeling and simulation of musculotendon dynamics. *Journal of Biomechanical Engineering*, *135*(2).

Miller, R. H. (2017). Joint loading in runners does not initiate knee osteoarthritis. *Exercise and Sport Sciences Reviews*, *45*(2), 87–95.

Miller, R. H., Edwards, W. B., Brandon, S. C., Morton, A. M., & Deluzio, K. J. (2014). Why don't most runners get knee osteoarthritis? a case for per-unit-distance loads. *Medicine & Science in Sports & Exercise*, *46*(3), 572–579.

Miller, R. H., Umberger, B. R., & Caldwell, G. E. (2012). Sensitivity of maximum sprinting speed to characteristic parameters of the muscle force–velocity relationship. *Journal of Biomechanics*, *45*(8), 1406–1413.

Miokovic, T., Armbrecht, G., Felsenberg, D., & Belavý, D. L. (2012). Heterogeneous atrophy occurs within individual lower limb muscles during 60 days of bed rest. *Journal of Applied Physiology*, *113*(10), 1545–1559.

Modenese, L., Ceseracciu, E., Reggiani, M., & Lloyd, D. G. (2016). Estimation of musculotendon parameters for scaled and subject specific musculoskeletal models using an optimization technique. *Journal of Biomechanics*, *49*(2), 141–148.

Modenese, L., & Kohout, J. (2020). Automated generation of three-dimensional complex muscle geometries for use in personalised musculoskeletal models. *Annals of Biomedical Engineering*, *48*(6), 1793–1804.

Modenese, L., Montefiori, E., Wang, A., Wesarg, S., Viceconti, M., & Mazzà, C. (2018). Investigation of the dependence of joint contact forces on musculotendon parameters using a codified workflow for image-based modelling. *Journal of Biomechanics*, *73*, 108–118.

Modenese, L., & Renault, J.-B. (2021). Automatic generation of personalised skeletal models of the lower limb from three-dimensional bone geometries. *Journal of Biomechanics*, *116*, 110186.

Moissenet, F., Cheze, L., & Dumas, R. (2011). *Introduction of contact forces minimization in the musculo-tendon forces optimization during gait* (Vol. Parts A & B).

Moo, E. K., Fortuna, R., Sibole, S. C., Abusara, Z., & Herzog, W. (2016). In vivo sarcomere lengths and sarcomere elongations are not uniform across an intact muscle. *Frontiers in Physiology*, *7*, 187.

Moreland, J. D., Richardson, J. A., Goldsmith, C. H., & Clase, C. M. (2004). Muscle weakness and falls in older adults: A systematic review and meta-analysis. *Journal of the American Geriatrics Society*, *52*(7), 1121–1129.

Moriggi, M., Vasso, M., Fania, C., Capitanio, D., Bonifacio, G., Salanova, M., Blottner, D., Rittweger, J., Felsenberg, D., Cerretelli, P., & Gelfi, C. (2010). Long term bed rest with and without vibration exercise countermeasures: Effects on human muscle protein dysregulation. *Proteomics*, *10*(21), 3756–3774.

Mulder, E. R., Gerrits, K., Kleine, B., Rittweger, J., Felsenberg, D., De Haan, A., & Stegeman, D. F. (2009). High-density surface emg study on the time course of central nervous and peripheral neuromuscular changes during 8 weeks of bed rest with or without resistive vibration exercise. *Journal of Electromyography and Kinesiology*, *19*(2), 208–218.

Myers, C. A., Laz, P. J., Shelburne, K. B., & Davidson, B. S. (2015). A probabilistic approach to quantify the impact of uncertainty propagation in musculoskeletal simulations. *Annals of Biomedical Engineering*, *43*(5), 1098–1111.

Narici, M. V., & De Boer, M. D. (2011). Disuse of the musculo-skeletal system in space and on earth. *European Journal of Applied Physiology*, *111*(3), 403–420.

Narici, M. V., Franchi, M., & Maganaris, C. (2016). Muscle structural assembly and functional consequences. *Journal of Experimental Biology*, *219*(2), 276–284.

Narici, M. V., & Maganaris, C. N. (2007). Plasticity of the muscle-tendon complex with disuse and aging. *Exercise and Sport Sciences Reviews*, *35*(3), 126–134.

National Advisory Committee for Aeronautics. (1958). *Notes on space technology.* https : / / ntrs . nasa . gov / api / citations / 19740074640 / downloads / 19740074640.pdf

Navacchia, A., Myers, C. A., Rullkoetter, P. J., & Shelburne, K. B. (2016). Prediction of in vivo knee joint loads using a global probabilistic analysis [031002]. *Journal of Biomechanical Engineering*, *138*(3).

Neptune, R. R., Wright, I. C., & van den Bogert, A. J. (1999). Muscle coordination and function during cutting movements. *Medicine and Science in Sports and Exercise*, *31*(2), 294–302.

Nichols, T. R., & Houk, J. C. (1976). Improvement in linearity and regulation of stiffness that results from actions of stretch reflex. *Journal of Neurophysiology*, *39*(1), 119–142.

Nilsson, J., & Thorstensson, A. (1989). Ground reaction forces at different speeds of human walking and running. *Acta Physiologica Scandinavica*, *136*(2), 217–227.

Novotny, S. C., Perusek, G. P., Rice, A. J., Comstock, B. A., Bansal, A., & Cavanagh, P. R. (2013). A harness for enhanced comfort and loading during treadmill exercise in space. *Acta Astronautica*, *89*, 205–214.

Ong, C. F., Geijtenbeek, T., Hicks, J. L., & Delp, S. L. (2019). Predicting gait adaptations due to ankle plantarflexor muscle weakness and contracture using physics-based musculoskeletal simulations. *PLOS Computational Biology*, *15*(10), e1006993.

Orselli, M. I. V., Franz, J. R., & Thelen, D. G. (2017). The effects of achilles tendon compliance on triceps surae mechanics and energetics in walking. *Journal of Biomechanics*, *60*, 227–231.

Osternig, L. R., Hamill, J., Lander, J. E., & Robertson, R. (1986). Co-activation of sprinter and distance runner muscles in isokinetic exercise. *Medicine & Science in Sports & Exercise*, *18*(4), 431–435.

Pandy, M. G. (2001). Computer modeling and simulation of human movement. *Annual Review of Biomedical Engineering*, *3*(1), 245–273.

Pavei, G., Biancardi, C. M., & Minetti, A. E. (2015). Skipping vs. running as the bipedal gait of choice in hypogravity. *Journal of Applied Physiology*, *119*(1), 93–100.

Pavei, G., & Minetti, A. E. (2016). Hopping locomotion at different gravity: Metabolism and mechanics in humans. *Journal of Applied Physiology*, *120*(10), 1223–1229.

Petersen, N., Jaekel, P., Rosenberger, A., Weber, T., Scott, J., Castrucci, F., Lambrecht, G., Ploutz-Snyder, L., Damann, V., & Kozlovskaya, I. (2016). Exercise in space: The european space agency approach to in-flight exercise countermeasures for long-duration missions on iss. *Extreme Physiology & Medicine*, *5*(1), 1–13.

Pincheira, P. A., Boswell, M. A., Franchi, M. V., Delp, S. L., & Lichtwark, G. A. (2022). Biceps femoris long head sarcomere and fascicle length adaptations after 3 weeks of eccentric exercise training. *Journal of Sport and Health Science*, *11*(1), 43–49.

Pizzolato, C., Lloyd, D. G., Sartori, M., Ceseracciu, E., Besier, T. F., Fregly, B. J., & Reggiani, M. (2015). Ceinms: A toolbox to investigate the influence of different neural control solutions on the prediction of muscle excitation and joint moments during dynamic motor tasks. *Journal of Biomechanics*, *48*(14), 3929–3936.

Porsa, S., Lin, Y.-C., & Pandy, M. G. (2016). Direct methods for predicting movement biomechanics based upon optimal control theory with implementation in opensim. *Annals of Biomedical Engineering*, *44*(8), 2542–2557.

Pouilles, J., Tremollieres, F., & Ribot, C. (1993). The effects of menopause on longitudinal bone loss from the spine. *Calcified Tissue International*, *52*(5), 340–343.

Prilutsky, B. I., & Zatsiorsky, V. M. (2002). Optimization-based models of muscle coordination. *Exercise and Sport Sciences Reviews*, *30*(1), 32.

Psatha, M., Wu, Z., Gammie, F. M., Ratkevicius, A., Wackerhage, H., Lee, J. H., Redpath, T. W., Gilbert, F. J., Ashcroft, G. P., Meakin, J. R., et al. (2012). A longitudinal mri study of muscle atrophy during lower leg immobilization following ankle fracture. *Journal of Magnetic Resonance Imaging*, *35*(3), 686–695.

Qaisar, R., Karim, A., & Elmoselhi, A. B. (2020). Muscle unloading: A comparison between spaceflight and ground-based models. *Acta Physiologica*, *228*(3), e13431.

Raasch, C. C., Zajac, F. E., Ma, B., & Levine, W. S. (1997). Muscle coordination of maximum-speed pedaling. *Journal of Biomechanics*, *30*(6), 595–602.

Rajagopal, A., Dembia, C. L., DeMers, M. S., Delp, D. D., Hicks, J. L., & Delp, S. L. (2016). Full-body musculoskeletal model for muscle-driven simulation of human gait. *IEEE Transactions on Biomedical Engineering*, *63*(10), 2068–2079.

Ramachandran, V., Wang, R., Ramachandran, S. S., Ahmed, A. S., Phan, K., & Antonsen, E. L. (2018). Effects of spaceflight on cartilage: Implications on spinal physiology. *Journal of Spine Surgery*, *4*(2), 433.

Rambaut, P. C., & Johnston, R. S. (1979). Prolonged weightlessness and calcium loss in man. *Acta Astronautica*, *6*(9), 1113–1122.

Redl, C., Gfoehler, M., & Pandy, M. G. (2007). Sensitivity of muscle force estimates to variations in muscle–tendon properties. *Human Movement Science*, *26*(2), 306–319.

Reeves, N. D., Maganaris, C. N., Ferretti, G., & Narici, M. V. (2002). Influence of simulated microgravity on human skeletal muscle architecture and function. *Life in Space for Life on Earth*, *501*, 373–374.

Reeves, N. D., Maganaris, C. N., Ferretti, G., & Narici, M. V. (2005). Influence of 90-day simulated microgravity on human tendon mechanical properties and the effect of resistive countermeasures. *Journal of Applied Physiology*, *98*(6), 2278–2286.

Reinbolt, J. A., Haftka, R. T., Chmielewski, T. L., & Fregly, B. J. (2008). A computational framework to predict post-treatment outcome for gait-related disorders. *Medical Engineering & Physics*, *30*(4), 434–443.

Richter, C., Braunstein, B., Staeudle, B., Attias, J., Suess, A., Weber, T., Mileva, K. N., Rittweger, J., Green, D. A., & Albracht, K. (2021a). Contractile behavior of the gastrocnemius medialis muscle during running in simulated hypogravity. *NPJ Microgravity*, *7*(1), 1–8.

Richter, C., Braunstein, B., Staeudle, B., Attias, J., Suess, A., Weber, T., Mileva, K. N., Rittweger, J., Green, D. A., & Albracht, K. (2021b). Gastrocnemius medialis contractile behavior is preserved during 30% body weight supported gait training. *Frontiers in Sports and Active Living*, *2*, 219.

Richter, C., Braunstein, B., Winnard, A., Nasser, M., & Weber, T. (2017). Human biomechanical and cardiopulmonary responses to partial gravity–a systematic review. *Frontiers in Physiology*, *8*, 583.

Riley, D. A., Bain, J. L. W., Thompson, J. L., Fitts, R. H., Widrick, J. J., Trappe, S., Trappe, T. A., & Costill, D. L. (2000). Decreased thin filament density and length in human atrophic soleus muscle fibers after spaceflight. *Journal of Applied Physiology*, *88*(2), 567–572.

Riley, D. A., Bain, J. L., Thompson, J. L., Fitts, R. H., Widrick, J. J., Trappe, S., Trappe, T. A., & Costill, D. L. (1998). Disproportionate loss of thin filaments in human soleus muscle after 17-day bed rest. *Muscle & Nerve*, *21*(10), 1280–1289.

Rittweger, J., Albracht, K., Flück, M., Ruoss, S., Brocca, L., Longa, E., Moriggi, M., Seynnes, O., Di Giulio, I., Tenori, L., et al. (2018). Sarcolab pilot study into skeletal muscle's adaptation to long-term spaceflight. *NPJ Microgravity*, *4*(1), 1–9.

Rittweger, J., Frost, H. M., Schiessl, H., Ohshima, H., Alkner, B., Tesch, P., & Felsenberg, D. (2005). Muscle atrophy and bone loss after 90 days' bed rest and the effects of flywheel resistive exercise and pamidronate: Results from the ltbr study. *Bone*, *36*(6), 1019–1029.

Ritzmann, R., Freyler, K., Kümmel, J., Gruber, M., Belavy, D. L., Felsenberg, D., Gollhofer, A., Kramer, A., & Ambrecht, G. (2018). High intensity jump exercise preserves posture control, gait, and functional mobility during 60 days of bed-rest: An rct including 90 days of follow-up. *Frontiers in Physiology*, 1713.

Salzman, A., Torburn, L., & Perry, J. (1993). Contribution of rectus femoris and vasti to knee extension an electromyographic study. *Clinical Orthopaedics and Related Research*, *290*, 236–243.

Sartori, M., Reggiani, M., Farina, D., & Lloyd, D. G. (2012). Emg-driven forward-dynamic estimation of muscle force and joint moment about multiple degrees of freedom in the human lower extremity. *PLOS ONE*, *7*(12), e52618.

Sasaki, K., & Neptune, R. R. (2010). Individual muscle contributions to the axial knee joint contact force during normal walking. *Journal of Biomechanics*, *43*(14), 2780–2784.

Saxby, D. J., Bryant, A. L., Modenese, L., Gerus, P., Killen, B., Konrath, J., Fortin, K., Wrigley, T. V., Bennell, K. L., & Cicuttini, F. M. (2016). Tibiofemoral contact forces in the anterior cruciate ligament-reconstructed knee. *Medicine and science in sports and exercise*, *48*(11), 2195–2206.

Schneider, S. M., Lee, S. M. C., Feiveson, A. H., Watenpaugh, D. E., Macias, B. R., & Hargens, A. R. (2016). Treadmill exercise within lower body negative pressure protects leg lean tissue mass and extensor strength and endurance during bed rest. *Physiological Reports*, *4*(15), e12892.

Schoenfeld, B. J. (2010). The mechanisms of muscle hypertrophy and their application to resistance training. *The Journal of Strength & Conditioning Research*, *24*(10), 2857–2872.

Schoenfeld, B. J. (2013). Is there a minimum intensity threshold for resistance training-induced hypertrophic adaptations? *Sports Medicine*, *43*(12), 1279–1288.

Schönau, E., Werhahn, E., Schiedermaier, U., Mokow, E., Schiessl, H., Scheidhauer, K., & Michalk, D. (1996). Influence of muscle strength on bone strength during childhood and adolescence. *Hormone Research in Paediatrics*, *45*(Suppl. 1), 63–66.

Schutte, L. M., Hayden, S. W., & Gage, J. R. (1997). Lengths of hamstrings and psoas muscles during crouch gait: Effects of femoral anteversion. *Journal of Orthopaedic Research*, *15*(4), 615–621.

Scott, J. P. R., Kramer, A., Petersen, N., & Green, D. A. (2021). The role of long-term head-down bed rest in understanding inter-individual variation in response to the spaceflight environment: A perspective review. *Frontiers in Physiology*, *12*, 9.

Scovil, C. Y., & Ronsky, J. L. (2006). Sensitivity of a hill-based muscle model to perturbations in model parameters. *Journal of Biomechanics*, *39*(11), 2055–2063.

Serrancolí, G., Falisse, A., Dembia, C., Vantilt, J., Tanghe, K., Lefeber, D., Jonkers, I., De Schutter, J., & De Groote, F. (2019). Subject-exoskeleton contact model calibration leads to accurate interaction force predictions. *IEEE Transactions on Neural Systems and Rehabilitation Engineering*, *27*(8), 1597–1605.

Serrancolí, G., Kinney, A. L., & Fregly, B. J. (2020). Influence of musculoskeletal model parameter values on prediction of accurate knee contact forces during walking. *Medical Engineering & Physics*, *85*, 35–47.

Seth, A., Hicks, J. L., Uchida, T. K., Habib, A., Dembia, C. L., Dunne, J. J., Ong, C. F., DeMers, M. S., Rajagopal, A., Millard, M., et al. (2018). Opensim: Simulating musculoskeletal dynamics and neuromuscular control to study human and animal movement. *PLOS Computational Biology*, *14*(7), e1006223.

Seynnes, O. R., Maganaris, C. N., De Boer, M. D., Di Prampero, P. E., & Narici, M. V. (2008). Early structural adaptations to unloading in the human calf muscles. *Acta Physiologica*, *193*(3), 265–274.

Sherman, M. A., Seth, A., & Delp, S. L. (2011). Simbody: Multibody dynamics for biomedical research. *Procedia Iutam*, *2*, 241–261.

Sibonga, J. D., Evans, H. J., Sung, H., Spector, E., Lang, T., Oganov, V., Bakulin, A., Shackelford, L., & LeBlanc, A. (2007). Recovery of spaceflight-induced bone loss: Bone mineral density after long-duration missions as fitted with an exponential function. *Bone*, *41*(6), 973–978.

Simons, J. C. (1964). An introduction to surface-free behaviour. *Ergonomics*, *7*(1), 23–36.

Skrinjar, L., Slavič, J., & Boltežar, M. (2018). A review of continuous contact-force models in multibody dynamics. *International Journal of Mechanical Sciences*, *145*, 171–187.

Slowman, S. D., & Brandt, K. D. (1986). Composition and glycosaminoglycan metabolism of articular cartilage from habitually loaded and habitually unloaded sites. *Arthritis & Rheumatism*, *29*(1), 88–94.

Smith, C. R., Vignos, M. F., Lenhart, R. L., Kaiser, J., & Thelen, D. G. (2016). The Influence of Component Alignment and Ligament Properties on Tibiofemoral Contact Forces in Total Knee Replacement. *Journal of Biomechanical Engineering*, *138*(2).

Souza, R. B., Baum, T., Wu, S., Feeley, B. T., Kadel, N., Li, X., Link, T. M., & Majumdar, S. (2012). Effects of unloading on knee articular cartilage t1rho and t2 magnetic resonance imaging relaxation times: A case series. *journal of Orthopaedic & Sports Physical Therapy*, *42*(6), 511–520.

Spatz, J., Fields, E., Yu, E., Pajevic, P. D., Bouxsein, M., Sibonga, J., Zwart, S., & Smith, S. (2012). Serum sclerostin increases in healthy adult men during bed rest. *The Journal of Clinical Endocrinology & Metabolism*, *97*(9), E1736–E1740.

Stäudle, B., Seynnes, O., Laps, G., Göll, F., Brüggemann, G.-P., & Albracht, K. (2020). Recovery from achilles tendon repair: A combination of postsurgery outcomes and insufficient remodeling of muscle and tendon. *Medicine and Science in Sports and Exercise*.

Stavnichuk, M., Mikolajewicz, N., Corlett, T., Morris, M., & Komarova, S. V. (2020a). A systematic review and meta-analysis of bone loss in space travelers. *npj Microgravity*, *6*(1), 1–9.

Stavnichuk, M., Mikolajewicz, N., Corlett, T., Morris, M., & Komarova, S. V. (2020b). A systematic review and meta-analysis of bone loss in space travelers. *NPJ Microgravity*, *6*(1), 1–9.

Steele, K. M., DeMers, M. S., Schwartz, M. H., & Delp, S. L. (2012). Compressive tibiofemoral force during crouch gait. *Gait & Posture*, *35*(4), 556–560.

Stein, T., Leskiw, M., Schluter, M., Donaldson, M., & Larina, I. (1999). Protein kinetics during and after long-duration spaceflight on mir. *American Journal of Physiology-Endocrinology And Metabolism*, *276*(6), E1014–E1021.

Suetta, C., Aagaard, P., Magnusson, S. P., Andersen, L. L., Sipilä, S., Rosted, A., Jakobsen, A. K., Duus, B., & Kjaer, M. (2007). Muscle size, neuromuscular activation, and rapid force characteristics in elderly men and women: Effects of unilateral long-term disuse due to hip-osteoarthritis. *Journal of Applied Physiology*, *102*(3), 942–948.

Swann, A., & Seedhom, B. (1993). The stiffness of normal articular cartilage and the predominant acting stress levels: Implications for the aetiology of osteoarthrosis. *Rheumatology*, *32*(1), 16–25.

Sylos-Labini, F., Ivanenko, Y. P., Cappellini, G., Portone, A., MacLellan, M. J., & Lacquaniti, F. (2013). Changes of gait kinematics in different simulators of reduced gravity. *Journal of Motor Behavior*, *45*(6), 495–505.

Tanner, R. E., Brunker, L. B., Agergaard, J., Barrows, K. M., Briggs, R. A., Kwon, O. S., Young, L. M., Hopkins, P. N., Volpi, E., Marcus, R. L., LaStayo, P. C., & Drummond, M. J. (2015). Age-related differences in lean mass, protein synthesis and skeletal muscle markers of proteolysis after bed rest and exercise rehabilitation. *The Journal of Physiology*, *593*(18), 4259–4273.

Tardioli, A., Malliaras, P., & Maffulli, N. (2012). Immediate and short-term effects of exercise on tendon structure: Biochemical, biomechanical and imaging responses. *British Medical Bulletin*, *103*(1), 169–202.

Tesch, P. A., Berg, H. E., Bring, D., Evans, H. J., & LeBlanc, A. D. (2005). Effects of 17-day spaceflight on knee extensor muscle function and size. *European Journal of Applied Physiology*, *93*(4), 463–468.

Thelen, D. G., Choi, K. W., & Schmitz, A. (2013). *Simultaneous prediction of muscle, ligament and tibiofemoral contact forces via optimally tracking subject-specific gait dynamics* (Vol. 1B) [V01BT27A005].

Thelen, D. G., & Anderson, F. C. (2006). Using computed muscle control to generate forward dynamic simulations of human walking from experimental data. *Journal of Biomechanics*, *39*(6), 1107–1115.

Thelen, D. G., Won Choi, K., & Schmitz, A. M. (2014). Co-simulation of neuromuscular dynamics and knee mechanics during human walking. *Journal of Biomechanical Engineering*, *136*(2), 021033.

Trappe, S., Costill, D., Gallagher, P., Creer, A., Peters, J. R., Evans, H., Riley, D. A., & Fitts, R. H. (2009). Exercise in space: Human skeletal muscle after 6 months aboard the international space station. *Journal of Applied Physiology*, *106*(4), 1159–1168.

Trappe, S., Creer, A., Minchev, K., Slivka, D., Louis, E., Luden, N., & Trappe, T. (2008). Human soleus single muscle fiber function with exercise or nutrition countermeasures during 60 days of bed rest [PMID: 18094071].

American Journal of Physiology-Regulatory, Integrative and Comparative Physiology, *294*(3), R939–R947.

Trappe, S., Creer, A., Slivka, D., Minchev, K., & Trappe, T. (2007). Single muscle fiber function with concurrent exercise or nutrition countermeasures during 60 days of bed rest in women. *Journal of Applied Physiology*, *103*(4), 1242–1250.

Trappe, S., Trappe, T., Gallagher, P., Harber, M., Alkner, B., & Tesch, P. (2004). Human single muscle fibre function with 84 day bed-rest and resistance exercise. *The Journal of Physiology*, *557*(2), 501–513.

Trappe, S., Trappe, T. A., Lee, G. A., Widrick, J. J., Costill, D. L., & Fitts, R. H. (2001). Comparison of a space shuttle flight (sts-78) and bed rest on human muscle function. *Journal of Applied Physiology*, *91*(1), 57–64.

Uchida, T. K., Hicks, J. L., Dembia, C. L., & Delp, S. L. (2016). Stretching your energetic budget: How tendon compliance affects the metabolic cost of running. *PLOS ONE*, *11*(3), e0150378–e0150378.

Valente, G., Crimi, G., Vanella, N., Schileo, E., & Taddei, F. (2017). Nmsbuilder: Freeware to create subject-specific musculoskeletal models for opensim. *Computer Methods and Programs in Biomedicine*, *152*, 85–92.

Valente, G., Pitto, L., Testi, D., Seth, A., Delp, S. L., Stagni, R., Viceconti, M., & Taddei, F. (2014). Are subject-specific musculoskeletal models robust to the uncertainties in parameter identification? *PLOS ONE*, *9*(11), e112625.

van den Bogert, A. J., Blana, D., & Heinrich, D. (2011). Implicit methods for efficient musculoskeletal simulation and optimal control. *Procedia IUTAM*, *2*, 297–316.

Van den Bogert, A. J., Geijtenbeek, T., Even-Zohar, O., Steenbrink, F., & Hardin, E. C. (2013). A real-time system for biomechanical analysis of human movement and muscle function. *Medical & Biological Engineering & Computing*, *51*(10), 1069–1077.

van den Bogert, A. J., Gerritsen, K. G., & Cole, G. K. (1998). Human muscle modelling from a user's perspective. *Journal of Electromyography and Kinesiology*, *8*(2), 119–124.

van den Bogert, A. J., & Nigg, B. M. (2006). Simulation. In B. M. Nigg & W. Herzog (Eds.), *Biomechanics of the musculo-skeletal system* (3rd ed., pp. 622–644). Wiley.

van der Krogt, M. M., Delp, S. L., & Schwartz, M. H. (2012). How robust is human gait to muscle weakness? *Gait & Posture*, *36*(1), 113–119.

van Ingen Schenau, G. J., & Bobbert, M. F. (1993). The global design of the hindlimb in quadrupeds. *Cells Tissues Organs*, *146*(2-3), 103–108.

Van Rossom, S., Smith, C. R., Thelen, D. G., Vanwanseele, B., Van Assche, D., & Jonkers, I. (2018). Knee joint loading in healthy adults during functional exercises: Implications for rehabilitation guidelines. *Journal of Orthopaedic & Sports Physical Therapy*, *48*(3), 162–173.

van Soest, A., Casius, L., & Lemaire, K. (2019). Huxley-type cross-bridge models in largeish-scale musculoskeletal models; an evaluation of computational cost. *Journal of Biomechanics*, *83*, 43–48.

Vanrenterghem, J., Nedergaard, N. J., Robinson, M. A., & Drust, B. (2017). Training load monitoring in team sports: A novel framework separating physiological and biomechanical load-adaptation pathways. *Sports Medicine*, *47*(11), 2135–2142.

Vanwanseele, B., Eckstein, F., Knecht, H., Spaepen, A., & Stüssi, E. (2003). Longitudinal analysis of cartilage atrophy in the knees of patients with spinal cord injury. *Arthritis & Rheumatism*, *48*(12), 3377–3381.

Vardy, A. N., de Vlugt, E., & van der Helm, F. C. (2012). Parameter estimation of the huxley cross-bridge muscle model in humans. *2012 Annual International Conference of the IEEE Engineering in Medicine and Biology Society*, 4827–4830.

Veerkamp, K., Waterval, N., Geijtenbeek, T., Carty, C., Lloyd, D., Harlaar, J., & van der Krogt, M. (2021). Evaluating cost function criteria in predicting healthy gait. *Journal of Biomechanics*, *123*, 110530.

Vico, L., & Hargens, A. (2018). Skeletal changes during and after spaceflight. *Nature Reviews Rheumatology*, *14*(4), 229–245.

Virgin Galactic. (2021). Virgin galactic successfully completes first fully crewed spaceflight. *www.virgingalactic.com*. Retrieved September 3, 2021, from https://www.virgingalactic.com/articles/virgin-galactic-successfully-completes-first-fully-crewed-spaceflight/

Wächter, A., & Biegler, L. T. (2006). On the implementation of an interior-point filter line-search algorithm for large-scale nonlinear programming. *Mathematical Programming*, *106*(1), 25–57.

Wang, J. H. (2006). Mechanobiology of tendon. *Journal of Biomechanics*, *39*(9), 1563–82.

Wang, J. H. C., & Li, B. (2010). Mechanics rules cell biology. *BMC Sports Science, Medicine and Rehabilitation*, *2*(1), 1–7.

Wang, M., Shen, J., Jin, H., Im, H.-J., Sandy, J., & Chen, D. (2011). Recent progress in understanding molecular mechanisms of cartilage degeneration during osteoarthritis. *Annals of the New York Academy of Sciences*, *1240*(1), 61–69.

Weber, T., Green, D. A., Attias, J., Sies, W., Frechette, A., Braunstein, B., & Rittweger, J. (2019). Hopping in hypogravity—a rationale for a plyometric exercise countermeasure in planetary exploration missions. *PLOS ONE*, *14*(2), e0211263.

Weir, J. P. (2005). Quantifying test-retest reliability using the intraclass correlation coefficient and the sem. *The Journal of Strength & Conditioning Research*, *19*(1), 231–240.

Werkhausen, A., Cronin, N. J., Albracht, K., Bojsen-Møller, J., & Seynnes, O. R. (2019). Distinct muscle-tendon interaction during running at different speeds and in different loading conditions. *Journal of Applied Physiology*, *127*(1), 246–253.

Werkhausen, A., Willwacher, S., & Albracht, K. (2021). Medial gastrocnemius muscle fascicles shorten throughout stance during sprint acceleration. *Scandinavian Journal of Medicine & Science in Sports*, *31*(7), 1471–1480.

Wesseling, M., Meyer, C., Corten, K., Desloovere, K., & Jonkers, I. (2018). Longitudinal joint loading in patients before and up to one year after unilateral total hip arthroplasty. *Gait & posture*, *61*, 117–124.

Widrick, J. J., Romatowski, J. G., Norenberg, K. M., Knuth, S. T., Bain, J. L. W., Riley, D. A., Trappe, S., Trappe, T. A., Costill, D. L., & Fitts, R. H. (2001). Functional properties of slow and fast gastrocnemius muscle fibers after a 17-day spaceflight [PMID: 11356784]. *Journal of Applied Physiology*, *90*(6), 2203–2211.

Widrick, J. J., Knuth, S. T., Norenberg, K. M., Romatowski, J., Bain, J. L., Riley, D. A., Karhanek, M., Trappe, S., Trappe, T. A., Costill, D., et al. (1999). Effect of a 17 day spaceflight on contractile properties of human soleus muscle fibres. *The Journal of Physiology*, *516*(Pt 3), 915.

Widrick, J. J., Norenberg, K. M., Romatowski, J., Blaser, C., Karhanek, M., Sherwood, J., Trappe, S., Trappe, T., Costill, D., & Fitts, R. (1998). Force-velocity-power and force-pca relationships of human soleus fibers after 17 days of bed rest. *Journal of Applied Physiology*, *85*(5), 1949–1956.

Widrick, J. J., Romatowski, J., Bain, J. L., Trappe, S., Trappe, T. A., Thompson, J. L., Costill, D. L., Riley, D. A., & Fitts, R. H. (1997). Effect of 17 days of bed rest on peak isometric force and unloaded shortening velocity of human soleus fibers. *American Journal of Physiology - Cell Physiology*, *273*(5), C1690–C1699.

Widrick, J. J., Trappe, S., Romatowski, J. G., Riley, D. A., Costill, D. L., & Fitts, R. H. (2002). Unilateral lower limb suspension does not mimic bed rest or spaceflight effects on human muscle fiber function. *Journal of Applied Physiology*, *93*(1), 354–360.

Williams, P. E., & Goldspink, G. (1978). Changes in sarcomere length and physiological properties in immobilized muscle. *Journal of Anatomy*, *127*(Pt 3), 459.

Wilson, C., Yeadon, M. R., & King, M. A. (2007). Considerations that affect optimised simulation in a running jump for height. *Journal of Biomechanics*, *40*(14), 3155–3161.

Wilson, J. (2021). Nasa's orion flight test and the journey to mars. *www.nasa.gov*. Retrieved September 3, 2021, from https://www.nasa.gov/content/nasas-orion-flight-test-and-the-journey-to-mars

Winnard, A., Scott, J., Waters, N., Vance, M., & Caplan, N. (2019). Effect of time on human muscle outcomes during simulated microgravity exposure without countermeasures—systematic review. *Frontiers in physiology*, *10*, 1046.

Winters, J. M. (1990). Hill-based muscle models: A systems engineering perspective. *Multiple muscle systems* (pp. 69–93). Springer.

Wisdom, K. M., Delp, S. L., & Kuhl, E. (2015). Use it or lose it: Multiscale skeletal muscle adaptation to mechanical stimuli. *Biomechanics and Modeling in Mechanobiology*, *14*(2), 195–215.

Wren, T. A., Rethlefsen, S., & Kay, R. M. (2005). Prevalence of specific gait abnormalities in children with cerebral palsy: Influence of cerebral palsy subtype, age, and previous surgery. *Journal of Pediatric Orthopaedics*, *25*(1), 79–83.

Yamashita-Goto, K., Okuyama, R., Honda, M., Kawasaki, K., Fujita, K., Yamada, T., Nonaka, I., Ohira, Y., & Yoshioka, T. (2001). Maximal and submaximal forces of slow fibers in human soleus after bed rest [PMID: 11408459]. *Journal of Applied Physiology*, *91*(1), 417–424.

Yang, D., & Morris, S. F. (1999). Neurovascular anatomy of the rectus femoris muscle related to functioning muscle transfer. *Plastic and Reconstructive Surgery*, *104*(1), 102–106.

Yeadon, M. R., Atha, J., & Hales, F. (1990). The simulation of aerial movement—iv. a computer simulation model. *Journal of Biomechanics*, *23*(1), 85–89.

Zahalak, G. I. (1981). A distribution-moment approximation for kinetic theories of muscular contraction. *Mathematical Biosciences*, *55*(1-2), 89–114.

Zajac, F. E. (1989). Muscle and tendon: Properties, models, scaling, and application to biomechanics and motor control. *Critical Reviews in Biomedical Engineering*, *17*(4), 359–411.

Zhao, Z., Li, Y., Wang, M., Zhao, S., Zhao, Z., & Fang, J. (2020). Mechanotransduction pathways in the regulation of cartilage chondrocyte homoeostasis. *Journal of Cellular and Molecular Medicine*, *24*(10), 5408–5419.

Żuk, M., Syczewska, M., & Pezowicz, C. (2018). Use of the surface electromyography for a quantitative trend validation of estimated muscle forces. *Biocybernetics and Biomedical Engineering*, *38*(2), 243–250.